Influence of creep and drying/wetting on the initial stress state of clays

by

Rutger (R.P.A.) Bosmans

in partial fulfillment of the requirements for the degree of

Master of Science
in Civil Engineering

at the Delft University of Technology,
to be defended publicly on Friday December 10, 2021 at 08:30 AM.

Student number:	4470699		
Thesis committee:	Prof. Dr. C. (Cristina) Jommi,	TU Delft, Geo Engineering,	Chair supervisor
	Dr. S. (Stefano) Muraro,	TU Delft, Geo Engineering	
	Dr. F. (Federico) Pisanò,	TU Delft, Offshore Engineering	
	MSc. C. (Ching-Yu) Chao,	TU Delft Geo Engineering	

Preface

The last 10 months and 2 days have been spent on the final project of my time as a student at Delft University of Technology. It has been a time with ups and downs like any other Master thesis project. Being stuck on a code for a month straight and contracting covid-19 leading to a two week isolation in my own room were definitely not easy but working on the project and seeing your model do what you hope it will do, realising that your communication and research skills are improving and on top of that even contributing something new to research are highs that far outweigh the lows and which I will not forget.

Over the past 10 months I have worked on a project which is very much included in my field of interest. The difficulties encountered in unsaturated soils are something which keeps coming back in the projects I do but next to this geo-engineering in general is something I find highly interesting. I can with confidence state that the choice for geo-engineering as my master was the correct one. In the past 2 years and a few months I have learned so much about the soil beneath our feet but also about modelling approaches, current day's challenges and in general the world out there. I am excited to find out what more there is to discover within this field.

Of course I could not have done this project on my own. A first and special thank you goes out to Cristina Jommi, my chair supervisor. Her knowledge about soils and modelling approaches is incredible and has been very valuable to the project. I am also very happy to have stuck with my promise of doing my Master thesis with her which I made after successfully defending my Bachelor thesis. Next to this, I would like to thank Stefano Muraro and Ching-Yu Chao. Stefano and Ching-Yu were always available if at any point I had questions and their practical view on the problems I was facing was very useful. Lastly I would like to thank Federico Pisanò for completing my supervision committee because without him graduating simply would not have been possible.

A final thank you goes out to everyone who has been there to support me during this final journey. My friends at university, my roommates at home, my teammates from hockey and all the other people who have been around me. Thank you very much! Without you the downs would have been much more difficult and the ups would have been celebrated less.

I hope you enjoy reading this thesis as much as I did writing it!

Rutger Bosmans
Delft, December 2021

Abstract

The coefficient of lateral earth pressure at rest (K_0) is an important parameter in any geotechnical problem since it provides information on the initial stress state, which governs the response of the soil to the proceeding stress changes. A proper determination of the stresses in any geotechnical problem is required to be able to predict the soil behaviour. Any change in the conditions the soil is subject to can alter the value of K_0, how this value changes for conventional stress histories such as loading and unloading is defined well. However, the influence of unconventional stress histories such as creep or drying/wetting cycles is not thoroughly understood. Since every soil is subjected to natural environmental stresses, resulting in creep and unsaturated conditions, it is interesting to look at their influences of the soil stress state expressed by K_0.

The goal of this work is to determine if it is possible to better understand what is happening to K_0 during creep and under unsaturated conditions and if the prediction of K_0 can be improved by accounting for these phenomena, with the focus being on clays. Literature showed that for saturated samples, the value of K_0 increases with time during creep. For unsaturated conditions it was found that K_0 decreases with an increase of suction.

In order to see if it is possible to improve the prediction of K_0, a model needed to be constructed. The starting point of this model was a saturated, elastoplastic model based on the SANICLAY model. The first step in extending this model was to include viscosity which was done by adopting Perzyna's overstress approach. The model was validated to experimental data on OostVaardersPlassen (OVP) clay obtained from literature and the validation showed that the model was satisfactory in predicting the soil behaviour.
Accounting for unsaturated conditions was done by adopting the average soil skeleton approach. Implementation was initially done in the original elastoplastic model. Again, the model was validated to experimental data obtained from the literature, this time unsaturated loading/unloading tests on London clay (LC) were used. The results showed that the model prediction was accurate up to suctions up to 600 kPa.
The final step in the model development was to include both Perzyna's and the average soil skeleton stress approach in the basic model giving an unsaturated elasto viscoplastic model version. Unsaturated creep tests on London clay were used to validate the model but the results showed that an uncoupled stress-suction approach gave inaccurate predictions. The viscous nucleus in Perzyna's approach was changed to become suction dependent and the results showed that the experimental data could be reproduced reasonably well.

The unsaturated elasto viscoplastic model was then used to analyse K_0 during the unsaturated creep tests. The results showed that the model predicted a decrease in K_0 with time for low loads and high suctions. For higher loads and low to moderate suctions, the model predicted an initial increase followed by a decrease. For all cases it was found that the value of K_0 decreased with suction.
The role of anisotropy on the model prediction was analysed by predicting the change in K_0 using an isotropic version of the model. This version also predicted a decrease at low loads and high suctions but an initial increase was no longer predicted to decrease. The decrease of K_0 with suction was still observed.
No experimental data was available to confirm either of the findings, comparing the results with the literature study showed that the decrease of K_0 with suction was previously observed. The decrease with time on the other hand was not found in previous work. However, the creep tests in previous works were performed on saturated samples and in general for a shorter time period which could show different results.

It is concluded that by accounting for creep and unsaturated conditions, the qualitative prediction of the soil behaviour can be improved. By accounting for coupled behaviour through an unsaturated viscous nucleus, the currently available unsaturated and time dependent experimental deformation data can be simulated accurately. The prediction of the change in stress state, due to these natural phenomena, is likely to be improved as well since the outcome of the model matches findings from the literature. However, due to the lack of experimental unsaturated time dependent data stating the change in K_0, no conclusions can be drawn on the importance of anisotropy and the quantitative model performance. What this work does offer is a good modelling tool to support future experiments or investigations into unsaturated creep behaviour.

Keywords: Coefficient of lateral earth pressure, Creep, Unsaturated Conditions, SANICLAY, Perzyna's approach, Average soil skeleton stress approach.

List of Tables

List of Figures

Nomenclature

Greek Letters

α	Rotation of plastic potential or viscous parameter defining shape of Φ or fitting parameter SWRC
β	Rotation of yield surface
δ	Kronecker delta (always has two subscripts)
ε	Strain
η	Ratio of deviatoric stress to mean stress
κ	Slope of rebound line in v - ln(p') space
κ^*	Slope of rebound line in ln(v) - ln(p') space
λ	Slope of virgin compression line in v - ln(p') space
λ^*	Slope of virgin compression line in ln(v) - ln(p') space
μ	Fluidity parameter
ν	Poisson's ratio
σ	Stress
τ	Shear stress
ϕ	Friction angle
ϕ^b	Additional friction angle
Φ	Viscous nucleus
χ	Effective stress parameter

Upper case Letters

C	Constitutive matrix or Rate of evolution of anisotropy
C_c	Compression index
C_s	Swelling index
F	Force
G_s	Specific gravity
K	Coefficient of lateral earth pressure
K_p	Coefficient of passive earth pressure or plastic multiplier parameter
L	Plastic multiplier
M_c	Slope of critical state line in p-q space (compression)
M_e	Slope of critical state line in p-q space (extension)
M_g	Critical stress ratio
N	Shape of the yield surface
N_Φ	Strain rate coefficient
S_r	Degree of saturation

Lower case Letters

a	Fitting parameter SWRC
b_1, b_2	Loading collapse parameters
c	Cohesion
c_M	Ratio M_e/M_c
e	Void ratio
f	Yield function
g	Plastic potential
k_f, k_g	Shape controlling parameters of the yield surface and plastic potential
m	Fitting parameter SWRC
n	Fitting parameter SWRC
n_{suc}	Exponent used in suction dependent viscous nucleus
p	Mean stress
p_c^s	Size of SYS
p_c^s	Size of DLS
q	Deviatoric stress
q_c	Cone resistance

r Material parameter
s Suction
s_{ref} Reference suction
s_{visc} Suction parameter used in suction dependent viscous nucleus
t Time
u Pore pressure
w Gravimetric water content
x Saturation limit of anisotropy

Superscripts

° Degree
’ Effective
$^{+}$ State of ionization
* Saturated (Relative in case of S_r^*)
^{ep} Elastoplastic
^{NC} Normally Consolidated
^{p} Plastic
^{vp} Viscoplastic

Subscripts

$_0$ Initial (or at rest in case of coefficient of lateral earth pressure) or preconsolidation pressure
$_1$ Vertical
$_a$ Air or axial
$_{aev}$ Air entry value
$_c$ Preconsolidation
$_{c0}$ Psysicochemical stress at saturated state used as reference
$_{cap}$ Capillary
$_{c,g}$ Preconsolidation pressure plastic potential
$_{cv}$ Constant volume
$_e$ Air entry point
$_E$ End of primary consolidation
$_f$ Failure
$_h$ Horizontal
$_{max}$, $_m$ Maximum
$_{net}$ Net stress, defined as total stress minus air pressure
$_p$ Passive (in case of time, void ratio or K_0, indicates end of primary consolidation)
$_{pc}$ Physicochemical
$_{res}$ Residual
$_s$ Suction
$_t$ External
$_v$ Vertical or Volumetric
$_w$ Water

Mathematical symbols

|| Absolute value
$\hat{}$ Average soil skeleton approach
$\langle\rangle$ Macauley brackets
$\frac{\partial}{\partial}$ Partial derivative
$\dot{}$ Time derivative
^{T} Transpose
{} Vector

Notation

In tables and lists, tensors are noted in bold, scalars are noted in regular font. Tensors are presented in Voigt notation, exploiting the symmetry of the tensors.

List of acronyms

AEV	Air Entry Value
CLS	Critical State Line
CPT	Cone Penetration Test
CRR	Cyclic Resistance Ratio
CRS	Constant Rate of Strain
DLS	Dynamic Loading Surface
EOP	End Of Primary
EP	Elastoplastic
EVP	Elasto viscoplastic
FEM	Finite Element Method
HCT	High Capacity Tensiometer
HOC	Highly OverConsolidated
LC	London Clay
MCC	Modified Cam Clay
MSL	Multi-Staged Loading
NC	Normally Consolidated
OCR	OverConsolidation Ratio
OVP	OostVaardersPlassen
REV	Representative Elementary Volume
SANICLAY	Simple ANIsotropic CLAY
SOC	Slightly OverConsolidated
SSCC	Suction Stress Characteristic Curve
SSL	Single-Stage Loading
SWRC	Soil Water Retention Curve
SYS	Static Yield Surface

Contents

1 Introduction

Knowledge of the stress state of a soil is essential at the start of any geotechnical project. How this stress state changes under applied loading conditions during the project is defined well. However, any soil has been, and will be, subjected to environmental influences such as creep and drying/wetting cycles. In order to properly analyse the soil stress state and its corresponding behaviour, these environmental influences need to be considered. An overview of the processes is schematically shown below.

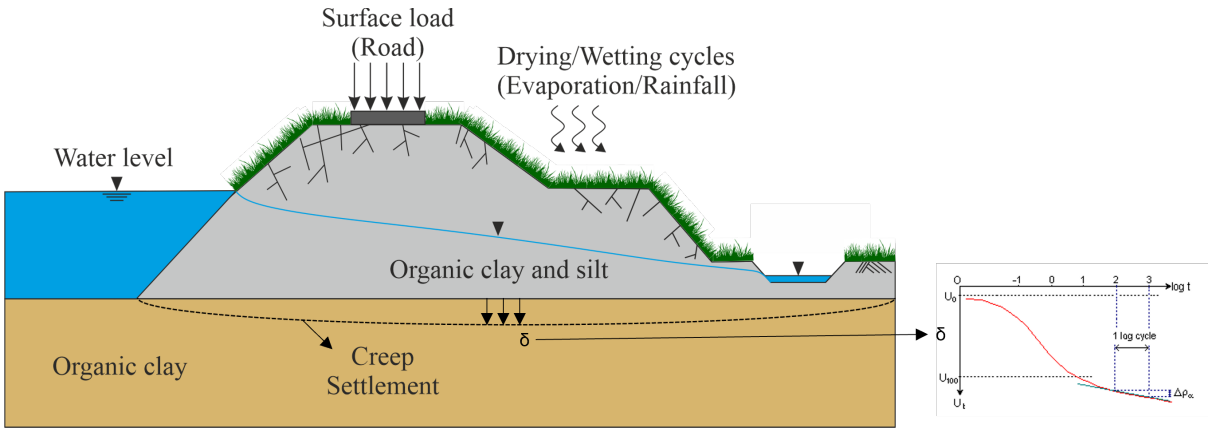

Figure 1: Schematic overview of the processes taking place. Settlement graph retrieved from GeotechniCAL (1996).

Time dependent behaviour of soils has been an important topic in research. Any soil exhibits not only immediate settlement under loading but also continues to deform for a long time, which is called creep. Creep is defined as the deformation under constant effective stress (Le et al., 2012). Several case studies show the importance of the prediction of the creep behaviour of a soil.
In Australia, a large part a bypass of the Pacific Highway had to be constructed on soft soil (Ballina clay). In order to determine the long term behaviour of this soil, trial embankments were constructed which were monitored for 3 years showing large secondary compression (Huang et al., 2006). As can be seen below, 100 days after start of the measurements, the settlement was approximately 20 mm. The measurements over a duration of 3 years show that the settlement increases to nearly 300mm over the duration with numerical predictions indicating that the settlement could increase to more than 400mm as time goes on.

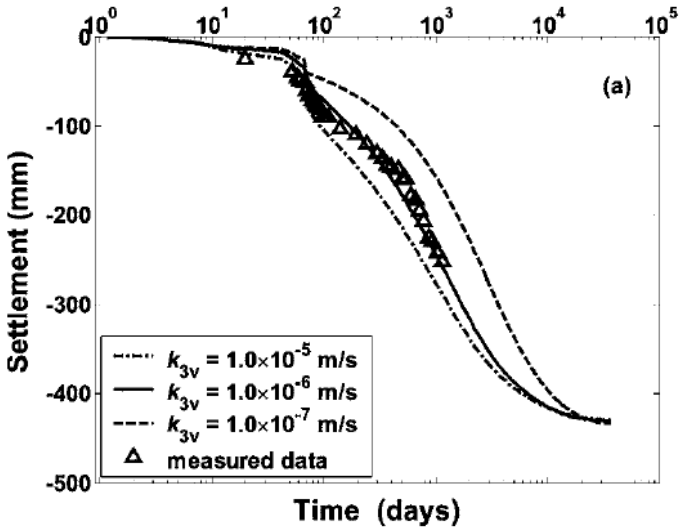

Figure 2: Ground surface settlement over time (Huang et al., 2006).

Another relevant project is the Chengde Airport in China which had to be constructed in a mountainous area. To do this, an embankment had to be constructed made of soft soil. The secondary settlement of this embankment could pose serious problems to the strict safety requirements for the airport. It was therefore of high importance to get a good prediction of the secondary settlement in an early phase of the design process (Yao et al., 2018).

The influence of drying on soils is often ignored in practice because there is a lot of uncertainty on the duration of the dry conditions and their effects are believed to quickly disappear upon wetting. However, the majority of natural soils used in engineering practice does experience unsaturated conditions during its required life span (Ellithy & Stark, 2020). Zhang et al. (2010) performed field studies in which slopes were analysed under artificial rainfall. Thousands of these slopes can be found and the conclusion of the field study was that due to drying and wetting cycles, cracks occured increasing the permeability and upon wetting a loss of suction was observed leading to a decrease in shear strength. The slopes failed consequently causing damage to infrastructure. Yang et al. (2019) numerically analysed one of these slopes using finite element analyses. They were able to predict the loss of suction due to continued wetting accurately. Using the determined hydraulic response, the Factor of Safety of the slope was determined accordingly. The results show that as the time increases (and the soil gets wetter) the Factor of Safety reduces. The highest decrease that was found was with a factor 5 indicating the importance of accounting for the hydraulic condition of a soil.

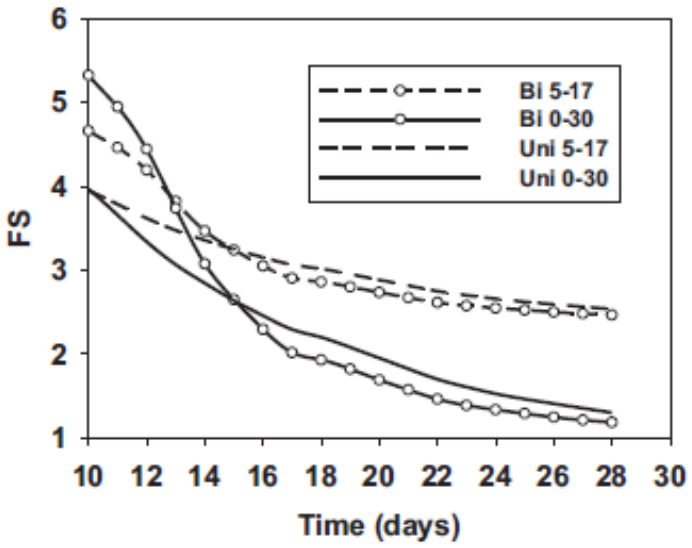

Figure 3: Factor of Safety over time with wetting (Yang et al., 2019).

1.1 Problem statement

The case studies above highlight the importance of accounting for environmental influences on the soil behaviour. In order to assess this behaviour, the stress state of the soil needs to be known. The vertical stress can easily be determined but the horizontal stress needs to be known as well. To determine the horizontal stress, the coefficient of lateral earth pressure (K_0) is used which is defined as the ratio between the horizontal and vertical effective stress.

$$K_0 = \frac{\sigma'_h}{\sigma'_v} \tag{1}$$

The importance of a proper K_0 determination is highlighted by Golpasand et al. (2018). They performed a numerical analysis of ground settlement around a tunnel construction and part of their research was to show the influence of K_0 on the settlement behaviour. Their results showed that not only the amount of settlement (figure 4) differed highly with K_0 but also the direction of the pressures acting on the tunnel changed with K_0.

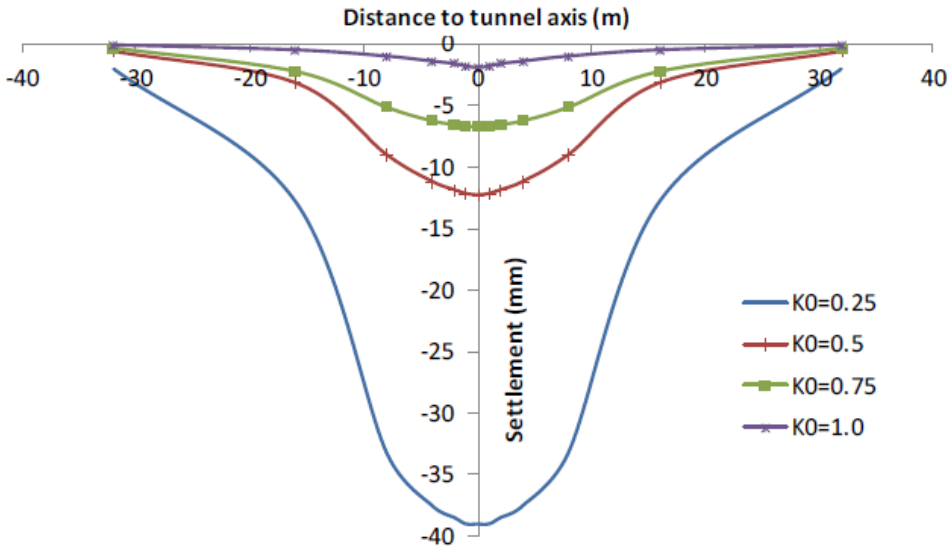

Figure 4: Ground settlement around tunnel with varying K_0 (Golpasand et al., 2018).

The problem being faced is that it is unclear yet how the environmental influences described earlier affect the value of K_0. The influence of both creep and drying/wetting on the soil behaviour has been highlighted by case studies and the importance of a proper K_0 determination is shown above. This makes it worthwhile to perform an analysis on the influence of creep and drying/wetting on K_0.

1.2 Objective

There are two main goals in this work. The first one is to get a better understanding of the processes going on in the soil during creep and drying/wetting as well as their influence on the soil stress state, expressed by K_0. The second goal is to use this understanding to improve the modelling of these natural phenomena. The focus of this goal will be on soft soils because of their relevant creep behaviour as shown above. With this goal in mind, the following research question is formulated.

'Can the prediction of K_0 be improved for unconventional stress histories including creep and drying/wetting cycles?'

In order to help answer this research question, the following subquestions are used. The answers of the subquestions together will define the answer to the research question stated above.

1. Is there an agreement in literature on the influence of creep and drying/wetting on the soil stress state and is there solid physical reasoning behind this?
2. How can the influences be validated?
3. What is the influence of drying/wetting on the creep behaviour of a soil?

Literature shows that soft soils exhibit anisotropic behaviour under loading and unloading conditions (Lo & Morin, 1972; Romero & Jommi, 2008; Yin & Karstunen, 2011). Because of this, it is interesting what the effect of anisotropy is on the initial stress state. Therefore, a fourth subquestion is formulated.

4. What is the influence of anisotropy on the initial stress state?

1.3 Approach

In order to answer the main research question, the subquestions need to be answered for which the following approaches will be used.

1. **Is there an agreement in literature on the influence of creep and drying/wetting on the soil stress state and is there solid physical reasoning behind this?**
   To see if there is an agreement, works from different researches will be analysed. The focus will be on proof for physical causes behind the different phenomena, experimental evidence on the influence of the phenomena on K_0 and different modelling approaches to capture these influences.
2. **How can the influences be validated?**
   A model will be constructed which accounts for both the influence of creep as well as drying/wetting. Initially, two model versions will be developed, one accounting for creep and one for unsaturated conditions. The output of these model versions will be compared to experimental data from the literature to see if the influences of the respective phenomena are captured accurately.
3. **What is the influence of drying/wetting on the creep behaviour of a soil?**
   The coupled behaviour of the two phenomena needs to be analysed. To do this, a model version is constructed that accounts both for creep and unsaturated conditions. This newly developed model needs to be tested to unsaturated, time dependent experimental data which has to be obtained from literature. Upon completion of the analysis, model adaptations might be required if the results show the need to. If this is indeed required, additional literature needs to be analysed to see if previous researchers have dealt with this problem before. If this is not the case, the potential model adaptation needs to be defined. Of course, the newest version of the model would need to be tested again to the experimental data to validated the coupled effect.
4. **What is the influence of anisotropy on the initial stress state?**
   Upon validation of the final model version, anisotropy will be turned off in the model. Redoing the same tests will isolate the effect the anisotropy had since potential differences in model output will be solely due to the effect of anisotropy. Comparing the model predictions with and without anisotropy will yield the answer to this research question.

1.4 Reading guide

Chapter 2 contains the literature study which is performed to gain insight in the problem and collect information on how the mentioned approaches can be executed properly. The adopted methodology is explained in chapter 3 including the model version serving as a starting point of the work. The implementation of the influence of creep is presented in chapter 4 after which the unsaturated conditions are included in chapter 5. Chapter 6 will contain the results obtained to help answer the main research question. These results are discussed in chapter 7 after which the conclusions and recommendations are given in chapter 8.

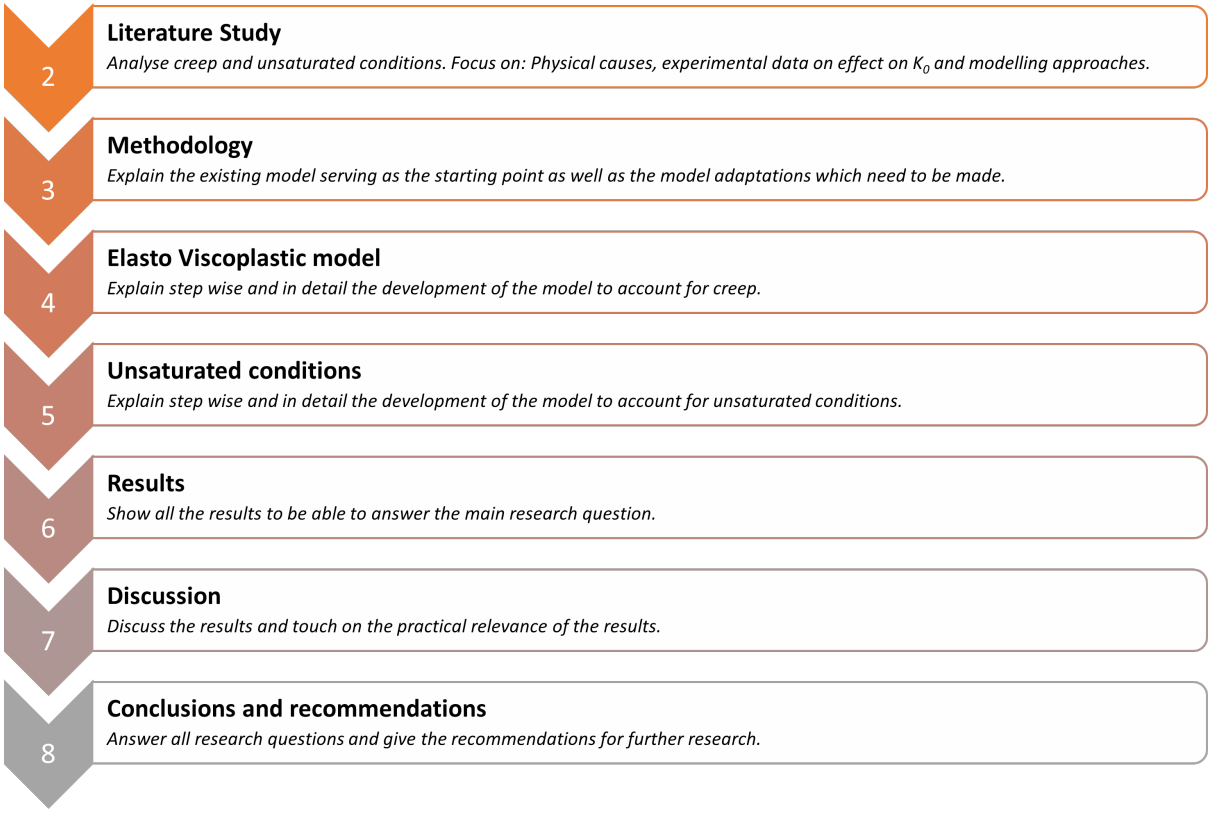

Figure 5: Reading guide thesis.

The answer to the first research question is found in the literature study. The second subquestion is answered in chapter 4 and the the first half of chapter 5. Subquestion 3 is answered in the second half of chapter 5 after which the final subquestion is answered in chapter 6. The answer to the main research question is given in the conclusions in chapter 7.

2 Literature Study

The literature study consists of three main parts. First, the well known relationships for K_0 for normally- and overconsolidated soils will be elaborated.
The second part focuses on creep. This part starts off by looking at the physical causes behind this phenomenon. After this, experimental data on the change of K_0 during creep is discussed. The part ends with an elaboration of Perzyna's overstress approach which is the modelling approach that will be used to account for creep.
The final part of the literature study goes in depth on the influence of unsaturated conditions. Different stress approaches to account for this influence are discussed first after which the suction stress principle is discussed to show the interactions going on in the soil under unsaturated conditions. Then, experimental data is discussed, this time focussing on the change of K_0 under unsaturated conditions. The chapter ends with an explanation of the average soil skeleton approach which is, similar to Perzyna's approach, the modelling approach which will be used.

2.1 Loading

In this section, the well known equations for K_0 for normally consolidated and overconsolidated soils are presented.

2.1.1 Normally consolidated soils

The first definition of the coefficient of lateral earth pressure was given by Donath (1891) who defined it as the ratio between total horizontal and vertical stress. The improvement of the definition using effective stresses was given by Bishop (1958) (Wijeyesekera & Mohamed, 2000).

The most important work on finding an expression to determine K_0 was done by Jaky (1944) and Jaky (1948). Analysing a slope of freestanding granular soil and determining sliding planes led to the following equation for K_0.

$$K_0 = (1 - \sin\phi') \frac{1 + \frac{2}{3}\sin\phi'}{1 + \sin\phi'} \tag{2}$$

Without further explanation this has been simplified into the well known equation for K_0 of normally consolidated soils.

$$K_0 = (1 - \sin\phi') \tag{3}$$

For a more precise derivation refer to Mesri and Hayat (1993). It should be noted that in the equations above ϕ' is the constant volume friction angle ϕ'_{cv} which can be determined by a triaxial or direct shear test. Equation (3) has been widely accepted as a good first prediction of K_0 for normally consolidated soils. Validation of equation (3) is shown below.

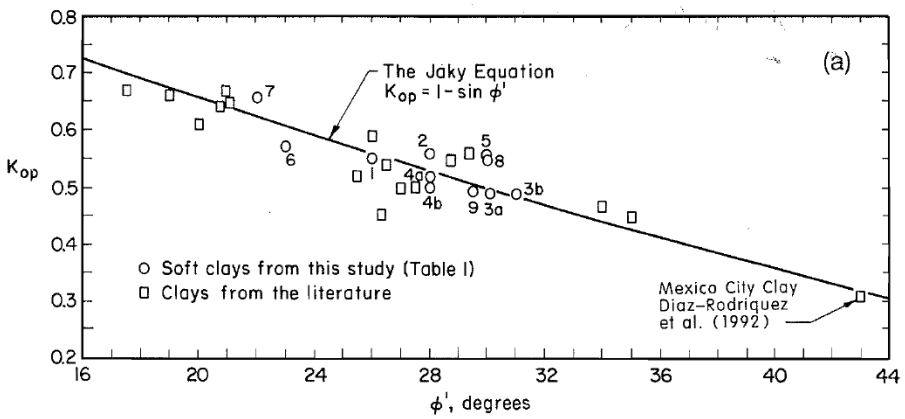

Figure 6: Validation of Jaky's equation (Mesri & Hayat, 1993).

2.1.2 Overconsolidated soils

Hendron (1963) found, based on experimental data, that in general during unloading the decrease of vertical stress is higher than the decrease of horizontal stress. By definition, this leads to an increase in K_0 following equation (1). An example of this behaviour is shown below from a test done by Brooker and Ireland (1965) on a cohesive soil (London clay). A test was performed where the soil sample was loaded axially with no radial deformation allowed. The radial stress required to maintain no radial deformation was registered and shown in the figure below. The lower line is the stress path during loading and the upper one during unloading. It can clearly be seen that under unloading of the sample, the vertical stress decreases more than the horizontal stress.

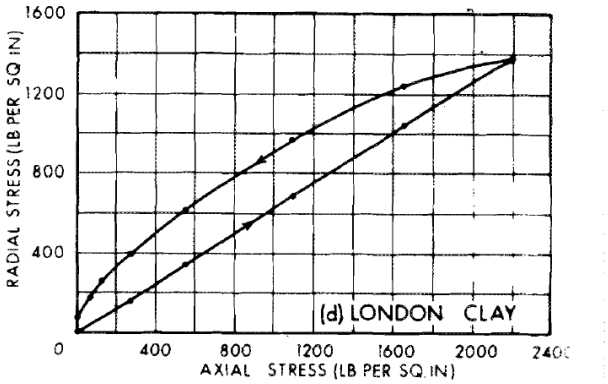

Figure 7: Stress path under loading and unloading for London clay (Brooker & Ireland, 1965).

Another consequence of unloading is an increase in the OverConsolidation Ratio (OCR) which is defined as follows:

$$OCR = \frac{\sigma'_{v,max}}{\sigma'_v} \tag{4}$$

where $\sigma'_{v,max}$ is the maximum vertical effective stress the soil has experienced in the past. Since during unloading $\sigma'_{v,max}$ remains constant and σ'_v decreases, the OCR increases. Above it was determined that K_0 increases as well during unloading which leads to the possibility of defining a relationship between the two. This has been experimentally confirmed by Brooker and Ireland (1965). The test results as in figure 7 is plotted but now with the OCR on the horizontal axis and K_0 on the vertical one. Only the solid line marked K_0 is of relevance in the figure below. The dashed lines indicate an asymptote of K_p (coefficient of passive earth pressure) which is not relevant in this work.

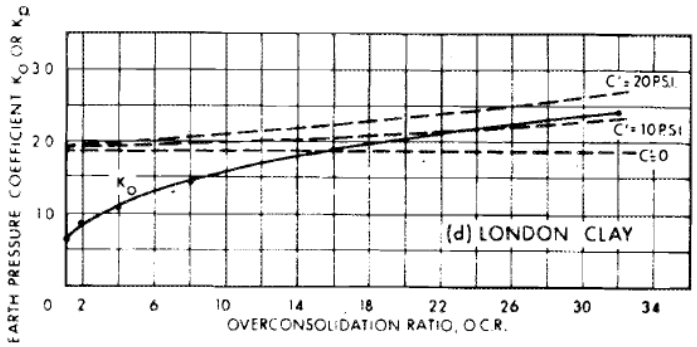

Figure 8: Relationship between K_0 and OCR for London clay (Brooker & Ireland, 1965).

Besides the tests by Brooker and Ireland (1965) on cohesive soils, Hendron (1963) performed tests on sands and found a similar relation as was found for clay. His results are shown below.

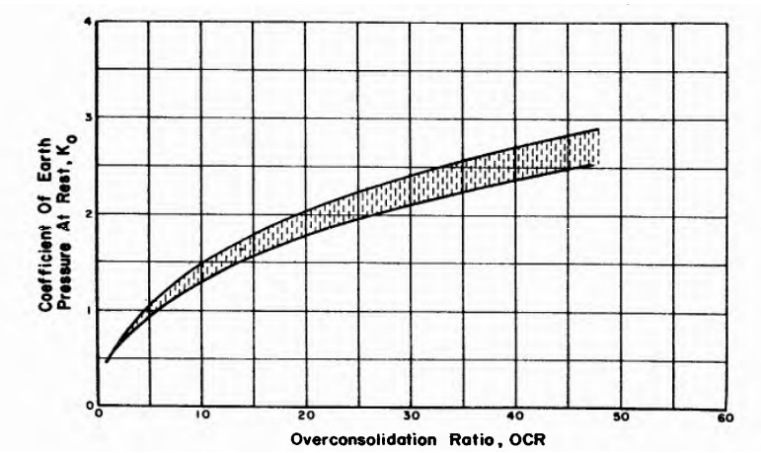

Figure 9: Relationship between K_0 and OCR for Pennsylvania sand (Hendron, 1963).

Following this, Schmidt (1966) analysed the data from Brooker and Ireland (1965) and a year later Schmidt (1967) looked at the data from Hendron (1963) after which he came up with a semi empirical relation between K_0 and OCR.

$$K_0 = b * OCR^a \tag{5}$$

Where a is the slope of the log K_0 vs log OCR curve and b is the intercept of this curve at OCR = 1. If the OCR is equal to one the soil is normally consolidated meaning equation (3) needs to be recovered leading to $b = 1 - \sin\phi'$. Following an extensive analysis of data on both clays and sands, Mayne and Kulhawy (1982) found that taking $a = \sin\phi'$ gave accurate results. Mesri and Hayat (1993) confirmed this finding by summarising available data of which the results are shown in figure 10.

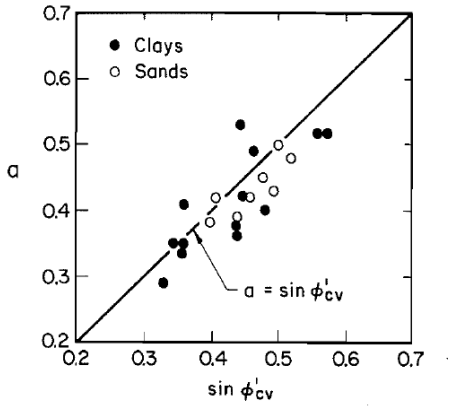

Figure 10: Data showing the fit of $a = \sin\phi'$ (Mesri & Hayat, 1993).

Concluding, the change in K_0 during unloading and reloading can be defined with a relationship between K_0 and OCR as follows.

$$K_0 = (1 - \sin\phi') * OCR^{\sin\phi'} \tag{6}$$

Mayne and Kulhawy (1982) describe other approaches to modelling the K_0-OCR relationship. Empirical approaches are mentioned as well as approaches using determination of swelling indices and a critical-state model. In general though, equation (6) is widely accepted and therefore no other approaches will be discussed here.

2.2 Creep

In this chapter the phenomenon of creep is analysed. To start off, causes of creep are explained. Then, experimental data is presented regarding the change in K_0 under creep. After that, Perzyna's overstress approach is elaborated on which is the approach used to model creep behaviour.

2.2.1 Causes

The term creep describes the deformation of a soil under constant effective stress. This deformation is most notably present in soft soils such as clays and peats. Le et al. (2012) have listed 5 possible causes of creep.

- Creep due to the Breakdown of Interparticle Bonds
- Creep due to Jumping of Molecule Bonds
- Creep due to Sliding Among Particles
- Creep due to Water Flows in a Double Pore System
- Creep due to the Structural Viscosity

The first three causes listed above focus on the interactions between the grains whereas the final two focus on the influence of the pore fluid. In the following, the causes will be explained briefly.

Different kinds of bonds form at the contacts between (clay) particles. Examples of these bonds are primary valence bonds or van der Waals forces. These bonds can be broken causing rearrangement of soil particles leading to further deformation (Le et al., 2012).
Reasons for the breakdown of these bonds are mentioned by Mesri (1973). He states that an increase in interparticle forces can cause shear strains or a change in particle spacing which make the particles move relative to each other. This relative movement can lead to the particle bonds to break. For this theory to hold, proof is needed that there is indeed a change in interparticle forces during secondary compression. To the best of the author's knowledge, no such experimental proof is available on clays.
For sands however, this proof can be found in the work of Wang and Gao (2013). They performed oedometer tests using a tactile pressure sensor inside the specimen to measure interparticle forces. The results showed that during secondary compression there is a redistribution of interparticle forces. The net effect is an increase in mean interparticle force as can be seen in figure 11 (Wang & Gao, 2013).

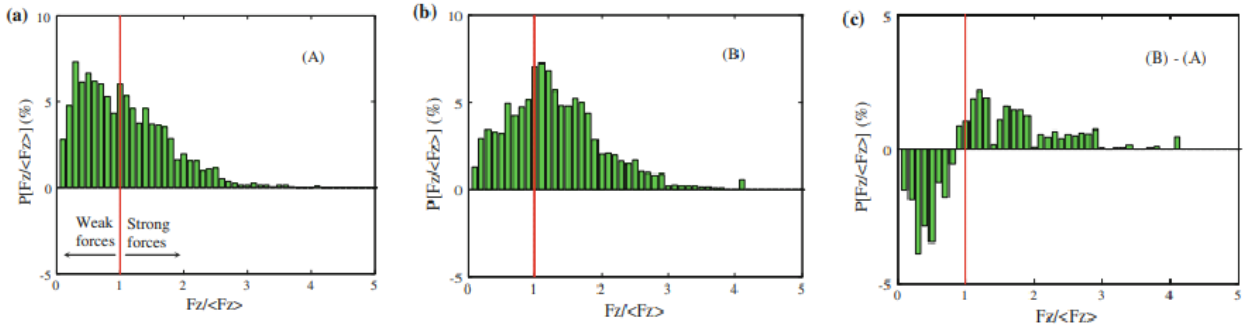

Figure 11: Distribution of interparticle forces. a) before secondary compression, b) after secondary compression, c) difference (Wang & Gao, 2013).

This experimental finding can support the theory by Mesri (1973) that breakdown of interparticle bonds can be due to a change in net interparticle force resulting in a change in interparticle spacing (Le et al., 2012). It needs to be stated though that no evidence for this theory is available for clays.

Jumping of bonds is defined as the movement of a particle from one position to another. The particles inside a soil are all in a certain position and under application of a force, such as a shear stress, the equilibrium position of the particle can change (Andersland & Douglas, 1970). In order to move to the new equilibrium position a certain amount of energy is needed to a) break the bonds the molecule has in its current position and b) push the particles on the path to the new position away. This required amount of energy is called the activation energy (Low, 1962). Kuhn and Mitchell (1993) suggested that the particles which are moving in the soil are oxygen atoms and that creep is partially caused by the displacement of these oxygen atoms within the contact surfaces of the clay grains. A schematic overview of the principle behind the activation energy is given in figure 12, it shows the energy needed for a molecule to move from position a to b.

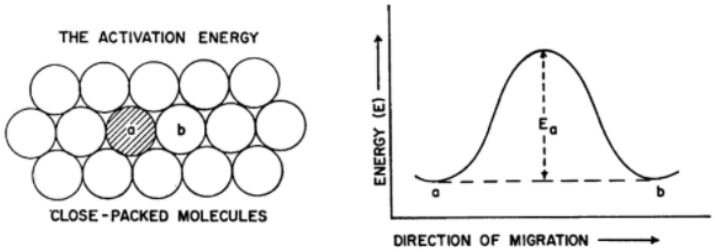

Figure 12: Schematic overview of the principle of activation energy (Low, 1962).

Gupta (1964) described retarded or viscous deformation as the change of soil orientation from a less to a more dispersed structure with the particles more parallel to each other. To realise this, particles have to move with respect to each other called sliding. If water is present in the soil it offers a bonding effect against sliding making the sliding process slower than it would be in a completely dry soil. The reorientation of particles is schematically shown in figure 13.

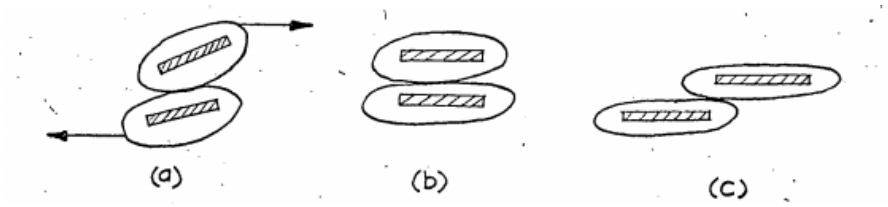

Figure 13: Movement of particles relative to each other (Gupta, 1964).

Kuhn and Mitchell (1993) developed a framework to describe the sliding among particles. The sliding of particles is caused by a shear force tangential to the particles. Since this sliding is viscous due to the presence of water as described above. This sliding is modelled as a dashpot in figure 14b.
At the contact surface between particles it is known that bonds form which result in a resistance against deformation. This resistance is present in both the normal and tangential direction and is therefore modelled as a spring in figure 14. This framework gives a visual representation of the processes playing a role within the sliding among particles in a soil during secondary compression.

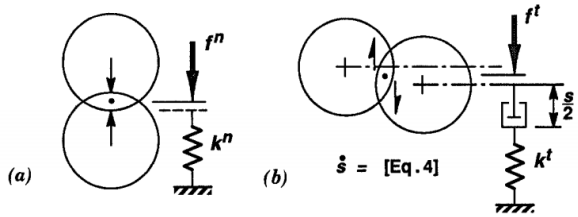

Figure 14: Framework of sliding among particles (Kuhn & Mitchell, 1993).

The last two causes focus on the influence of the pore fluid. The main consideration is to divide the soil in a macro- and microstructure. The macrostructure consists of larger grains and pores whereas the microstructure is formed by clay clusters between the larger grains. The pores inside these clay clusters are smaller than the large pores in the macrostructure. This consideration was first introduced on peats (Adams, 1963; de Jong, 1966, 1968) after which Zeevaert (1986) applied it to describe clay. Two types of pores (Macro and Micro) are included in this system and therefore it is referred to as double porosity. An overview is shown in figure 15 (Le et al., 2012).

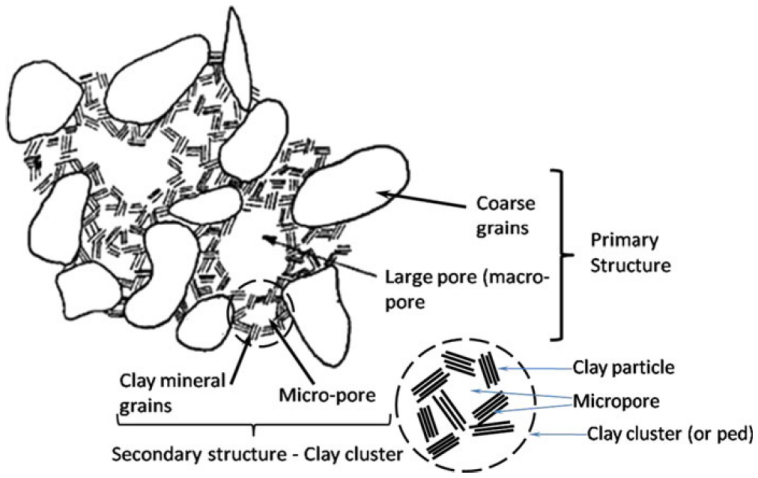

Figure 15: Macro- and microstructure in clay (Le et al., 2012).

Under pressure, water from the micropores is expelled into the macropores. This causes deformation in the micropores leading to creep compression (Le et al., 2012). Zeevaert (1986) stated that since the microstructure consists mainly of clay mineral grains, the water in these micropores is adsorbed forming a water film around the grains. Because of this, the draining of micropores has a highly viscous character and the process is slow. Akagi (1994) performed experiments to test this micropore theory. He prepared samples in such a way that Ca^{2+} ions would be present in the pore fluid in the micropores and Na^{+} ions in the macropores. The pore fluid drained from the sample during primary- and secondary compression was quantitatively tested for the concentration in cations. The findings showed that during secondary compression the concentration Ca^{2+} in the drained fluid was a lot higher indicating that during secondary compression water drains from the micropores. This increase in Ca^{2+} concentration lead to the conclusion that during secondary compression deformation of micropores is taking place. The results of one of the experiments is shown below in figure 16 where t_E indicates the time at the end of primary consolidation.

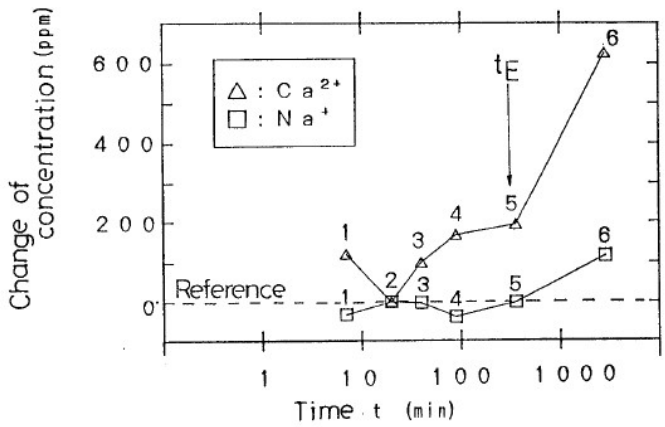

Figure 16: Compression and cation concentration over time (relevant part of figure taken from Akagi (1994)).

The final cause for creep described by Le et al. (2012) is called structural viscosity. What is meant by this is that there is plastic structural resistance against compression within the clay since the water is adsorbed to the clay grains. Creep compression is then defined as the deformation of clay clusters due to the viscous flow of water. Work is also mentioned from researchers who concluded that the viscosity of the water has an insignificant influence on secondary compression. They stated that the electrical loading of water molecules has an impact on the attractive and repulsive forces. Which of these two theories is preferred is not discussed but it can be concluded that the flow of water from micropores is delayed because of forces between the water and clay grains causing a delay in compression which results in creep (Le et al., 2012).
Akagi (1994) mentioned that secondary compression is due to the flow of water from micropores which can be described as viscous since the pore fluid is closely adsorbed to the surfaces of the clay particles.
A case can be made saying that structural viscosity is not a standalone cause of creep but is an addition to the double pore system. As described earlier, creep can be explained by drainage from micropores, this drainage is delayed because of the viscous character of this pore fluid due to interactions between the water and the clay particles.

2.2.2 Experimental data on K_0 development during creep

The first literature reference on the behaviour of K_0 under creep is found in Schmertmann (1983). He asked a simple question about creep, namely: 'Will $K_0 = \sigma'_h/\sigma'_v$ of a normally consolidated cohesive soil increase or decrease during secondary aging in 1-D compression?' (Schmertmann, 1983). This question was asked to 40 geotechnical engineers of which half said K_0 would increase, 25% said K_0 would stay the same, 12.5% said K_0 would decrease and the rest did not know. No experimental evidence was given but this is the first indication of what happens to K_0 during secondary compression (Schmertmann, 1983).

Kavazanjian and Mitchell (1984) were the first researches to perform lab tests following the publication of Schmertmann. Their reasoning was that any soil would reach a value of $K_0 = 1$ given enough time because this would represent a minimal energy state. Under the presence of a deviatoric stress, soil bonds would continue to break causing deformation of the sample in the direction of the deviatoric stress to undo the imbalance of energy.
They ran triaxial cells tests on specimens of undisturbed mud to test their theory. It was found that K_0 increased from 0.53 to 0.58 over a time span of 10000 min (∼7 days) after EOP (End Of Primary) consolidation (figure 17) (Kavazanjian & Mitchell, 1984).

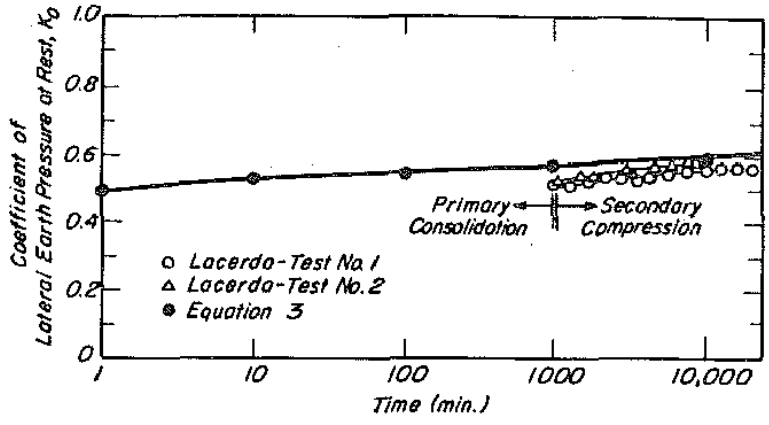

Figure 17: K_0 as a function of time (Kavazanjian & Mitchell, 1984).

There is no general acceptance for the theory that K_0 has to approach unity but even if there was, it has been shown that the time for this state to be reached would be so long that K_0 approaching unity is of little practical importance (Mesri & Castro, 1987). What Kavazanjian and Mitchell (1984) did show was an increase in K_0 with time.

The next research regarding K_0 under creep was performed by Mesri and Castro (1987). Four clays were tested in a special triaxial cell with a bellophram bushing assembly. A load cell inside the triaxial cell guaranteed constant axial loads over long periods of time. The temperature was kept constant and the cell pressure was adapted to make sure a 1D compression condition was present at all times. The results are shown below in figure 18.

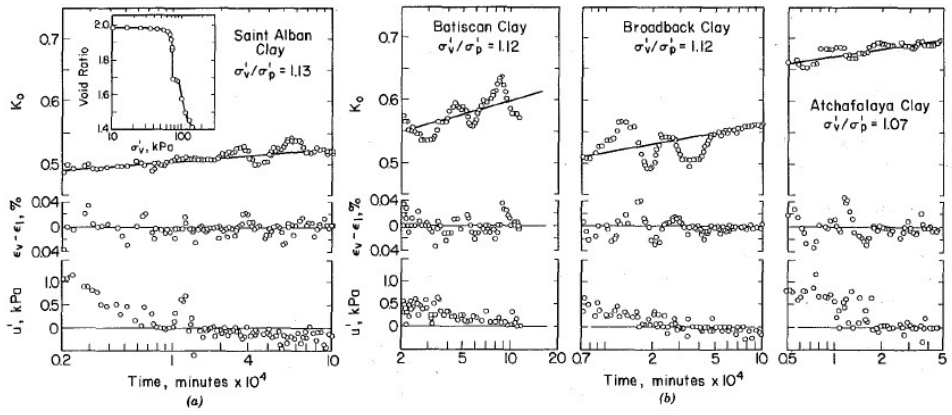

Figure 18: K_0 as a function of time for the four different clays (Mesri & Castro, 1987).

The measurements are denoted by the dots and it can clearly be seen that for all specimens the value of K_0 increases with time. The experimental data is not following a very clear path for all specimens and the authors stated that this was due to possible problems with the measurements. Problems are the deviations from the 1D compression condition denoted by $\varepsilon_v - \varepsilon_1$ nonequal zero and the accuracy of the measured volume changes which was influenced by leakage in and out of the sample.

In 1993, Mesri and Hayat (1993) performed tests on 11 soft clays using triaxial cells and special oedometers allowing for the measurement of horizontal stress. All specimens were loaded beyond their preconsolidation pressure and after this left subjective to creep for a large time range ($t/t_p = 6$ to 4856, where t_p is the time required to complete primary consolidation). Their results show a significant scatter (due to experimental problems) in the amount of change of K_0 with time but in all cases a positive change was found thus showing that K_0 increases with time. The results are not presented in a clear way and thus not included in this thesis but can be found in Mesri and Hayat (1993).
A finding of the authors which was presented in a clear way is that when the vertical effective stress was kept constant, the horizontal effective stress increased over time. An example of this is presented in the figure below.

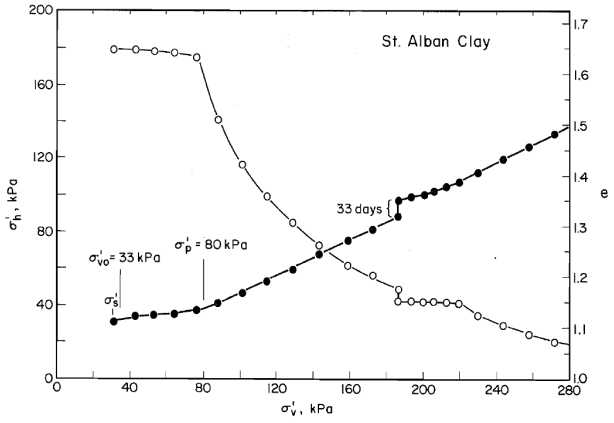

Figure 19: σ'_h vs σ'_v for the St. Alban clay (Mesri & Hayat, 1993).

This increase with time was not observed for all 11 samples. What was observed for all samples is that, no matter if σ'_h increased or not, the slope of the stress path upon reloading is a lot smaller than the slope during consolidation. The slope of the stress path during consolidation is indicated by K_{0p} (the coefficient of lateral earth pressure at rest for normally consolidated young soils). Figure 19 shows that after reloading, the slope of the stress path initially is almost flat after which it goes back to the same slope observed during consolidation. Therefore, the soil moves towards a K_{0p} stress state upon continued loading. In order to reach this K_{0p} stress state, the vertical stress has to increase more than the horizontal stress as is observed by the near flat line after secondary compression. The corollary of this is that K_0 decreases which means that to reach K_{0p}, the value of K_0 has to decrease and therefore K_0 must have increased during secondary compression.
The argumentation above shows a second proof of an increase in K_0 which can still be observed even if no increase of σ'_h is observed.

More recent experiments are included in the work performed by Grimstad et al. (2021). In their paper the results from two Norwegian master theses are analysed namely the ones from Sletten (2015) and Gjengstø (2016). Both performed split-ring oedometer tests on Tiller clay of which the results are shown below (figure 20).

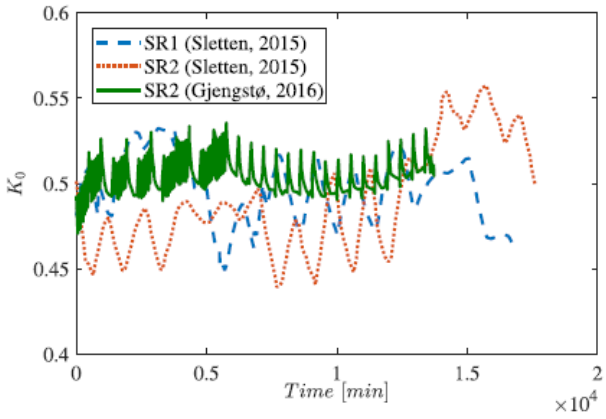

Figure 20: K_0 evolution over time (Grimstad et al., 2021).

The time scale in figure 20 is roughly 2 weeks and no clear trend can be seen. The large variations in the measurements is assigned to variations in temperature to which the sensors in the oedometer are very sensitive (Gjengstø, 2016). Grimstad et al. (2021) argued that next to this problem there is an overarching problem with the measurements being that the timescale in the lab is a few weeks whereas the timescale in situ is thousands of years. However, Lindgård and Ofstad (2017) performed in situ tests on the same clay using earth pressure cells. Several problems were encountered during testing of which the most important ones are breaking of the cells and disturbance of the soil due to cell installation. This caused results with a huge amount of scatter. At the same depth of 5m, values for K_0 were reported in the range of 0.61-1.0. The conclusion which can be made though is that for all tests an in situ value of K_0 was higher than the values found in the lab (around 0.5) suggesting an increase of K_0 when the soil is left alone for an extended period of time.

All of the tests above have been performed on clays. However, data on other soils is available as well. Krieg and Goldscheider (1993) performed oedometer tests on peat specimens. Their findings showed that on the short term the development of K_0 differed between specimens which was most likely caused by the stress history of each sample. The long term behaviour showed that for all samples there was a linear increase of K_0 with time during the measurement period.

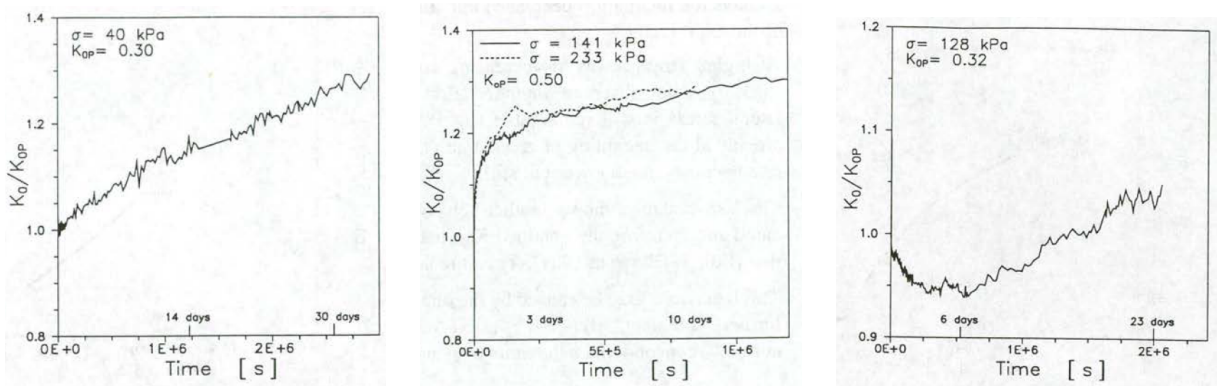

Figure 21: K_0 evolution over time, low stress level (left), high stress levels (middle), overconsolidated sample (right) (Krieg & Goldscheider, 1993).

The final research worth elaborating is the one performed by Wijeyesekera and Mohamed (2000). They tested kaolonites with different bentonite contents in a multi-purpose consolidometer which was able to measure horizontal and vertical total stresses as well as the pore water pressure. The results from their tests are shown in figure 22. The number after KB indicates the mass percentage of bentonite in the sample.

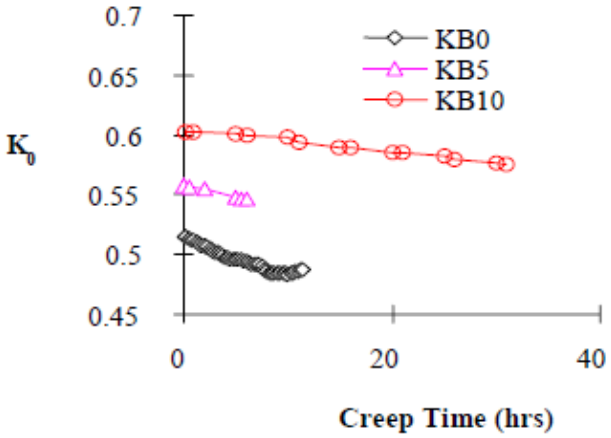

Figure 22: K_0 evolution over time (Wijeyesekera & Mohamed, 2000).

As can be seen the value of K_0 decreases for all samples. The reason for this was the reorientation of clay packets as a result of remaining excess pore water pressure. The authors claimed that after this decrease the value of K_0 would remain constant. Grimstad et al. (2021) argued however that these tests to not give conclusive results. The duration of the test is too short (1 to 2 days) and when looking at a test performed by Wijeyesekera and Mohamed (2000) for a longer period of time an increase in K_0 can be seen after the initial decrease (figure 23).

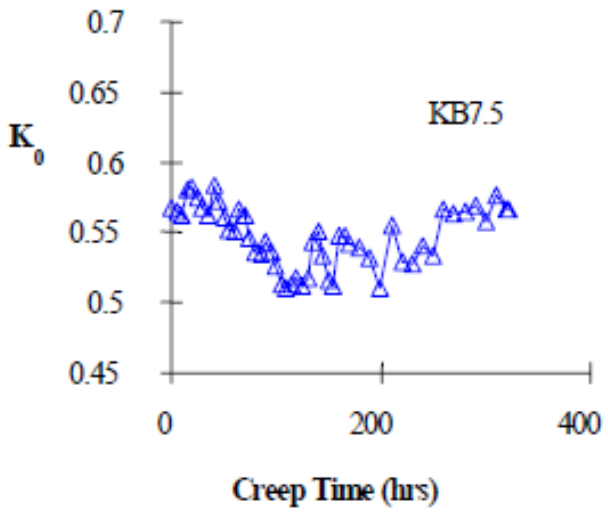

Figure 23: K_0 evolution over time (Wijeyesekera & Mohamed, 2000).

Grimstad et al. (2021) interpreted these results by saying an initial decrease does not rule out a long term increase. Cementation (thixotropy) effects could explain the initial decrease, an argument in favour of this is that 'the higher the bentonite content the greater the decrease in K_0 observed during this first period.' (Grimstad et al., 2021). This finding cannot be directly derived from figure 22 but if the data were to be extrapolated this could very well be true.

2.2.3 Perzyna's approach

As has been stated before, creep behaviour of a soil is retarded or viscous. In other words, the behaviour of a soil is dependent on time. In order to model this behaviour, viscosity needs to be implemented in the model. This is done using Perzyna's approach which is explained here.

It is widely accepted that total strains can be split into an elastic, reversible part and a plastic, irreversible part. The long term, viscous strains mentioned above are irreversible and therefore should be included in the plastic strain component. One of the most popular approaches to model the plastic strain rate is developed by Peryzna (1963).

In this approach the plastic strain rate is determined as follows (Lazari et al., 2019).

$$\dot{\varepsilon}^{vp} = \mu \Phi(f) \frac{\partial g}{\partial \sigma'} \tag{7}$$

where: μ Fluidity parameter (= 1/viscosity)
Φ Viscous nucleus (Lazari et al., 2019) or overstress function (Heeres et al., 2002)
f, g Yield function and plastic potential

The idea behind this approach is that it is possible for the rate-independent yield function (f) to become larger than 0, so-called overstress. If this is the case, a stress point is outside of the yield function and plastic, viscous strains occur (Heeres et al., 2002). The amount of plastic strains (or the magnitude of the plastic strain rate) is defined by the distance of this point to the yield surface. The direction of plastic strain is governed by the stress derivative of the plastic potential. The parameter μ controls the rate of plastic strain and is simply a scalar (Lazari et al., 2019). A visual interpretation of this approach is given below (Liingaard et al., 2004).

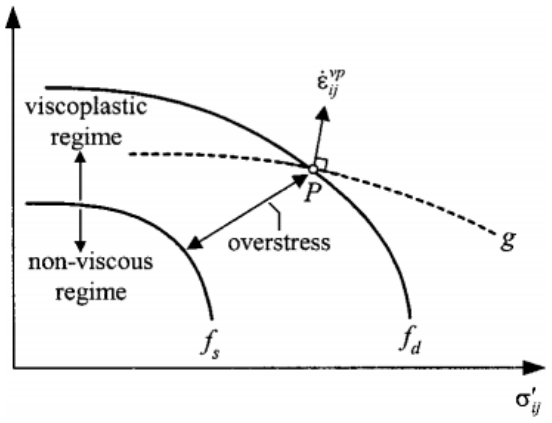

Figure 24: Visualisation of overstress principle (Liingaard et al., 2004).

Lazari et al. (2019) give two definitions for the viscous nucleus function, the first one being the most common and the second one being useful for loose sands specifically.

$$\Phi(f) = \langle (\frac{f}{|p'|})^{\alpha} \rangle = \langle \overline{f}^{\alpha} \rangle \tag{8a}$$

$$\Phi(f) = \exp \alpha \overline{f} \tag{8b}$$

where $\langle\rangle$ are the Macauley brackets meaning that if the value between these brackets is smaller than 0, the value of the expression is set to 0. This is required to make sure that viscoplastic strains only occur if the value of the yield function is larger than zero. α is a viscous parameter defining the shape of $\Phi(f)$ (Lazari et al., 2019). Note that in equation (8) the yield function is made dimensionless by dividing the yield function by the absolute value of the mean effective stress (p').

2.3 Unsaturated conditions

In this section, the influence of unsaturated conditions on the soil stress state is elaborated upon. First, two simple stress approaches are mentioned to introduce the principle. Then, the suction stress approach is explained to discuss the interactions taking place in the soil. After that, experimental data from the literature on the K_0 value is discussed using the explained approaches. The chapter ends with an explanation of the average soil skeleton stress principle which is the approach that will be included to model the influence of unsaturated conditions.

2.3.1 Simple stress approaches

Lu and Likos (2006) mention four approaches to describe the effect of unsaturated conditions on the stress state.

1. Bishop's effective stress approach attributed to Bishop (1959).
2. Independent stress state variable approached credited to Fredlund and Morgenstern (1977).
3. Modified stress variable approaches developed by various researchers
4. The suction stress approach found in for example Lu and Likos (2006)

The first two will be touched upon in this subchapter, the suction stress approach will be explained in the next one. The modified stress variable approaches are not treated here because of their different conceptual levels.

Bishop's effective stress approach uses a modified form of the classical Terzaghi effective stress formulation to include the effect of unsaturated conditions. The formulation is given below.

$$\sigma' = \sigma - u_a + \chi(u_a - u_w) \tag{9}$$

where:
- σ' Effective stress
- σ Total stress
- u_a Air pressure
- u_w Pore water pressure
- χ Effective stress parameter

The effective stress parameter χ is a function of saturation. It varies between 0 and 1 and accounts for the influence of matric suction $(u_a - u_w)$ on the effective stress (Lu & Likos, 2006).
Abrantes and de Campos (2019) stated that the effective stress parameter can be calculated as follows.

$$\begin{cases} \chi = 1 & \text{for s} < s_e \\ \chi = (\frac{s}{s_e})^r & \text{for s} \geq s_e \end{cases} \tag{10}$$

where:
- s Matric suction $(u_a - u_w)$
- s_e Suction at the air entry point
- r Material parameter

The Bishop's effective stress approach is well known in the literature and used often. Lu and Likos (2006) mention however that both theoretical and experimental problems with a proper determination of χ limit the applicability of the method.

The independent stress state variable approach credited to Fredlund and Morgenstern (1977) is explained in Fredlund and Rahardjo (1993). They looked at the equilibrium conditions for an unsaturated soil containing the forces for the air phase, the water phase and contractile skin combined with the total equilibrium equation for a soil element. Using this equilibrium, three independent sets of normal stresses could be extracted being

$(\sigma - u_a)$, $(u_a - u_w)$ and u_a. $(\sigma - u_a)$ is called the net stress, $(u_a - u_w)$ the matric suction and u_a is the air pressure which is used as a reference pressure in this case. Assuming the pore water and the soil particles are incompressible u_a can be eliminated leaving $(\sigma - u_a)$ and $(u_a - u_w)$ as the stress variables for an unsaturated soil (Fredlund & Rahardjo, 1993). The stress variables are shown below (figure 25).

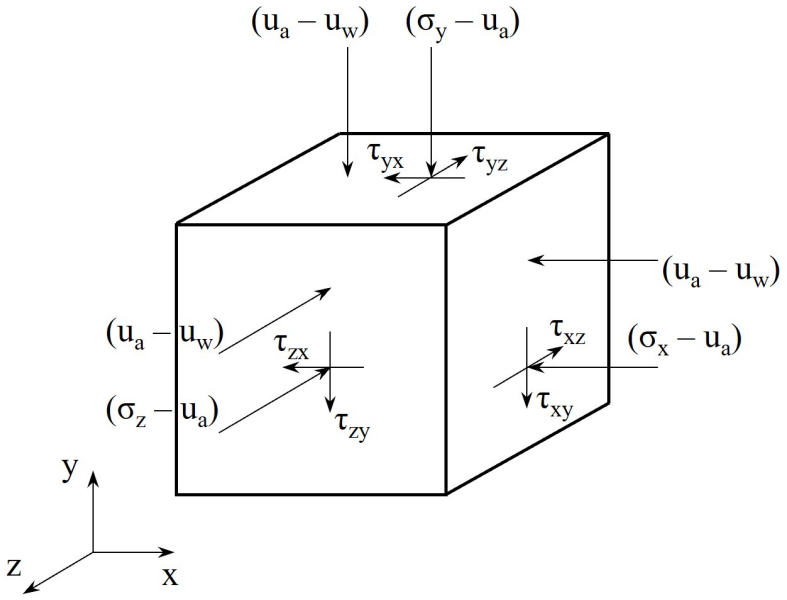

Figure 25: The stress variables for an unsaturated soil element. Redrawn from Fredlund and Rahardjo (1993).

As stated above, the equilibrium equation formed by Fredlund and Rahardjo (1993) uses the air pressure as a reference pressure. The equilibrium equation can also be formed by using either the σ or u_w as a reference pressure resulting in different stress state variables. However, using the air pressure is best option for engineering practice since it separates the effects of a change in normal stress and pore water pressure. Also, for most engineering problems the air pressure is atmospheric meaning it can be set to zero (Fredlund & Rahardjo, 1993).
Lu and Likos (2006) explained that usage of the independent stress approach requires extra variables when for example calculating failure criteria. Experimental difficulties occur in determining these parameters and it is also not certain how valid these parameters are at different saturation levels. An example of such a material parameter is the additional friction angle ϕ^b included in the Mohr-Coulomb failure criterion when using independent stress variables shown below. These problems have limited the applicability of the method.

$$\tau_f = c' + (\sigma - u_a)tan\phi' + (u_a - u_w)tan\phi^b \tag{11}$$

2.3.2 Suction stress approach

The final concept which will be explained uses a variable called the suction stress. The idea behind the concept is that the effect of desaturation on a soil element needs to be explicitly defined. The reason why this approach is explicitly mentioned is not because it will be used in this project but because it gives a clear insight of what is happening in a soil element when the element is unsaturated.
In a soil element, three types of forces can be distinguished. The first type are active 'skeletal' forces propagating through the soil grains, the second type are active local forces at the interparticle contacts and the final type is the passive interparticle contact force counterbalancing the first two types.
In saturated soils it is sufficient to model only type 1 and 3 forces since the system can be seen as an equivalent continuum medium. Because of this all forces travel through the system and therefore the system can be described using macroscopic stresses defined at the boundaries. This is done for example in Terzaghi's effective stress principle. Under unsaturated conditions, however, the soil-water system can no longer be seen

as a continuum and the effect of the pore pressure can no longer be modelled as a macroscopic stress. Instead, the pore pressure disintegrates into several microscopic forces acting at the grain level (Lu & Likos, 2006). The researchers proposed that it would be possible to gather the second type of force under a new macroscopic stress variable called the suction stress. This suction stress accounts for van der Waals forces, cementation forces and capillary forces, among others.
Physically, the forces included in the concept of suction stress depend on the physical and chemical properties of the soil-water system and are therefore referred to as physicochemical forces (F_{pc}). These forces are not propagating through the soil skeleton and are therefore not included in a macroscopic stress approach like Terzaghi's effective stress principle. Methods used in practice do attempt to capture the effect of these forces. An example of this is the effective cohesion in the Mohr-Coulomb failure criterion (equation (11)) (Lu & Likos, 2006).

The basis for the derivation of the suction stress is shown in figure 26 which shows a Representative Elementary Volume (REV) with all contributing forces.

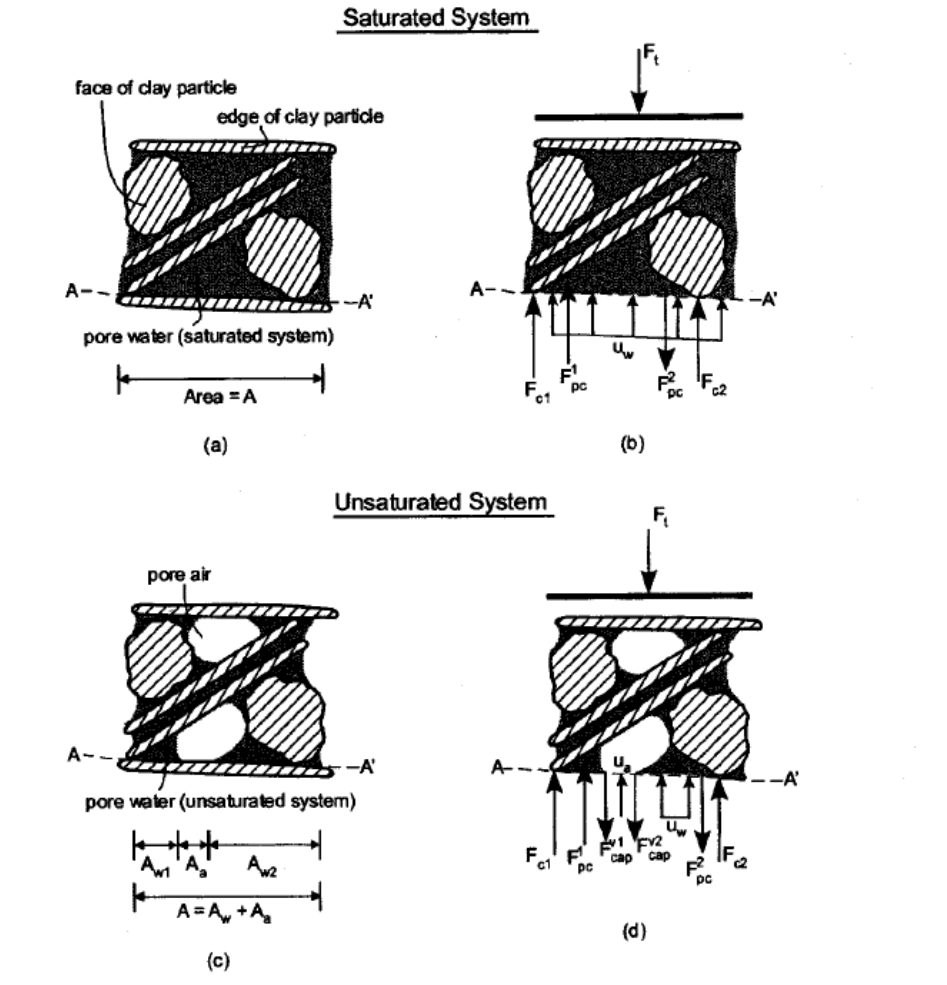

Figure 26: REV with contributing forces, saturated above and unsaturated below (Lu & Likos, 2006).

Using the REV for unsaturated soils (figure 26d) and dividing all forces by their respective areas the following equation can be determined.

$$\sigma' = \sigma_t - u_a + \sigma_{pc} + \sigma_{cap} + \chi(u_a - u_w) \tag{12}$$

Note that σ_t represents an external force and the subscript t does not indicate tensile. This equation can be rewritten to include suction stress.

$$\sigma' = \sigma_t - u_a + \sigma'_s + \sigma_{c0} \tag{13}$$

In the equation above σ'_s is the suction stress and σ_{c0} is the physicochemical stress at saturated state used as a reference. With this, the suction stress becomes.

$$\sigma'_s = \sigma_{pc} + \sigma_{cap} + \chi(u_a - u_w) - \sigma_{c0} \tag{14}$$

All terms in the equation above depend on the saturation level of the soil so therefore the suction stress can be expressed as a function of saturation. Defining this relationship results in a curve which is called the Suction Stress Characteristic Curve (SSCC). An example of an SSCC is given below (Lu & Likos, 2006).

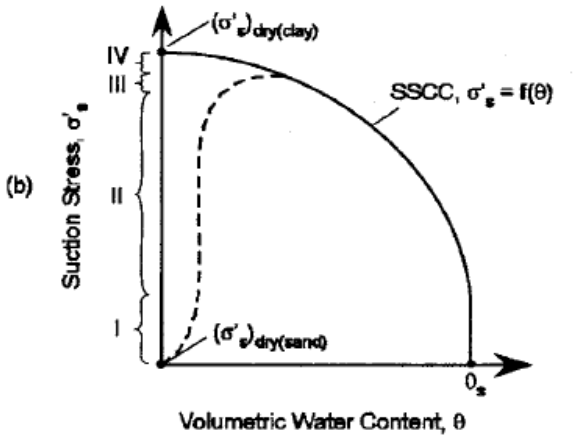

Figure 27: Example of an SSCC for clay and sand (Lu & Likos, 2006).

Using the suction stress principle, Lu et al. (2010) defined the effective stress as follows.

$$\sigma' = (\sigma - u_a) - \sigma_s, \text{ with } \sigma_s = -(u_a - u_w)S_e \tag{15}$$

Where S_e is the effective saturation defined as

$$S_e = \frac{S_r - S_{r,res}}{1 - S_{r,res}} \tag{16}$$

with S_r the regular saturation and $S_{r,res}$ the residual saturation.

S_e can also be calculated as a function of matric suction using for example Van Genuchten's Soil Water Retention Curve (SWRC) model shown below.

$$S_e = \{\frac{1}{1 + [\alpha(u_a - u_w)]^n}\}^{1-1/n} \tag{17}$$

In the equation above, n and α are empirical fitting parameters. α is the inverse of the air entry pressure for a saturated soil and n is a parameter indicating pore size distribution.
Using this equation, the effective stress can be determined as follows.

$$\sigma' = \sigma - u_a + (u_a - u_w) \qquad u_a - u_w \leq 0 \tag{18a}$$

$$\sigma' = \sigma - u_a + \frac{u_a - u_w}{(1 + [\alpha(u_a - u_w)]^n)^{(n-1)/n}} \qquad u_a - u_w \geq 0 \tag{18b}$$

The above equations together with figure 26 serve to give insight in all the processes going in the soil under unsaturated conditions (Lu et al., 2010).

2.3.3 Experimental data on K_0 changes under unsaturated conditions

In this section, the behaviour of K_0 under varying levels of saturation is elaborated. Work from researchers is presented who use the different approaches explained above.

The first tests on unsaturated clay samples are performed by Zhang et al. (2009). Triaxial K_0 consolidation tests were performed on 16 samples of expansive clay with different saturation levels. During the tests axial and radial stresses were monitored as well as the pore water pressure. The radial stress was increased at a rate of 10 kPa/h up to a predetermined maximum. During this loading, the axial stress was increased accordingly to keep no radial deformation. After reaching the desired radial stress, it was kept constant and the specimens were consolidated until the axial deformation reached less than 0.01 mm per hour. The axial stress vs radial stress graph for the four samples with a maximum radial stress of 50 kPa is shown below.

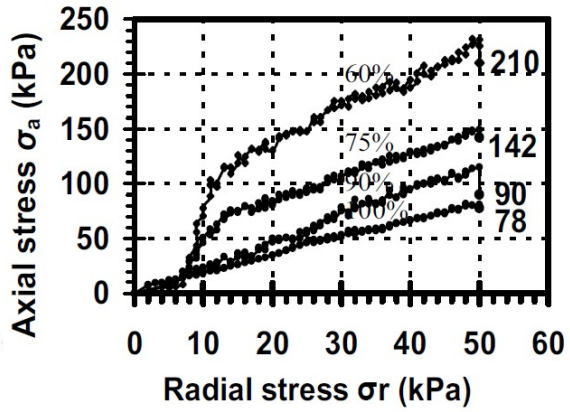

Figure 28: Variation of axial stress with radial stress under different degrees of saturation (Zhang et al., 2009).

It can be seen that for a high degree of saturation the relationship is linear whereas for a low degree of saturation the relationship is nonlinear initially. The reason for this is that at low degrees of saturation the soil structure is able to resist the axial stress better initially. After a certain point the soil structure collapses and the relationship becomes linear. Another point worth mentioning is that the axial stress decreases towards an ultimate stress when the radial stress remains constant. Using the measured stresses, the researchers calculated the effective stresses using Bishop's effective stress principle (equation (9)) and K_0 accordingly. Their results are shown below.

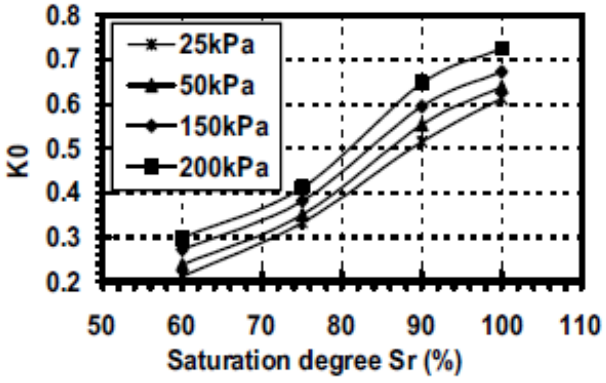

Figure 29: Variation of K_0 with degree of saturation (Zhang et al., 2009).

It can clearly be seen that the data shows that K_0 increases with degree of saturation. The variation in K_0 can be as high as a factor 3 over an increase in degree of saturation with 40%.

Oh et al. (2013) performed tests on fourteen samples, 10 clayey sand and 4 silty sand, in a suction controlled triaxial setup. Different matric suctions were applied on the samples. During loading, radial strains were prohibited meaning a K_0 consolidation path was followed. Their findings showed that when the matric suction was increased, a lower horizontal stress was found at the same vertical stress. This directly means that K_0 decreases with an increase in matric suction.

The obtained results were collected and plotted in one figure with K_0 on the vertical axis (both using effective- and total stresses) and matric suction on the horizontal axis (figure 30). It can be seen that there is a decrease in K_0 with an increase in matric suction for the clayey sand when total stresses are considered. The effective stresses were calculated using the suction stress approach from section 2.3.2 and it can be seen that K_0 calculated using the effective stresses is constant no matter the applied suction. This suggests that the suction stress approach yields a unique value for K_0.

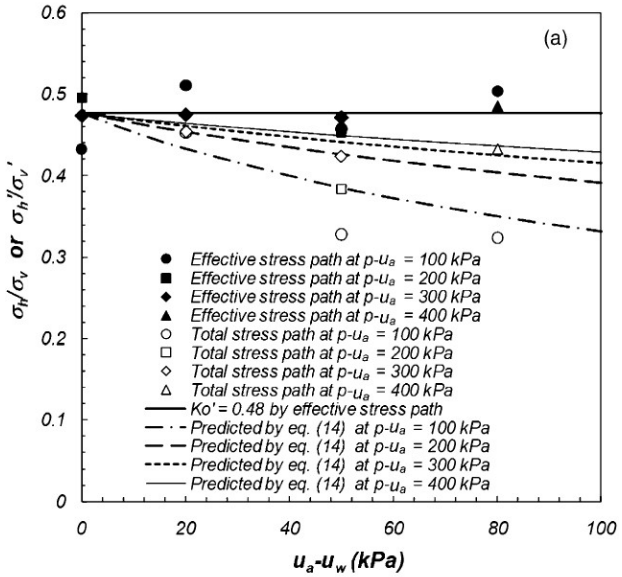

Figure 30: Variation of K_0 with matric suction for a clayey sand (Oh et al., 2013).

Pirjalili et al. (2020) used a new device to evaluate K_0 in a suction-controlled system. Using this device, Firouzkouh clay and a Sand-Kaolin mixture were tested at different void ratios and matric suction levels. The effective stresses were calculated using Bishop's effective stress approach and the corresponding K_0 value with it. The findings show a decrease of K_0 with increasing matric suction.

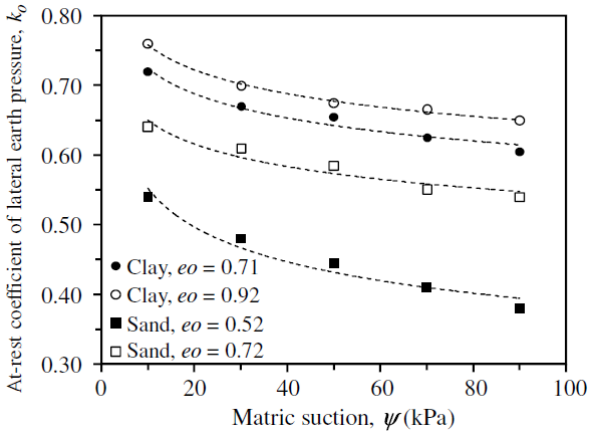

Figure 31: Variation of K_0 with matric suction (Pirjalili et al., 2020).

Tests on saturated and unsaturated samples on the same soil were performed by Abrantes and de Campos (2019). Different triaxial chambers were used for the saturated and the unsaturated tests. The soil which was tested was a high plasticity clay. The results of the tests show a constant value of K_0 of 0.36 under saturated conditions. For unsaturated conditions the results are shown in figure 32

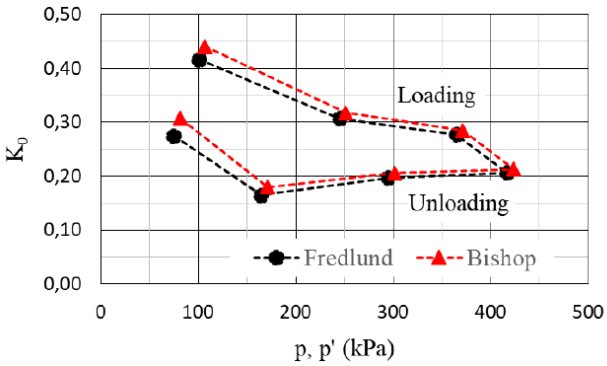

Figure 32: K_0 under loading and unloading calculated using both Bishop's and Fredlund's approaches, matric suction = 10 kPa (Abrantes & de Campos, 2019).

It can be seen that there is a change in K_0 value under different loading conditions. In general however, the value of K_0 in the unsaturated conditions is lower than the value of 0.36 found for the saturated sample. A point worth noting is that the difference in prediction by Bishop's (equation (9)) and Fredlund's approach is small.

de Campos et al. (2021) tested residual gneiss samples using a triaxial chamber similar to the one used by Abrantes and de Campos (2019). Their findings showed that K_0 decreased with suction no matter if it was expressed using total stresses (Fredlund's approach) or effective stresses (Bishop's approach). The results are shown in figure 33.

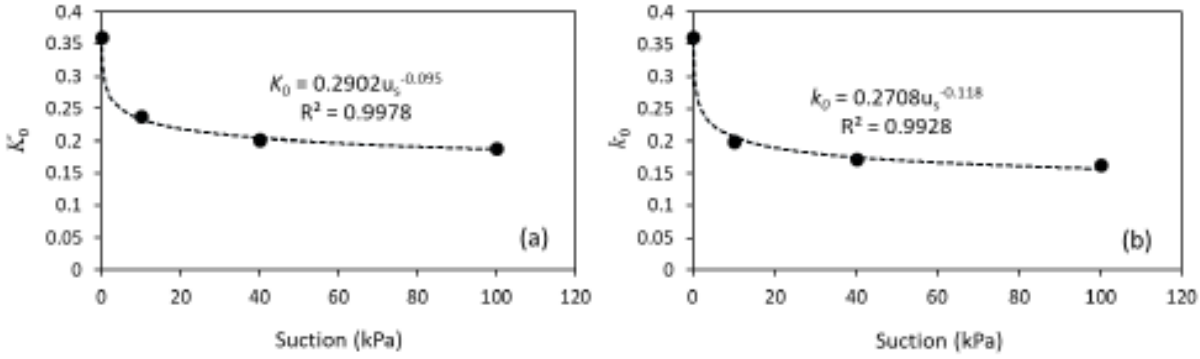

Figure 33: Variation of K_0 under suction, defined in effective stresses (a) and total stresses (b) (de Campos et al., 2021).

2.3.4 Unsaturated constitutive modelling

The conceptual approach presented by Jommi (2000) will be adopted in the following.

Bishop's formulation (equation (9)) can be rewritten in tensor formulation as shown below.

$$\sigma'_{hk} = \sigma_{hk} - u_a\delta_{hk} + \chi(u_a - u_w)\delta_{hk} \tag{19}$$

Where δ_{hk} is the Kronecker delta. A general constitutive law in incremental form, relating the rate of change in stresses to the rate of change in stress through a constitutive matrix.

$$\dot{\varepsilon}_{ij} = C^{ep}_{ijhk}\dot{\sigma}'_{hk} \tag{20}$$

On the contrary, models using two stress variables usually use the elastoplastic matrix linked to the net stress and define an explicit dependence on the suction level giving the following expression.

$$\dot{\varepsilon}_{ij} = C^{ep}_{ijhk}(\dot{\sigma}'_{hk} - \dot{u}_a\delta_{hk}) + C^{s}_{ijhk}(\dot{u}_a - \dot{u}_w)\delta_{hk} \tag{21}$$

As can be seen, an extra constitutive matrix (C^s_{ijhk}) is used to model the suction influence on the strain rates. To avoid doing this, a single stress approach can be used which adopts a stress variable called the average soil skeleton stress. It is defined as the difference between the total stress and the weighted average of the air and pore water pressure. The saturation degree is used as the weighing factor.

$$\hat{\sigma}_{hk} = \sigma_{hk} - [S_r u_w + (1 - S_r)u_a]\delta_{hk} \tag{22}$$

This definition can directly be substituted in equation (20) without the need for an extra constitutive tensor. By rewriting equation (22) it can be shown that an increase in matric suction can be considered as an increment to the isotropic stress. Experimental data show that when starting from saturated conditions, applying a suction increases the shear and volumetric stiffness which can be modelled as an increment to the isotropic stress. This part of the soil behaviour is therefore modelled correctly by using the average soil skeleton stress as a single stress variable (Jommi, 2000).

Using equation (22), an increase in suction would lead to a decrease of the preconsolidation stress. However, for unsaturated soils, it has been observed that an increase of suction leads to a increase in the apparent preconsolidation stress. This behaviour is not modelled by only using the average soil skeleton stress.
Another aspect of unsaturated soils is that under wetting the soil experiences swelling and/or collapse depending on the net stress level which is something not modelled either by the average soil skeleton stress. This second point is backed up by available experimental evidence in which triaxial tests were performed on sands. In these tests, a conventional compression path was followed after which the isotropic stress was reduced while keeping the deviatoric stress constant. By reducing the isotropic stress, an increase in the void ratio would intuitively be expected. At higher stress levels though, the soil samples underwent compaction. This can be interpreted as a structural collapse of the soil skeleton (Jommi, 2000).

Neither of the two points above are able to be modelled by using a single stress variable approach like the average soil skeleton stress. However, Jommi (2000) states that both the increase in apparent preconsolidation pressure and the collapse upon wetting of the soil cannot be interpreted as being caused solely by an increase or decrease of the mean pressure on the soil. Both effects are more similar to bonding and debonding when looking at it from a macroscopic point of view. This bonding and debonding can be seen as the macroscopic equivalent of the interactions between the air-water interface and the soil skeleton.

In order to reproduce both the increase in the preconsolidation pressure and the collapsing behaviour observed upon wetting, Jommi (2000) suggests to modify the hardening rule for the preconsolidation pressure. Merely substituting the average soil skeleton stress would give:

$$\hat{p}_0 = (p^*_0 - S_r s) \tag{23}$$

where $\hat{p}_0$ and p_0^* are the mean preconsolidation pressures under unsaturated and saturated conditions respectively. Equation (23) shows that increasing the suction in this case would result in a decrease in the mean preconsolidation pressure. Because of this an adaptation to the equation is required.

$$\hat{p}_0 = (p_0^* - S_r s) + h(S_r) \tag{24}$$

The term $h(S_r)$ is a (positive) function of the degree of saturation. In order to evaluate $h(S_r)$ at a given suction level, a relationship between suction and degree of saturation is required. This relation is found in the Soil Water Retention Curve (SWRC). Using both $h(S_r)$ and a proper SWRC, an accurate description of the increase in preconsolidation pressure can be obtained. Since the suction and the degree of saturation are related trough the SWRC, it is also possible to define h as a function of suction. However, defining h as a function of the degree of saturation has the advantage that the function can be defined in such a way that as the degree of saturation approaches one, the unsaturated mean preconsolidation pressure becomes equal to the saturated one. An example of an implementation of h as a function of the degree of saturation will be given in section 5.1.

Another advantage of adopting this approach is that effects of void ratio and drying/wetting can be included in the SWRC. At the same suction value, a different degree of saturation can be found based on whether this suction was obtained by drying or wetting of the soil. This phenomenon where, depending on whether the soil experiences drying or wetting, different degrees of saturation are found at the same suction is known as hysteresis.

3 Methodology

In this section, the methodology used to answer the research questions will be explained. The basis of the project is a saturated elastoplastic model based on the SANICLAY (Simple ANIsotropic CLAY) model as found in Dafalias et al. (2006). In order to be able to answer the research questions, this model needs to be extended so that it is able to account for creep and the influence of unsaturated conditions. As is described in the literature study above, creep will be accounted for by introducing viscosity in the model through Perzyna's approach. The influence of unsaturated conditions will be accounted for by adopting the average soil skeleton approach given by Jommi (2000). The final goal is to have an unsaturated elasto viscoplastic soil model to be able to assess the development of K_0 over time at different suction levels and see if the observed behaviour is in line with what was found in the literature. The remainder of this chapter first explains the starting point of the model after which the extensions of this model following in the next chapters will be touched on shortly.

3.1 Elastoplastic model

As described above, the starting point of the model is based on the SANICLAY model (Dafalias et al., 2006). In this thesis, the yield surface and plastic potential from Dafalias et al. (2006) are adopted but altered slightly. McDowell and Hau (2004) suggest an extra degree of freedom for the Modified Cam Clay model to help control the shape of the yield surface and plastic potential, this same change is adopted here. Both are given in the equations below and the adaptation (the extra degree of freedom) is found in k_f and k_g respectively.

$$f = (-p\beta + q)^2 + \frac{(N^2 - \beta^2)p^2}{(k_f - 1)} - \frac{(N^2 - \beta^2)(\frac{p}{p_c})^{\frac{2}{k_f}} p_c^2}{(k_f - 1)} = 0 \tag{25}$$

$$g = (-p\alpha + q)^2 + \frac{(M_g^2 - \alpha^2)p^2}{(k_g - 1)} - \frac{(M_g^2 - \alpha^2)(\frac{p}{p_{c,g}})^{\frac{2}{k_g}} p_{c,g}^2}{(k_g - 1)} = 0 \tag{26}$$

where:	p	Mean effective stress
	α, β	Non-dimensional anisotropic variables accounting for the coupling of deviatoric and volumetric plastic strain rates
	q	Deviatoric stress
	M_g	Critical stress ratio
	N	Shape of the yield surface
	k_f, k_g	Shape controlling parameters of yield surface and plastic potential respectively
	p_c, $p_{c,g}$	Initial size of yield surface and plastic potential

The critical stress ratio (M_g) is equal to M_c if the stress ratio η (q/p) is bigger than α and equal to M_e if it is smaller. M_c and M_e are the slopes of the critical state lines in p-q space in compression and extension respectively. Regarding k_g, the value of this parameter is always kept equal to 2.0 in this work.
The equations above contain 3 internal variables (p_c, α and β), the change of each of these variables is governed by their respective hardening laws. For the sake of simplicity, the hardening law for α is assumed to be equal to β as suggested by Dafalias and Taiebat (2013).

$$\dot{p}_c = \langle L \rangle \bar{p}_c = \langle L \rangle \left(\frac{1+e}{\lambda - \kappa} \right) p_c \left(\frac{\partial g}{\partial p} \right) \tag{27}$$

$$\dot{\beta} = \langle L \rangle \bar{\beta} = \langle L \rangle \left(\frac{1+e}{\lambda - \kappa} \right) C \left(\frac{p}{p_c} \right)^2 |\frac{\partial g}{\partial p}| |\eta - x\beta| (\beta^p - \beta) \tag{28}$$

where:	e	Void ratio
	λ, κ	Slopes of normal compression and rebound curves respectively
	η	Stress ratio (q/p)
	x	Saturation limit of anisotropy
	C	Rate of evolution of anisotropy

Note that if $\eta/x > \beta$, then $\beta^p = M_c$ and if $\eta/x < \beta$, then $\beta^p = -M_e$. Also note that $\langle\rangle$ denote the Macauley brackets making sure that when L is bigger than 0, $\langle L\rangle$ = L and when L is smaller than 0, $\langle L\rangle = 0$.
The equations above are formulated in triaxial stress space for the sake of simplicity. In the existing elastoplastic code (which will be touched on in the next paragraph), the equations are included in multiaxial stress space. For the extension of the equations to multiaxial stress space, refer to chapter 3 of Dafalias et al. (2006).

The plastic strain rate is given by the flow rule and is already present in the two equations above. The term $\langle L\rangle * \frac{\partial g}{\partial p}$ is the flow rule for the volumetric plastic strain rate ($\dot{\varepsilon}_v^p$).

The plastic multiplier L is defined as follows.

$$L = \frac{1}{K_p}\left(\frac{\partial f}{\partial p}\dot{p} + \frac{\partial f}{\partial q}\dot{q}\right) \tag{29}$$

with,

$$K_p = -\left(\frac{\partial f}{\partial p_c}\bar{p}_c + \frac{\partial f}{\partial \beta}\bar{\beta}\right) \tag{30}$$

where $\bar{p}_c$ and $\bar{\beta}$ are calculated from equation (27) and equation (28) respectively.

3.2 Model extensions

The elastoplastic model based on SANICLAY is already available in a mechanical driver capable of modelling the soil behaviour assuming saturated conditions. This code will be extended step by step to eventually reach an unsaturated elasto viscoplastic model. The next two chapters will focus on the steps being taken to develop this model. The first step is adapting the model to make it elasto viscoplastic which will be explained in detail in the next chapter. After that, the elastoplastic model is taken again and this time the influence of unsaturated conditions is included. This development is described in chapter 5. After both adaptations are done separately, a combined model version is constructed which is the final unsaturated elasto viscoplastic model. This final model version is also included in chapter 5.

Both chapters 4 and 5 will have a similar outline. First, the changes in the model formulation will be touched on. After this, experimental data that is taken from the literature is elaborated upon. Both chapters will then touch on the determination of the model parameters which is followed by the model validation in which the model output is compared to the earlier mentioned experimental data. Each chapter will end with a short conclusion on the respective model version. Which model version is described in which chapter is highlighted in figure 34 below.

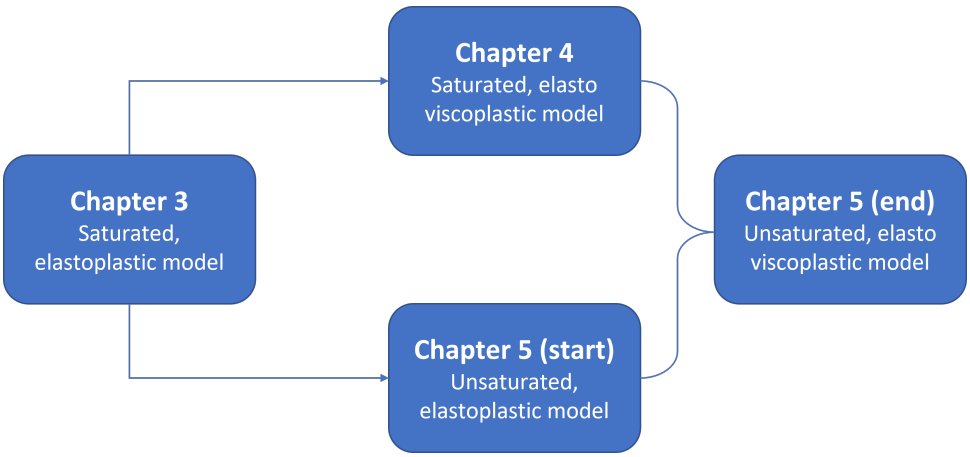

Figure 34: Flowchart of Methodology spread over chapters 3 to 5.

4 Elasto Viscoplastic model

This chapter will go in detail on the implementation of time dependency in order to model creep using Perzyna's approach as described in section 2.2.3. This implementation is broken down in steps starting with the required model changes. After this, the experimental data obtained from the literature is explained in two steps. First, the material which is used to validate the model is elaborated upon after which the tests performed on this material are explained. Following this is the parameter calibration performed to match the model parameters to the material and testing program. Then, the model validation itself is performed in which numerical output from the elasto viscoplastic model is compared to the gathered experimental data. The chapter ends with conclusions that can be drawn based on the model validation.

4.1 Model formulation

To implement Perzyna's overstress approach in the model, two changes are required to the elastoplastic model described in section 3.1. The first change is in the calculation of the plastic strains which is now done using Perzyna's approach instead of using a plastic multiplier. The second change is that in the hardening laws the new viscoplastic volumetric strain needs to be included. The choice for the viscous nucleus is also explained. Both changes will be explained in detail below.

As stated above, in the elastoplastic model variant from the previous section, the plastic strains were calculated by using a plastic multiplier and the derivative of the plastic potential. By adopting Perzyna's overstress approach, the plastic strains are now calculated through the equation below. Note that this equation is very similar to equation (7) but that the derivative of the plastic potential has been normalised. This is done to make sure the derivative of the plastic potential only governs the direction of plastic strains and the magnitude is defined by the term $\mu\Phi(f)$.

$$\dot{\varepsilon}^{vp} = \mu\Phi(f)\frac{\frac{\partial g}{\partial \sigma'}}{\frac{\partial g}{\partial \sigma'} \cdot \frac{\partial g}{\partial \sigma'}} \tag{31}$$

where:

	μ	Fluidity parameter (1/s)
	$\Phi(f)$	Viscous nucleus
	$\frac{\partial g}{\partial \sigma'}$	Gradient of plastic potential

The viscous nucleus in this work is adopted from Rezania et al. (2016). They based their viscous nucleus using a Static Yield Surface (SYS) and a Dynamic Loading Surface (DLS) which can be visualised as shown below.

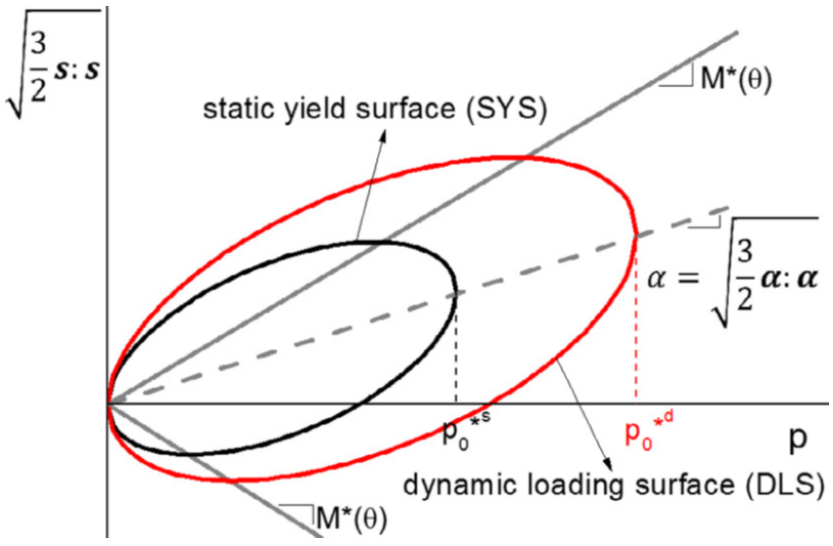

Figure 35: Visualisation of SYS and DLS (Rezania et al., 2016).

The SYS is the current size of the yield surface and does not have to go through the stress point. The DLS is the version of the yield surface which can be seen as an inflated/deflated version of the SYS and always goes through the stress point the soil is currently in. The viscous nucleus makes use of the so-called overstress which is the distance between the DLS and the SYS and can be calculated as follows.

$$\Phi(f) = \langle \exp(N_\phi * (\frac{p_c^d}{p_c^s} - 1)) - 1 \rangle \tag{32}$$

In the equation above, N_ϕ is the strain rate coefficient which needs to be calibrated. p_c^s is the size of the SYS and p_c^d is the size of the DLS. Again, Macauley brackets are used, this time to make sure that no viscoplastic strains occur inside the yield surface. This is the most common approach although some literature suggests creep strains inside the yield surface as well (Cresseri & Jommi, 2005; Liingaard et al., 2004). In this work, creep strains are modelled to only be present if the stress state is outside of the yield surface. The possibility of including creep inside the yield surface as well will be discussed later. In Rezania et al. (2016), $p_{c,g}$ is used for p_c^d which is the size of the plastic potential. This is done because an associated flow rule is used and therefore the plastic potential is equal to the DLS. In this work, a non associated flow rule is used and therefore p_c^d needs to be explicitly used.

Equation (31) only governs the rate of change in the viscoplastic strains. To obtain the increment in viscoplastic strains, a multiplication with a time interval is required. In the model this is obtained by giving each loading step a corresponding timestep by which the viscoplastic strain rate is multiplied with.

In the elastoplastic model, the hardening laws (equations (27) and (28)) both depend on the volumetric strain rate which was calculated by multiplying the plastic multiplier (L) with the derivative of the plastic potential to the mean stress.
In the viscoplastic model, the volumetric strain rate is calculated in a different way. Equation (31) calculates the strain rate for each of the stress components so the volumetric strain rate is simply the strain rates of the principle stresses added together. Noted down as an equation this becomes.

$$\dot{\varepsilon}_v^{vp} = \{1\ 1\ 1\ 0\ 0\ 0\}^T \cdot \dot{\varepsilon}^{vp} \tag{33}$$

To help clarify this change, the new hardening laws are given below.

$$\dot{p}_c = \left(\frac{1+e}{\lambda-\kappa}\right) p_c\ \dot{\varepsilon}_v^{vp} \tag{34}$$

$$\dot{\beta} = \left(\frac{1+e}{\lambda-\kappa}\right) C \left(\frac{p}{p_c}\right)^2 |\dot{\varepsilon}_v^{vp}||\eta - x\beta|(\beta^p - \beta) \tag{35}$$

Again, these equations are noted in rate of change. To get an increment in either of the internal variables, the equations simply need to be multiplied with a time increment.

By changing the way the plastic strains are calculated and updating the hardening laws, the model has been changed from elastoplastic (EP) to elasto viscoplastic (EVP).

4.2 Material description

The data that is being used to validate the EVP model is taken from two theses, namely the ones from Polinder (2019) and Wegman (2020). Both of these theses contain tests on the well known OostVaardersPlassen (OVP) clay.

The reason why both theses used OVP clay as their soil is because it is assumed to be representative for Dutch organic soils. Their samples were prepared as follows. A 100 kg sample was taken in April 2017 and was first mixed in a vacuum mixer to remove air bubbles. After this, de-aired water was added and the sample was mixed for 10 hours. Then, the samples were consolidated to bring down their water content. This was done using K_0-consolidation at a pressure of 40 kPa, this process took 172 days (Wegman, 2020). The following characteristics can be assigned to the soil.

Table 1: OVP Clay characteristics (Polinder, 2019).

Property	Unit	Value
Unit weight	[kN/m^3]	14.0
Specific gravity	[-]	2.53
Mass content clay	[%]	26
Mass content silt	[%]	71
Mass content sand	[%]	3
Organic content	[%]	9.5
Liquid limit	[%]	120
Plastic limit	[%]	37

4.3 Test description

This section describes the tests that are performed on the OVP clay and whose results will be used in the validation of the EVP model. From these tests, three will be used briefly in the parameter determination in the next section. These three tests are the stress path in p'-q space and the void ratio vs log(p') plots from Wegman (2020) and a 10 day ageing deformation test by Polinder (2019). These tests will be explained in detail below. In the parameter determination these tests will only be used briefly to get a first visualisation of the model performance. Because of this, all the test results that are presented below will be used in the model validation which is the penultimate section of this chapter.

4.3.1 Wegman (2020) tests

Wegman (2020) performed triaxial tests on OVP clay samples. Their goal was to test samples at different OverConsolidation Ratios (OCRs). In the EVP model validation, three samples will be used. One is Normally Consolidated (NC), one is Slightly OverConsolidated (SOC) and one is Highly OverConsolidated (HOC). In the following, the testing procedure is explained and the experimental results from Wegman (2020) are presented.

The first step in the test program is to consolidate the samples. For all samples the same procedure was followed. Initially, the samples are isotropically consolidated until about 20 kPa (this is below the preconsolidation pressure). After this, the deviatoric stress is increased until the K_0 line is reached. This results in a stress path in p'-q space with a slope of 3:1. Upon reaching the K_0 line, a stress path is followed at constant stress ratio (η) to make sure the sample stays on the K_0 line. This is continued until the desired preconsolidation pressure is reached. For the overconsolidated samples, an unloading path is applied as well. During unloading, the vertical stress is reduced to obtain the desired OCR. After completion of the consolidation, the samples are ready for the shearing process to start. Shearing is performed undrained at a rate of 1% strain/hr. Wegman (2020) presents their data in several graphs showing separately the consolidation, unloading and shearing paths for several samples. Shown below are the complete experimental stress paths for the relevant sample. These are obtained by extracting the experimental data from the figures by Wegman (2020) and are presented in this way for the sake of clarity.

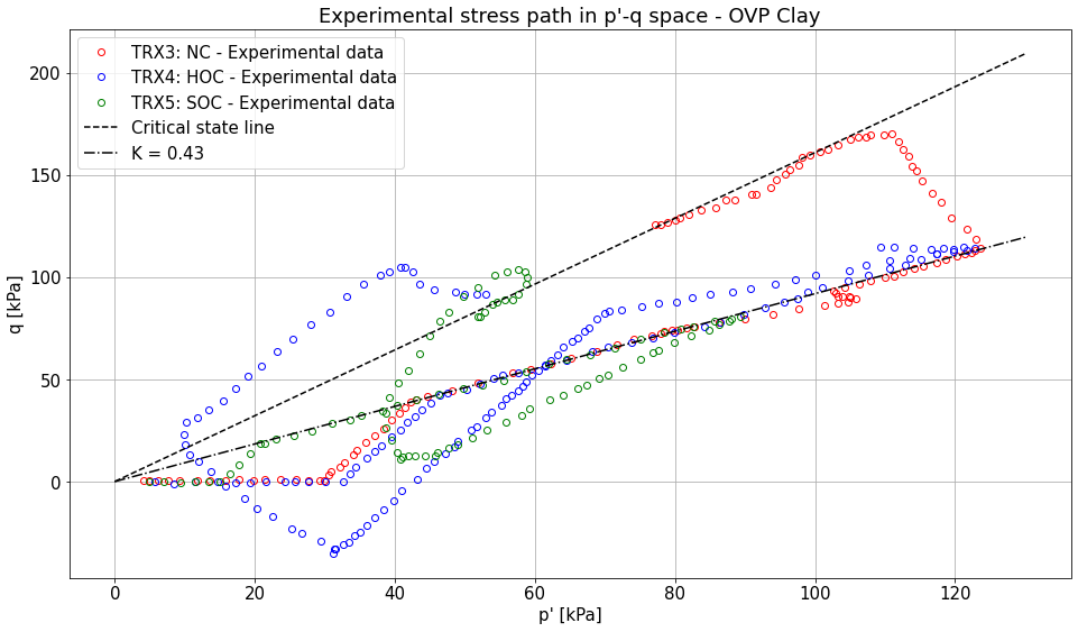

Figure 36: Stress path in p'-q space, TRX_3 is the Normally Consolidated (NC) sample, TRX_4 the Highly OverConsolidated (HOC) one and TRX_5 the Slightly OverConsolidated (SOC) one - Data taken from Wegman (2020).

As is shown in the figure caption, the used tests are TRX_3, 4 and 5 which are normally consolidated, highly overconsolidated and slightly overconsolidated respectively.

Wegman (2020) presents additional results next to the stress paths shown above. Two of these results are the deviatoric stress and excess pore pressure during shearing vs the axial strain. These graphs are presented below. Note that the axial strain at the start of shearing is taken as 0%.

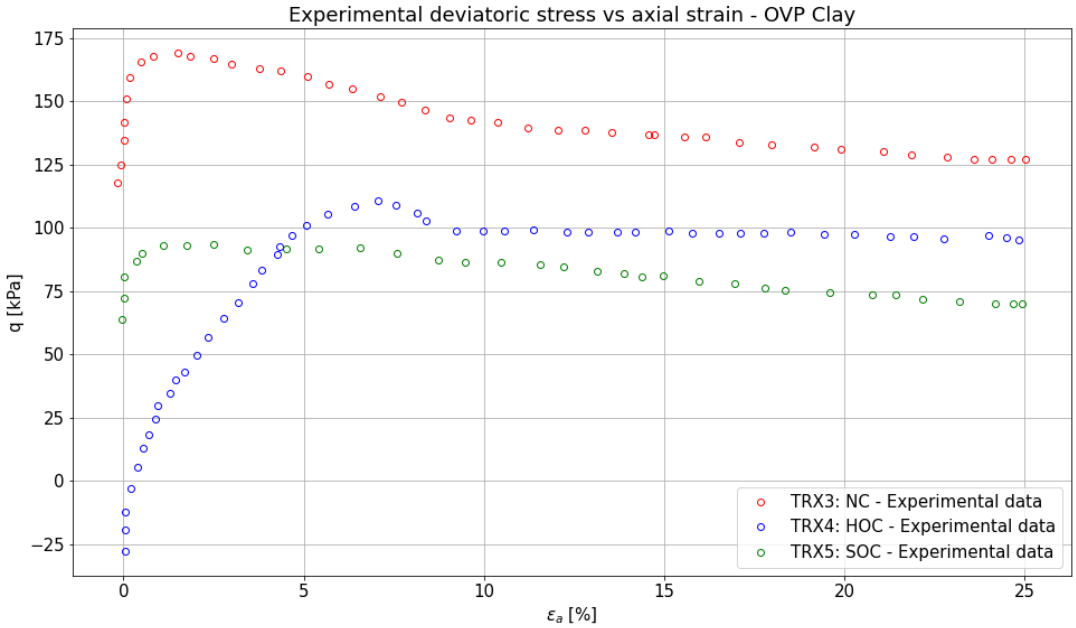

Figure 37: Deviatoric stress development with axial strain during shearing - Data taken from Wegman (2020).

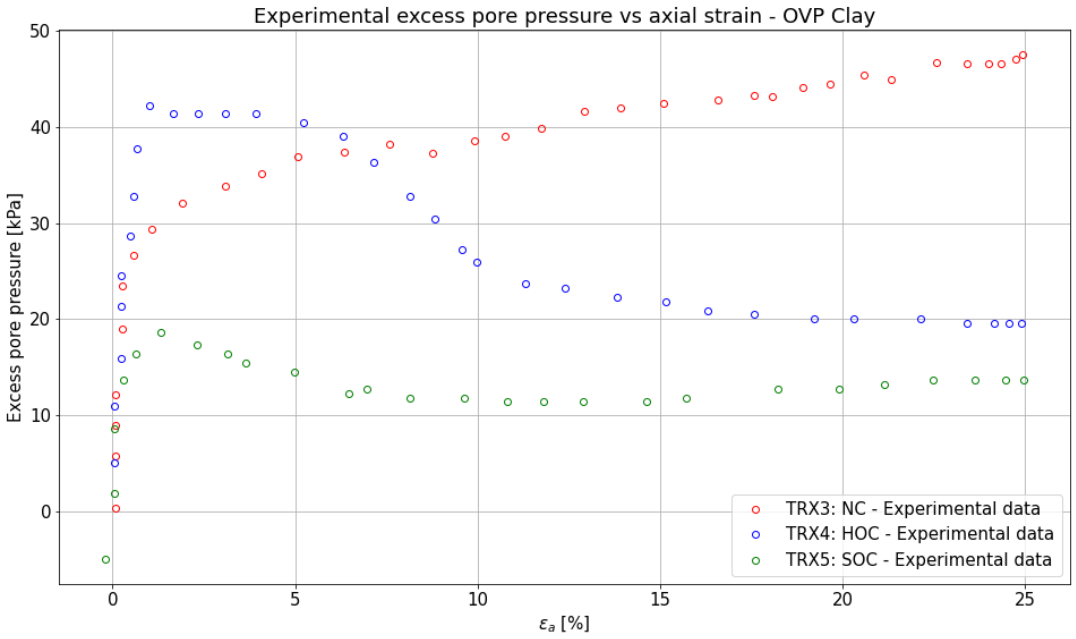

Figure 38: Excess pore pressure development with axial strain during shearing - Data taken from Wegman (2020).

For the model validation, it is interesting to look at the stress paths not only in p'-q space but also in σ'_v-σ'_h space. Wegman (2020) presented for each of the samples the development of the stresses and strains with time throughout the tests. At a multitude of moments in time, both the vertical and horizontal effective stress are taken from these plots to be able to create the stress paths in σ'_v-σ'_h space. This stress path is presented below. For the sake of clarity, the symbols are connected with lines because otherwise the figure would be too difficult to read. In the model validation presented later these lines will be removed.

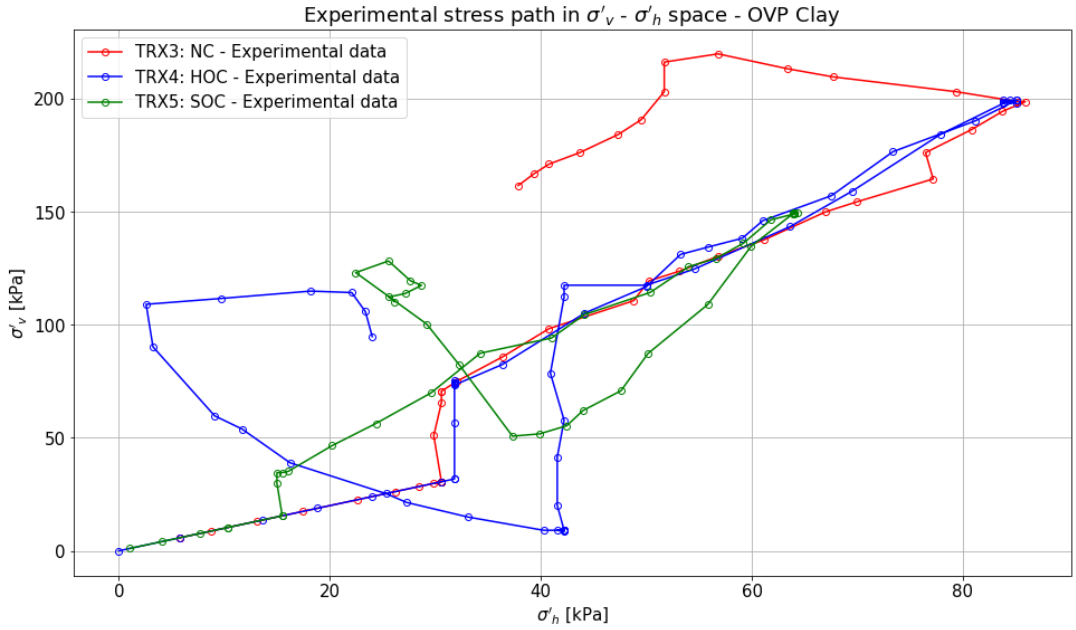

Figure 39: Stress paths in σ'_v-σ'_h space - Data taken from Wegman (2020).

The final plot from Wegman (2020) which will be used is the monitored void ratio throughout the test. This is presented in figure 40 with p' on the logarithmic horizontal axis. Different stages of the test can be seen, the initial part of the test is on the reloading branch which shows stiff behaviour. After the preconsolidation pressure is exceeded, the behaviour is less stiff corresponding with the primary loading branch. Upon completion of the loading stage, unloading stages can clearly be seen as well. It should be noted that after unloading, a waiting period was applied before shearing was started. During this waiting period an increase in the void ratio due to a rebound of the soil is observed for the highly overconsolidated sample. A rebound like this is not commonly measured and therefore is likely to not be the true soil behaviour. The void ratio was determined based on the water extortion during the triaxial test in order to get a consistent measurement of the void ratio, this is not the usual practice though and therefore measurement errors might have affected the results (Wegman, 2020). The final part which is present is the undrained shearing stage where p' changes but the void ratio remains constant. The final values are indicated with big markers.

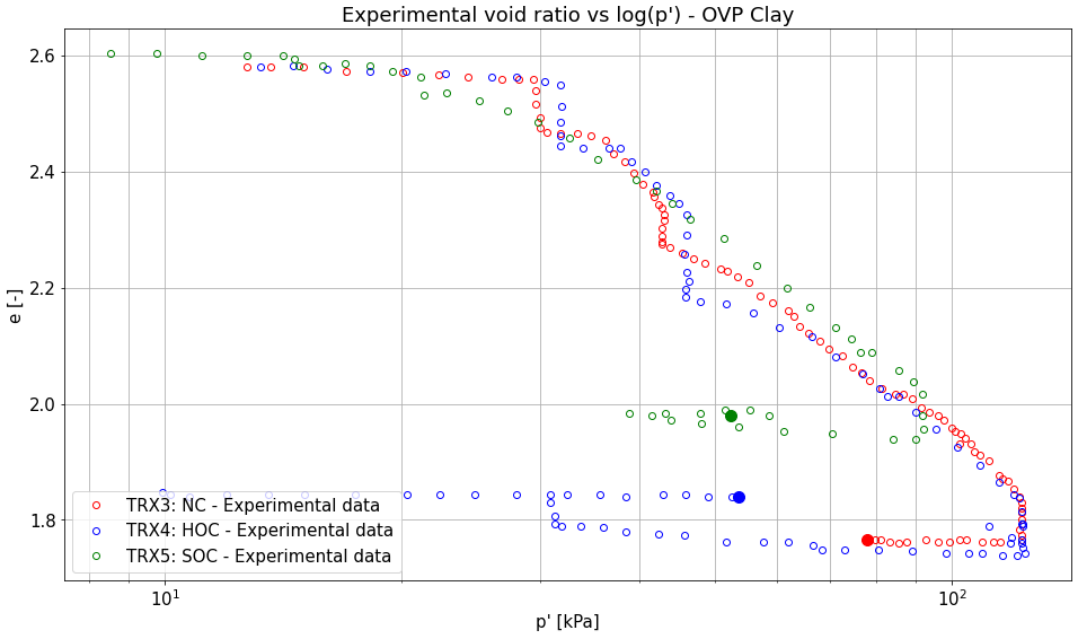

Figure 40: Void ratio vs log mean effective stress - Data taken from Wegman (2020).

4.3.2 Polinder (2019) tests

Using the OVP clay, Polinder (2019) performed K_0-CRS (Constant Rate of Strain) tests. From their results, two tests are used to help with the model validation. The first test is a 10 day ageing test in which a sample is loaded, then left to age for 10 days and then loaded again after which it is unloaded. The idea behind this test is that after the first loading stage, a certain isotach is reached. During ageing, the soil moves away from this isotach which is reached again upon reloading. The principle behind isotachs is explained by Polinder (2019). The testing equipment governed the vertical stress and measured the horizontal one at the same time. The results are plotted in two graphs, one shows the stress path in p'-q space and the other one shows the vertical and horizontal stresses over time. Both graphs will be used in the model validation with the goal being to see how well the model predicts the stress development over time as well as assessing the ability of the model to follow the experimental stress path. Shown below is first the stress path in p'-q space after which the effective stress vs time plot is presented.

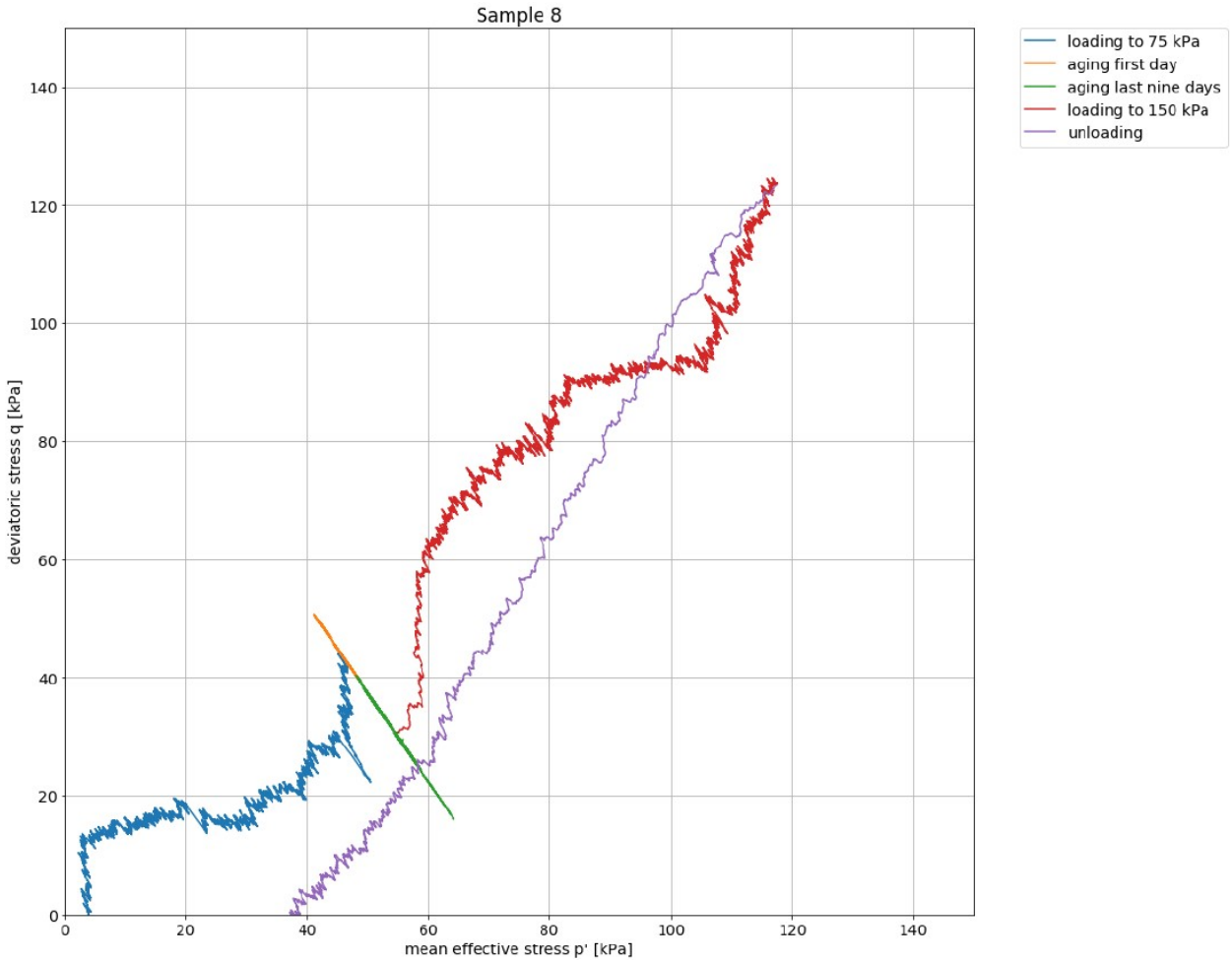

Figure 41: Stress path in p'-q space - 10 days ageing (Polinder, 2019).

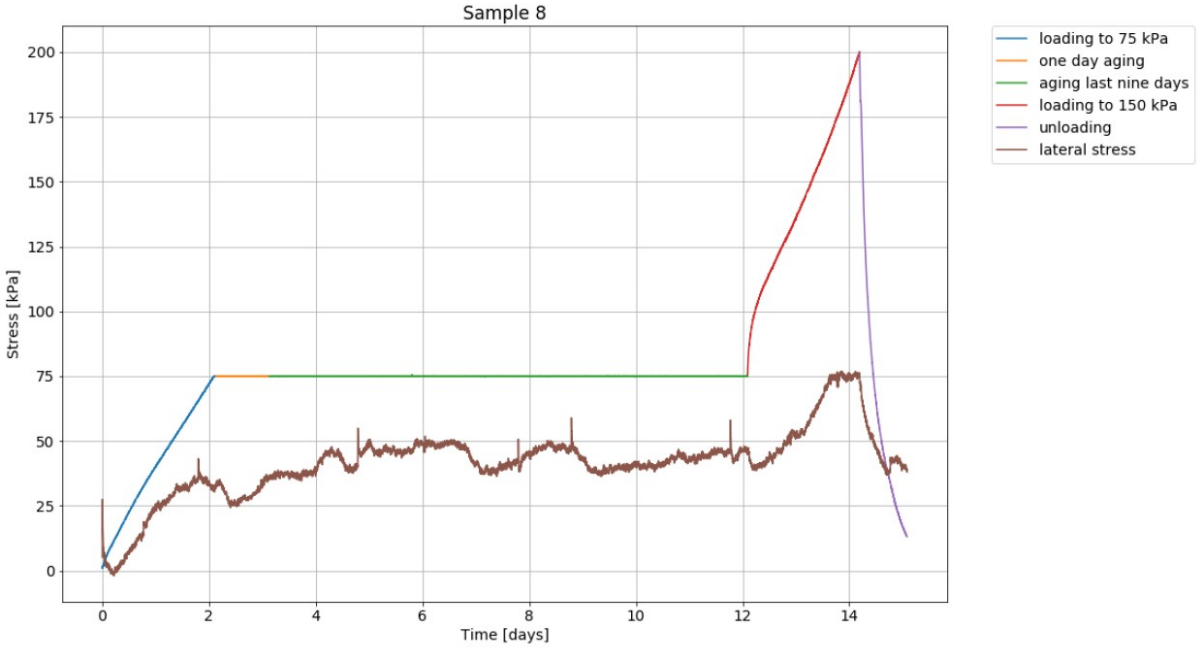

Figure 42: Measured imposed vertical and effective horizontal stresses in time - 10 days ageing (Polinder, 2019).

The second test is an ageing test in which the change in void ratio is monitored. Two samples are compared which are loaded to the same vertical effective stress, then left to rest for 10 and 30 days respectively after which they are loaded again. With this test the ability of the model to predict the creep behaviour of the soil is tested. The test results are shown below, sample 8 is the 10 days ageing sample and sample 16 the 30 days one. In this figure, two additional samples (13 and 14) are presented. Due to power failures during their tests, the data belonging to these samples is not used.

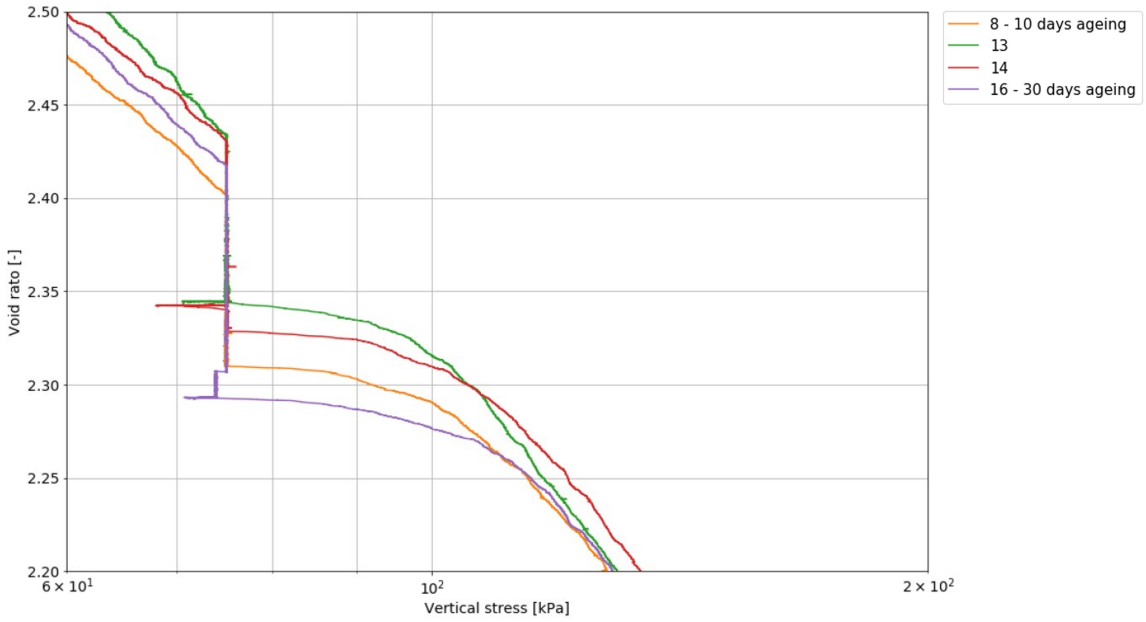

Figure 43: Void ratio vs log vertical effective stress - Sample 8 is subjective to 10 days ageing, sample 16 to 30 days ageing, the other two samples are not used (Polinder, 2019).

4.4 Parameter determination

The EVP model uses 12 parameters and 6 initial state variables which all need to be calibrated to the soil that is being used. The parameter determination is explained in detail below.

The parameters needed to validate the elasto viscoplastic model are divided in three groups. These are:

- Elastoplastic parameters

M_c	Value of stress ratio q/p at critical state in compression
c_M	M_e/M_c
λ^*	Slope of compression line in ln(ν)-ln(p') plane - Calculated from λ as $\lambda^* = \lambda$ / (1 + e_0)
κ^*	Slope of rebound line in ln(ν)-ln(p') plane - Calculated from κ as $\kappa^* = \kappa$ / (1 + e_0)
ν	Poisson's ratio
N	Shape of the yield surface (1)
x	Saturation limit of anisotropy under constant stress ratio
C	Rate of evolution of anisotropy
k_f	Shape of the yield surface (2)
k_g	Shape of the plastic potential (always equal to 2.0)

- Viscosity parameters

μ	Fluidity parameter
N_ϕ	Strain rate coefficient

- Initial state variables

$\boldsymbol{\varepsilon_0}$	Initial strain
$\boldsymbol{\sigma_0}$	Initial total stress
$\boldsymbol{\alpha_0}$	Initial rotation of plastic potential
$\boldsymbol{\beta_0}$	Initial rotation of yield surface
$p_{c,0}$	Initial mean preconsolidation pressure
e_0	Initial void ratio

First, the parameters from the first and third group are determined. This is done using the elastoplastic (EP) version of the model (see section 3.1) which does not yet include the viscosity parameters. Parameter determination is done by taking the values either directly from the literature or calculating them based on equations from the literature.

4.4.1 Elastoplastic model parameters

The elastoplastic parameters are determined first. Two parameters can directly be taken from Wegman (2020). He states that $M_c = 1.61$ and $M_e = 1.35$ leading to $c_M = 0.84$. λ and κ can be determined from the data in figure 40. κ is the slope of the reloading line and λ the slope of the virgin compression line. Using the normally consolidated sample, λ and κ are determined as shown below.

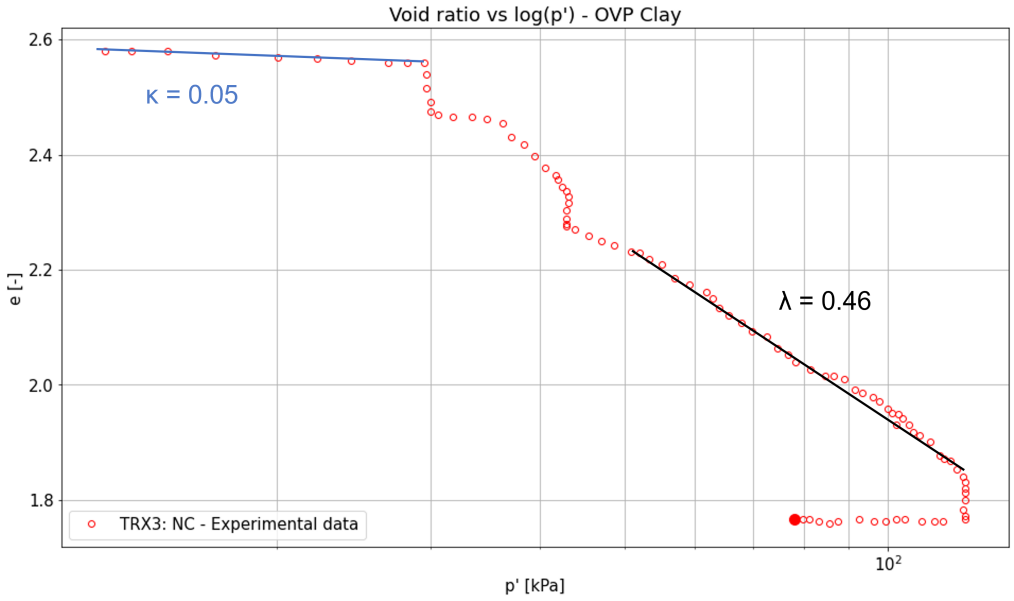

Figure 44: Determination of λ and κ using the normally consolidated deformation data from Wegman (2020).

With the initial void ratio of 2.59, λ^* becomes 0.46 / (1 + 2.59) = 0.13, similarly κ^* becomes 0.014. Fern et al. (2017) states a value of 0.2 for the Poisson's ratio (ν) of OVP clay.

The parameter values for N and x need to be determined according to Dafalias et al. (2006). They state that x can be calculated as follows.

$$\frac{\eta_k}{x} = \frac{B * \varepsilon * \eta_k^3 + \eta_k^2 + [2(1-\kappa/\lambda) - BM_c^2]\varepsilon\eta_k - M_c^2}{2\varepsilon(1-\kappa/\lambda)}, \text{ with } B = -\frac{2(1+\nu)}{9(1-2\nu)}\frac{\kappa}{\lambda} \tag{36}$$

Using a K_0 loading path, ε is equal to 3/2 and η_k is equal to η_{k_0} which can be calculated as $\frac{3(1-K_0)}{1+2K_0}$. K_0 can be calculated using Jaky's relationship (equation (3)). Wegman (2020) reports a value of 40.1° for the critical state friction angle. K_0 can now be estimated as 1 - sin(40.1) = 0.36.
Now that κ, λ, M_c, ν and K_0 are known, it can be determined that η_k is 1.12 and B is -0.05 leading to an x value of 1.71. Note that here κ and λ are used and not κ^* and λ^*.

N on the other hand can be calculated using the following expression.

$$\frac{p_f}{p_{k_0}} = \left(\frac{N^2 - \eta_{k_0}^2}{N^2 - 2\eta_{k_0}M_c + M_c^2}\right)^{(1-\kappa/\lambda)} \tag{37}$$

This equation assumes a normally consolidated clay. In figure 36, TRX_3 is the normally consolidated test so therefore this test should be used to determine p_f and p_{k_0}. p_{k_0} is the p value at the end of K_0 consolidation and is equal to 123 kPa. p_f is the p value at critical state and as can be seen in figure 36 is roughly equal to 100 kPa. All other values have already been calculated above. With these values, N is determined to be 1.48.

The parameters that still need to be determined are k_f and C. For the sake of simplicity and in absence of experimental evidence, k_f is assumed to be equal to k_g as 2.0.

The value for C has to be determined through the execution of trial runs with the other parameters known. This process is relatively simple since Dafalias et al. (2006) states that C often varies between 3 and 20. A sensitivity analysis was performed within this range (figures 93a and 93b) which can be used in determining the value of C.

4.4.2 Initial state variables

The initial state variables are determined next. The first variable that is looked at is the mean preconsolidation pressure. The value for this parameter can be determined using the sample preparation description. Since it is known that the samples are K_0-consolidated to 40 kPa vertical stress and the value of K_0 is known to be 0.36, the mean preconsolidation pressure can directly be calculated to be equal to 22.9 kPa.
Figures 39 and 42 show that for both theses the initial stress is small and therefore it is set to 5 kPa isotropic ($\sigma_0 = 5$ kPa). The initial strain is assumed to be zero ($\varepsilon_0 = 0$).
α_0 and β_0 can be determined using Dafalias et al. (2006). For the sake of simplicity, β_0 will be taken equal to α_0 (as done in Dafalias and Taiebat (2013)) which is calculated as η_k/x (Dafalias, 1987). With η_k and x as mentioned above, α_0 is equal to 0.65. In the model, the rotation needs to be given in multiaxial space instead of as a scalar. This can easily be converted though leading to $\beta_0 = \alpha_0$ = [-0.65/3*1, -0.65/3*1, 0.65/3*2, 0.0, 0.0, 0.0].
The initial void ratio for the samples of Wegman (2020) is averaged as 2.59 whereas Polinder (2019) reports an initial void ratio of 2.61 for their samples.

Below is a comprehensive overview of the determined parameter values with only the value for C left to be determined.

Table 2: Elastoplastic parameter values - OVP Clay.

Parameter	Meaning	Value
M_c	Value of stress ratio q/p at critical state in compression	1.61
c_M	M_e/M_c	0.84
λ^*	Slope of compression line in ln(ν)-ln(p') plane	0.13
κ^*	Slope of rebound line in ln(ν)-ln(p') plane	0.014
ν	Poisson's ratio	0.20
N	Shape of the yield surface (1)	1.48
x	Saturation limit of anisotropy under constant stress ratio	1.71
C	Rate of evolution of anisotropy	TBD[1]
k_f	Shape of the yield surface (2)	2.0
k_g	Shape of the plastic potential (always equal to 2.0)	2.0

[1] TBD = To Be Determined

Table 3: Initial state variables - OVP Clay.

Parameter	Unit	Meaning	Value
$\boldsymbol{\varepsilon_0}$	[-]	Initial strain	[0.0, 0.0, 0.0, 0.0, 0.0, 0.0]
$\boldsymbol{\sigma_0}$	[kPa]	Initial total stress	[5.0, 5.0, 5.0, 0.0, 0.0, 0.0]
$\boldsymbol{\alpha_0}$	[-]	Initial rotation of plastic potential	[-0.65/3*1, -0.65/3*1, 0.65/3*2, 0.0, 0.0, 0.0]
$\boldsymbol{\beta_0}$	[-]	Initial rotation of yield surface	[-0.65/3*1, -0.65/3*1, 0.65/3*2, 0.0, 0.0, 0.0]
$p_{c,0}$	[kPa]	Initial mean preconsolidation pressure	22.9
e_0	[-]	Initial void ratio	2.59 (Wegman, 2020), 2.61 (Polinder, 2019)

The value for C will be set to 4 as a first approximation. The reason for this is that it was found that for high values of C, the model ran into convergence problems.

Using the set of parameters shown above, a first model run is performed using the elastoplastic model. The model output is compared to data from Wegman (2020). More specifically, the stress paths in p'-q space and the void ratio vs log(p') plot are used. The reason for this is that together these graphs give insight in both the stress and deformation prediction of the model. The results are presented below, the symbols show the experimental data and the lines the corresponding numerical predictions.

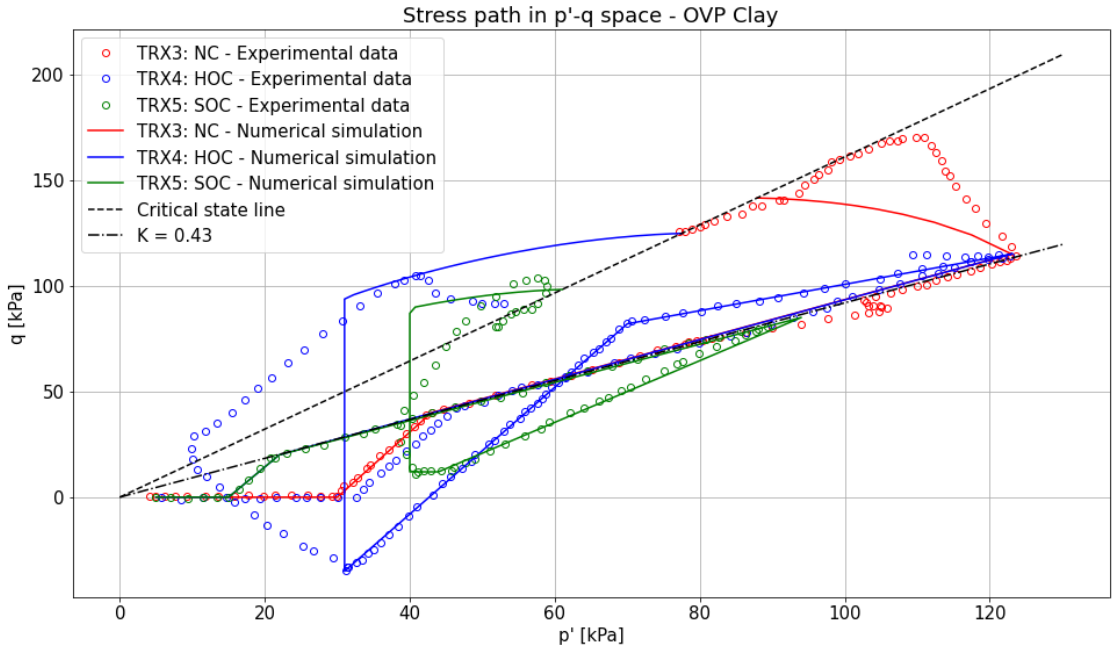

(a) EP model prediction for the stress path in p'-q space.

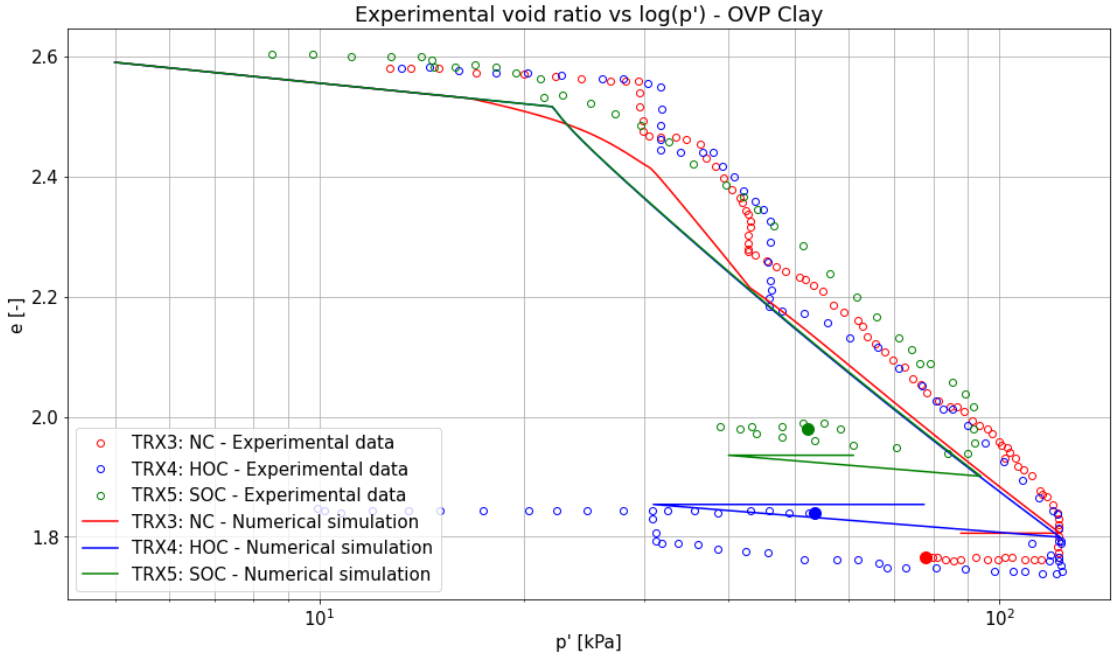

(b) EP model prediction for the change in void ratio with mean effective stress.

Figure 45: Model prediction using the first set of EP parameters - Experimental data from Wegman (2020).

The results show that there are definitely viscous influences in the experimental data. This can clearly be seen in figure 45b where deformation at a constant mean effective stress is observed. Because of this, more information on the creep behaviour is needed before comments can be made regarding potential tuning of parameters or the model performance.

4.4.3 Elasto Viscoplastic model parameters

In order to model the creep behaviour that is shown in the experimental data, the elasto viscoplastic (EVP) model is needed. This model introduces two new parameters (μ, N_ϕ) which both need to be determined. To do this, test data from Polinder (2019) is used involving the void ratio vs $\log(\sigma'_v)$ plot of a sample which has been left subjective to creep for 10 days (figure 43).
Unfortunately, no literature on OVP clay is available to give a first guess of the parameter values. Because of this, Rezania et al. (2016) is used as a starting point in which the viscosity parameters are given for Kawasaki clay as $\mu = 7\text{e-}6\ \text{s}^{-1}$ and $N_\phi = 12$. Using these parameters as well as a performed sensitivity analysis (figures 95 and 96) it is found that $\mu = 3\text{e-}10\ \text{s}^{-1}$ and $N_\phi = 9$ gives a good fit to the experimental data. The obtained result with these parameter values is shown below.

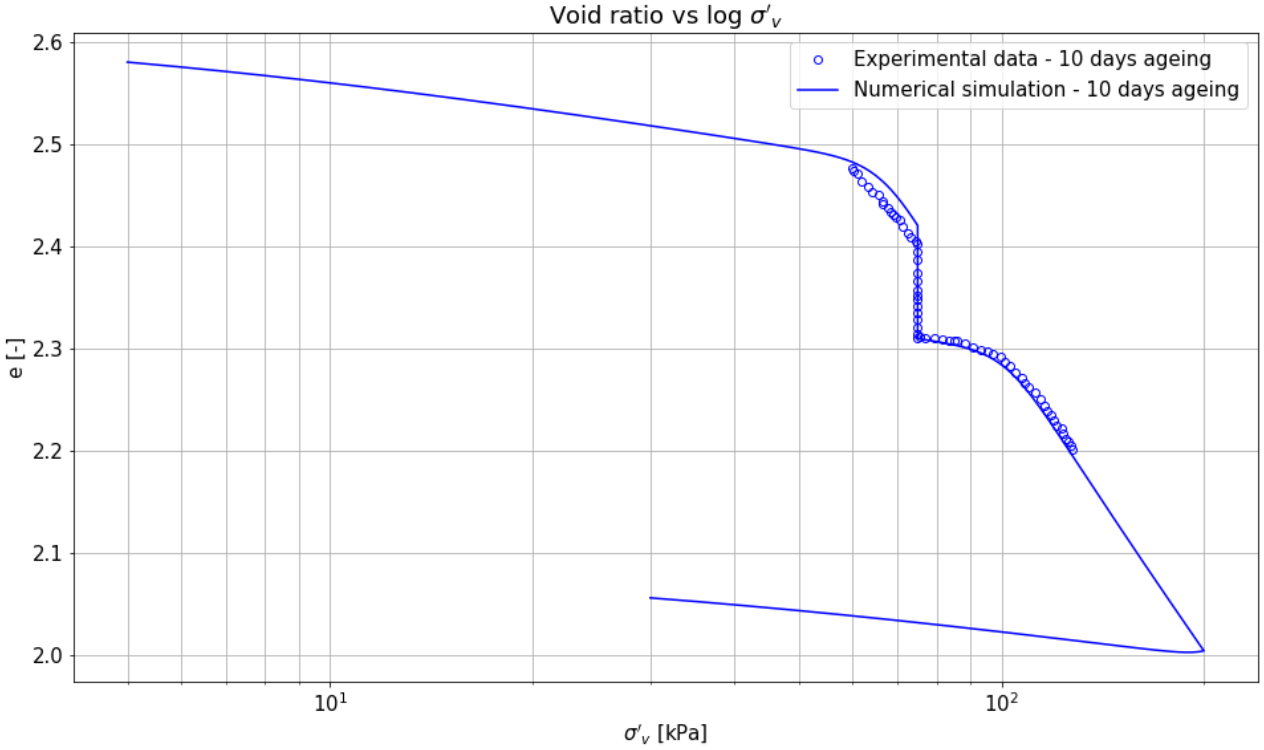

Figure 46: Determination viscosity parameters - Void ratio vs $\log(\sigma'_v)$ (experimental data from Polinder (2019)).

4.4.4 Overview determined parameters

Shown below are the determined parameters for the EVP model having used both data from Wegman (2020) and Polinder (2019).

Table 4: Elastoplastic parameter values - OVP Clay - EVP Model.

Parameter	Meaning	Value
M_c	Value of stress ratio q/p at critical state in compression	1.61
c_M	M_e/M_c	0.84
λ^*	Slope of compression line in ln(ν)-ln(p') plane	0.13
κ^*	Slope of rebound line in ln(ν)-ln(p') plane	0.014
ν	Poisson's ratio	0.20
N	Shape of the yield surface (1)	1.48
x	Saturation limit of anisotropy under constant stress ratio	1.71
C	Rate of evolution of anisotropy	4
k_f	Shape of the yield surface (2)	2.0
k_g	Shape of the plastic potential (always equal to 2.0)	2.0

Table 5: Elasto viscoplastic parameter values - OVP Clay - EVP Model.

Parameter	Unit	Meaning	Value
μ	[s^{-1}]	Fluidity parameter	3e-10
N_ϕ	[-]	Strain rate coefficient	9

Table 6: Initial state variables - OVP Clay - EVP Model.

Parameter	Unit	Meaning	Value
$\boldsymbol{\varepsilon_0}$	[-]	Initial strain	[0.0, 0.0, 0.0, 0.0, 0.0, 0.0]
$\boldsymbol{\sigma_0}$	[kPa]	Initial total stress	[5.0, 5.0, 5.0, 0.0, 0.0, 0.0]
$\boldsymbol{\alpha_0}$	[-]	Initial rotation of plastic potential	[-0.65/3*1, -0.65/3*1, 0.65/3*2, 0.0, 0.0, 0.0]
$\boldsymbol{\beta_0}$	[-]	Initial rotation of yield surface	[-0.65/3*1, -0.65/3*1, 0.65/3*2, 0.0, 0.0, 0.0]
$p_{c,0}$	[kPa]	Initial mean preconsolidation pressure	22.9
e_0	[-]	Initial void ratio	2.59 (Wegman, 2020), 2.58 (Polinder, 2019)

4.5 Elasto viscoplastic model validation

Using the determined set of parameters, the EVP model now needs to be validated by comparing the model output to the experimental data. In the following paragraphs this validation will be done starting by using the data from Wegman (2020). Afterwards, the data from Polinder (2019) will be used to help in the model validation.

4.5.1 Validation using Wegman (2020) data

The first step in validating the EVP model is by using the experimental data from Wegman (2020). As a reminder, triaxial tests were performed on samples with different levels of overconsolidation. These samples are Normally Consolidated (NC), Slightly OverConsolidated (SOC) and Highly OverConsolidated (HOC). The experimental data can be found in figures 36 to 40. The first set of results is obtained by using the parameter values as determined above (tables 4 and 5), the results are initially presented below using only the stress path in p'-q space and the void ratio vs log(p') plot.

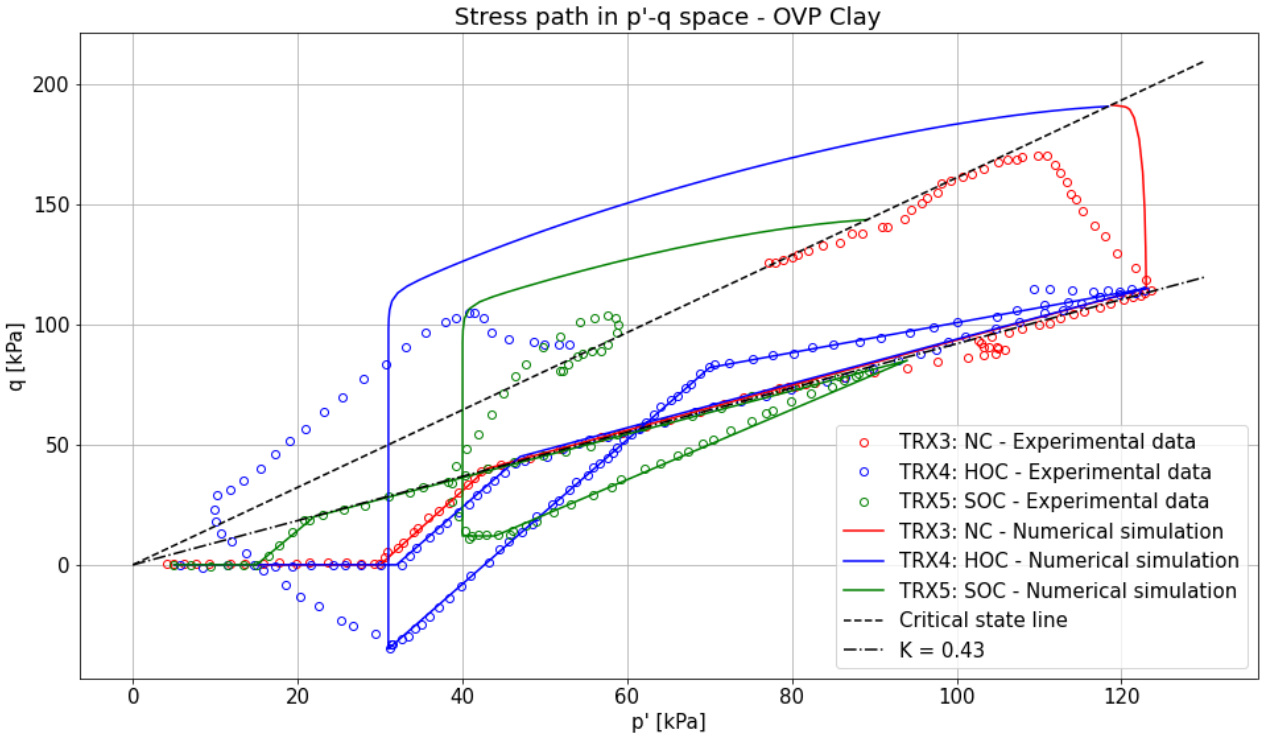

(a) EVP model prediction for the stress path in p'-q space.

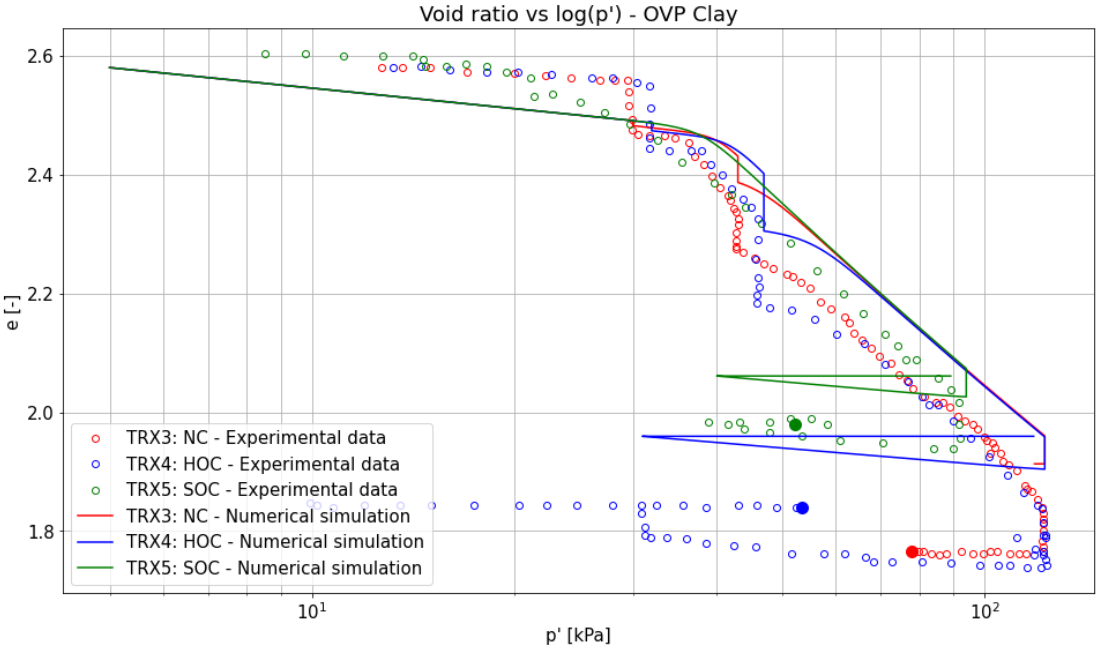

(b) EVP model prediction for the change in void ratio with mean effective stress.

Figure 47: Model prediction using the EVP model and the initial set of detemrined parameters - Experimental data from Wegman (2020).

It can be seen that the results have changed compared to the original EP model (figures 45a and 45b). Adopting the EVP model apparently requires altering of some of the parameters. Figure 47a shows that the model predicts the samples to go towards the critical state line too late during shearing. Shown below are the stress paths with yield surfaces for the model runs performed with the EP and EVP model. The EVP model shows both the SYS (Static Yield Surface) and the DLS (Dynamic Loading Surface) as explained at the start of this chapter.

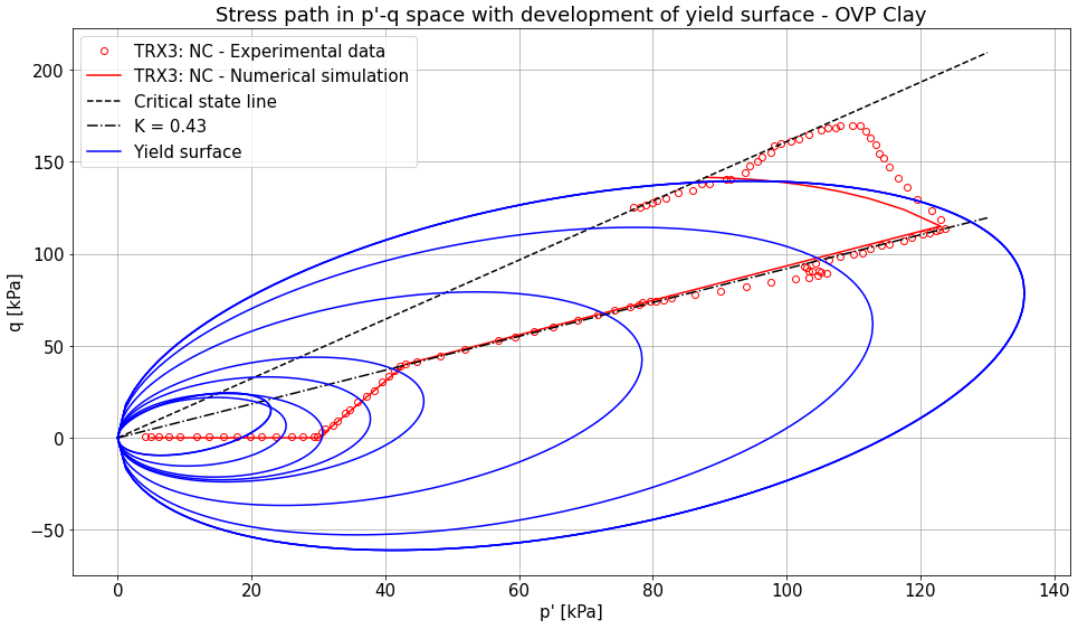

(a) Stress path with yield surface for sample TRX_3 using the EP model.

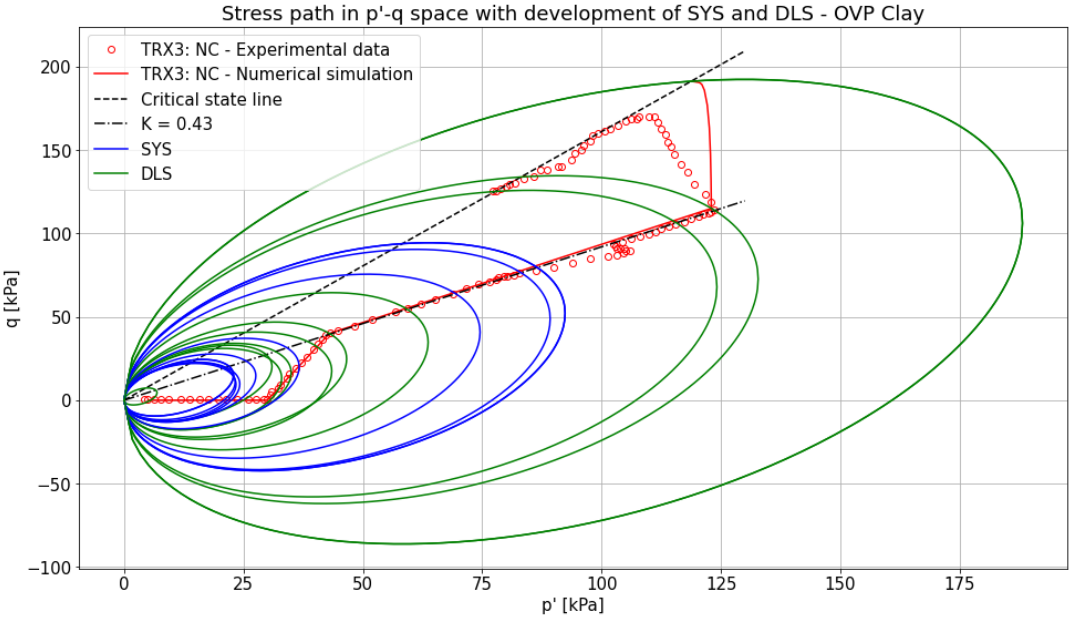

(b) Stress path with SYS and DLS for sample TRX_3 using the EVP model.

Figure 48: Yield surface development for the EP and EVP model.

Figure 48b shows that in the EVP model, the DLS (which always goes through the stress point) is too big. Changing the size of the DLS would mean that p_{cd} would need to be altered which is not desired. Another option to improve the stress path in the EVP model is to change the shape of the DLS. If it is flattened, the stress path will move towards the CSL earlier. Using a performed sensitivity analysis with the EVP model (appendix A.3), N and k_f (the parameters governing the shape of the DLS) are changed to become 1.00 and 3.5 respectively. Figure 47b indicates that the amount of deformation at a constant stress is too small, therefore the viscosity parameters need to be increased to make sure that the model predicts enough deformation. N_ϕ is set to 13 and μ to 8e-10 s^{-1} to account for this. Finally, it was found that x should be changed to 1.80. With these new parameters the results look as follows.

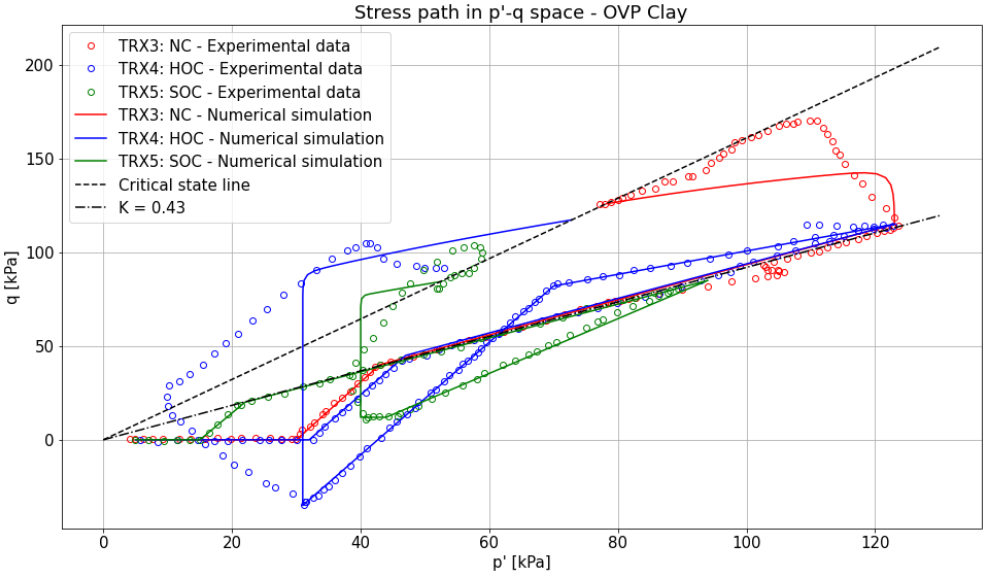

Figure 49: Model prediction for the stress path in p'-q space using the EVP model and the altered set of determined parameters (experimental data from Wegman (2020)).

The new stress path with SYS and DLS for sample TRX_3 is shown below.

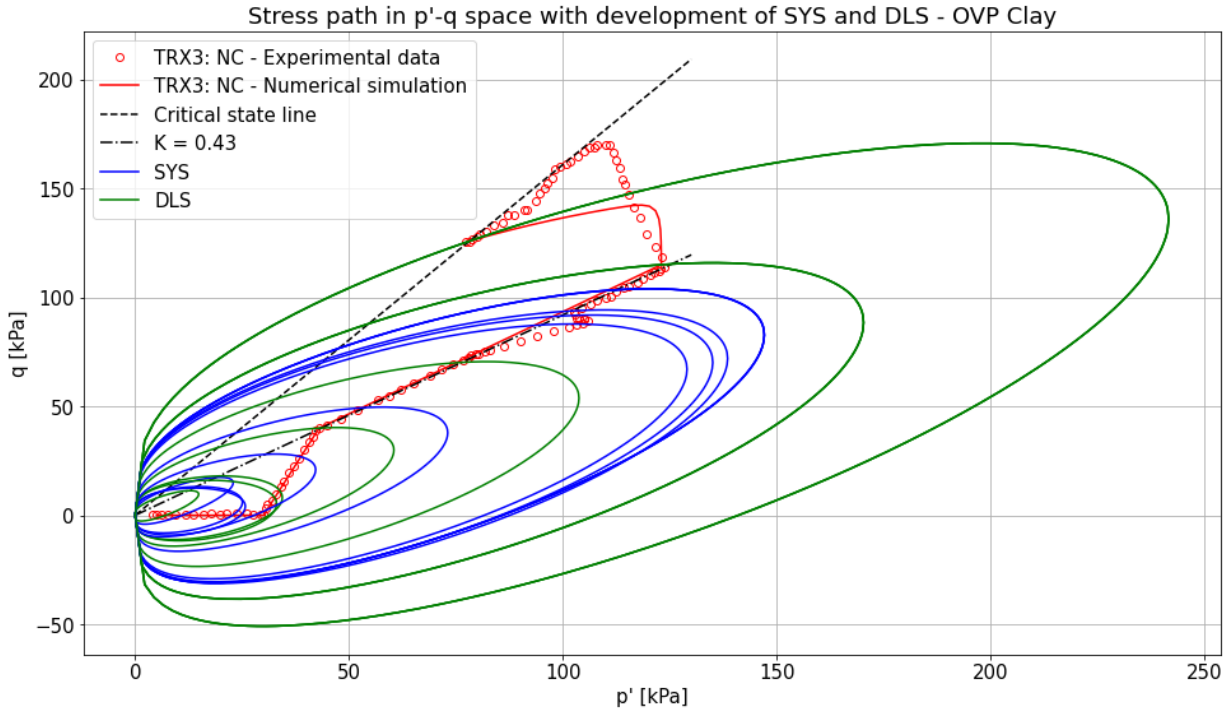

Figure 50: Stress path with SYS and DLS for sample TRX_3 using the tuned EVP model.

It can be seen that with the new shape of the DLS, the stress path is forced to go to the critical state line faster which is in correspondence with the experimental data. The rest of the results are presented next.

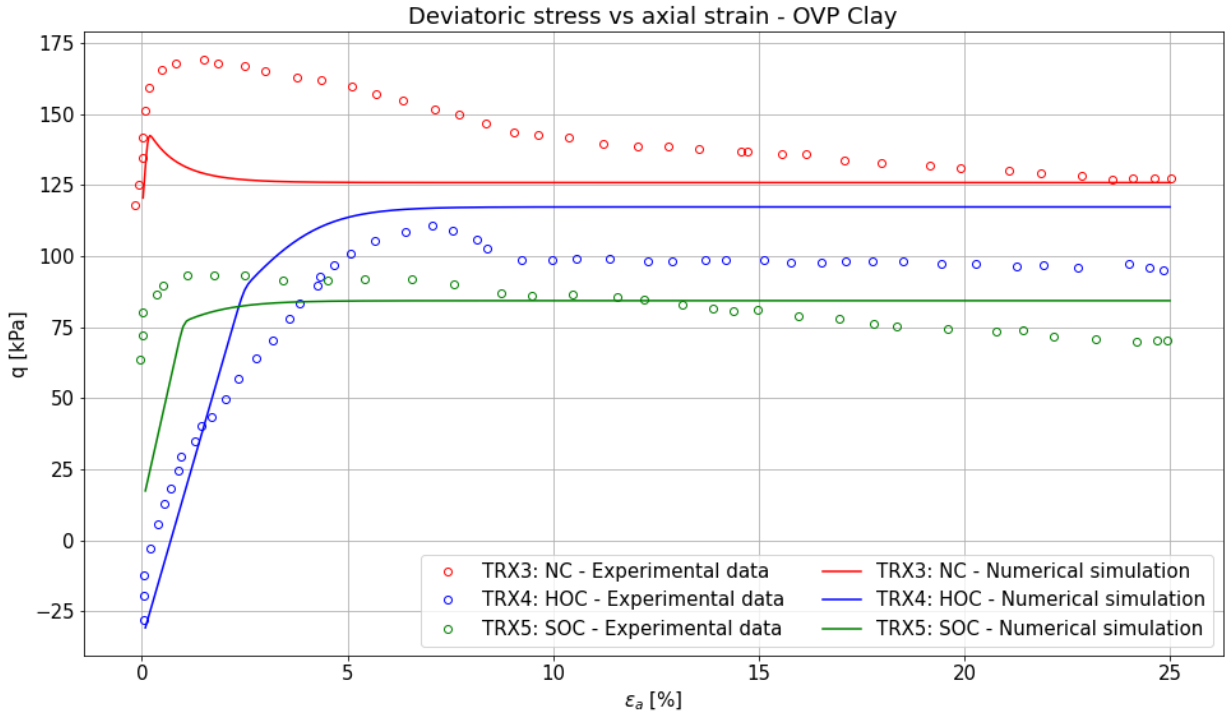

(a) Deviatoric stress vs axial strain during triaxial shearing.

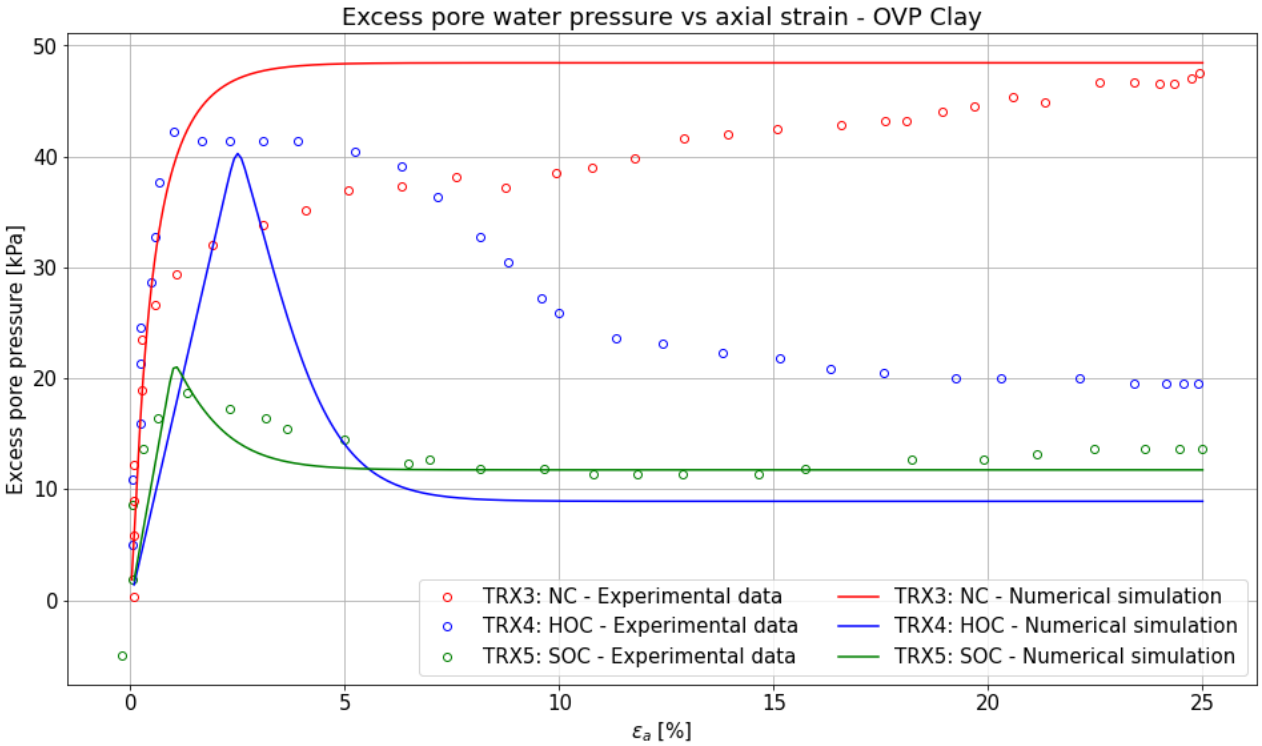

(b) Pore water pressure vs axial strain during triaxial shearing.

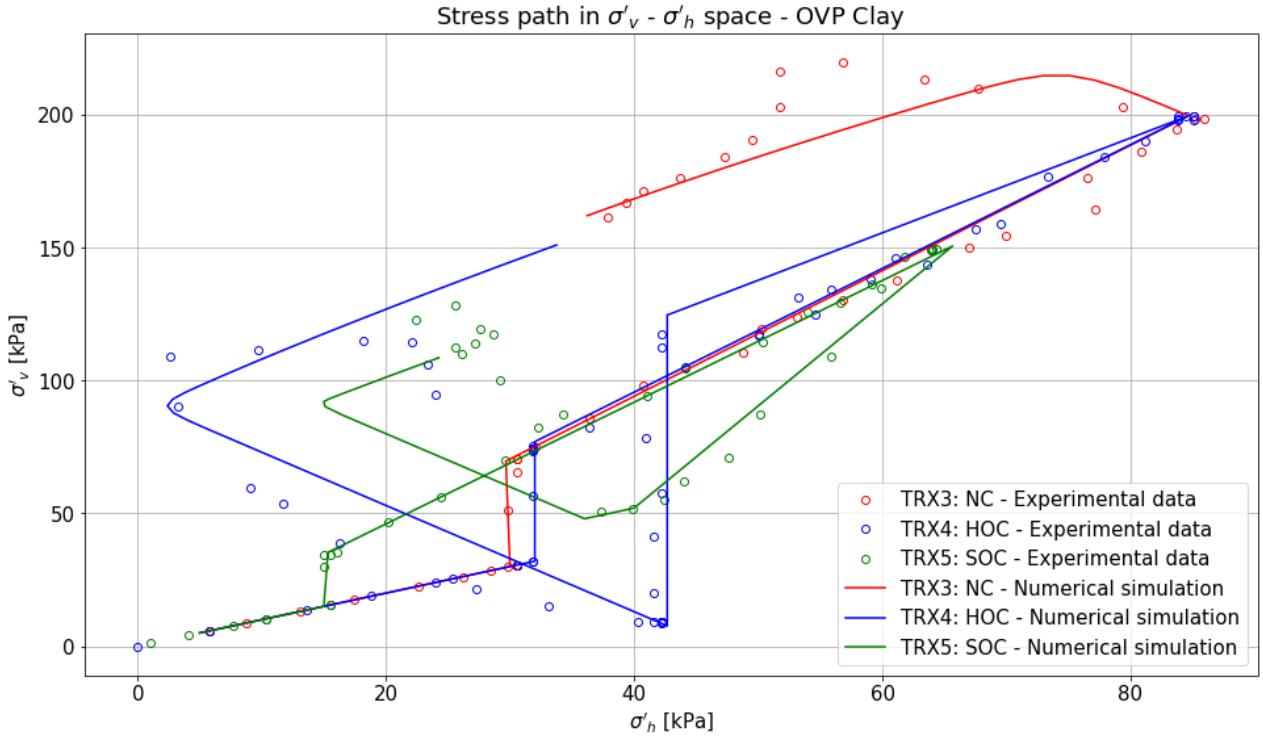

(c) Stress path in σ'_v-σ'_h space.

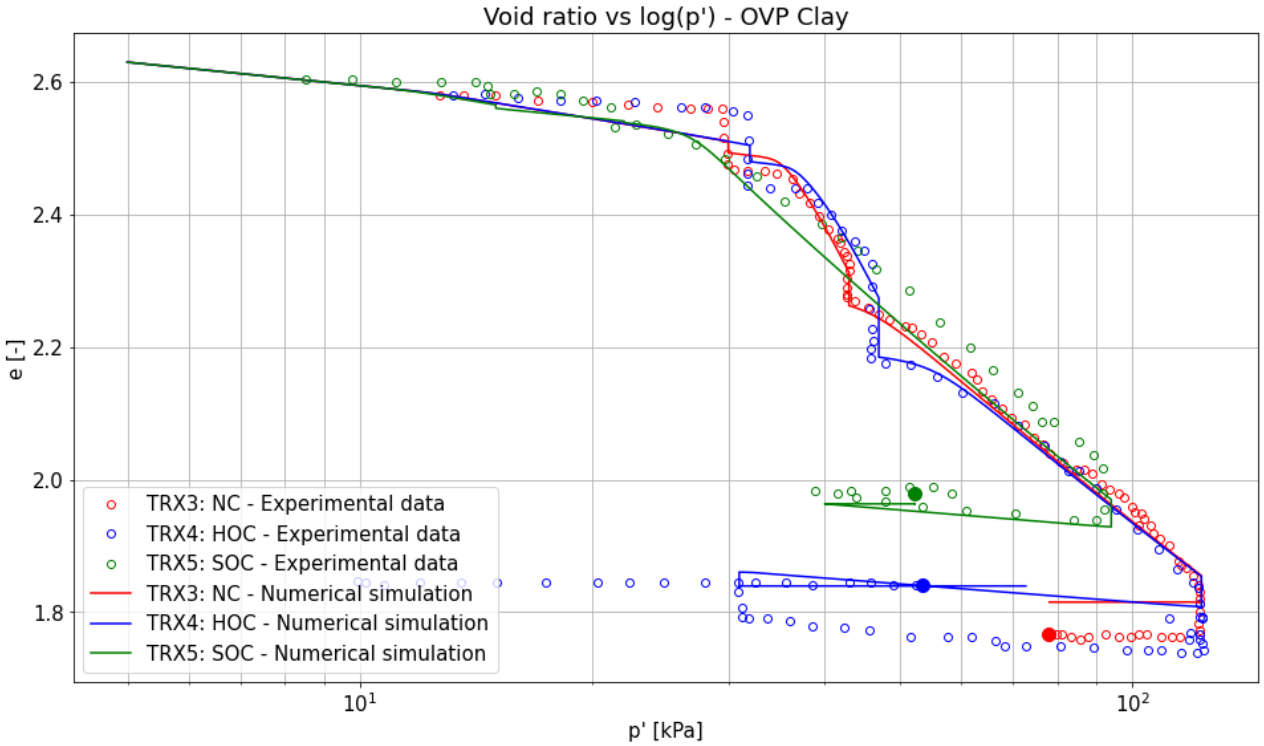

(d) Change in void ratio with mean effective stress.

Figure 51: EVP model predictions compared to experimental data from Wegman (2020).

From the figures above the following things can be noted. First of all, looking at figure 49, it can be seen that the model follows the stress paths quite well. Since only one set of parameters is used, the NC sample underpredicts the experimental data during shearing and the HOC sample overpredicts the experimental data. There is no solution for this other than using different parameters for the different sample which is not desirable.
The excess pore pressure development shown in figure 51b shows that the peak pore pressure is predicted quite accurately for the samples. Again, it can be seen that the NC and HOC samples differ from the experimental data in opposite directions. What is meant is that in this case the NC sample overpredicts the experimental data and the HOC sample underpredicts the data. In general, the trend the model follows is satisfactory.
Finally, looking at the deformation behaviour presented in figure 51d it can be concluded that the model predicts creep reasonably well. Whenever there is a break between loading steps and the sample is subjective to creep the model predicts this accurately. As stated before, the increase of the void ratio when the mean effective stress is kept constant after shearing is not commonly observed. It is therefore deemed correct that the model does not predict this behaviour.

4.5.2 Validation using Polinder (2019) data

As described earlier in section 4.3, two tests are taken from Polinder (2019) to help evaluate the model performance. The first one is a test where a sample is loaded, then left to age for 10 days, then loaded again after which it is unloaded. The experimental stress path is plotted in two plots, effective stresses (vertical and horizontal) vs time and in p'-q space. Using the tuned parameters after the validation on the data from Wegman (2020) the following prediction for the effective stresses over time is obtained.

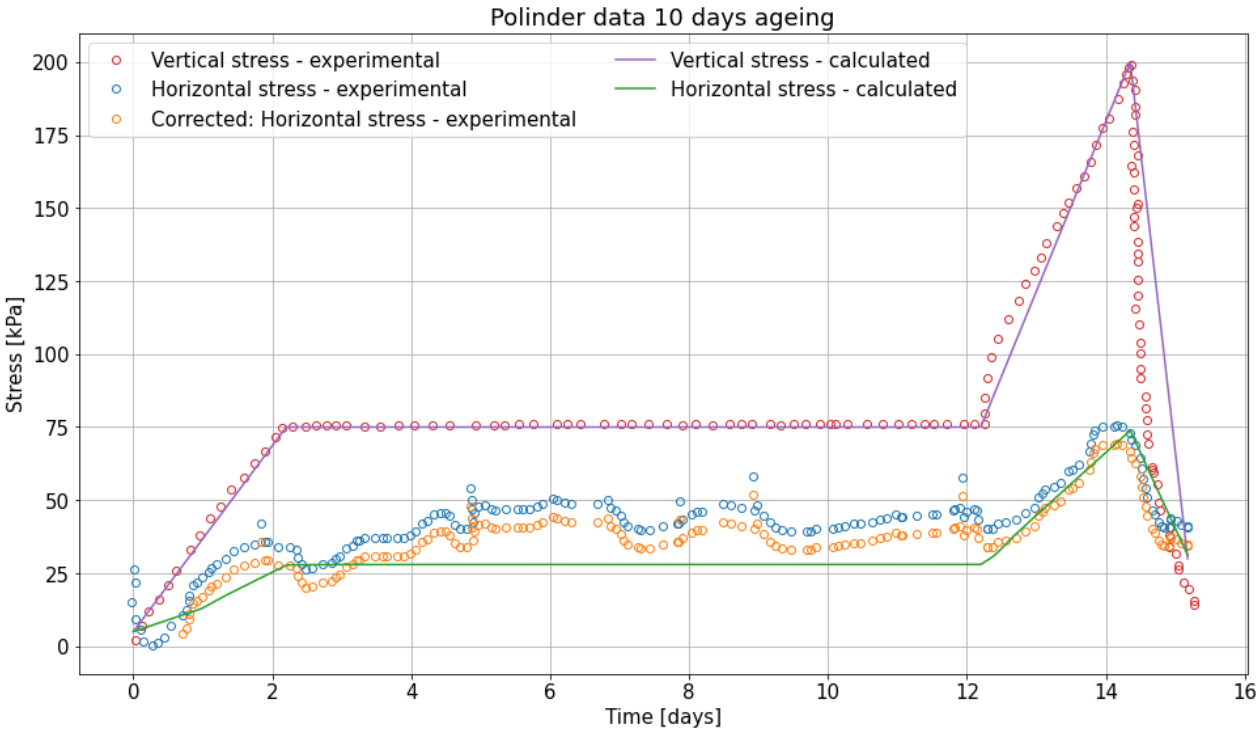

Figure 52: Stresses vs time - 10 days ageing (experimental data from Polinder (2019)).

In the figure above, the red and blue dots are the experimental vertical and horizontal effective stress respectively and the purple and green lines the model outputs. Looking at the horizontal effective stress, it can be seen that the experimental data is quite significantly higher than the model prediction. However, when looking at the start of the test it can be seen that the data already shows a significant horizontal effective stress. This is likely due to experimental problems, Polinder (2019) states that the measurement apparatus was prone to stick and slip behaviour especially at low stresses which can explain this initial measured stress. Because of this, the experimental data has been corrected resulting in the orange dots for the horizontal effective stress.

It can be seen that in general the model output fits the experimental data well. The vertical stress is governed both experimentally and numerically so it is no surprise that this fit is almost perfect. The fit to the horizontal stress is less exact but looking at the general trend it shows good correspondence. The most interesting part of the data is the 10 day ageing time starting slightly after 2 days. The experimental horizontal stress does not follow a clear trend but roughly increases slightly. The horizontal stress model output appears to be constant which would not be in line with the experimental findings. Since the vertical effective stress is constant during the ageing period, a change in horizontal effective stress can be seen in the value of K_0. Shown below is both the experimental and numerical K_0 starting from 10 day ageing period. The reason for this is that the initial experimental data is inconsistent as explained above.

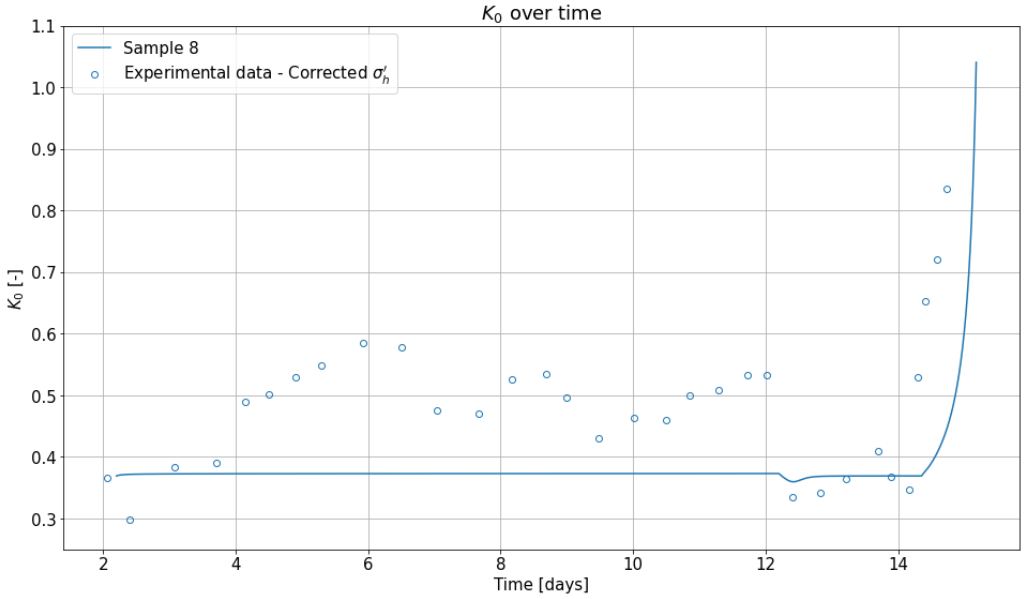

Figure 53: K_0 vs time - 10 days ageing (experimental data from Polinder (2019)).

Figure 53 shows that during ageing, the model does predict a very small increase in K_0 (mainly present initially) but this change is a lot smaller than the experimental change. Polinder (2019) mentions that the measurement of the lateral stresses could not be quantified due to stick and slip behaviour in the K_0-ring. Next to this, the experimental data shows similar behaviour to the K_0 tests on Tiller clay (figure 20). For these tests Gjengstø (2016) mentions that the variations in measured data are due to temperature fluctuations which could very well be the case in this data as well. After loading is applied again the model prediction matches the experimental data well which continues through the unloading stage.

Next to the change in horizontal stress during the 10 day ageing period, the change in preconsolidation pressure is analysed as well. Shown below is the same figure as above but this time p_c is presented. Note that for p_c no experimental data is available so no comparison can be made.

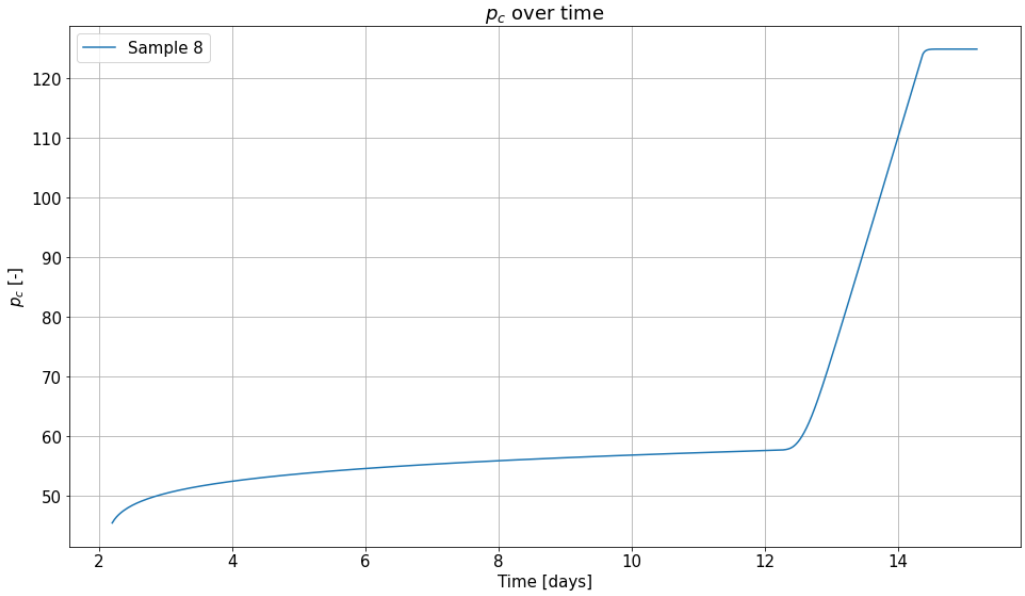

Figure 54: p_c vs time - 10 days ageing.

It can be seen that during ageing the preconsolidation pressure increases. This increase is rapid initially and then slows down significantly. This behaviour was to be expected since the yield surface moves towards the stress point, the expansion of the yield surface in each timestep is based on the distance to the stress point so initially the expansion is rapid and as the yield surface gets closer to the stress point it expands less.

As has been stated before, the stress path given in figure 52 is also presented in p'-q space. Shown below are two figures, the one on the left shows the stress path using the raw experimental data. The plot on the right shows the stress path upon correction of the horizontal stress. These two correspond to the blue and orange dots in figure 52 respectively.

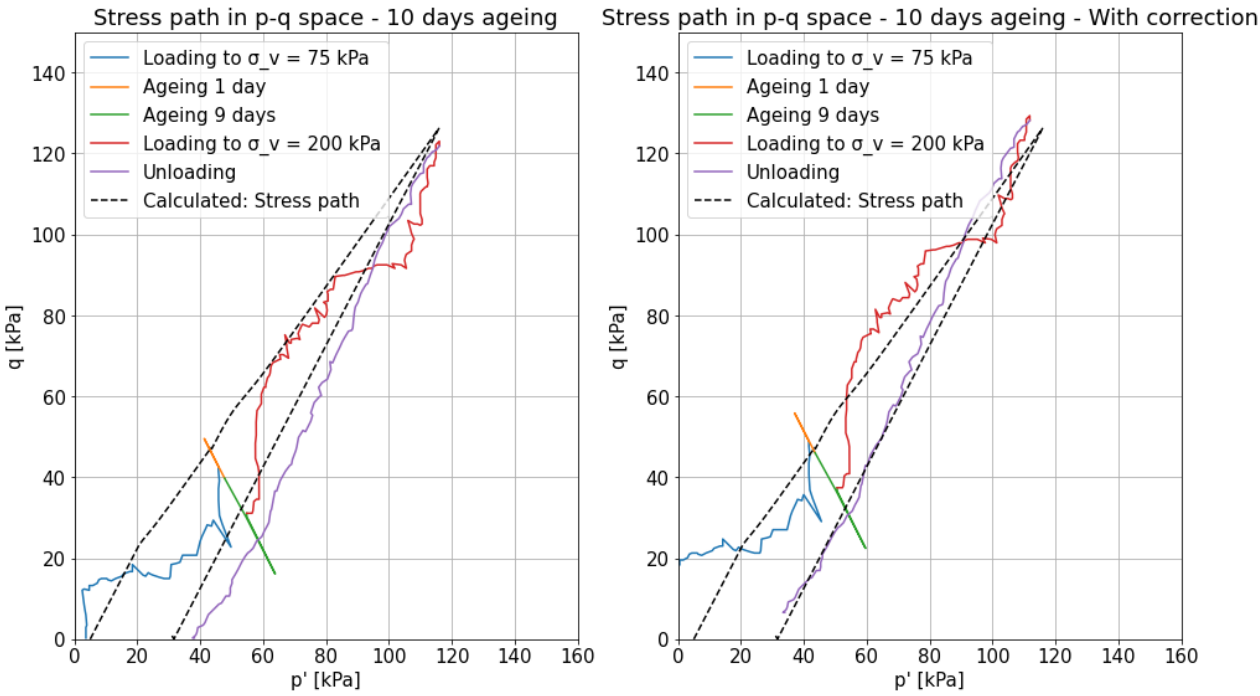

Figure 55: Stress path in p'-q space - 10 days ageing (experimental data from Polinder (2019).

As can be seen, the model follows the general trend of the stress path well. The details of the stress path such as the ageing behaviour shown in orange and green are not captured by the model. This is similar to what was seen in figures 52 and 53 where the horizontal experimental stress changed a lot more than the numerically predicted one. Overall the results can be stated to be satisfactory.

The second test used from Polinder (2019) evaluates the ageing behaviour of the soil (and can thus be used to test the ageing behaviour of the model). Shown below is a figure in which two samples are loaded to a certain effective stress after which they are left to age for 10 and 30 days respectively and then loaded again. It comes as no surprise that the sample that is left to age for longer shows more deformation since there is more time for the sample to creep. Slowing down of the creep behaviour can clearly be seen as well since the additional deformation in the extra 20 days is only a fraction of the deformation that was present in the first 10 days.

When looking at the model performance it can be seen that the model predicts this increase in deformation accurately. The reloading branch is predicted less accurately and the void ratio is underpredicted.

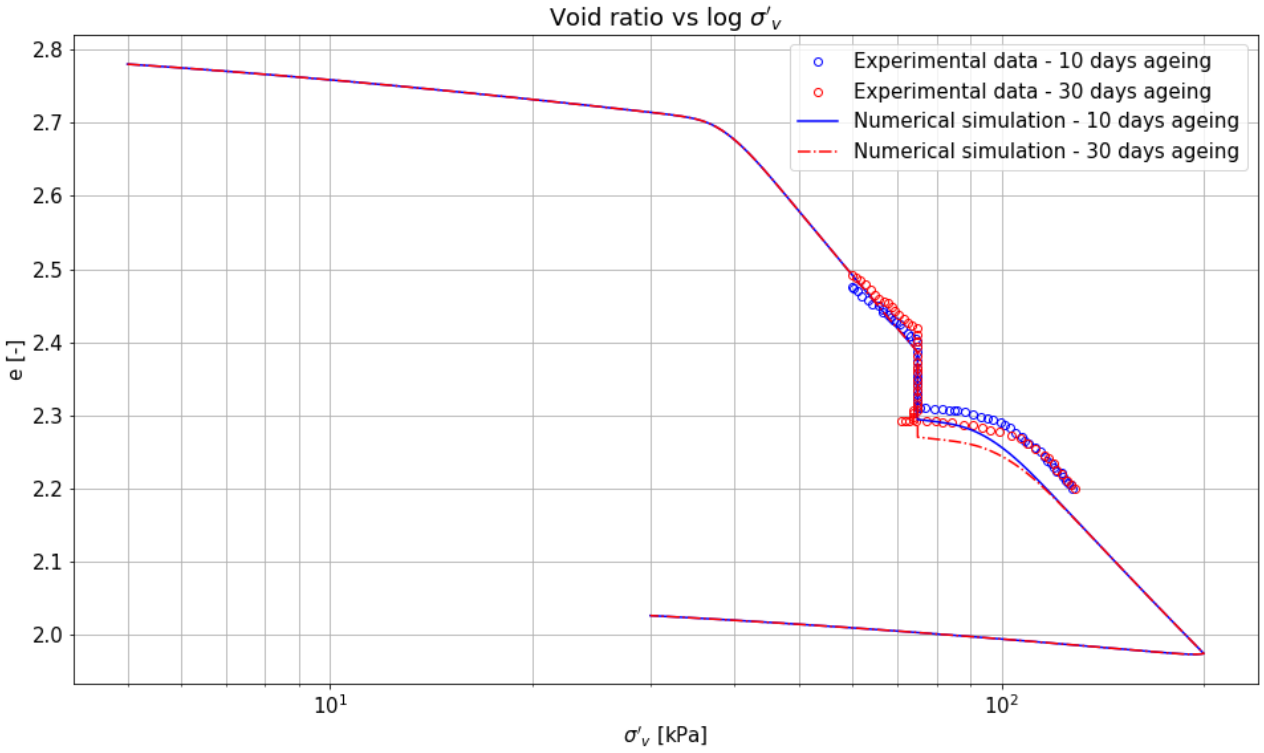

Figure 56: Void ratio vs $\log(\sigma'_v)$ for differently aged samples (experimental data from Polinder (2019)).

4.5.3 Overview final parameters

Shown below are the final values of all parameters used in the EVP model.

Table 7: Elastoplastic parameter values - OVP clay - EVP Model - Final values.

Parameter	Meaning	Value
M_c	Value of stress ratio q/p at critical state in compression	1.61
c_M	M_e/M_c	0.84
λ^*	Slope of compression line in ln(ν)-ln(p') plane	0.13
κ^*	Slope of rebound line in ln(ν)-ln(p') plane	0.014
ν	Poisson's ratio	0.20
N	Shape of the yield surface (1)	1.00
x	Saturation limit of anisotropy under constant stress ratio	1.80
C	Rate of evolution of anisotropy	4
k_f	Shape of the yield surface (2)	3.5
k_g	Shape of the plastic potential (always equal to 2.0)	2.0

Table 8: Elasto viscoplastic parameter values - OVP clay - EVP Model - Final values.

Parameter	Unit	Meaning	Value
μ	[s^{-1}]	Fluidity parameter	8e-10
N_ϕ	[-]	Strain rate coefficient	13

Table 9: Initial state variables - OVP clay - EVP Model - Final values.

Parameter	Unit	Meaning	Value
$\boldsymbol{\varepsilon_0}$	[-]	Initial strain	[0.0, 0.0, 0.0, 0.0, 0.0, 0.0]
$\boldsymbol{\sigma_0}$	[kPa]	Initial total stress	[5.0, 5.0, 5.0, 0.0, 0.0, 0.0]
$\boldsymbol{\alpha_0}$	[-]	Initial rotation of plastic potential	[-0.65/3*1, -0.65/3*1, 0.65/3*2, 0.0, 0.0, 0.0]
$\boldsymbol{\beta_0}$	[-]	Initial rotation of yield surface	[-0.65/3*1, -0.65/3*1, 0.65/3*2, 0.0, 0.0, 0.0]
$p_{c,0}$	[kPa]	Initial mean preconsolidation pressure	22.9
e_0	[-]	Initial void ratio	2.63 (Wegman, 2020), 2.78 (Polinder, 2019)

4.6 Conclusions

From sections 4.5.1 and 4.5.2 it can be concluded that the EVP model works accurately. The overall performance is good with some difficulties in predicting samples with different OCRs using one set of parameters or the prediction of the stress increase during ageing. In general though, the model captures the majority of the qualitative soil behaviour under different stress paths or test conditions. Because of this the model is deemed to be working accurately enough.

5 Unsaturated conditions

This chapter will explain in detail all the steps that are taken to develop and validate the unsaturated version of the model. In order to keep the development process simple, the influence of unsaturated conditions is first implemented in the original elastoplastic model and afterwards in the elasto viscoplastic model. Because of this, there are two unsaturated model versions. Both of these versions will be validated with the elastoplastic (EP) model first and the elasto viscoplastic (EVP) model second.

For the unsaturated elastoplastic model version, another SANICLAY model version is already available implemented in a hydromechanical driver that is able to account for the entire hydraulic stress history of the sample. Because both the saturated and unsaturated viscoplastic model versions are only available in a mechanical driver, the model validation of the unsaturated EP model will be done using the mechanical driver as has been done in the previous section. For the determination of the parameters and the state variables though, the hydromechanical driver will be used.

This chapter has a similar outline to the previous one. First of all, the adaptations that need to be made to the model to account for unsaturated conditions will be explained. After this, the experimental data from the literature which is used is explained in two steps. The first step is a description of the material that is being used in this literature after which the tests that are performed on this material are explained. This is followed by the parameter calibration required for the model to reproduce the tests results. The chapter ends with the model validation comparing the model output with the experimental data after which the findings are shortly concluded.

5.1 Model formulation

As was explained in section 2.3.4, the average soil skeleton stress approach will be used in order to account for unsaturated conditions in the model. To include this approach in the model, two changes need to be made. The first one is in the way the stress is calculated and the second change is the update in preconsolidation pressure due to the desaturation of the soil. These changes are highlighted below.

The stress in the model is now calculated in the following way.

$$\hat{\sigma}_{hk} = \sigma_{hk} - [S_r u_w + (1 - S_r)u_a]\delta_{hk} \tag{38}$$

The subscripts hk and the corresponding Kronecker delta make sure that only the normal stresses are updated and not the shear stresses.

This can be rewritten as

$$\hat{\sigma}_{hk} = \sigma_{hk} - u_a\delta_{hk} + S_r(u_a - u_w)\delta_{hk} \tag{39}$$

And simplified as

$$\hat{\sigma}_{hk} = \sigma_{net,hk} + S_r s\delta_{hk} \tag{40}$$

The preconsolidation pressure is determined as shown below. This equation will be referred to as the loading collapse rule in the remainder of this thesis.

$$\hat{p_c} = p_c^*\{1 + b_1[exp[b_2(1 - S_r^*)] - 1]\} \tag{41}$$

where:	$\hat{p_c}$	Unsaturated preconsolidation pressure
	p_c^*	Saturated preconsolidation pressure
	b_1, b_2	Model parameters
	S_r^*	Relative degree of saturation

p_c^* is the saturated preconsolidation pressure as it has been used up until now. Its hardening law is given in equation (27). It can be seen that the loading collapse has a slightly different shape than what was proposed by Jommi (2000). She proposed that $\hat{p}_c$ should be calculated as follows: $\hat{p}_c = (p_c^* - S_r s) + h(S_r)$, in the loading

collapse this function dependent on the degree of saturation is present but p_c^* is not first decreased with $S_r s$.

S_r^* is defined as

$$S_r^* \begin{cases} 1 & \text{for } S_r > S_{r,aev} \\ \frac{S_r - S_{r,res}}{S_{r,aev} - S_{r,res}} & \text{for } S_{r,aev} > S_r > S_{r,res} \\ 0 & \text{for } S_r < S_{r,res} \end{cases} \tag{42}$$

where: $S_{r,aev}$ Degree of saturation at the air entry value
$S_{r,res}$ Residual degree of saturation

The relation between the degree of saturation and suction is governed by the Soil Water Retention Curve (SWRC). The one that is adopted is Van Genuchten's SWRC as found in Romero and Jommi (2008).

$$S_r = C(s)[\frac{1}{1+(\alpha s)^n}]^m;\ C(s) = 1 - \frac{ln[1+\frac{s}{a}]}{ln(2)} \tag{43}$$

where α, n, m and a are fitting parameters.

5.2 Material description

No unsaturated time dependent data is available on OVP clay so therefore this soil cannot be used to help validate the unsaturated EVP model being developed in this chapter. The experimental data therefore had to be found in another piece of literature. Rezania et al. (2020) performed tests on London clay (LC), both loading/unloading as well as creep tests were performed on this clay at different levels of suction.

The London clay which was used was cored from the New Hook Farm in the Isle of Sheppey in the UK. The natural LC had a very high air entry value (AEV) (several MPa) due to the abundance of fine grained material. Because of this, larger sized aggregates were introduced in the sample to lower the AEV to a few hundred kPa to allow for testing at different water contents. Reconstituted soil samples were obtained by mixing the soil mixture described above with distilled water to about 1.5 times the liquid limit. Then, the slurry was consolidated at a vertical stress of 80 kPa for 5 days using a Perspex consolidometer. After this, the samples were quickly unloaded to minimize swelling and water absorption. At this point, samples could be taken from the apparatus in order to perform saturated tests. For unsaturated tests, the samples were taken from the consolidometer and air-dried to the desired water content. When this was reached, the samples were stored in air-tight containers for one week in order to obtain moisture equilibrium. Upon completion of these steps, samples were taken by pushing the oedometer ring into the samples (Bagheri et al., 2020; Rezania et al., 2020).

The table below shows the characteristics that are known about the natural soil.

Table 10: London clay characteristics (Rezania et al., 2020).

Property	Unit	Value
Mass content clay	[%]	64
Mass content silt	[%]	34
Mass content sand	[%]	2
In situ water content	[%]	29-35
Plastic limit	[%]	19-24
Liquid limit	[%]	70-78
Specific gravity	[-]	2.67
Vertical hydraulic conductivity at 20 °C	[m/s]	2.5e-10
Classification	[-]	High plasticity clay

5.3 Test description

This section will contain a description of the tests performed by Rezania et al. (2020). They performed two sets of tests, the first one being loading/unloading tests and the second set being a set of creep tests at different suctions. The first set is used to validate the EP version of the model, the second set is used in the EVP model validation. Similar to the previous chapter, some of the tests will be used in the parameter determination as well. In this case three loading/unloading test and one creep test are used for this purpose. The loading/unloading tests are the saturated sample, and samples with an initial suction of 513 and 1907 kPa. The parameter determination for the EP model is only done using the hydromechanical driver so the model validation of the mechanical driver is not influenced by this. The creep test that is used is a saturated sample with an applied load of 178 kPa. What all these tests mean is explained in below in detail.

5.3.1 Tests for EP model

In order to evaluate the elastoplastic version of the unsaturated model, tests are required where the time variable is not of importance yet. This data is found from multi-staged loading (MSL) tests in Rezania et al. (2020). In these tests, samples are loaded in multiple steps and following this unloaded in multiple steps as well. For saturated samples, conventional oedometer cells were used and loading was applied in 24h intervals. In each loading step the load was doubled starting at 11 kPa and ending at 1421 kPa. After reaching this load, the sample was unloaded, again in 24h intervals with halving the load at each step until 44 kPa was reached. The 24h intervals were used to ensure dissipation of built up pore water pressures during loading and to ensure complete swelling during unloading (Rezania et al., 2020).
For unsaturated samples, specimens were places in suction monitored oedometer cells which were equipped with high-capacity tensiometers (HCT) to measure the suction throughout the tests. Again, loading was applied in 24h intervals with the load being doubled after each step. This time around, the final loading step was smaller than a doubling of the previous load. This was done to avoid disturbance of the structural properties of the specimens (Rezania et al., 2020).

During all tests, the authors state that no water was expelled and therefore it can be stated that the tests were carried out at constant water content. The suction is not constant throughout the test since due to deformation during loading the degree of saturation increases and the suction decreases. Because of this, the samples are identified by their water content and corresponding initial suction value.

In total, 5 samples with different initial suction values are used as well as the saturated sample. These initial suction values are: 326, 433, 513, 1405 and 1907 kPa respectively. The table below shows the loading paths used for the samples, this is followed by a figure showing the experimental data.

Table 11: Loading paths for loading/unloading tests (from Rezania et al. (2020)).

Initial suction (s_0) [kPa]	Loading path [kPa]
Saturated (0)	11-22-44-89-178-355-710-1421-710-355-178-44
326, 433 and 513	22-44-89-178-355-710-1110-710-355-178-89-44-22-11
1405 and 1907	5-50-100-200-300-400-500-580-500-400-300-200-100-50-25

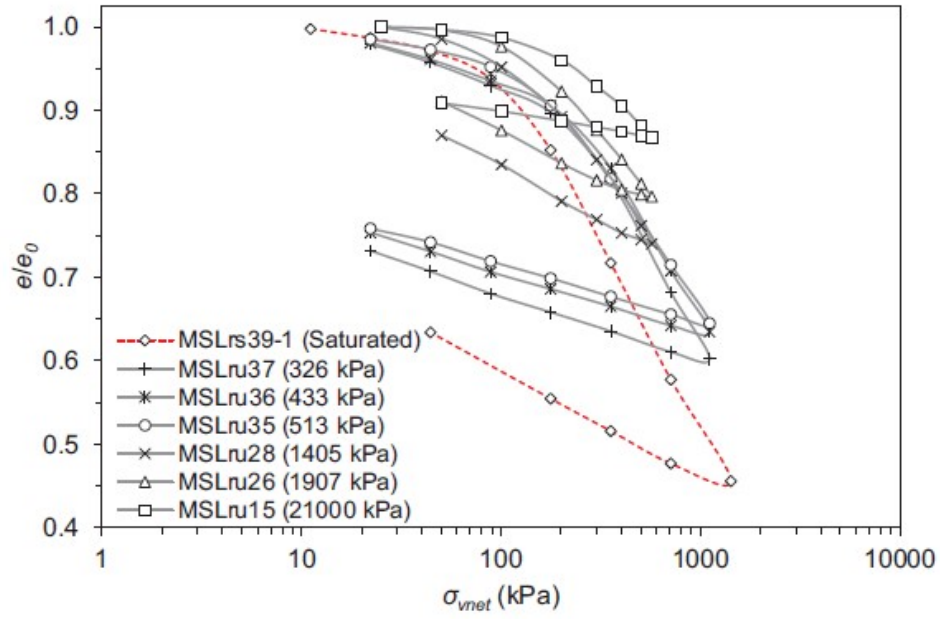

Figure 57: Experimental loading/unloading results on London clay from Rezania et al. (2020).

From the results, it can be seen that as the initial suction value increases, the total deformation decreases. Next to this, the slope of the primary loading curves decreases with an increase of initial suction as well. This last behaviour can also be seen in the development of the compression parameters (expressed in C_c and C_s, subscript c for compression and s for swelling) with suction as reported by the authors. Note that in figures 57 and 58, a test with an initial suction of 21000 kPa is included as well. In this work this test is excluded because the suction level is so high that it is deemed unrealistic for the applications of interest in this work.

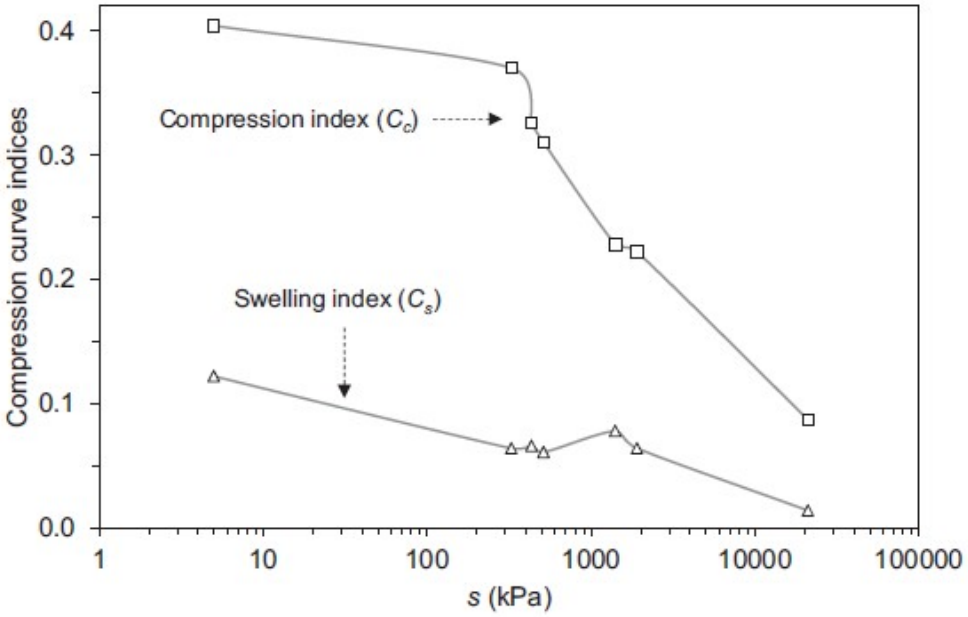

Figure 58: Development of compression parameters with suction (Rezania et al., 2020).

5.3.2 Tests for EVP model

Unsaturated creep data is available from single-stage loading (SSL) tests from Rezania et al. (2020). Reconstituted samples were used to avoid problems regarding the coupled effects of suction and soil structure. A load was applied in a single step after which the specimens were left subjective to creep. Only one loading step was used to make sure that loading effects and creep between loading stages could not influence the results. To avoid problems caused by sudden loading, the load was applied slowly with a rate of 8 to 10 kPa per hour. After the load was applied, the specimens were left subjective to creep for 19 to 94 days. It should be noted that, regarding total stresses, all specimens were loaded beyond their preconsolidation pressures to make sure the creep response in a normally consolidated state was evaluated. However, the present suction causes an apparent preconsolidation pressure, this causes the initial creep response to be relatively stiff. Both saturated and unsaturated samples were tested. For the saturated samples, the conventional oedometer cells were used similar to the MSL tests. Five samples were tested that were loaded to 178, 222, 355, 444 and 666 kPa respectively. For the unsaturated samples, the suction monitored oedometer cells equipped with HCTs were used again (Rezania et al., 2020).

Different combinations of applied loads and initial suction values were used to be able to assess both the potential influence of load and suction on the creep response of the specimens. The table below summarises all the different tests that were performed. Again, the results are presented after the table. Only the unsaturated samples are treated in detail because of their higher significance in the model validation and their more complex test program.

Table 12: Combinations of loads and initial suction values for creep tests (from Rezania et al. (2020)).

Initial suction (s_0) [kPa]	Water content (w) [%]	Applied load (σ_{vm}) [kPa]	Test duration [days]
326	37	666	28
326	37	444	29
326	37	355	36
433	36	666	28
433	36	444	21
433	36	355	34
513	35	355	34
513	35	222	34
513	35	178	27
1405	28	666	20
1405	28	444	21
1405	28	355	28
1907	26	222	23
1907	26	178	23

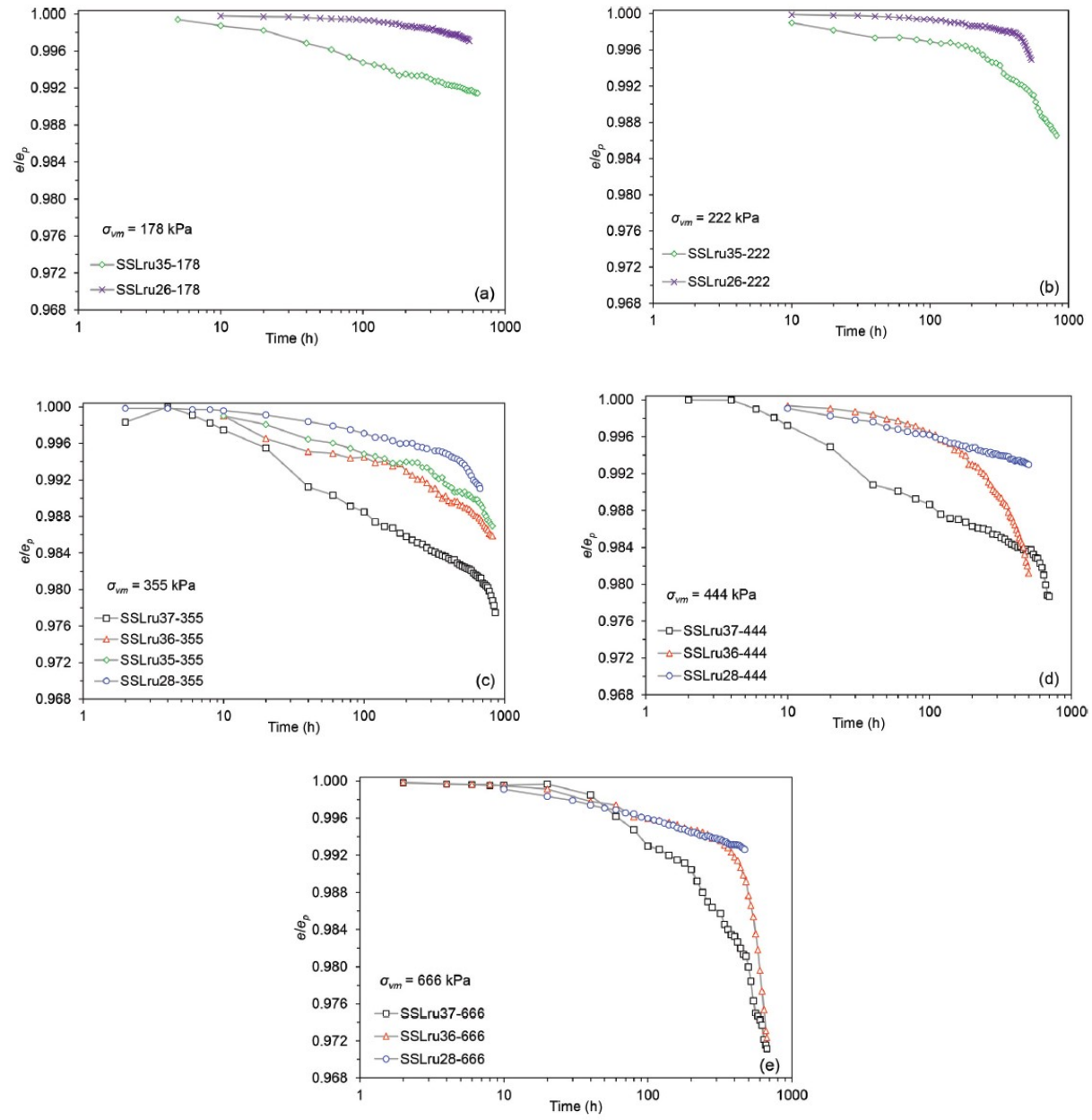

Figure 59: Results of unsaturated SSL tests at different stress level from Rezania et al. (2020).

The data in figure 59 is presented on a normalised axis dividing the void ratio by e_p which is the void ratio at the end of primary consolidation and is measured 24h after completion of loading.
Looking at this data, several observations can be made. The first and most obvious one is that as the initial suction increases, the creep deformation decreases. This is most clearly shown in figure 59c where 4 samples are presented with different initial suction values and all are loaded to 355 kPa. The higher the initial suction is (the lower the initial water content), the less creep deformation is present.
Next to this, the authors state that the response is stress dependent as well but that this dependency is mostly present at the end of the tests. What is most likely meant by this is the slope increase that is observed when a sample with the same initial suction is loaded to a higher stress. The problem with this observation though is that this is not always the case. When the samples with initial suction 1405 kPa (water content 28%) and loads 355, 444 and 666 kPa are compared it can be seen that an increase in the slope is observed at the end of the loading stage when 355 kPa is applied. When a load of 444 and 666 kPa is applied, this increase is not

spotted. Because of this, the stress dependency cannot be defined clearly.
The final takeaway is that the creep response appears to be suction dominated. Looking at the samples with 1405 kPa initial suction again, it can be seen that when the load changes from 444 to 666 kPa (load increase of 50%), the creep response remains more or less the same. This dominance of suction does reduce when the initial suction decreases. A good example of this are the samples with an initial suction of 433 kPa (water content 36%), looking at the plots with loads 355, 444 and 666 kPa again, it can be seen that as the load increases the creep response increases as well. This shows that the suction dominance decreases as the suction itself reduces.

5.4 Parameter determination

In order to be able to get the model to reproduce the experimental results which are explained above, the model parameters need to be calibrated to the used material which in this case is London clay. Shown below is an overview of all the parameters in the model. The hydromechanical model that is used in the parameter determination (except for the viscosity parameters since the model is only elastoplastic) uses λ and κ instead of λ^* and κ^*. After all parameters are determined and the mechanical model is used for the model validation, the values for λ^* and κ^* will be given.

- Elastoplastic parameters

M_c	Value of stress ratio q/p at critical state in compression
c_M	M_e/M_c
λ	Slope of compression line in ν-ln(p') plane
κ	Slope of rebound line in ν-ln(p') plane
ν	Poisson's ratio
N	Shape of the yield surface (1)
x	Saturation limit of anisotropy under constant stress ratio
C	Rate of evolution of anisotropy
k_f	Shape of the yield surface (2)
k_g	Shape of the plastic potential (always equal to 2.0)

- Initial state variables

$\boldsymbol{\varepsilon_0}$	Initial strain
$\boldsymbol{\sigma_0}$	Initial total stress
$\boldsymbol{\alpha_0}$	Initial rotation of plastic potential
$\boldsymbol{\beta_0}$	Initial rotation of yield surface
$p^*_{c,0}$	Initial mean preconsolidation pressure
e_0	Initial void ratio

- Unsaturated parameters

b_1, b_2	Loading collapse parameters
$S_{r,aev}$	Degree of saturation at air entry value
$S_{r,res}$	Residual degree of saturation
a, n, m, α	Fitting parameters SWRC

- Viscosity parameters

μ	Fluidity parameter
N_ϕ	Strain rate coefficient

The hydromechanical model is capable of including the drying process to the desired suction before sampling as is done in the sample preparation. Because of this, the state variables will be determined twice. Once before drying (the initial state) and once after drying which is right before loading. The state variables before loading are required to initialise the mechanical model which is used in the model validation. After all parameters are determined using the hydromechanical driver, this driver will be used to simulate only the drying process in order to obtain the state variables before loading (after drying) as well.

5.4.1 EP parameters

First of all, the elastoplastic parameters are determined. To do this, use is made of the PhD thesis of Gasparre (2005) who performed extensive laboratory testing on London clay. The following parameters were determined.

- $M_c = 0.85$ (taken from figure 7.11)
- $\lambda = 0.168$ (taken from table 7.1)
- $\kappa = 0.064$ (taken from table 7.1)
- $\phi'_{cv} = 21.3°$(given on page 234)

Note that the brackets indicate where in the PhD thesis the parameter values are taken from. These references do not refer to figures, tables or pages in this thesis.
For the sake of simplicity, c_M is assumed to be 1. Collins and Yu (1996) report a value of 0.3 for the Poisson's ratio.

This leaves N, x, C and k_f to be determined. N and x are calculated following Dafalias et al. (2006) resulting in 1.27 and 1.84 respectively. Experience has shown that in general N is lower than M_c though so as a first attempt it will be set equal to M_c. C and k_f are set to 4 and 2.0 initially respectively and will be changed if the results require them to.

5.4.2 Initial state variables

Since the samples are consolidated at a vertical stress of 80 kPa as is mentioned in section 5.2, the mean preconsolidation pressure can be determined by using K_0. Because the samples are reconstituted and afterwards consolidated, the samples are normally consolidated at the end of the consolidation stage and therefore Jaky's relationship (equation (3)) can be used to calculate K_0. As shown above, Gasparre (2005) gives 21.3° for ϕ'_{cv}. This leads to $K_0 = 0.64$ and with it $p^*_{c,0} = 61$ kPa. The initial void ratio is given by Rezania et al. (2020) as 0.93. Just like in section 4.4.2, it is assumed that the initial strain (ε_0) is zero and that after the unloading post consolidation a small stress is still present leading to $\sigma_0 = 5.0$ kPa isotropic. The initial stress is assumed to be equal to 11.0 kPa isotropic for the saturated sample since that is the stress level at which the void ratio is normalised in figure 57.
The initial rotation is determined as η_k/x as explained by Dafalias (1987). η_k is calculated as $\frac{3(1-K_0)}{1+2K_0}$ and with K_0 known this becomes 1.47. With x equal to 1.84, the initial rotation becomes 0.26. The hydromechanical driver is formulated in triaxial space so the initial rotation is stated as a scalar. Again, α_0 is assumed to be equal to β_0.

Table 13: Initial state variables - London clay.

Variable	Unit	Value
$\boldsymbol{\varepsilon_0}$	[-]	[0.0, 0.0, 0.0, 0.0, 0.0, 0.0]
$\boldsymbol{\sigma_0}$[1]	[kPa]	[5.0, 5.0, 5.0, 0.0, 0.0, 0.0]
$\boldsymbol{\alpha_0}$	[-]	0.26
$\boldsymbol{\beta_0}$	[-]	0.26
$p^*_{c,0}$	[kPa]	61.0
e_0	[-]	0.93

[1] The saturated sample started at an isotropic pressure of 11 kPa, all unsaturated samples at 5 kPa.

The required suction is obtained by setting the air pressure as 0 relative to the atmospheric pressure and changing the water pressure to become negative equal to the desired suction.

5.4.3 Unsaturated parameters

The unsaturated parameters belong to the loading collapse rule (b_1 and b_2) and the Soil Water Retention Curve ($S_{r,aev}$, $S_{r,res}$, a, n, m and α). The parameters belonging to the SWRC will be determined first. Rezania et al. (2020) reports the following SWRC for London clay. Only the drying path is analysed since the samples are prepared by drying them from a saturated state.

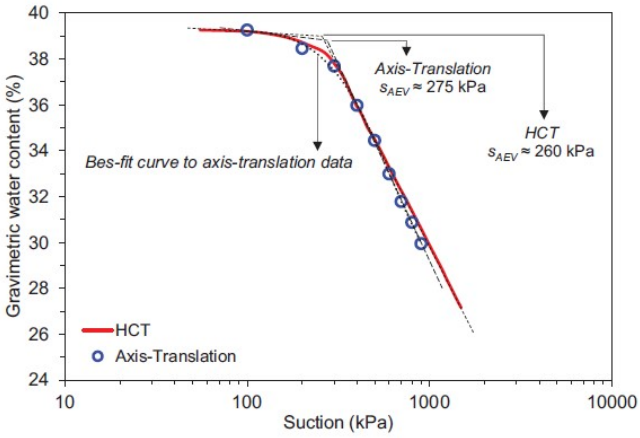

Figure 60: Soil Water Retention Curve determined for the main drying path of London clay (Rezania et al., 2020).

It has to be noted that the SWRC above is reported in gravimetric water content vs suction. The equation for the SWRC that is used in this work (Van Genuchten's SWRC) relates degree of saturation to suction (equation (43)). Therefore, the following relationship needs to be used to convert degree of saturation to gravimetric water content.

$$w * G_s = S_r * e \tag{44}$$

In the equation above, G_s is the specific gravity which Rezania et al. (2020) reports to be 2.67. In order to calibrate the SWRC parameters (a, n, m and α), trial runs need to be executed. Starting values for the parameters are taken from Romero and Jommi (2008) and a sensitivity analysis was performed which is reported in appendix A.4.1. With this, it was found that using a = 1e6 kPa, n = 4.5, m = 0.05 and α = 0.0036 kPa^{-1} resulted in a good fit to the experimental SWRC as is shown below.

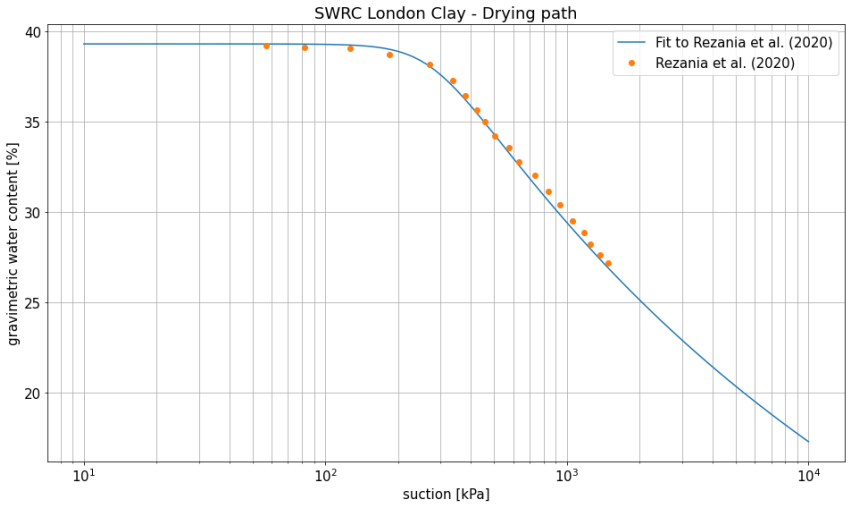

Figure 61: Fitted SWRC to the experimentally obtained one.

Using the fitted SWRC parameters, the degree of saturation at the air entry value (AEV) and the residual degree of saturation can be determined. Figure 60 shows that the air entry value is at a suction of 260 kPa (the axis translation technique introduced an error causing it to give a different AEV (Bagheri et al., 2020)), at this suction the degree of saturation is 0.97 ($S_{r,aev}$). It is assumed that the residual degree of saturation can be taken at a suction value of 1e5 kPa. At this value, the degree of saturation is 0.23 ($S_{r,es}$).

The other parameters belonging to the unsaturated part of the model are b_1 and b_2 and are relevant for the loading collapse rule (equation (41)). The loading collapse rule governs the expansion of the yield surface due to desaturation. Therefore, the values for b_1 and b_2 can be determined by comparing experimental mean preconsolidation values to the numerically predicted ones. The moment at which this comparison will be made is after the drying stage since before the drying stage the samples are saturated so b_1 and b_2 do not affect the results and during the loading stage they need to be known already in order to simulate the tests.
Unfortunately, the experimental preconsolidation pressures are not given by Rezania et al. (2020). Because of this, a possible range of values needs to be determined based on the information that is presented by the authors. Using the average soil skeleton stress approach, there are two contributions to the average stress. The first one is the net stress and the second one is the influence of the suction. How these contributions are determined is explained in detail below.

The first step in defining the experimental preconsolidation pressure is by looking at the net preconsolidation stress which can be found by using the loading/unloading data. Shown below is the test result for the sample with an initial suction of 513 kPa. As can be seen, two lines are drawn, the first one is parallel to the stiff branch of the data (this branch is assumed to be in the elastic domain) and another one parallel to the plastic domain of the deformation graph. The preconsolidation pressure can be estimated by the value at the point where the two lines intersect.

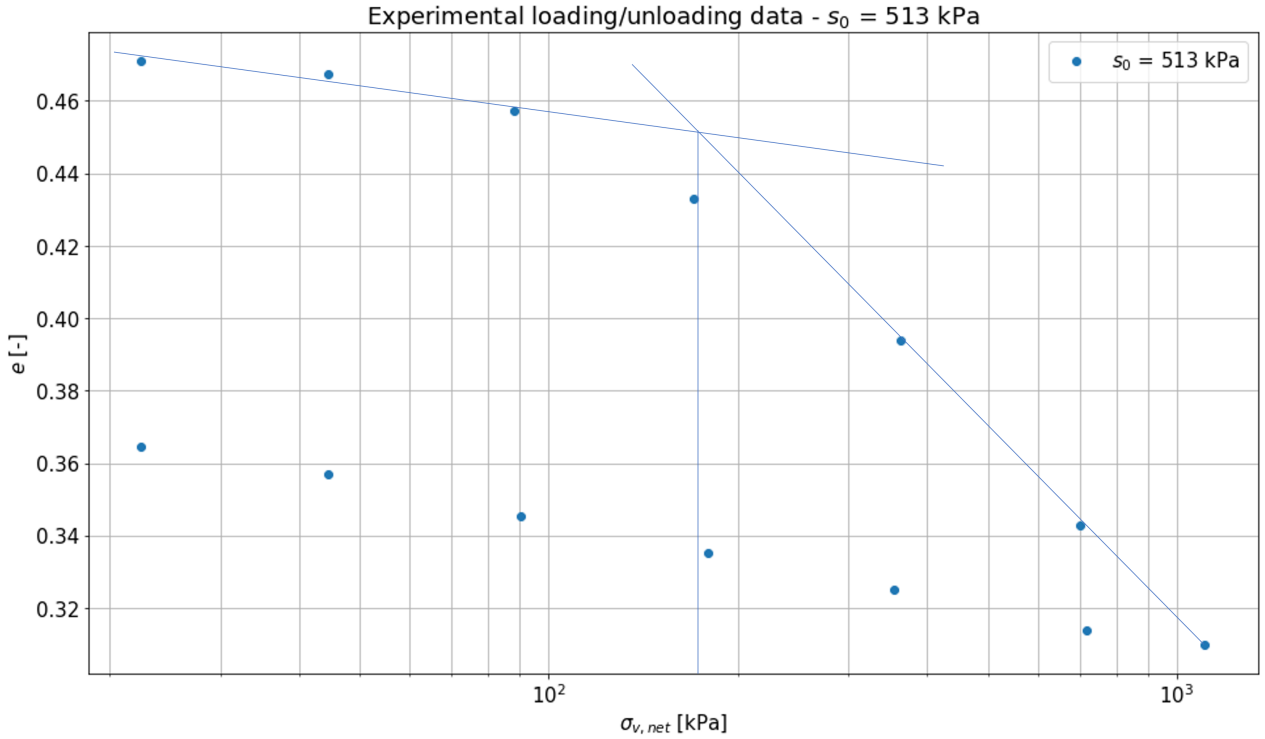

Figure 62: Determination of $\sigma_{v,net,c}$ for the sample with an initial suction of 513 kPa.

There are two things that need to be noted from the figure above. The first one is that the net vertical preconsolidation stress is determined. Because after drying the soil is in an isotropic stress state, the vertical stress is equal to the mean stress so therefore no corrections need to be made.

The second point is that in the figure above, the y-axis is not normalised whereas the original data in figure 57 was presented on a normalised scale. The reason why this is done is because on a normalised scale, the procedure performed above cannot be done. The non-normalisation is done by multiplying the vertical axis with the void ratio after drying. This void ratio is obtained by simulating a drying analysis in the hydromechanical driver. For this drying analysis b_1 and b_2 were assumed to be 0.11 and 8.2 respectively as was found in Romero and Jommi (2008). Due to a lack of better options no better guess for the parameters could be used. The process explained above is repeated for all samples. As has been stated in section 5.3.1, samples were tested at initial suction values of 326, 433, 513, 1405 and 1907 kPa. The vertical net preconsolidation pressures that were found for each of these samples are reported below. For the sake of completeness, the obtained initial void ratios after drying (before loading) used in the non-normalising of the y-axes are reported as well.

Table 14: Experimental net vertical preconsolidation stresses.

		Initial suction [kPa]				
Variable	Unit	326	433	513	1405	1907
e_0 (Before loading)	[-]	0.53	0.50	0.48	0.36	0.33
$\sigma_{v,net,c}$	[kPa]	246	240	172	120	128

The second contribution the the preconsolidation pressure is the role of suction. Rezania et al. (2020) reports the suction values at each load throughout the loading/unloading tests so with the vertical net preconsolidation pressure known, the corresponding suction value can be determined. Shown below is the suction vs load graph for the sample with an initial suction of 513 kPa.

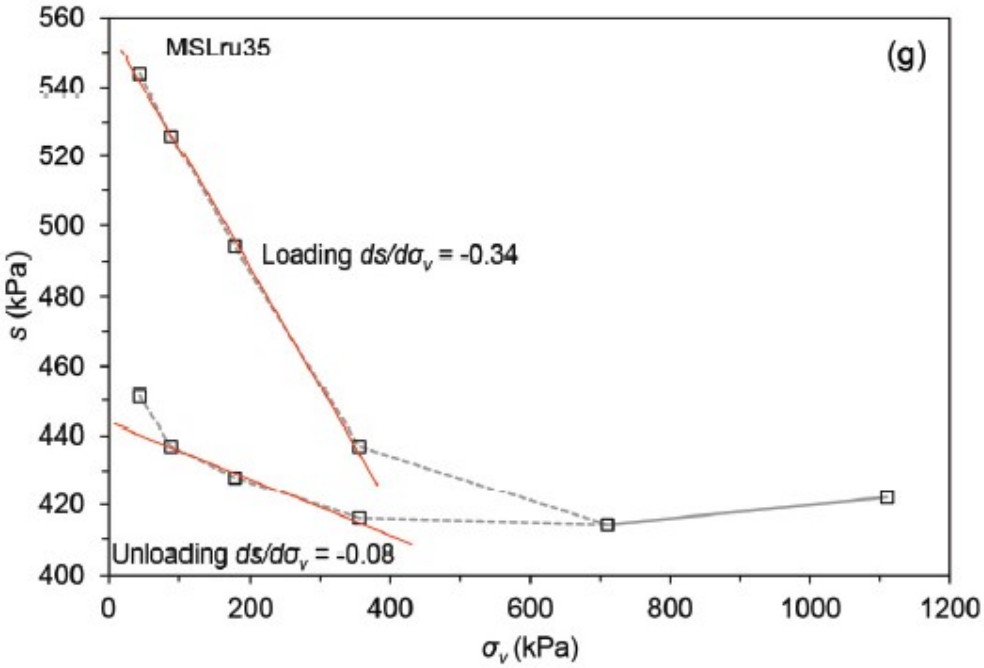

Figure 63: Suction development vs the applied load. Note that since u_a is zero at all times, σ_v is equal to $\sigma_{v,net}$ (Rezania et al., 2020).

It can be seen that at the determined $\sigma_{v,net,c}$ of 172 kPa, the suction is about 500 kPa. Using the calibrated SWRC from the start of this subchapter, the degree of saturation can be determined corresponding to this suction level. Doing so gives a degree of saturation of 0.872 and therefore the role of suction (known as $S_r s$) can be calculated to be 500*0.872 = 436 kPa. Together with the net preconsolidation pressure of 172 kPa,

the average soil skeleton mean preconsolidation pressure is determined to be 608 kPa. This procedure is again repeated for all samples and the results are presented in the table below. Note that for the sample with $s_0 =$ 1907 kPa, Rezania et al. (2020) did not report the value of suction during the tests so this procedure could not be done for this sample.

Table 15: Determination of experimental preconsolidation pressure. Note that after drying the stress state is isotropic so $\sigma_v =$ p.

		Initial suction [kPa]				
Variable	Unit	326	433	513	1405	1907
e_0 (Before loading)	[-]	0.53	0.50	0.48	0.36	0.33
$\sigma_{v,net,c}$	[kPa]	246	240	172	120	128
suc at $\sigma_{v,net,c}$	[kPa]	275	388	500	1260	N/A[1]
S_r at $\sigma_{v,net,c}$	[-]	0.967	0.918	0.872	0.710	N/A[1]
$\hat{p}_c$ - Using suction at $\sigma_{v,net,c}$	[kPa]	511	596	608	1015	N/A[1]

[1] N/A = Not Available

In order to obtain a range of possible experimental preconsolidation pressures and because the steps above could not be performed for the sample with $s_0 = 1907$ kPa, an additional way of determining the role of suction needed to be used. This second method is by assuming either drained or undrained conditions and calculating relevant values of suction and degree of saturation correspondingly. Rezania et al. (2020) report that their tests are performed at constant water content which would lead to the assumption that the tests are performed undrained. However, looking at figure 63, it can be seen that the suction change is relatively small for a large range of $\sigma_{v,net}$. If the tests were performed perfectly undrained, it would be expected that the suction would drop to values closer to zero as the sample deformed and the degree of saturation increased towards one. Next to this, the hydromechanical driver was used to predict the deformation behaviour governing the provided suction throughout the test using a preliminary set of parameters. This prediction was compared to the one using a drained and undrained analysis and it was found that the results are much closer to a drained analysis than an undrained one. Because of this, it is likely that during the tests some drainage was allowed and therefore the tests are partially drained behaviour. This finding will be touched on later in this chapter as well to confirm the choice of a drained approach.
In a drained analysis, the suction is constant throughout the test. With this known, the contribution of suction is now determined with the reported initial suction values and their corresponding degrees of saturation. This way of determining the contribution of suction yields new possible values for the experimental mean preconsolidation pressure as is reported in table 16 below.

Table 16: Determination of experimental preconsolidation pressure using two methods.

		Initial suction [kPa]				
Variable	Unit	326	433	513	1405	1907
e_0 (Before loading)	[-]	0.53	0.50	0.48	0.36	0.33
$\sigma_{v,net,c}$	[kPa]	246	240	172	120	128
$S_{r,0}$	[-]	0.945	0.899	0.868	0.693	0.646
s_0	[kPa]	326	433	513	1405	1907
$\hat{p}_c$	[kPa]	554	629	617	1094	1361

Using section 5.4.3 and table 16, a range of experimental average mean preconsolidation pressures is obtained. With this known, numerical prediction can be generated of which the output can be compared to the experimental results. Numerical predictions are obtained using three sets of b_1 and b_2, these are 4.0/2.0, 2.0/1.0 and 1.0/0.5 respectively. The results of these analyses and the obtained experimental window are presented below.

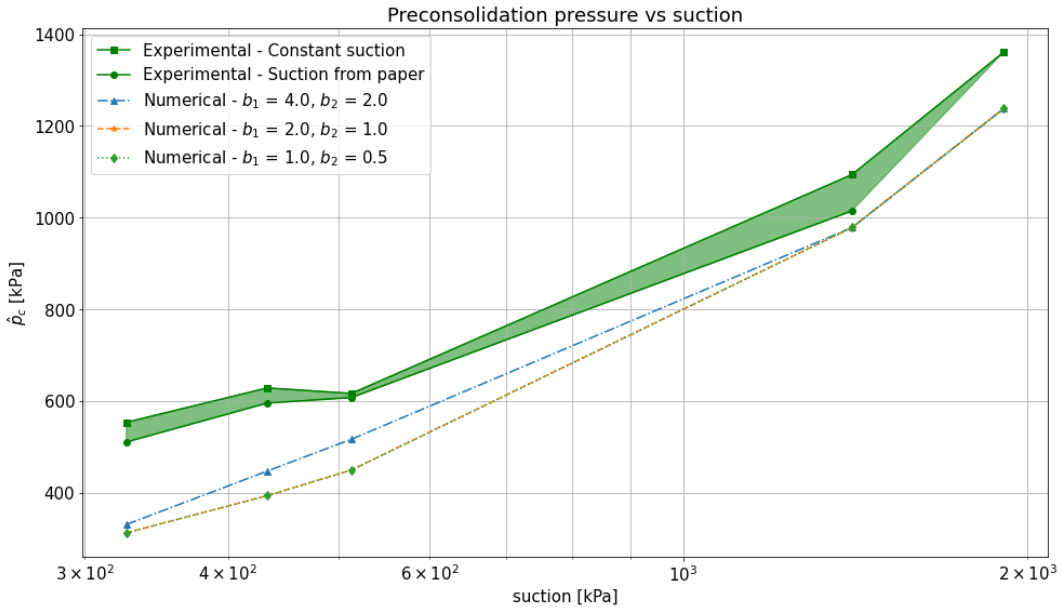

Figure 64: Numerical vs experimental preconsolidation pressure with suction for three sets of b_1 and b_2.

It can be seen that no set of b_1 and b_2 matches the experimental data accurately. The set using $b_1 = 4.0$ and $b_2 = 2.0$ is the closest to the experimental window and therefore these values will be selected as a first approximation.

With all parameters are known, the loading/unloading tests can be simulated. As has been stated before, this is only done using the hydromechanical driver since this driver can simulate the drying process. Because of this, the initial values for the state variables are the ones before drying which are known rather accurately. The results for the saturated sample and the samples with $s_0 = 513$ and 1907 kPa are shown below using drained analyses. For the sample with $s_0 = 513$ kPa, an additional analysis is performed where at each loading step the suction is governed following figure 63.

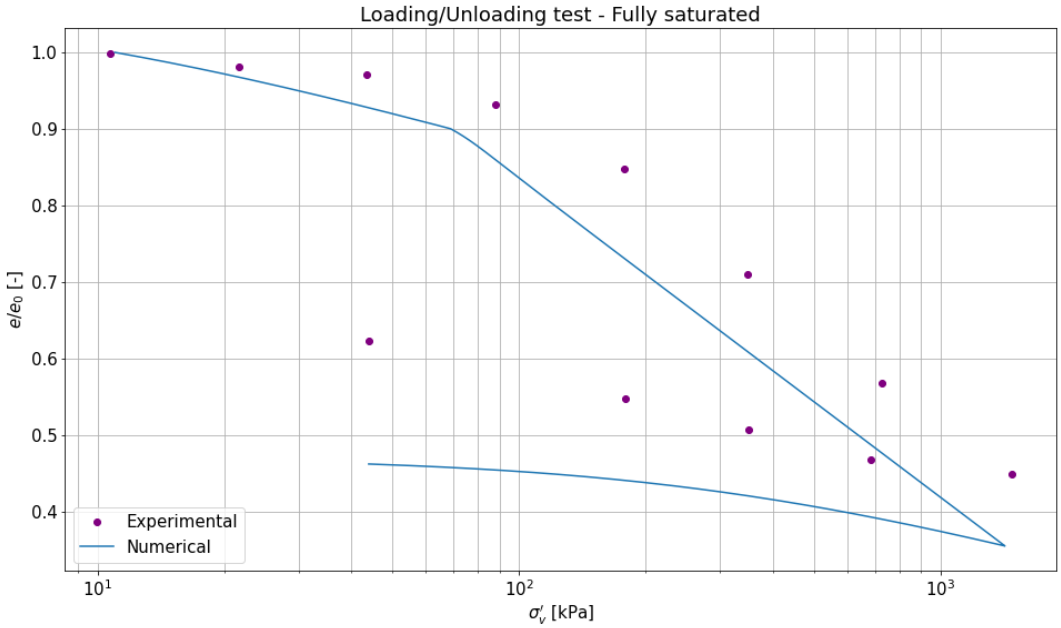

(a) Saturated sample.

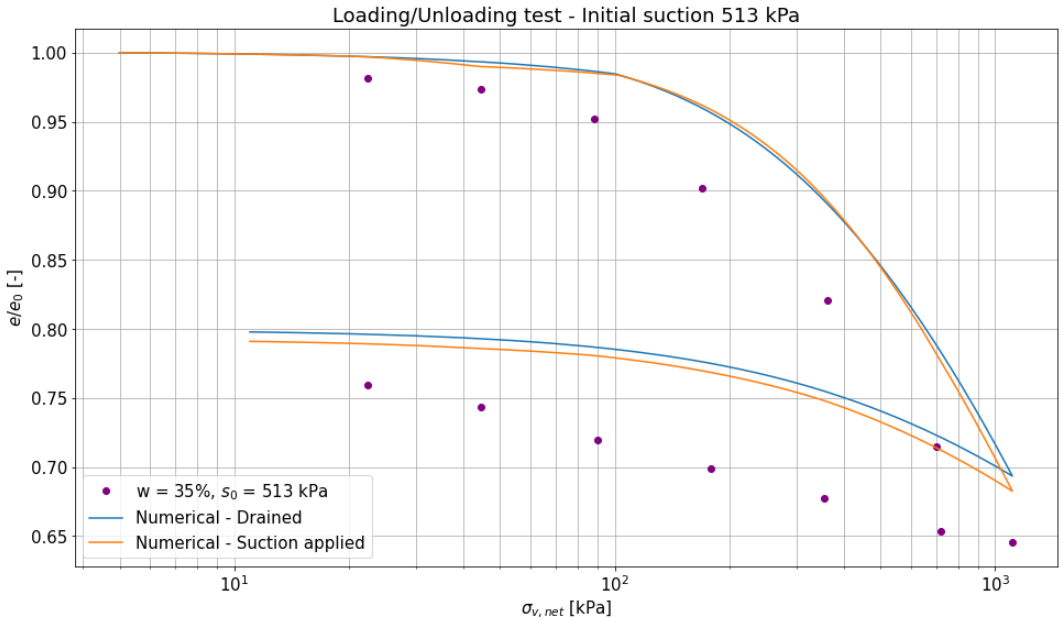

(b) $s_0 = 513$ kPa.

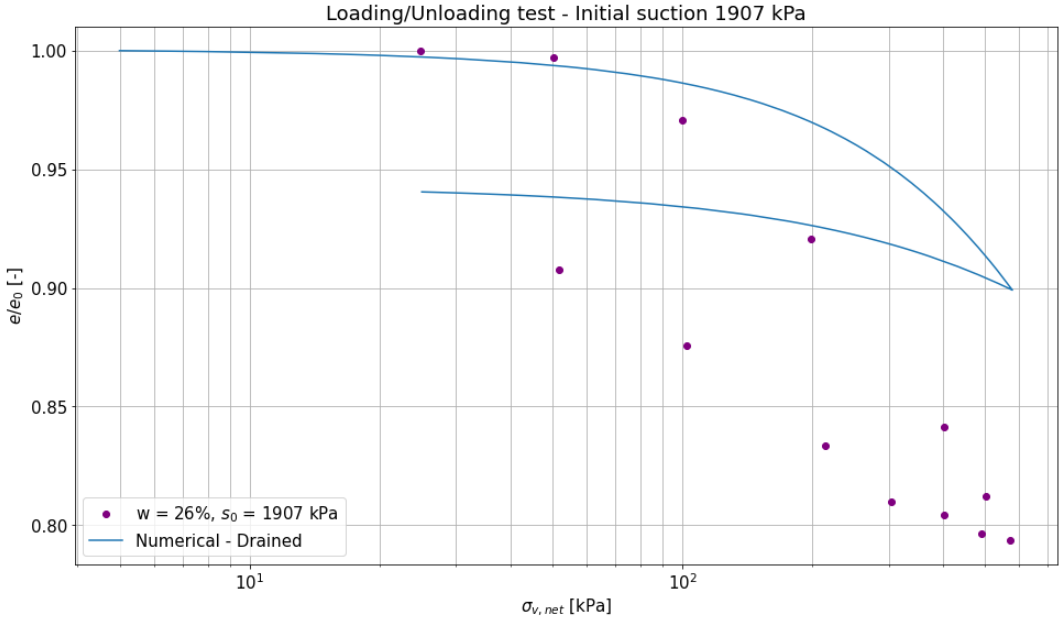

(c) $s_0 = 1907$ kPa.

Figure 65: Deformation behaviour predicted using a drained analysis in the hydromechanical driver.

There are three main conclusions that can be drawn from the three figures above. The first one is that a drained analysis is very close to the analysis where the suction is governed throughout the test. Because of this, it is concluded that it is better to perform drained analyses rather than undrained ones.

The second one is that the value of κ is not correct. Looking at the figure belonging to the saturated sample (figure 65a), it can be seen that the initial model response shows too much deformation and that during unloading the model predicts too little rebound. Since κ governs both slopes, it can only be tuned to match one of the branches accurately. It is decided to focus on the initial response of the soil rather than the

unloading response and therefore κ is lowered to a value of 0.040.

The final takeaway is that for the unsaturated samples, the assumption that the initial response of the soil is elastic does not fit the material response properly. Figure 65b shows that the initial slope of the numerical output is a lot smaller than the experimental data. Only after the plastic domain is entered does the numerical output match the experimental data better. Looking at the followed stress path shown below, it can be seen that due to the high b_1 and b_2, the yield surface is pushed out at a high rate during drying causing the stress state to be inside the yield surface at the end of drying.

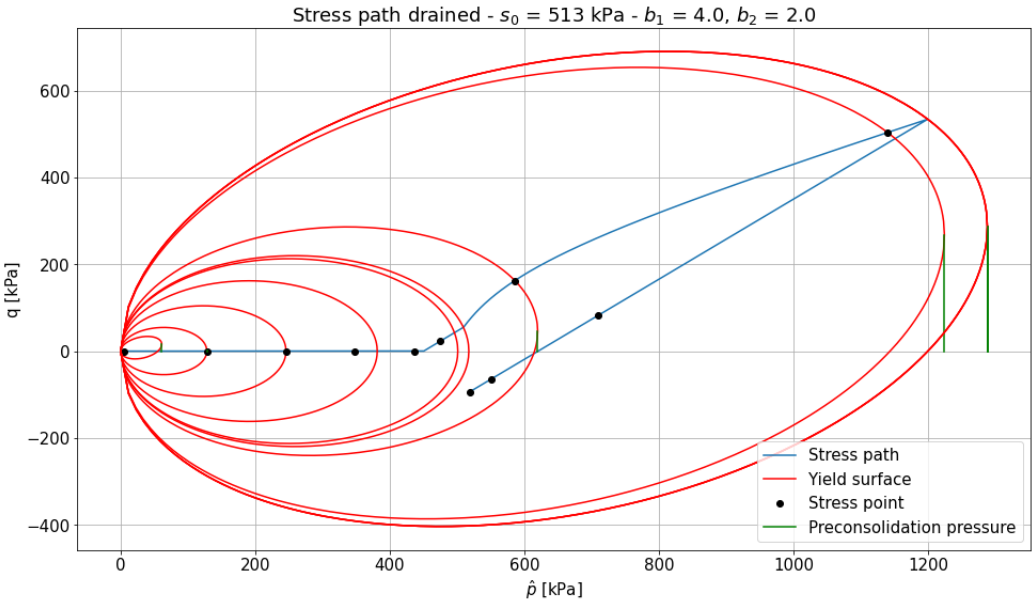

Figure 66: Full stress path including drying - s_0 = 513 kPa.

Instead, it could be the case that the sample touched the yield surface earlier than expected by looking at the experimental data. If the stress point is on the yield surface at the end of drying instead of in it and therefore the full loading part of the test is in the plastic domain, the experimentally observed behaviour can still be explained. It can be seen that the experimental data during loading has roughly two branches, the first one shows relatively stiff behaviour (this part was assumed to be elastic initially) and the second branch is much steeper and is clearly in the plastic domain (figure 65b). The initial stiff response can be allocated to the fact that the soil after drying is in an isotropic stress state and upon loading it transitions to a K_0 stress state. During this transition, the mean stress does not increase as much which can explain less deformation at an increase of the vertical stress. Figure 66 shows that when the soil reaches the plastic domain, the slope of the stress path during transition to the K_0 line is a lot steeper than the slope of the stress path after this line has been reached. This argumentation can explain the initial stiff response as an alternative to the originally assumed elastic branch.
Another argument for this reasoning is that Rezania et al. (2020) only speak of a compression index and a swelling index but not of a reloading index (figure 58). If indeed the loading part of the test is completely in the plastic domain, there is no reloading branch and the only elastic part of the test is the unloading part during which the soil swells.

An important consequence of this is that the way the experimental preconsolidation pressure was determined is incorrect. The procedure performed in figure 62 determining $\sigma_{v,net,c}$ cannot be done since a line alongside the elastic domain cannot be drawn. A consequence of this is that determining the suction at $\sigma_{v,net,c}$ using figure 63 cannot be done since $\sigma_{v,net,c}$ cannot be determined. Shown below is an updated version of figure 64 where the experimental average mean preconsolidation pressure is now only determined using a drained approach. Next to this, the contribution of $\sigma_{v,net,c}$ has been removed leaving only the influence of suction and degree of saturation to determine $\hat{p}_c$.

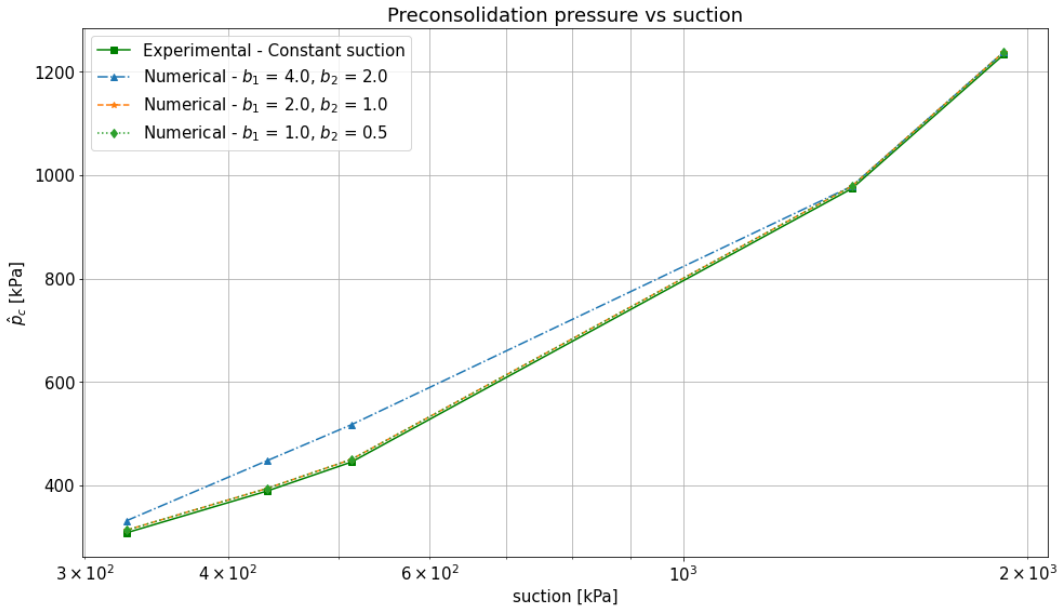

Figure 67: Updated numerical vs experimental preconsolidation pressure with suction for three sets of b_1 and b_2.

It can be seen that the experimental domain is now a line since only one way of determining the preconsolidation pressure was used. It can also be seen that with the updated values, the numerical preconsolidation pressure matches the experimental one for low values of b_1 and b_2. In the following, the updated version of figures 65a to 65c are reported with $\kappa = 0.040$, $b_1 = 1.0$ and $b_2 = 0.5$.

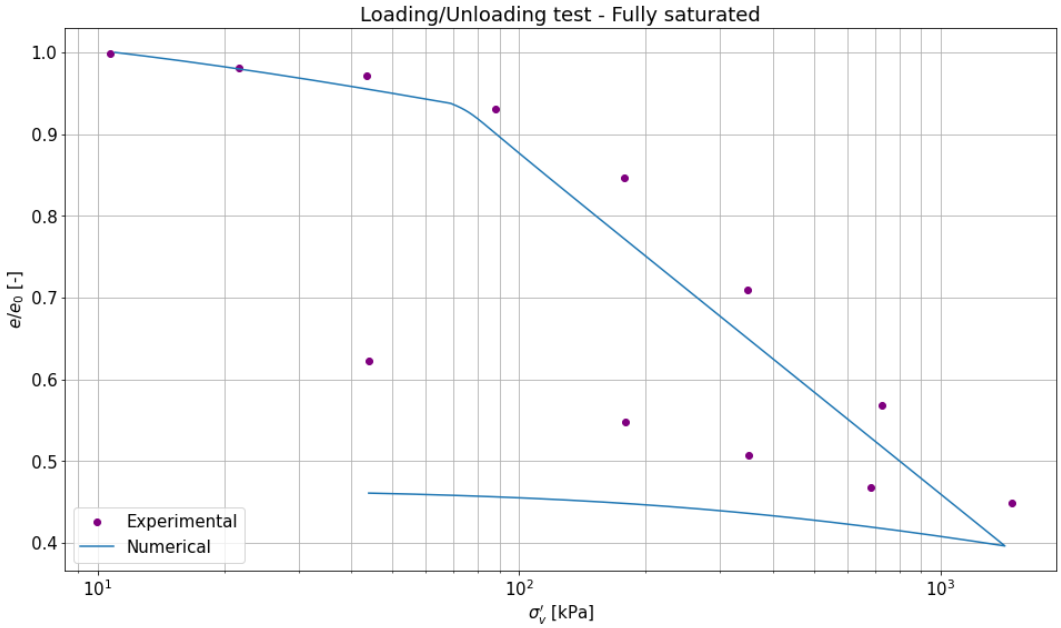

(a) Saturated sample.

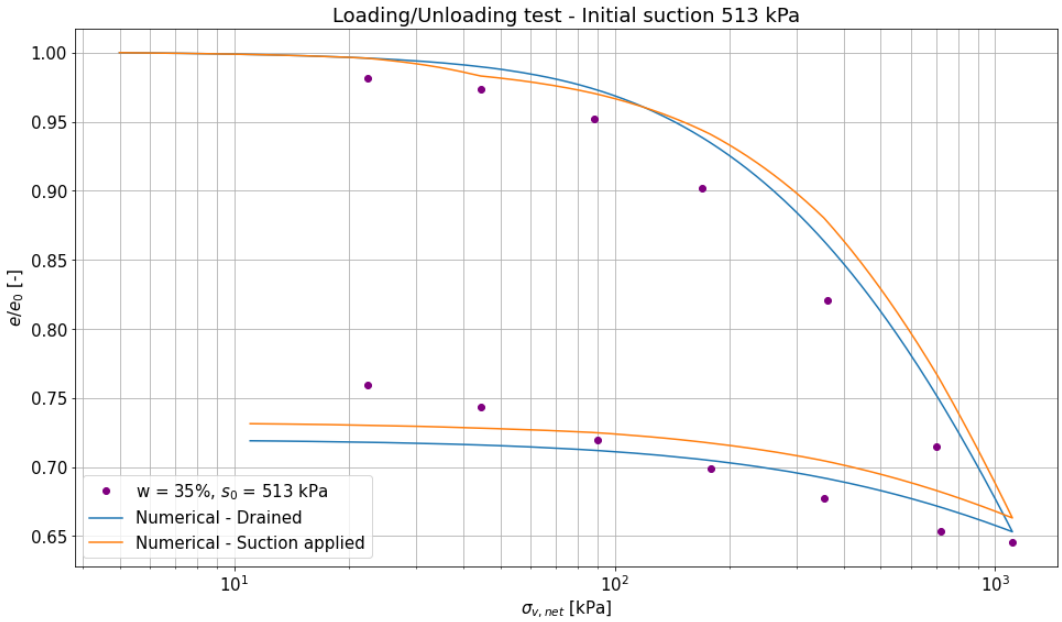

(b) $s_0 = 513$ kPa.

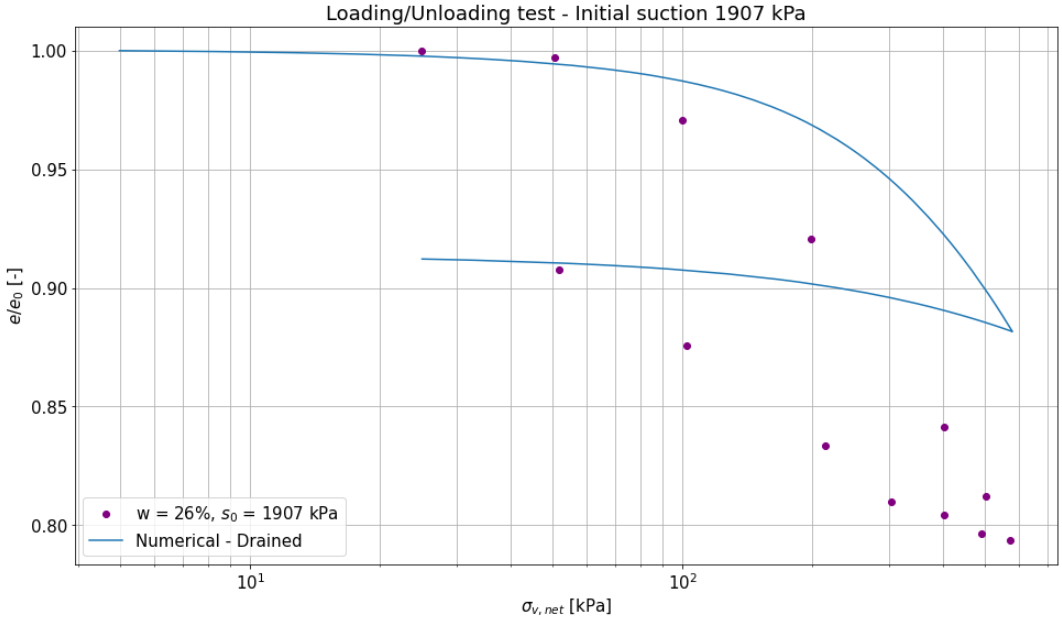

(c) $s_0 = 1907$ kPa.

Figure 68: Updated deformation behaviour predicted using a drained analysis.

It can be seen that the fit for the saturated sample and the sample with $s_0 = 513$ improved significantly. The high suction sample still does not have a good fit but possible reasons for this will be addressed later. Because of this, the elastoplastic and unsaturated parameters are deemed to be calibrated.

5.4.4 State variables after drying

As was stated before, in order to use the model version implemented in the mechanical driver, the state variables need to be known before the loading part of the test. These are obtained by performing a drying analysis with the hydromechanical driver using the calibrated parameters above. The results are reported in the table below. To keep the table organised, only the principle strains and stresses are reported, all shear values are zero. This time around the suction values are shown in the rows, this is because otherwise it was not possible to fit the table properly to the page.

Table 17: Initial state variables before loading (after drying) - London clay.

	Variable				
Initial suction [kPa]	$\boldsymbol{\varepsilon_0}$	$\boldsymbol{\sigma_0}$ [kPa]	$p^*_{c,0}$ [kPa]	α_0	e_0
Saturated	[0.0, 0.0, 0.0]	[11.0, 11.0, 11.0]	61.0	0.26	0.93
326	[0.064, 0.075, 0.075]	[5.0, 5.0, 5.0]	308.05	0.0	0.56
433	[0.072, 0.083, 0.083]	[5.0, 5.0, 5.0]	376.83	0.0	0.52
513	[0.076, 0.087, 0.087]	[5.0, 5.0, 5.0]	422.00	0.0	0.50
1405	[0.105, 0.116, 0.116]	[5.0, 5.0, 5.0]	835.92	0.0	0.38
1907	[0.114, 0.125, 0.125]	[5.0, 5.0, 5.0]	1034.68	0.0	0.34

5.4.5 Viscosity parameters

There are two viscosity parameters of which the values need to be determined. These are μ ([s^{-1}], fluidity parameter) and N_ϕ ([-], strain rate coefficient). Their values are determined through a sensitivity analysis which is given in appendix A.2.2. The sample that is tested is a saturated sample with $\sigma_{vm} = 355$ kPa. The reason for this is that using a saturated sample, the viscosity parameters can be determined without any potential influence of suction, the sample with $\sigma_{vm} = 355$ kPa is chosen since it is the median load level and therefore deemed most representative. It is found that the best fit is obtained for $\mu =$ 1e-8 s^{-1} and $N_\phi = 13$. The result with these parameters is shown below. Note that in this case the unsaturated EVP mechanical driver is used with all parameter values as determined above.

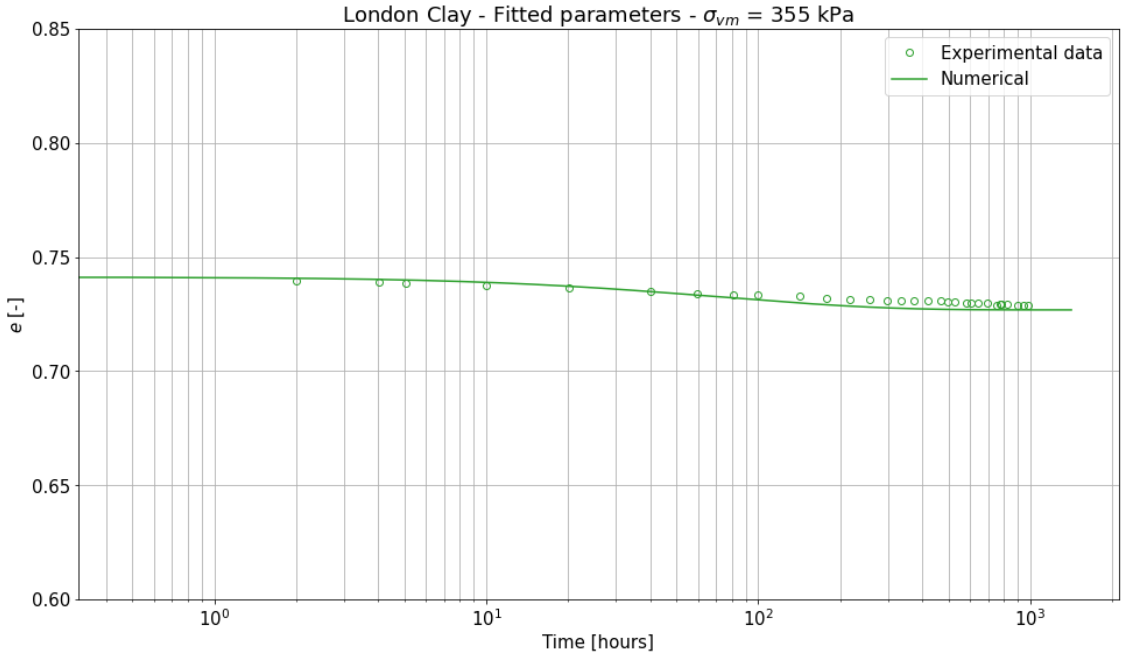

Figure 69: Best fitted viscosity parameter London clay - experimental data from Rezania et al. (2020).

In the figure above, the results are presented on a non-normalised y-axis whereas in the original data (figure 59), the results are presented on a normalised y-axis. Because of this, the original vertical axis only ranges from 0.968 to 1.000 which is an extremely small range. The model prediction will never be perfect and any deviation from the experimental data will look exaggerated on such a small axis. On the non-normalised axis shown above, it is possible to assess the model behaviour qualitatively. As was stated in section 5.3.2, the normalisation is done by multiplying the experimental data with e_p which is the void ratio 24 hours after consolidation. Its value is taken from the numerical outcome since the researchers did not provide the values and therefore there are no better options than to take it from the model output.

5.4.6 Overview parameters

Shown below is an overview of the parameters used in both drivers. Note that in the mechanical driver, λ^* and κ^* are used. Because the initial void ratio changes between samples, these values changes even though the original λ and κ are constant throughout the test.

Table 18: Overview elastoplastic parameters including λ and κ - London clay.

Parameter	Unit	Value
M_c	[-]	0.85
c_M	[-]	1.0
λ	[-]	0.168
κ	[-]	0.040
ν	[-]	0.3
N	[-]	0.85
x	[-]	1.84
C	[-]	4.0
k_f	[-]	2.0
k_g	[-]	2.0
α	[kPa^{-1}]	0.0036
n	[-]	4.5
m	[-]	0.05
a	[kPa]	1e6
b_1	[-]	1.0
b_2	[-]	0.5
$S_{r,aev}$	[-]	0.97
$S_{r,res}$	[-]	0.23

Table 19: Overview viscosity parameters - London clay.

Parameter	Unit	Value
μ	[s^{-1}]	1e-8
N_ϕ	[-]	13

Table 20: Overview initial state variables - London clay.

Variable	Unit	Value
$\boldsymbol{\varepsilon_0}$	[-]	[0.0, 0.0, 0.0, 0.0, 0.0, 0.0]
$\boldsymbol{\sigma_0}$[1]	[kPa]	[5.0, 5.0, 5.0, 0.0, 0.0, 0.0]
α_0	[-]	0.26
β_0	[-]	0.26
$p^*_{c,0}$	[kPa]	61.0
e_0	[-]	0.93

[1] The saturated sample started at an isotropic pressure of 11 kPa, all unsaturated samples at 5 kPa.

Table 21: Overview state variables after drying - London clay.

	Variable					
Initial suction [kPa]	$\boldsymbol{\varepsilon_0}$	$\boldsymbol{\sigma_0}$ [kPa]	$p^*_{c,0}$ [kPa]	α_0	β_0	e_0
Saturated	[0.0, 0.0, 0.0]	[11.0, 11.0, 11.0]	61.0	0.26	0.26	0.93
326	[0.064, 0.075, 0.075]	[5.0, 5.0, 5.0]	308.05	0.0	0.0	0.56
433	[0.072, 0.083, 0.083]	[5.0, 5.0, 5.0]	376.83	0.0	0.0	0.52
513	[0.076, 0.087, 0.087]	[5.0, 5.0, 5.0]	422.00	0.0	0.0	0.50
1405	[0.105, 0.116, 0.116]	[5.0, 5.0, 5.0]	835.92	0.0	0.0	0.38
1907	[0.114, 0.125, 0.125]	[5.0, 5.0, 5.0]	1034.68	0.0	0.0	0.34

As has been stated above, λ^* and κ^* change for each sample due to the different initial void ratio (table 21). As a reminder, λ^* and κ^* are obtained from the original λ and κ by dividing by $1 + e_0$. This gives the following parameter values. Note that all other parameters remain the same when used in the mechanical driver and are therefore not repeated again.

Table 22: Overview λ^* and κ^* values for each sample - London clay.

	Initial suction [kPa]					
Variable	Saturated	326	433	513	1405	1907
e_0 (repeated)	0.93	0.56	0.52	0.50	0.38	0.34
λ^*	0.087	0.108	0.111	0.112	0.122	0.125
κ^*	0.021	0.026	0.026	0.027	0.029	0.030

5.5 Model validation

With all parameters are known, model runs can be executed and the numerical output can be compared to the experimental data to help validate the model. First, the unsaturated elastoplastic model will be validated after which the unsaturated elasto viscoplastic model is assessed. Throughout the model validation, only the mechanical driver is used as was done in the previous chapter as well. For the elastoplastic model version, the hydromechanical driver is available as well. A comparison between the results of both drivers can be found in appendix B which shows they predict very similar deformation plots leading to the conclusions that the mechanical driver can be used to model the loading/unloading tests and that it is correct to run the analyses drained instead of undrained.

5.5.1 EP model

As has been explained in section 5.3.1, loading/unloading tests are performed where both the loading and unloading were done in multiple steps of 24 hours each. These tests were performed on a saturated sample and 6 unsaturated samples of which 1 was deemed unrealistic due to its extremely high suction of 21000 kPa. This means that in total 6 tests are used in the model validation. Shown below are the results for all six samples.

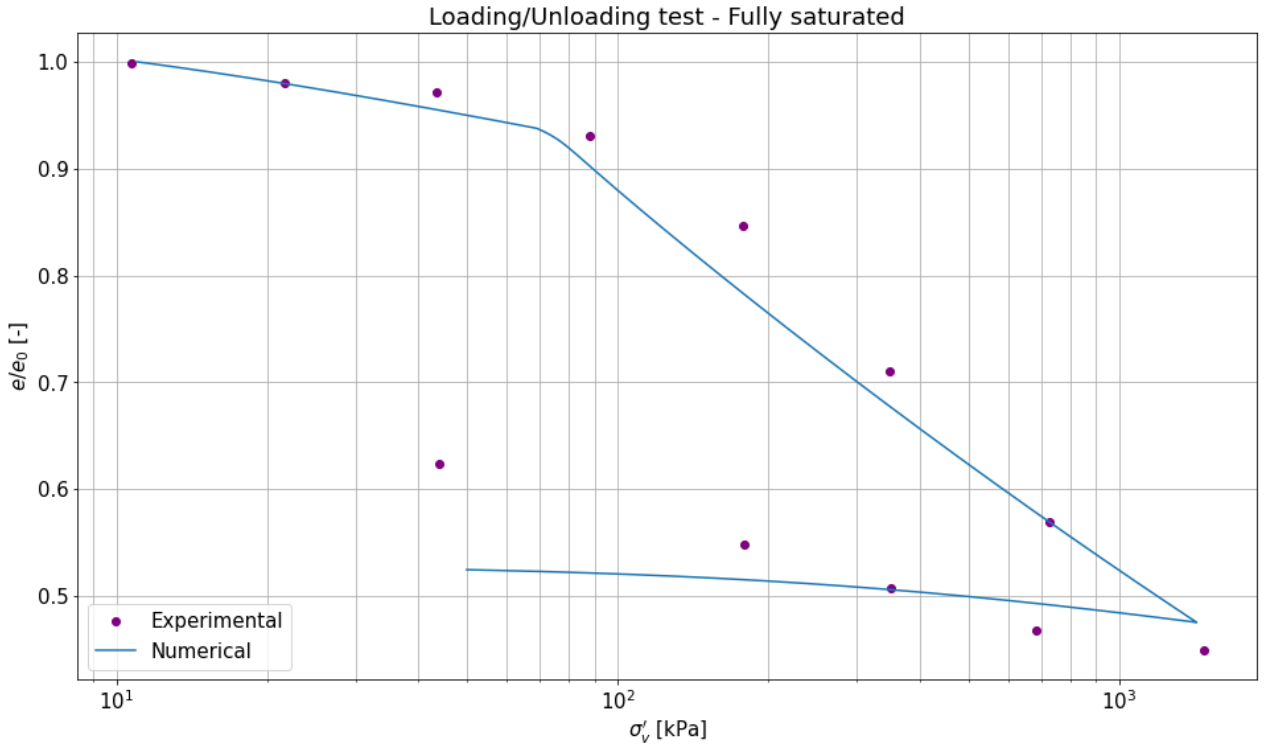

(a) Saturated sample.

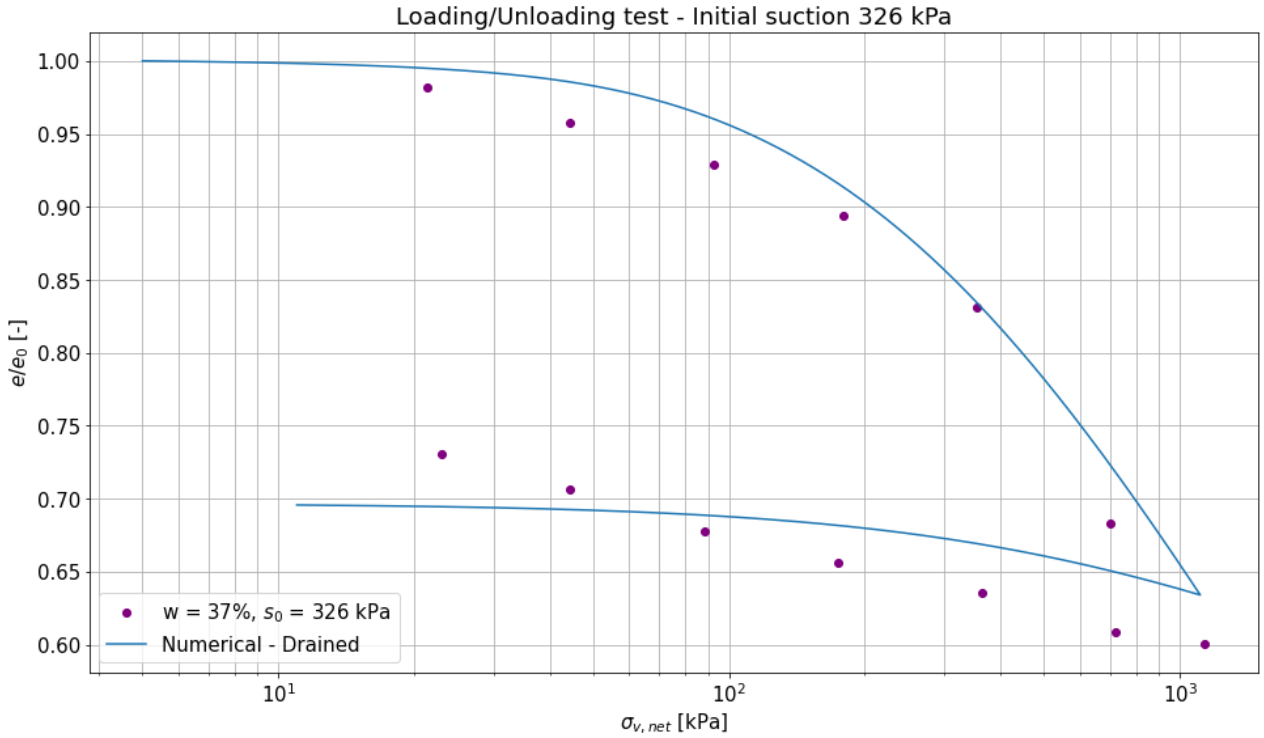

(b) $s_0 = 326$ kPa.

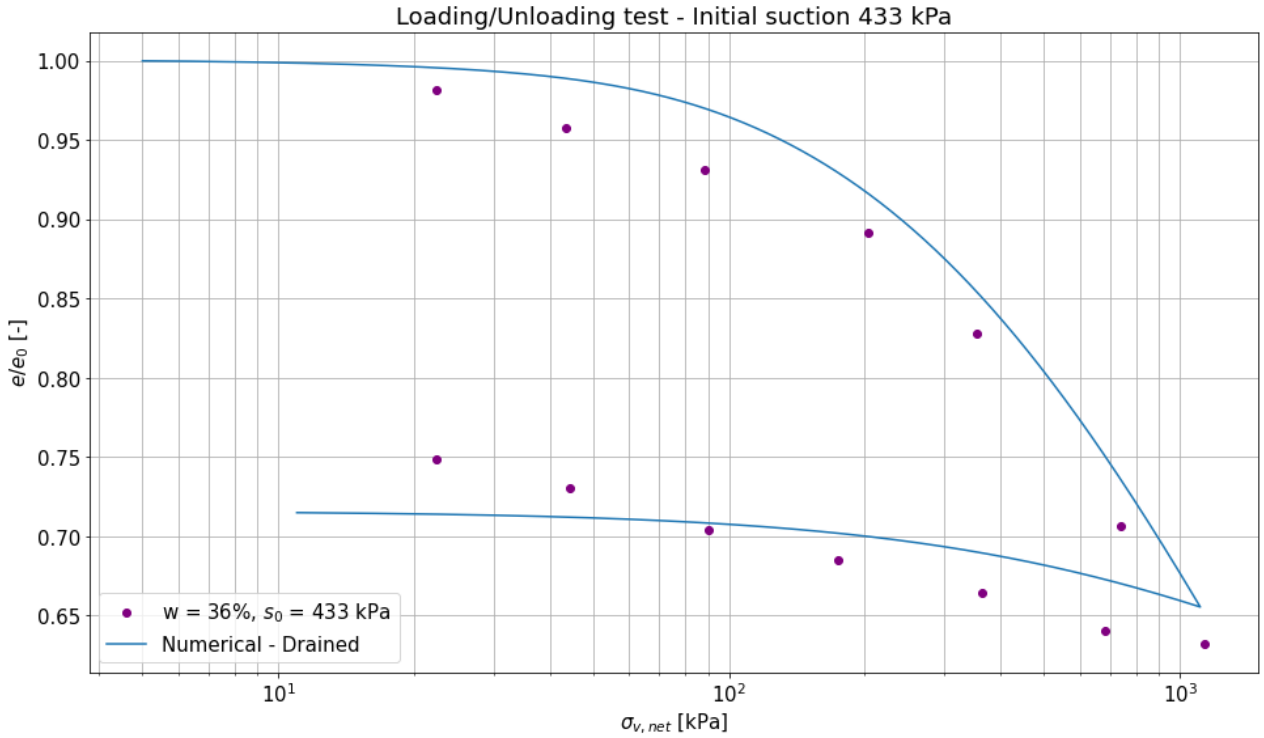

(c) $s_0 = 433$ kPa.

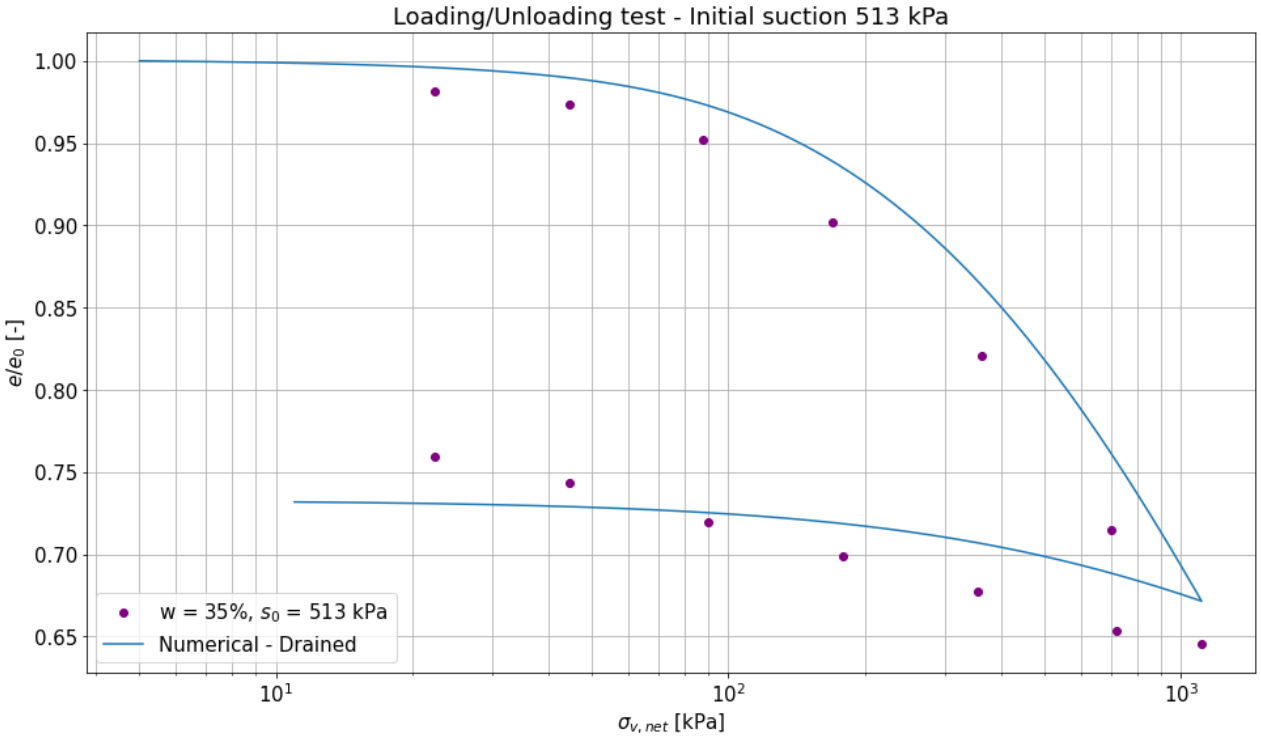

(d) $s_0 = 513$ kPa.

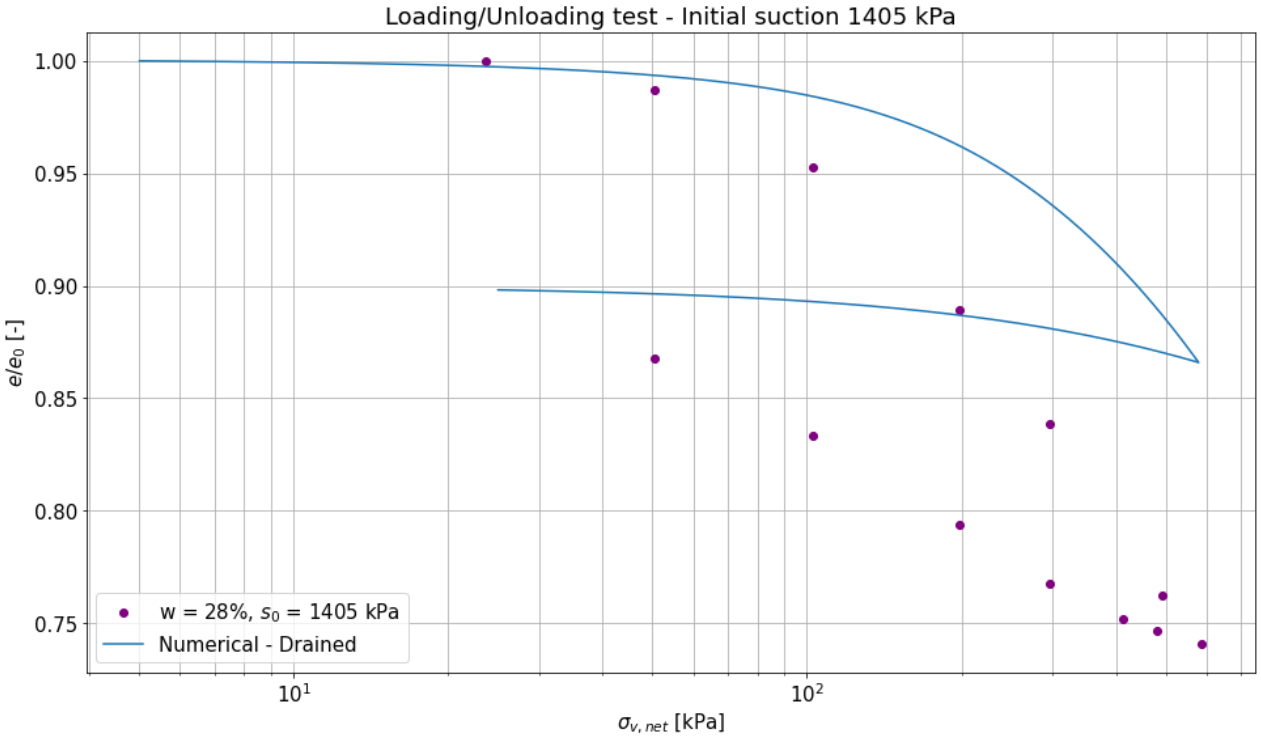

(e) $s_0 = 1405$ kPa.

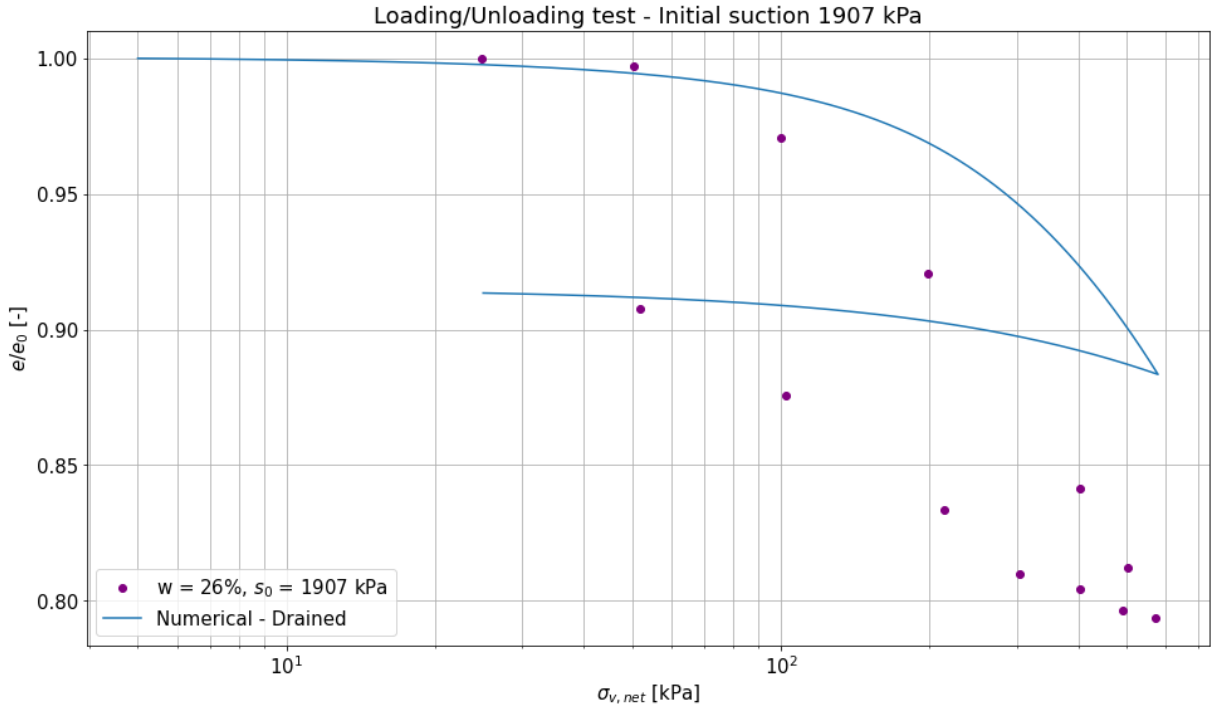

(f) s_0 = 1907 kPa.

Figure 70: Deformation behaviour predicted by the mechanical driver.

The results show that up until a suction of 513 kPa, the model prediction is satisfactory. The deformation during loading is slightly overpredicted for the saturated sample and slightly underpredicted for the unsaturated samples. The unloading branches are also not followed accurately but the problem that is being faced is that if κ were to be increased to match the unloading behaviour better, then the reloading branch of the saturated sample would be overpredicted leading to a wrong model prediction as was already shown in section 5.4.3.

For samples with a higher initial suction, the model predictions are worse. Not only is the deformation at the maximum load heavily underpredicted, the slopes of the unloading lines are incorrect and the deformation during the transition from an isotropic stress state to a K_0 one is almost none.

There are several reasons why the results become worse at higher suction. The most obvious cause is the Soil Water Retention Curve. There are two problems with the SWRC that can affect the model results. The first one is that the SWRC reported by Rezania et al. (2020) is given as gravimetric water content vs suction. In order to translate the gravimetric water content to degree of saturation equation (44) is used. The inherent problem with using this equation is that a constant void ratio is assumed. As the suction increases the sample deforms and the void ratio decreases introducing an error. Of course, as the suction increases, the sample deforms more and this error increases as well.
Another problem with the SWRC is that it is determined using two methods (Axis translation and through the High Capacity Tensiometers) as can be seen in figure 60. The two methods start deviating in SWRC prediction at around 600 kPa suction and the first method does not measure beyond 1000 kPa suction. This introduces uncertainty in the SWRC above 600 kPa and definitely above 1000 kPa.

Other potential causes for the worse results at higher suctions are the uncertainty in initial void ratio and the sampling technique. The initial void ratio is determined using a drying analysis in the hydromechanical driver but this drying analysis might give slightly different results than what the researchers measured in their work. If the initial void ratio is smaller, deviations to the value matter a lot more relatively. For example, a difference of 0.01 in initial void ratio is more significant if the initial void ratio is 0.34 than when the initial void ratio is 0.58.

The sampling technique is the final cause which can explain the worse results at high suctions. The samples were first prepared in blocks and then dried before an oedometer ring was penetrated to obtain the actual samples. As the suction increases, the block from which the sample is taken from is drier and therefore harder to sample from. It could be the case that during sampling disturbances to the soil structure were introduced which might result in a higher deformation measured. The numerical model does not contain any destructuration effects and would not be able to predict this.
There is no proof for either of these final causes but they serve as reasoning as to why the results turned out the way they did.

Since the results for suctions of 1400 kPa or higher are no longer accurate and below this value the results were found to be accurate, the model is deemed to be validated for suctions up to 1 MPa. For higher suctions the model performance is worse and results at high suction values need to be treated with care.

5.5.2 EVP model

Section 5.3.2 explained the unsaturated creep tests that were performed by Rezania et al. (2020). In this section, the calibrated model output will be compared to the experimental data. In figure 59, Rezania et al. (2020) present their results in five graphs. Each graphs contains the model output for all of the samples that are loaded to the same σ_{vm}. In this section, the results are presented in a slightly different way. Shown below are three graphs with each graph showing the creep deformation behaviour for samples with the same suction. Initially only the saturated sample and the samples with suction of 513 and 1405 kPa are presented. The reason for this is that for the initial results it is enough to only look at a part of the model performance to assess if adaptations need to be made. In selecting these samples, the saturated performance is covered and a low and a high suction sample are selected. Next to this, one of the samples with 513 kPa suction is tested at the lowest load (σ_{vm} = 178 kPa) and one of the 1405 kPa suction samples is tested at the highest load (σ_{vm} = 666 kPa).

Again, the data is presented on a non-normalised y-axis as is done in section 5.4.5. Using this axis it is possible to assess the model performance qualitatively.

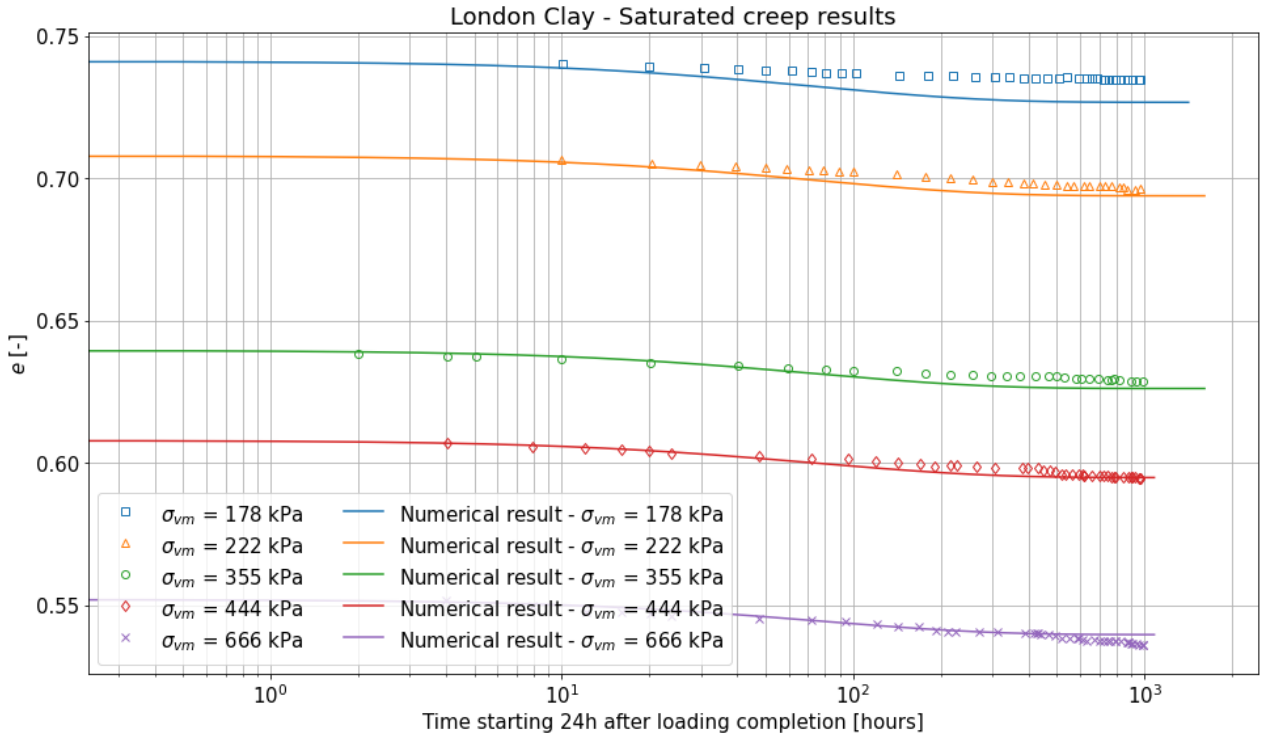

(a) Saturated sample.

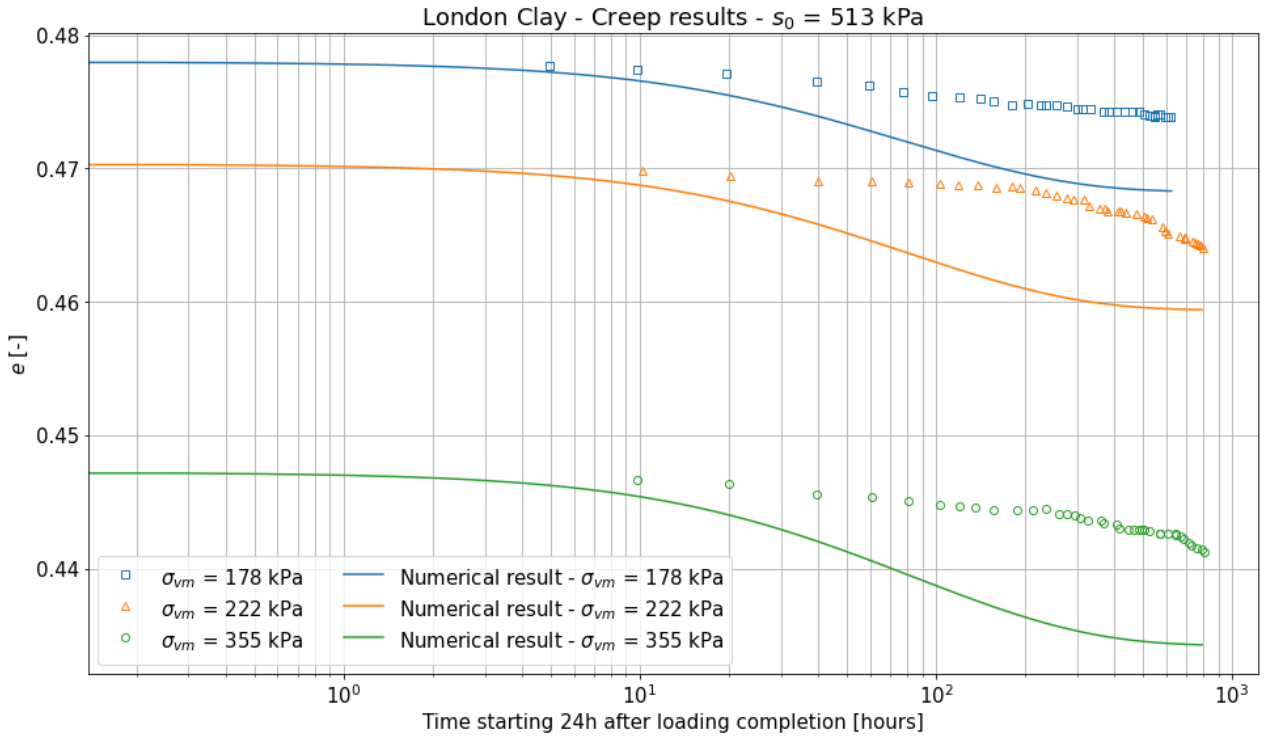

(b) s_0 = 513 kPa.

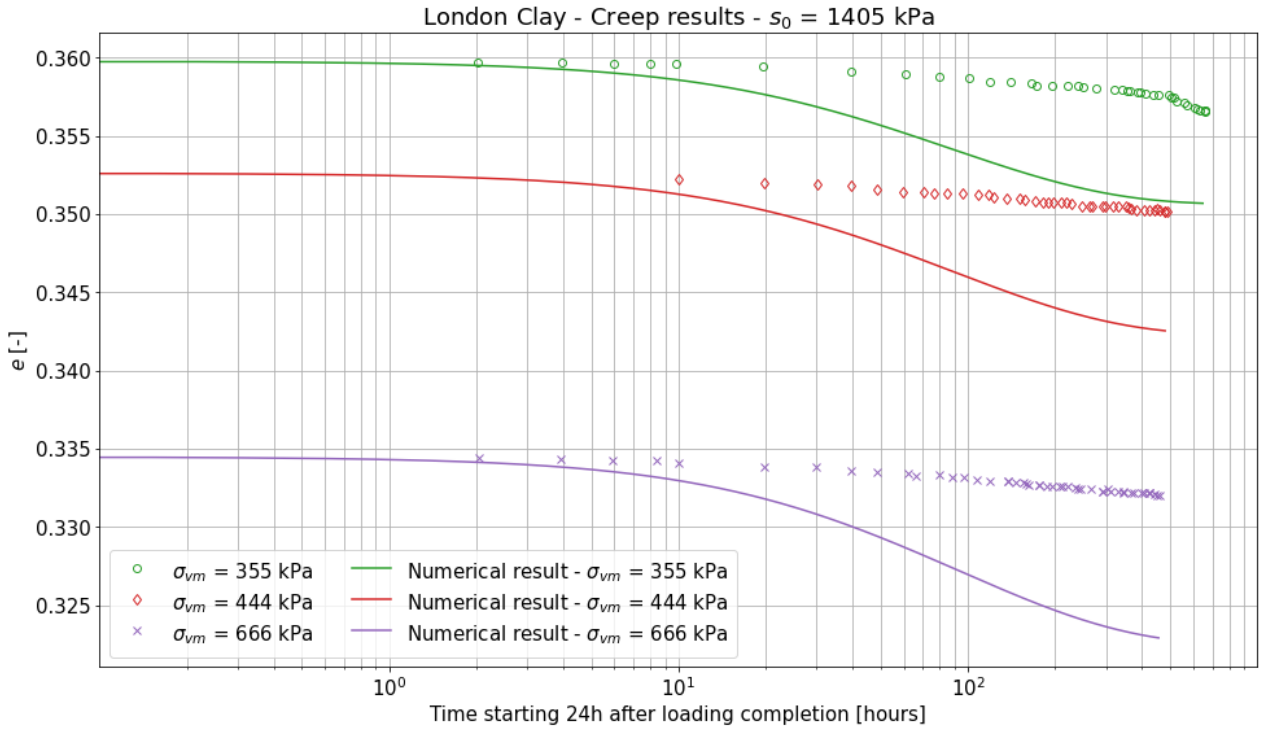

(c) s_0 = 1405 kPa.

Figure 71: Creep deformation behaviour predicted by the mechanical driver.

The results show that the model predicts the creep behaviour to occur too quickly. This deviation from the experimental data increases as the suction increases. Because of this, it is decided to make an adaptation to the model. More precisely, a new version of the viscous nucleus is proposed. A literature review was performed to see if a suction dependent viscous nucleus has been used before but no research was found. It is therefore to the best of the author's knowledge that the proposed change is a new contribution to research. The new version of the viscous nucleus is shown below.

$$\Phi(f) = \langle \exp(N_\phi * (\frac{\hat{p}_c^d}{\hat{p}_c^s} - 1)) - 1 \rangle * \left(\frac{s_{ref}}{s_{visc}}\right)^{n_{suc}} \tag{45}$$

where,

$$s_{visc} = \begin{cases} s & \text{for s} > s_{ref} \\ s_{ref} & \text{for s} < s_{ref} \end{cases}$$

A point worth noting is that the preconsolidation pressure and the size of the DLS are now both their unsaturated variants denoted with a hat. The unsaturated preconsolidation pressure is determined by multiplying the saturated one with the loading collapse rule (equation (41)). The size of the DLS on the other ($\hat{p}_c^d$) is also denoted with a hat even though this value is not obtained through the loading collapse rule. Instead, the DLS always goes through the stress point and since the stresses are now expressed with the average soil skeleton stress, the DLS which goes through this stress point is also denoted with a hat.

The change with comparison to the old viscous nucleus (equation (32)) is the final, suction dependent, term. Adding this term causes the viscous nucleus to be smaller due to the influence of suction and therefore slow down the creep strains. Since it is inversely related to the suction, the decrease in creep strain rate is higher at higher suctions which is what is needed according to the results presented above. The newly introduced parameters s_{ref} and n_{suc} are calibrated by executing trial runs. Because a change like this has not been done before, reference literature for potential starting values for s_{ref} and n_{suc} is not available and therefore trial and error is the only option to determine their values. This process is aided by a sensitivity analysis performed in appendix A.4.2.

With these changes, new results are obtained which are shown below.

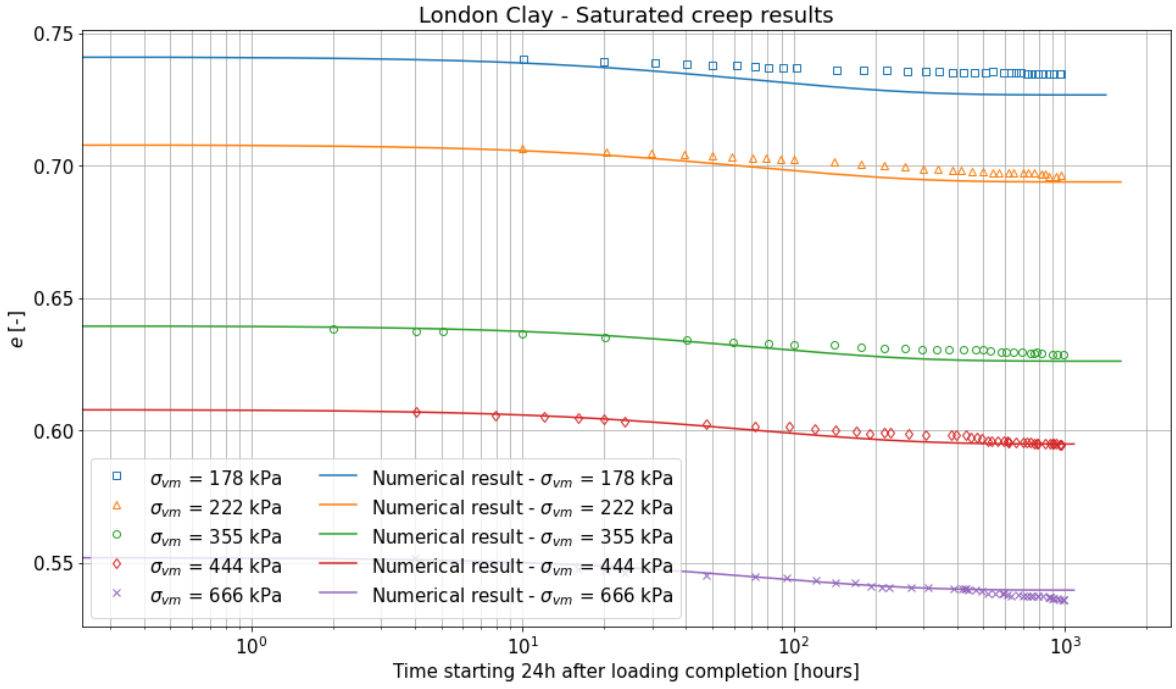

(a) Saturated sample.

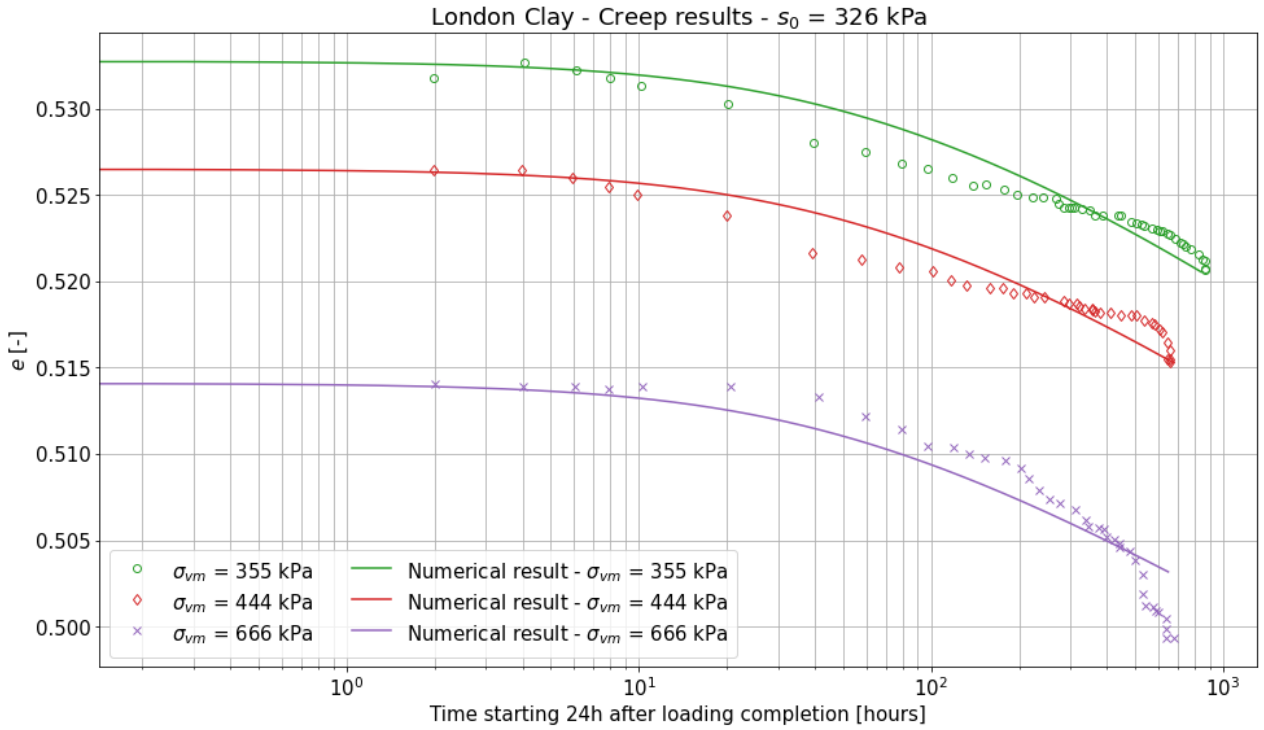

(b) s_0 = 326 kPa.

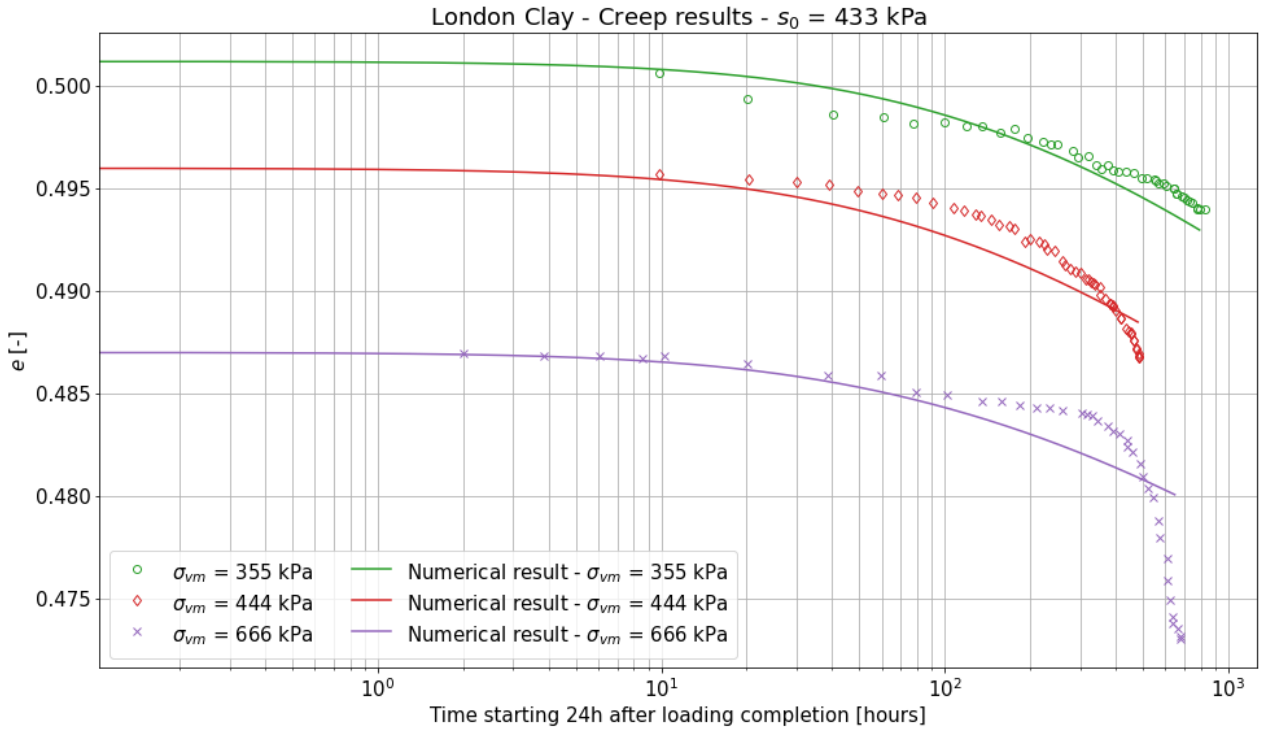

(c) s_0 = 433 kPa.

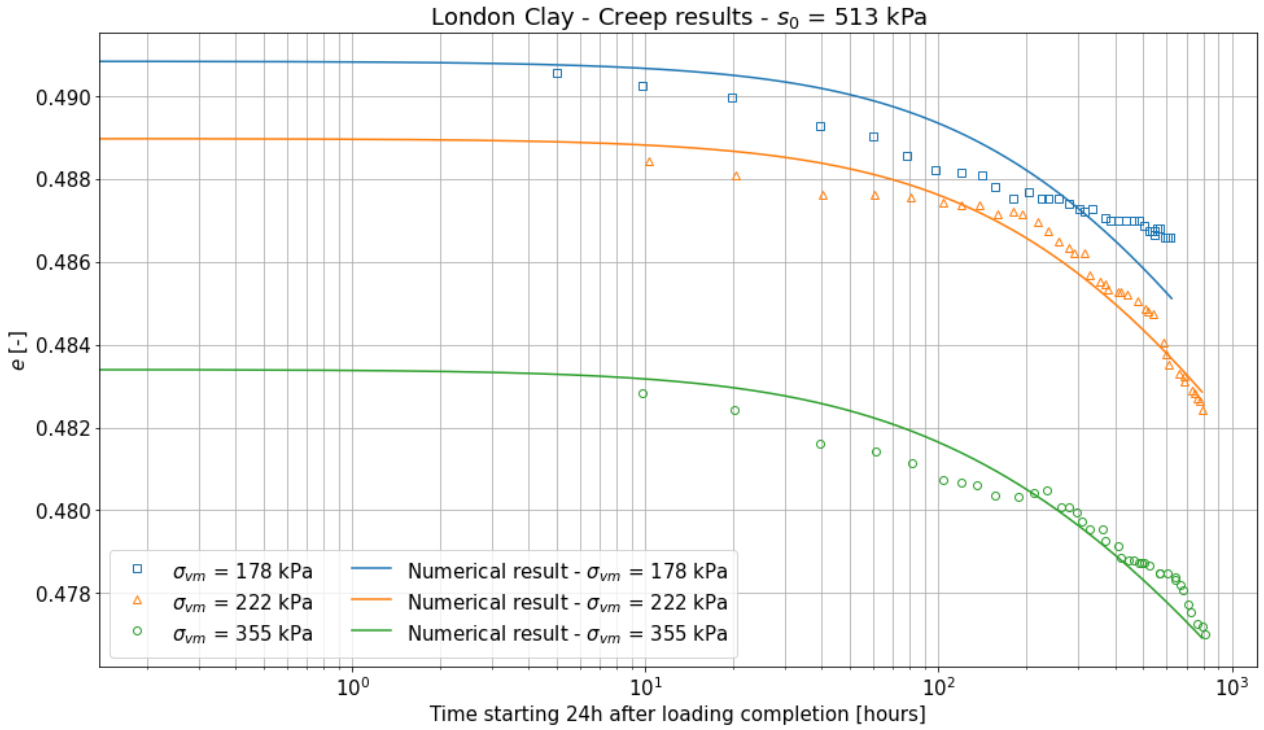

(d) s_0 = 513 kPa.

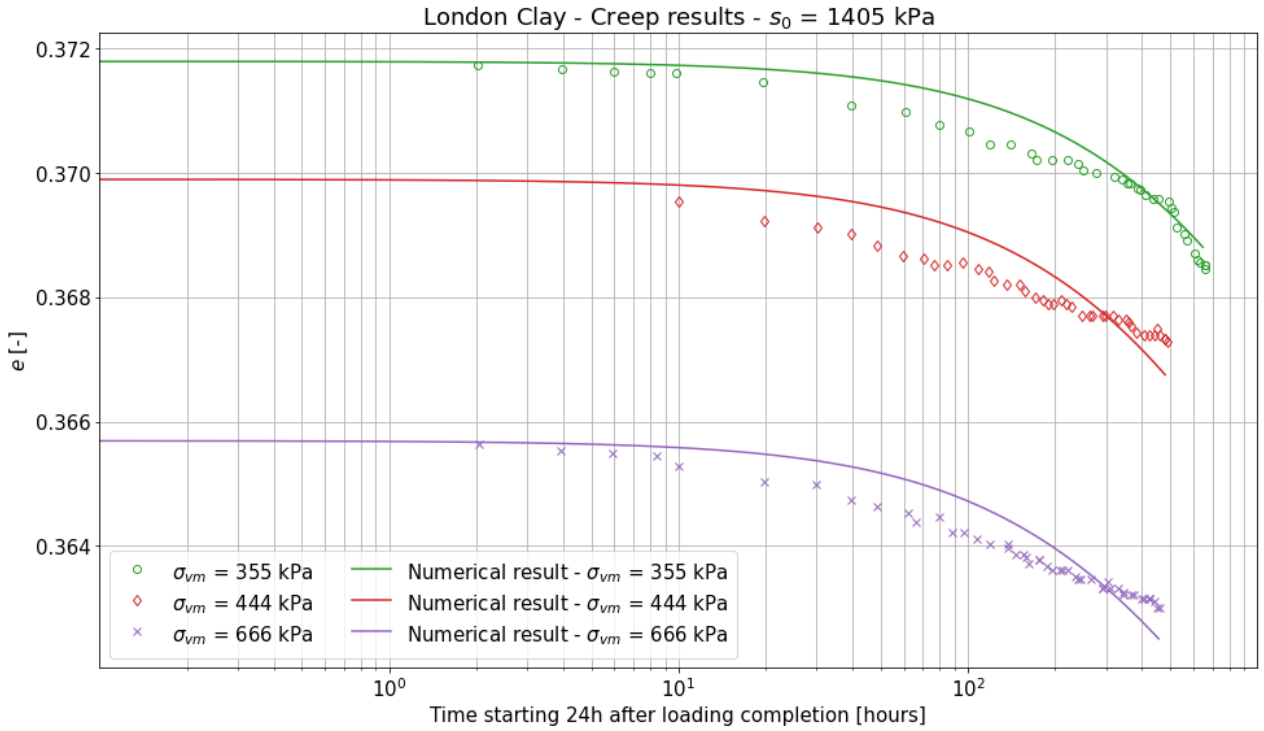

(e) s_0 = 1405 kPa.

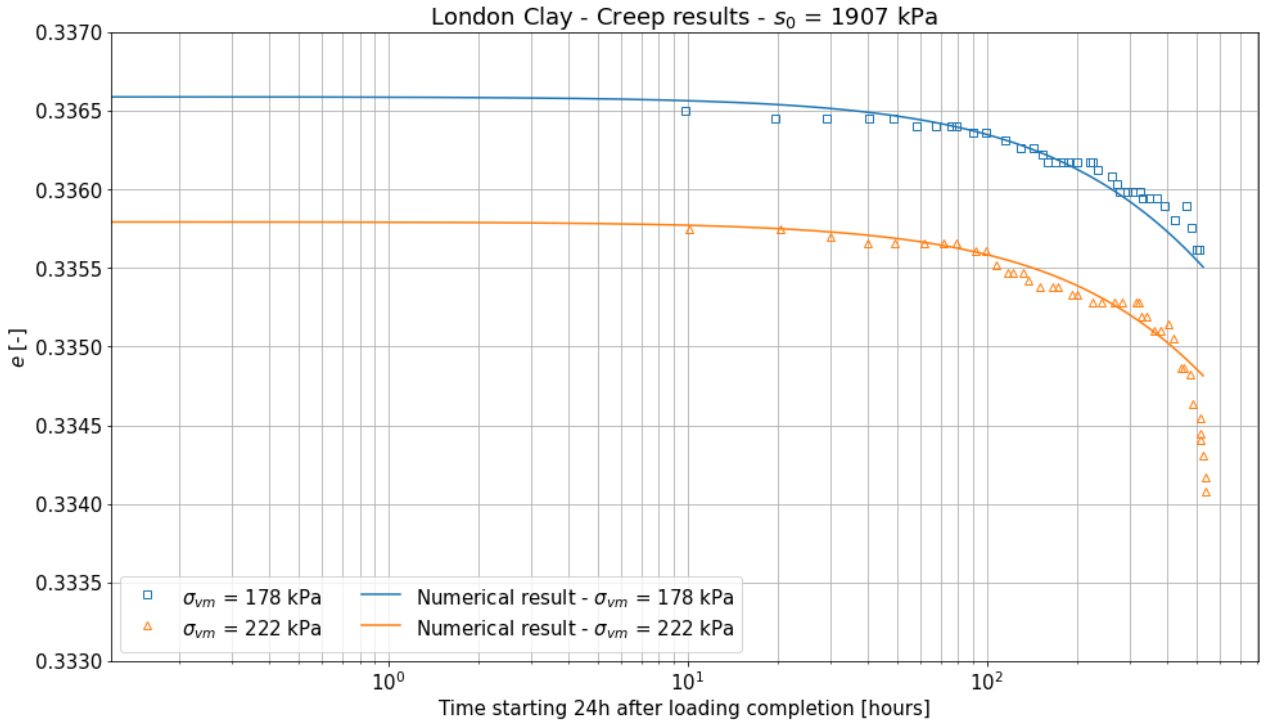

(f) s_0 = 1907 kPa.

Figure 72: Creep deformation behaviour predicted by the mechanical driver using the updated viscous nucleus.

The results show that with the updated viscous nucleus, the results improve significantly. The creep deformation prediction is now accurate and the model no longer predicts the creep deformation to occur too quickly. It can be seen that the model does show some difficulty in predicting the accelerated creep deformation at the end of the test. This is most clearly seen in figure 72c for the sample with σ_{vm} = 666 kPa. As was touched on in section 5.3.2 this accelerated behaviour is not consistently present throughout the tests and therefore it is difficult to assess whether it is the real soil behaviour or if it could be caused by randomness in the sampling. Rezania et al. (2020) only tested one sample for each combination of suction and load which makes it difficult to draw a conclusion on whether or not the accelerated behaviour should be captured by the model.

For each of the samples, a combination of s_{ref} and n_{suc} was selected to obtain the results. Shown below are the plots of the development of s_{ref} and n_{suc} with suction for each of the different applied σ_{vm}.

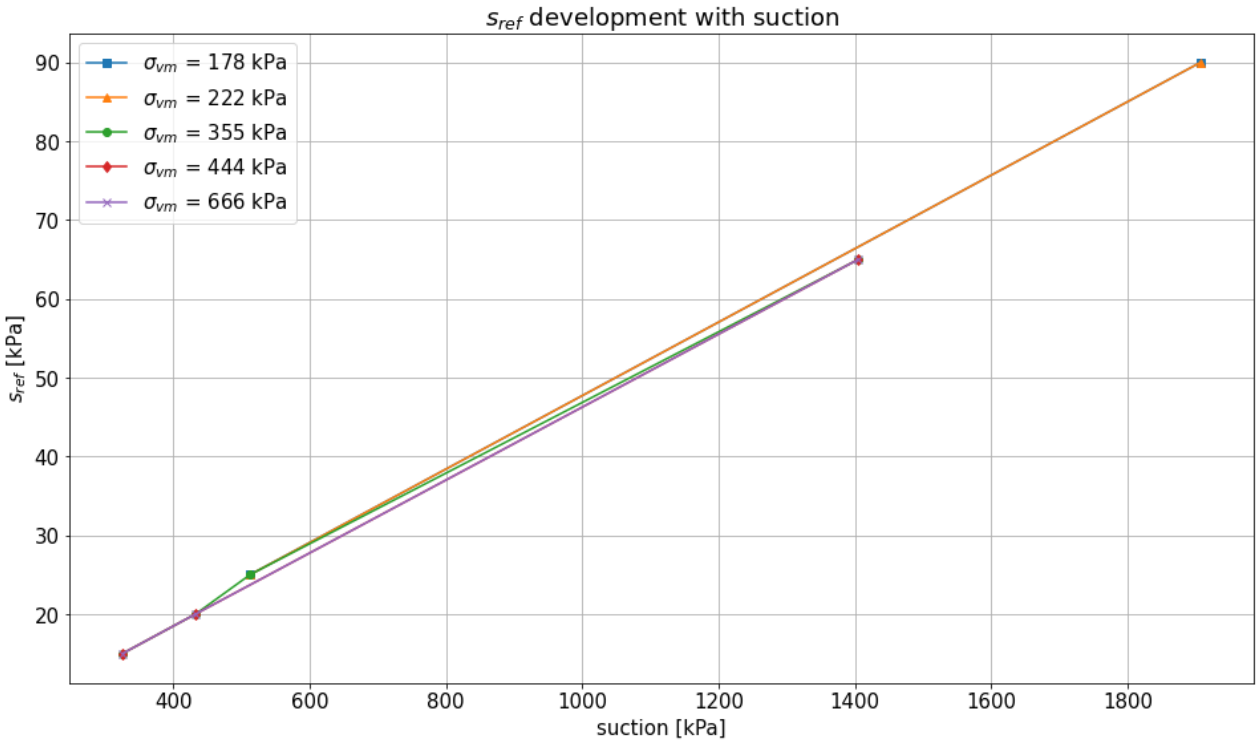

Figure 73: Development of s_{ref} with suction for each of the applied σ_{vm}.

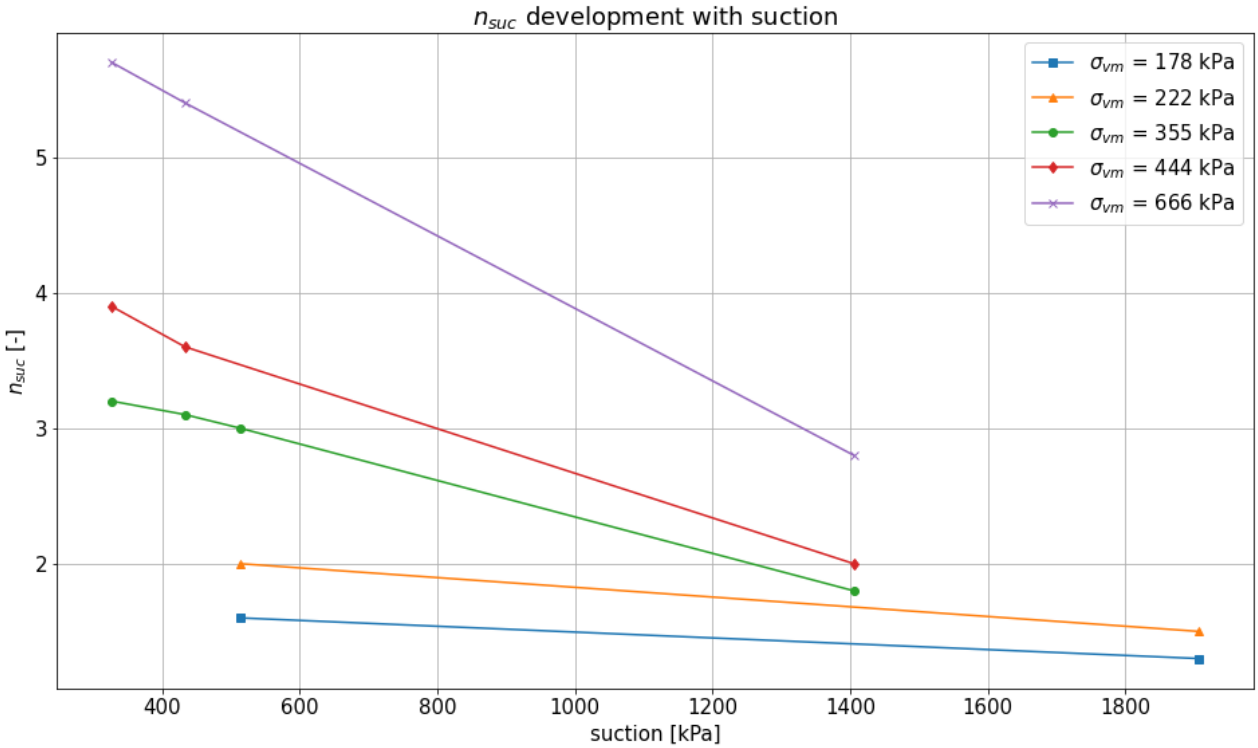

Figure 74: Development of n_{suc} with suction for each of the applied σ_{vm}.

It can be seen that s_{ref} linearly increases with suction and does not differ between applied loads. What this implies is that the term s_{ref}/s_{visc} in the viscous nucleus is a constant fraction as long as the suction is higher than s_{visc}. n_{suc} on the other hand decreases with suction, this decrease is roughly linear as well but the slope of this line and the value of n_{suc} at zero suction changes as the stress changes.
An important takeaway of the figures above is that there is a potential relationship for both s_{ref} and n_{suc} with suction and stress. Because of this, it is theoretically be possible to only give one value for s_{ref} and n_{suc} and then let the model determine the correct value based on the current stress and suction. This potential relationship is an argument in favour of the model adaptation. If on the other hand the two plots shown above showed significant scatter it would mean that by changing the parameter values from sample to sample effectively comes down to curve fitting the model output to the experimental data which is not desired.

Looking at the overall improvement and performance of the model, the unsaturated EVP model is deemed to be validated and can now be used to produce the final results in order to answer the main research question. The final results are presented in the next chapter.

5.5.3 Overview final parameters

In this paragraph, the final parameter values are presented. The parameters are almost identical to the parameters shown in section 5.4.6 with the exception for C. However, for the sakes of overview and completeness, all parameter values are given here again similar to what was done in the previous chapter.

Table 23: Elastoplastic parameters including λ and κ - London clay - Final values.

Parameter	Unit	Value
M_c	[-]	0.85
c_M	[-]	1.0
λ	[-]	0.168
κ	[-]	0.040
ν	[-]	0.3
N	[-]	0.85
x	[-]	1.84
C	[-]	0.0
k_f	[-]	2.0
k_g	[-]	2.0
α	[kPa^{-1}]	0.0036
n	[-]	4.5
m	[-]	0.05
a	[kPa]	1e6
b_1	[-]	1.0
b_2	[-]	0.5
$S_{r,aev}$	[-]	0.97
$S_{r,res}$	[-]	0.23

Table 24: Viscosity parameters - London clay - Final values.

Parameter	Unit	Value
μ	[s^{-1}]	1e-8
N_ϕ	[-]	13

Table 25: Initial state variables - London clay - Final values.

Variable	Unit	Value
$\boldsymbol{\varepsilon_0}$	[-]	[0.0, 0.0, 0.0, 0.0, 0.0, 0.0]
$\boldsymbol{\sigma_0}$[1]	[kPa]	[5.0, 5.0, 5.0, 0.0, 0.0, 0.0]
α_0	[-]	0.26
β_0	[-]	0.26
$p^*_{c,0}$	[kPa]	61.0
e_0	[-]	0.93

[1] The saturated sample started at an isotropic pressure of 11 kPa, all unsaturated samples at 5 kPa.

Table 26: State variables after drying - London clay - Final values.

	Variable					
Initial suction [kPa]	$\boldsymbol{\varepsilon_0}$	$\boldsymbol{\sigma_0}$ [kPa]	$p^*_{c,0}$ [kPa]	α_0	β_0	e_0
Saturated	[0.0, 0.0, 0.0]	[11.0, 11.0, 11.0]	61.0	0.26	0.26	0.93
326	[0.064, 0.075, 0.075]	[5.0, 5.0, 5.0]	308.05	0.0	0.0	0.56
433	[0.072, 0.083, 0.083]	[5.0, 5.0, 5.0]	376.83	0.0	0.0	0.52
513	[0.076, 0.087, 0.087]	[5.0, 5.0, 5.0]	422.00	0.0	0.0	0.50
1405	[0.105, 0.116, 0.116]	[5.0, 5.0, 5.0]	835.92	0.0	0.0	0.38
1907	[0.114, 0.125, 0.125]	[5.0, 5.0, 5.0]	1034.68	0.0	0.0	0.34

Note that the desired suction is obtained by setting the water pressure to the negative value of the suction.

Table 27: λ^* and κ^* values for each sample - Used in the mechanical driver - London clay - Final values.

	Initial suction [kPa]					
Variable	Saturated	326	433	513	1405	1907
e_0 (repeated)	0.93	0.56	0.52	0.50	0.38	0.34
λ^*	0.087	0.108	0.111	0.112	0.122	0.125
κ^*	0.021	0.026	0.026	0.027	0.029	0.030

5.6 Conclusions

From sections 5.5.1 and 5.5.2 it can be concluded that the implementation of the unsaturated conditions is done correctly in the mechanical driver. For the elastoplastic model, difficulties with uncertainty in the experimental data limited a full assessment of the model performance especially at higher suctions but for suction up to 513 kPa the model worked accurately. In developing the elasto viscoplastic model, it was found that the viscous nucleus needed to be made suction dependent. A literature review showed that this has not been done before so therefore this part of the work can definitely be seen as a contribution to research. With a suction dependent viscous nucleus, the model was able to predict creep deformation accurately after which it was concluded that the unsaturated elasto viscoplastic model performs satisfactory and is therefore deemed to be validated.

6 Results

In this section, the results required to answer the main research question are presented. The results are split in three subsections. The first two focus on the K_0 development over time using anisotropic and isotropic approaches respectively. The final part presents the development of the apparent preconsolidation pressure with time.

6.1 Anisotropic K_0 development

In order to be able to answer the main research question. K_0 vs time plots are required at different suction levels. This is needed because using these plots, the time dependency of K_0 can be addressed to draw conclusions on the development during creep. The runs are required at different suction levels as well to be able to see if the change in K_0 with suction is in agreement with what was found in the literature study.

The required plots are obtained from the unsaturated EVP model. It was unfortunately not possible to perform unsaturated lab tests since the required testing equipment was not ready to be used. Therefore, the already validated unsaturated EVP results from the previous chapter are used and presented in a different way to obtain the required plots as explained above. In the previous chapter, the creep deformation over time was analysed by comparing the model results to experimental data published by Rezania et al. (2020). The model output included the values of all state variables throughout the test. This means that next to the void ratio, all the stresses are available as well which means that K_0 can be determined. Because the deformation behaviour predicted by the model was checked and validated using the experimental data, it can be assumed that the stress prediction of the model is in line with what could be found experimentally. Therefore, the results from figures 72a to 72f are used again but this time plotted as K_0 vs time.

Shown below are all the results, they are presented in graphs where in each graph the samples are given that are loaded to the same σ_{vm} and have different suction values. The reason for this is that in doing so, the behaviour with time can be assessed but the change with suction can also be seen directly. Interpretation of the results will follow in the next chapter.

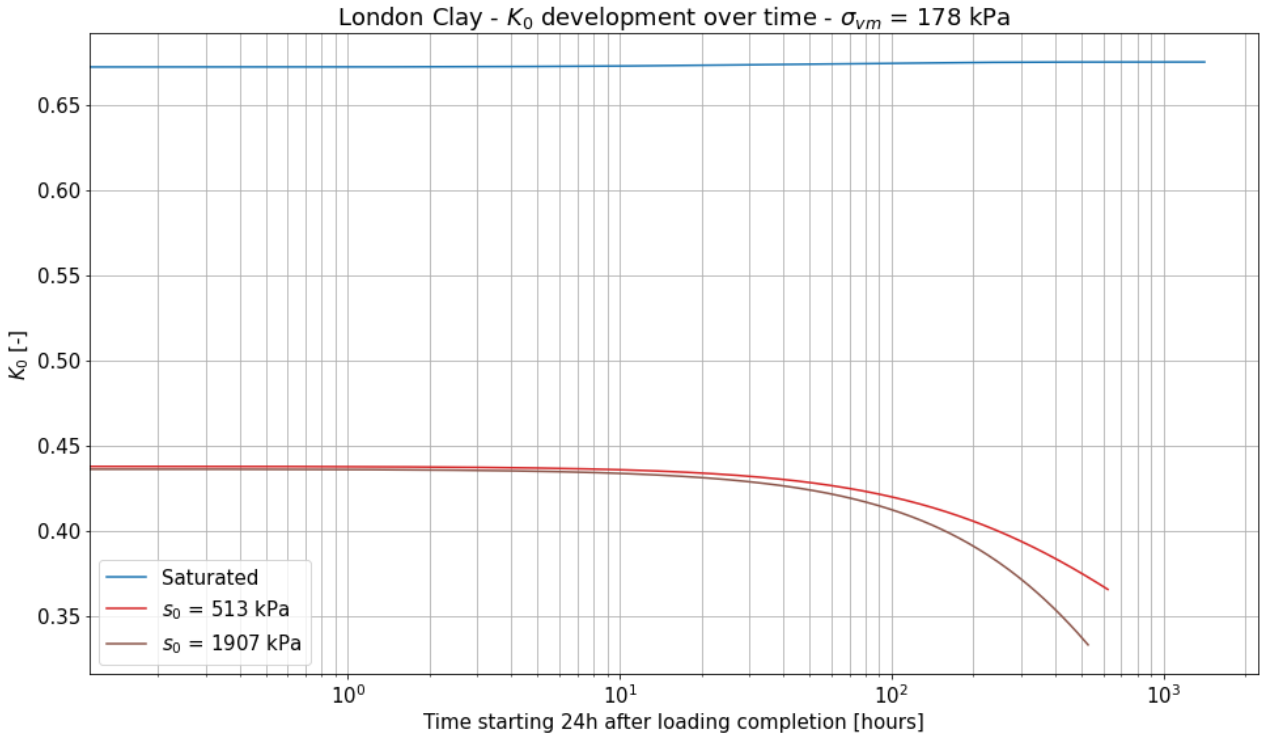

(a) σ_{vm} = 178 kPa.

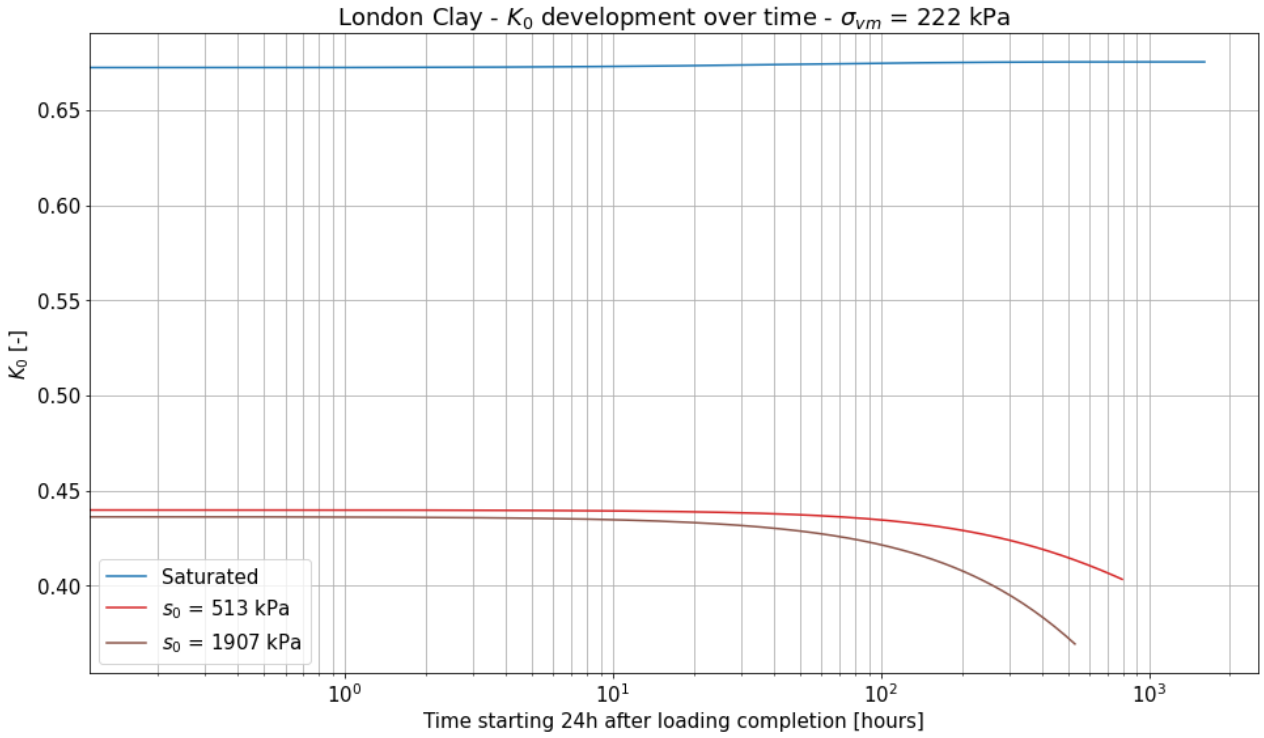

(b) σ_{vm} = 222 kPa.

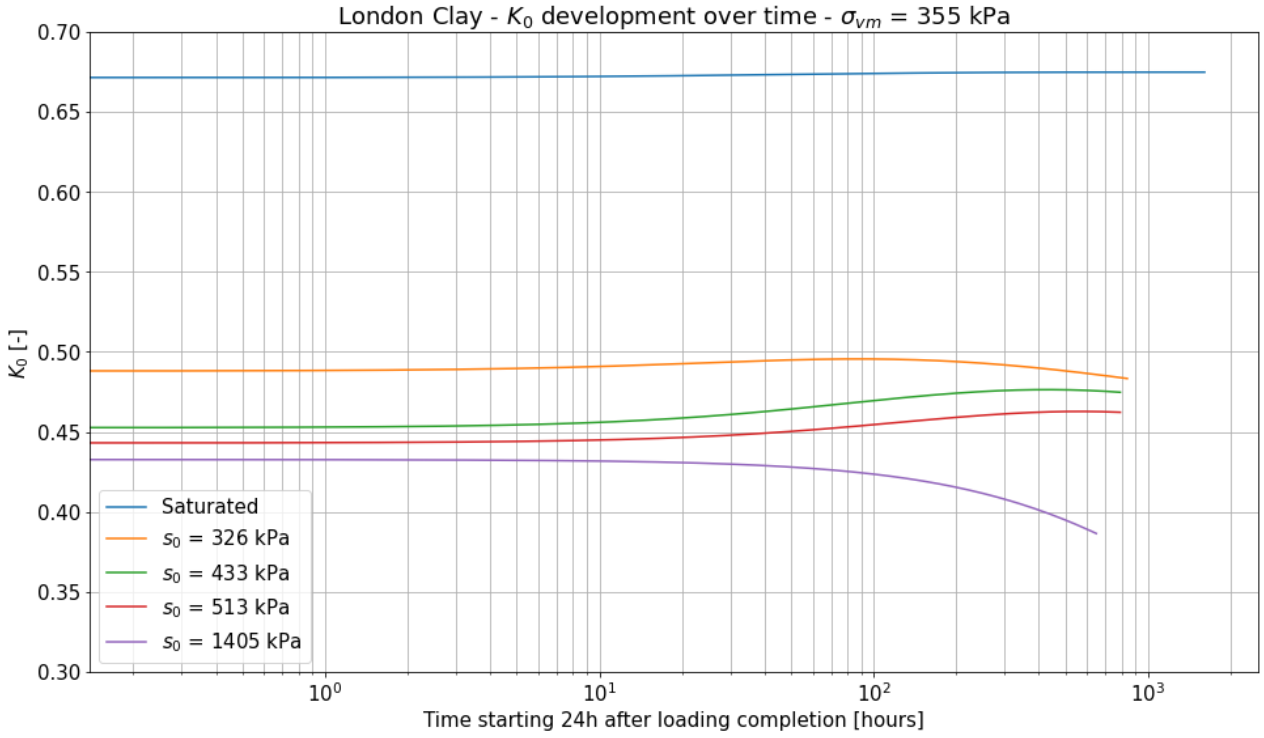

(c) σ_{vm} = 355 kPa.

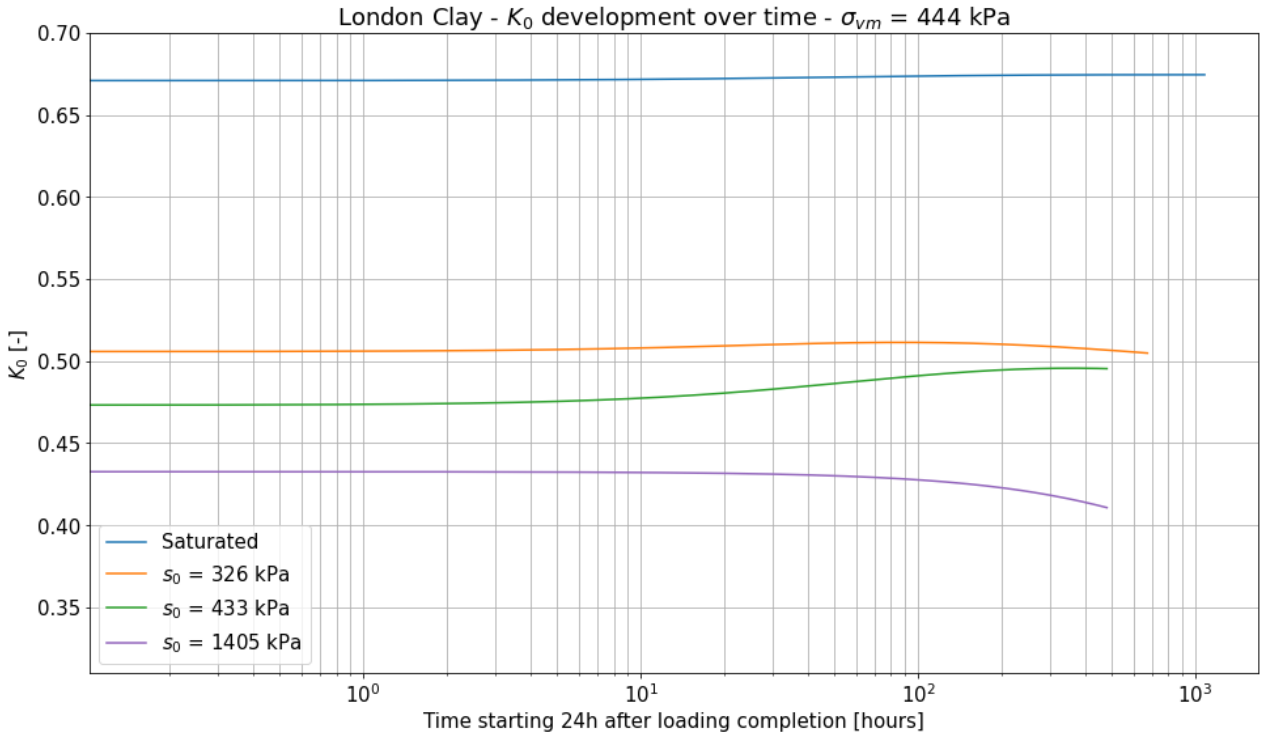

(d) σ_{vm} = 444 kPa.

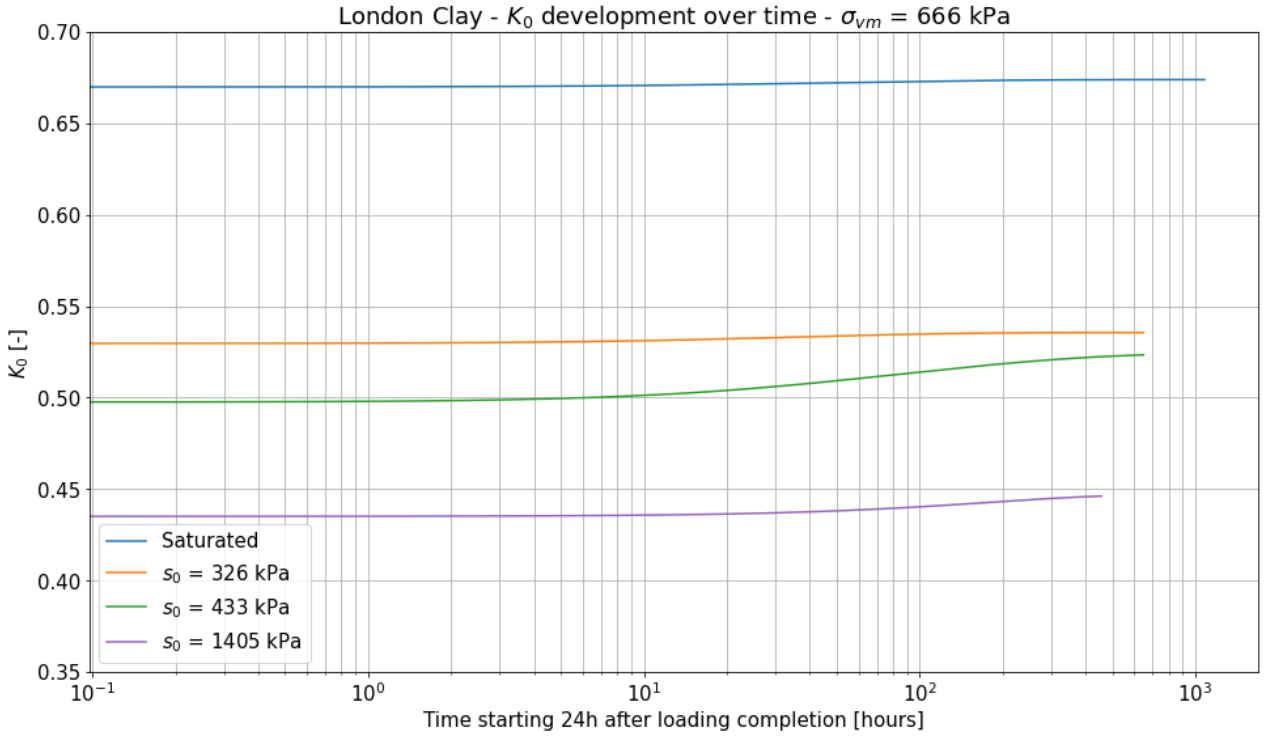

(e) σ_{vm} = 666 kPa.

Figure 75: K_0 development over time.

The results are less straightforward than expected. Depending on the combination of total stress and suction, different trends are predicted. All saturated samples show a small increase of K_0 with time but this increase is in the order of 1% only and is therefore not clearly visible in the figures above. For low loads (178 and 222 kPa) there is a monotonic decrease when the samples become desaturated. Figure 75c shows that at a higher load (σ_{vm} = 355 kPa) the value of K_0 increases initially at moderate suctions (326, 433 and 513 kPa). For the higher suction value of 1405 kPa a monotonic decrease is still observed. The lowest suction level of 326 kPa shows that after the initial increase, a decrease is observed.
This initial increase followed by a decrease is also present in figure 75d. In order to see what happens as time increases, model runs were performed where a very long (>100 years duration) creep test was simulated for the samples with σ_{vm} = 444 kPa. The results of this simulation are shown below with the long duration runs indicated with dotted lines.

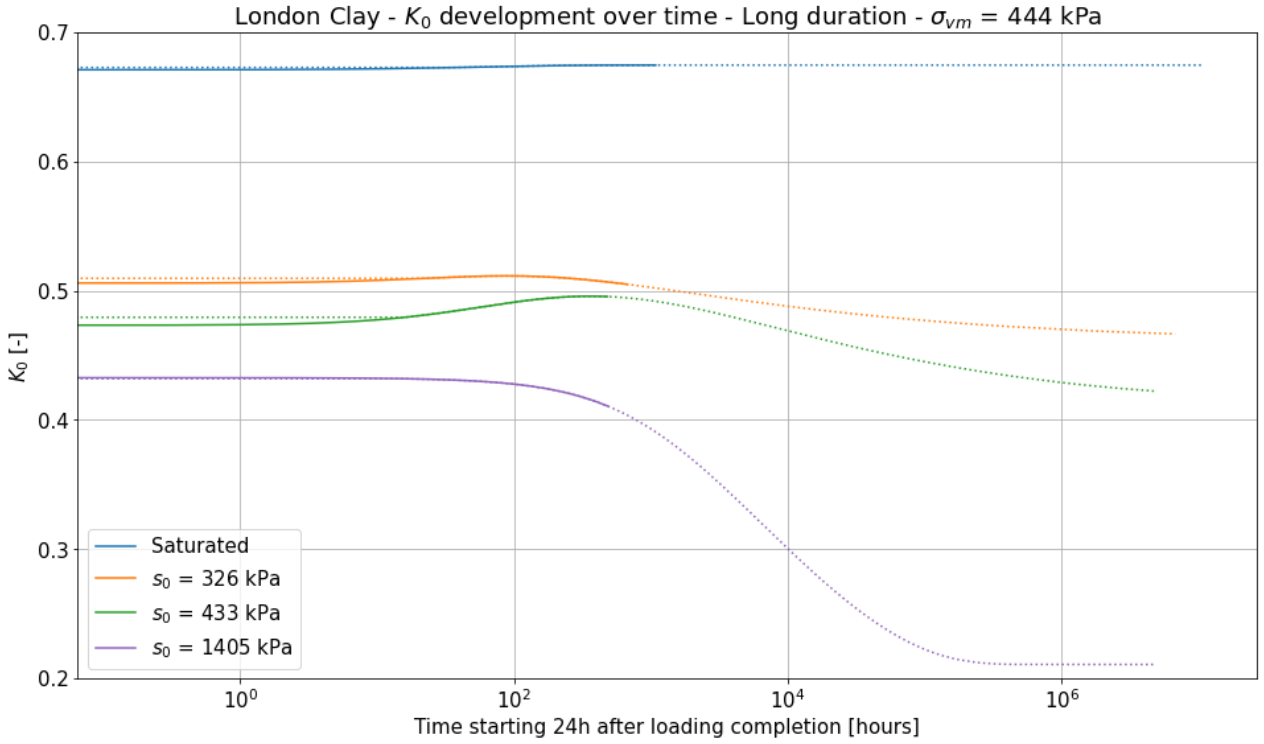

Figure 76: K_0 development over time - Long duration test - σ_{vm} = 444 kPa.

It can be seen that the decrease continues until the yield surface reaches the stress point and a change in K_0 is no longer observed. For the sample with s_0 = 1405 kPa a monotonic decrease is found.

6.2 Isotropic K_0 development

In order to answer subquestion 4 focused on the influence of anisotropy, it is required to isolate what the contribution of anisotropy is to the obtained results. To analyse this, the parameter accounting for the rate of evolution of anisotropy (C) is set to 0. Together with no initial rotation (which was found at the end of the drying stage), the tests are redone following a completely isotropic approach. The results of these simulations are shown below, in the figures, the original results obtained by the anisotropic approach are indicated with a dashed line.

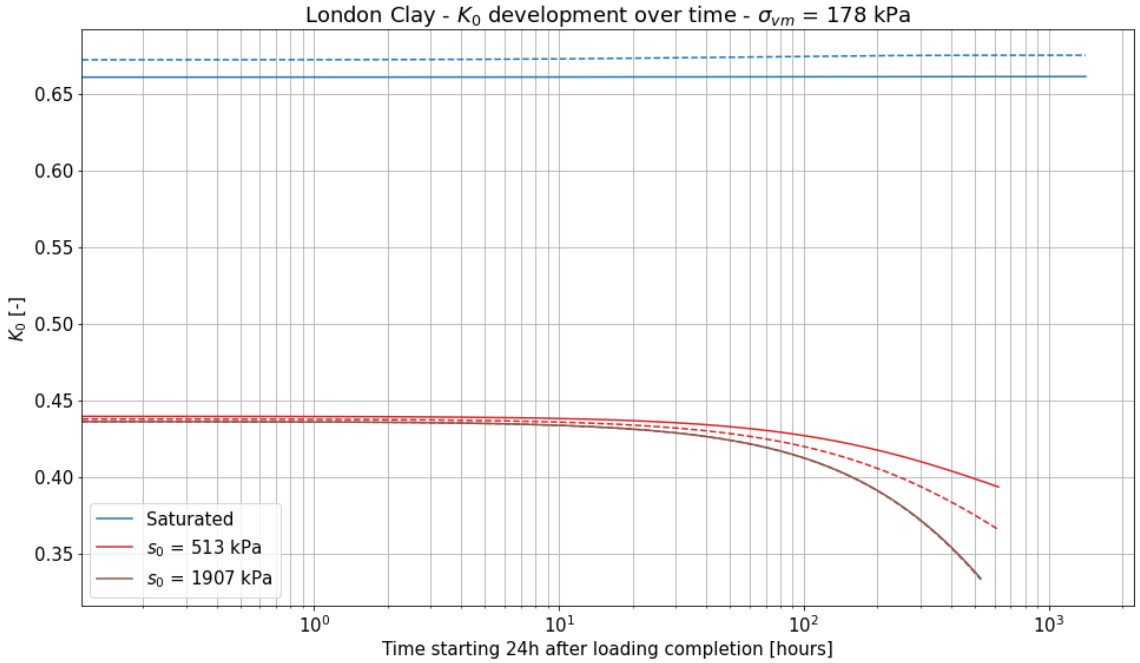

(a) σ_{vm} = 178 kPa.

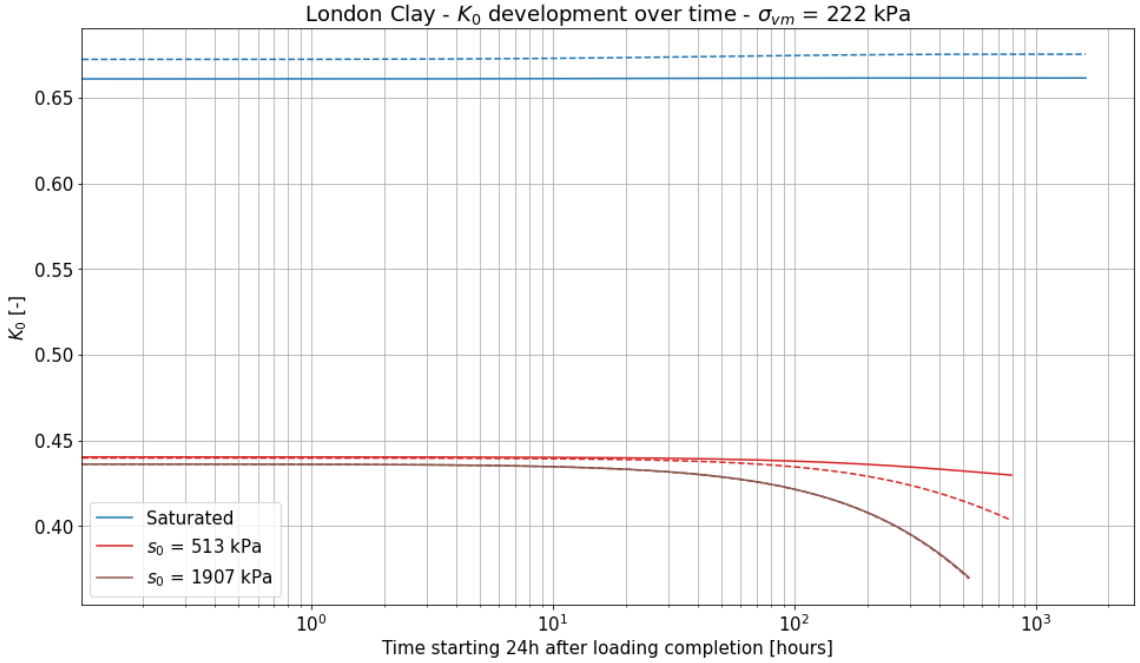

(b) σ_{vm} = 222 kPa.

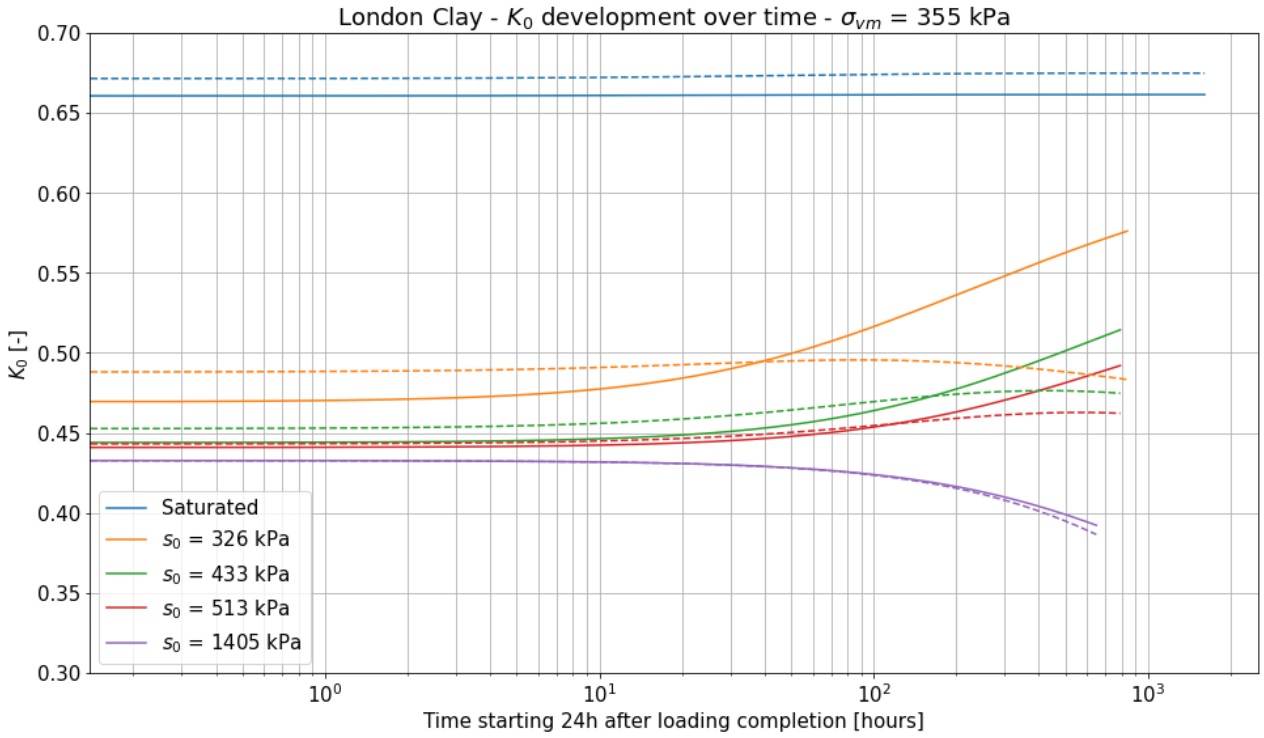

(c) σ_{vm} = 355 kPa.

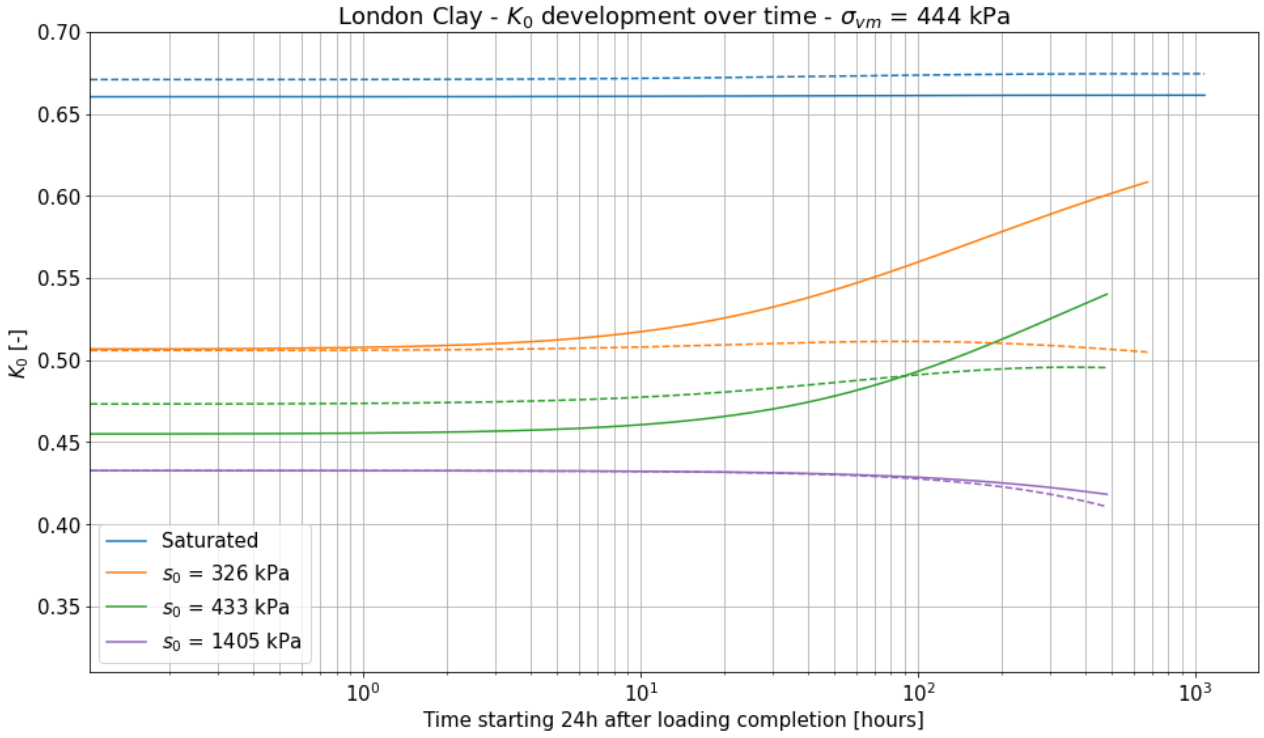

(d) σ_{vm} = 444 kPa.

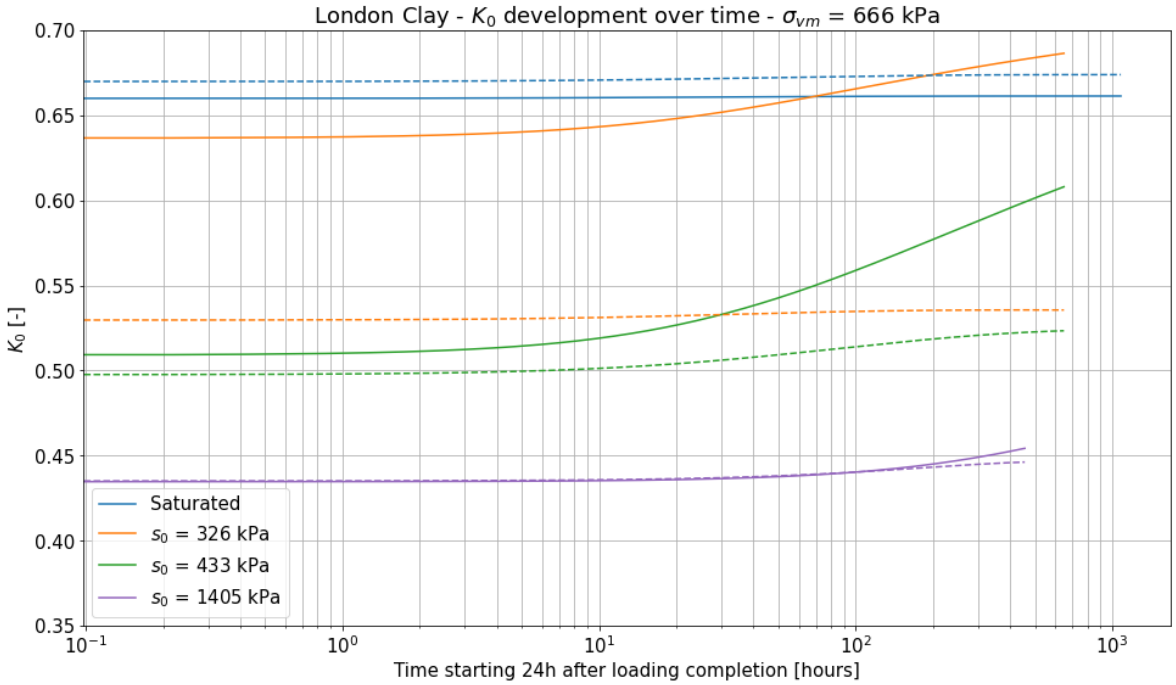

(e) σ_{vm} = 666 kPa.

Figure 77: K_0 development over time - Isotropic approach.

The results show a different trend which will be analysed more in depth in the next chapter. Shown below is again a model simulation with a duration of more than 100 years to show the long term trend of the K_0 prediction. The long duration simulations are indicated by a dotted and dash-dotted line for the anisotropic and isotropic approaches respectively.

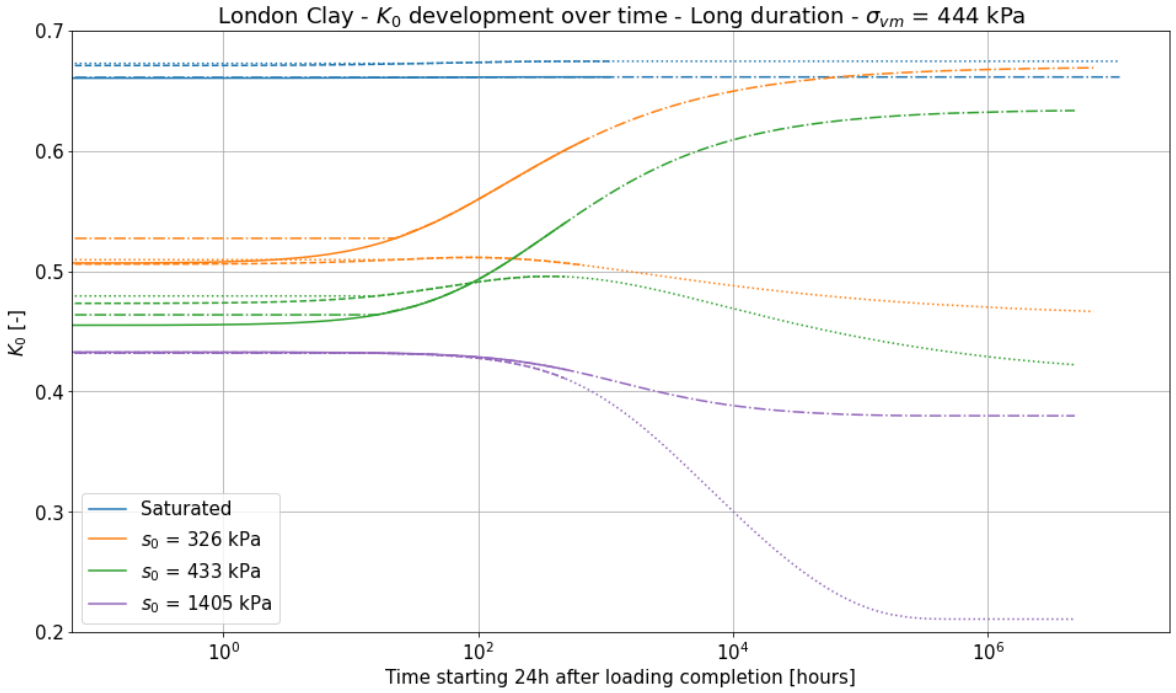

Figure 78: K_0 development over time - Isotropic approach - Long duration test - σ_{vm} = 444 kPa.

Turning anisotropy off in the model changed the deformation prediction slightly. Because the creep deformation data is the only experimental data available, it was made sure that the model without anisotropy also matched this data well. In order to get a good correspondence between experimental data and isotropic model prediction, the values of n_{suc} needed to be changed slightly. The new deformation plots are not presented again since they are very similar to the plots shown in the previous chapter. The updated n_{suc} vs suction graph is presented below. Again, the dashed lines indicate the previously found values when using the anisotropic approach.

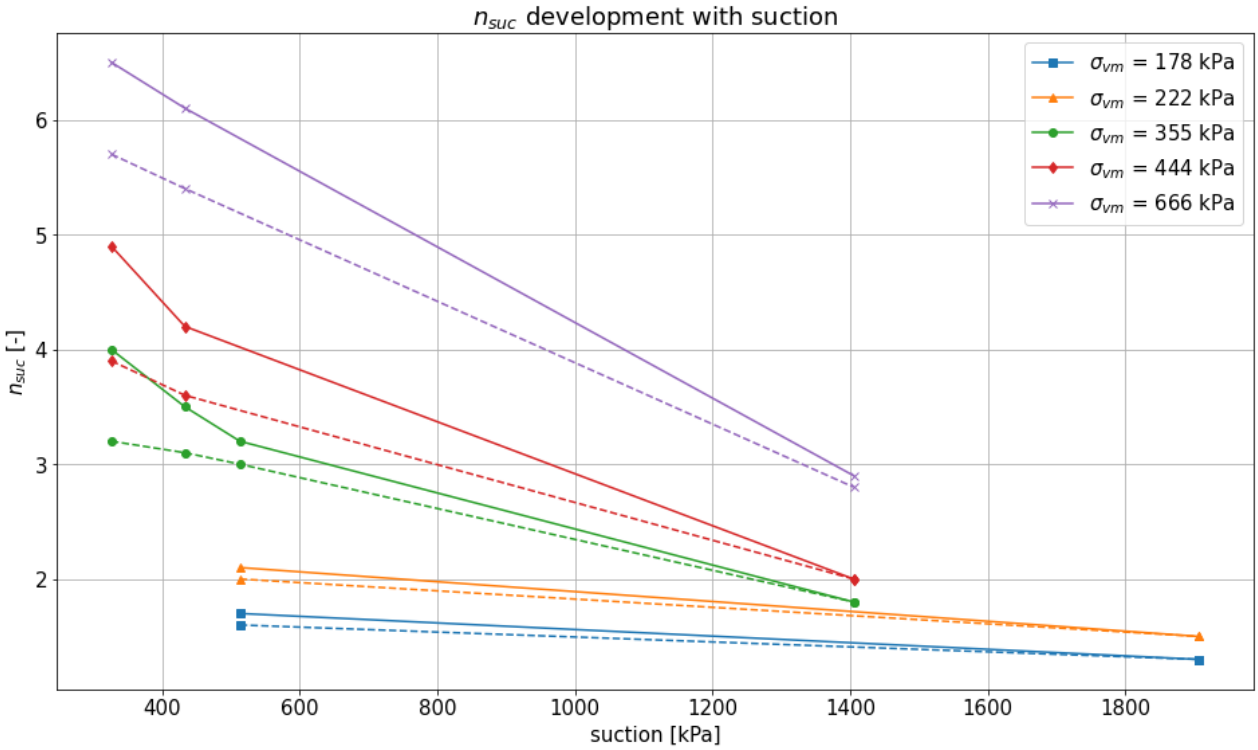

Figure 79: Development of n_{suc} with suction for each of the applied σ_{vm} - Solid lines indicate the isotropic approach, dashed lines the anisotropic one.

The values of s_{ref} remained the same for all samples so therefore figure 73 did not change.

6.3 $\hat{p}_c$ development

In order to get a full assessment of the soil stress state, the development of the preconsolidation pressure needs to be known. Using the same model runs as in the previous section, the change of $\hat{p}_c$ with time is now presented. All titles are labeled apparent preconsolidation pressure, this is because the preconsolidation pressure changes even though no change in the soil stress state is imposed (Leonards & Altschaeffl, 1964). Again, the anisotropic results are presented using dashed lines and the isotropic results using solid lines.

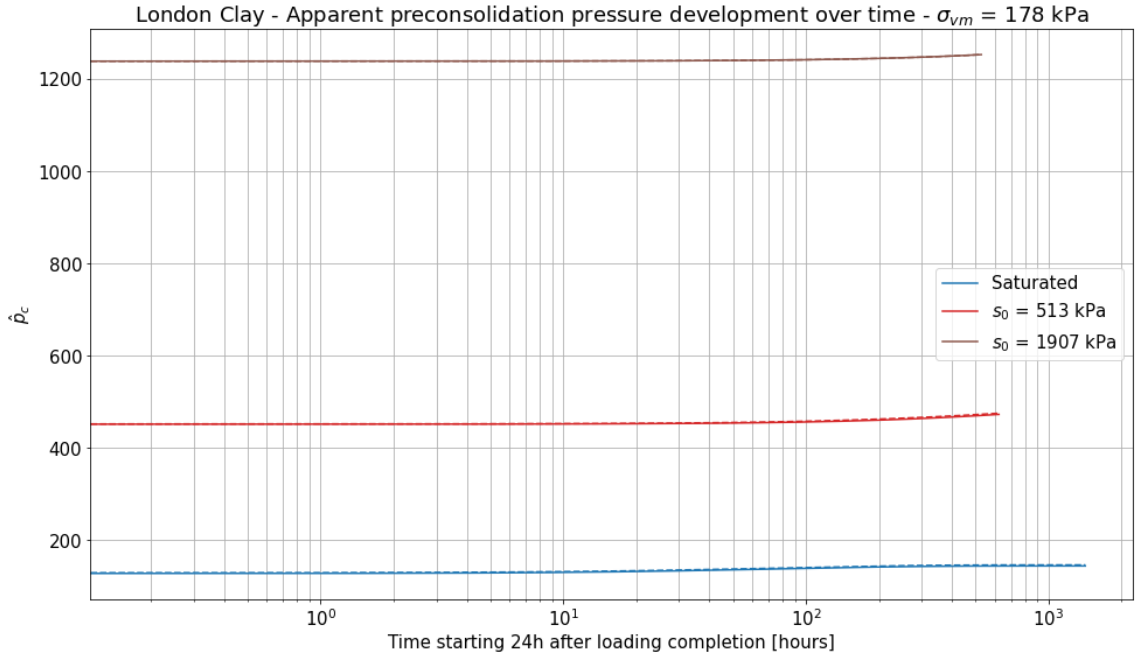

(a) σ_{vm} = 178 kPa.

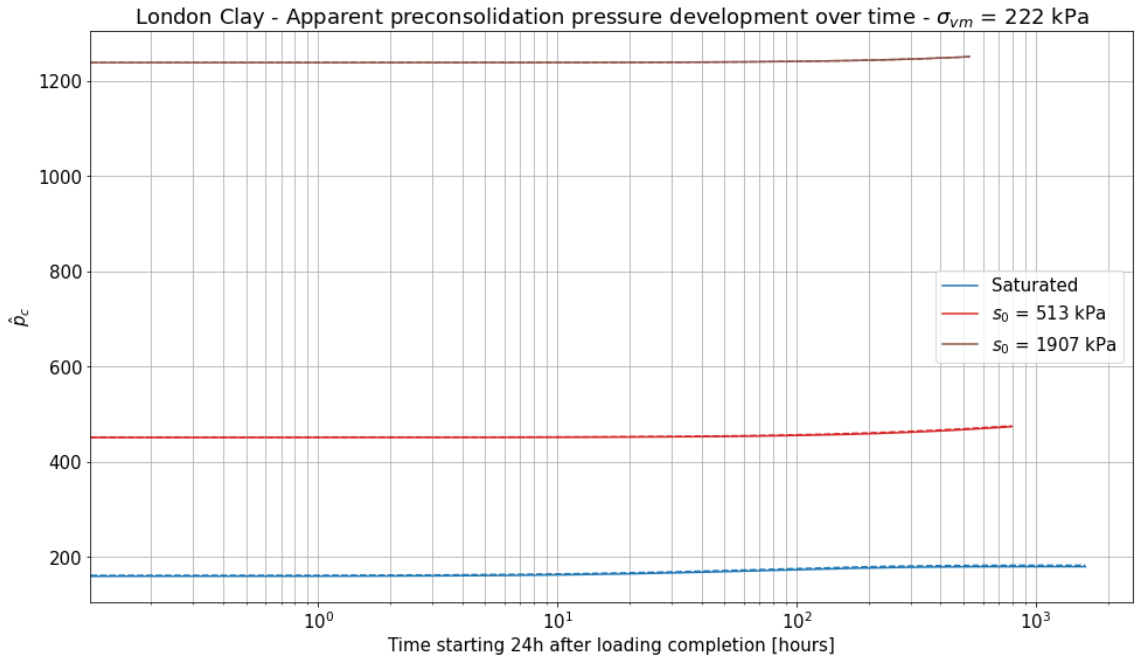

(b) σ_{vm} = 222 kPa.

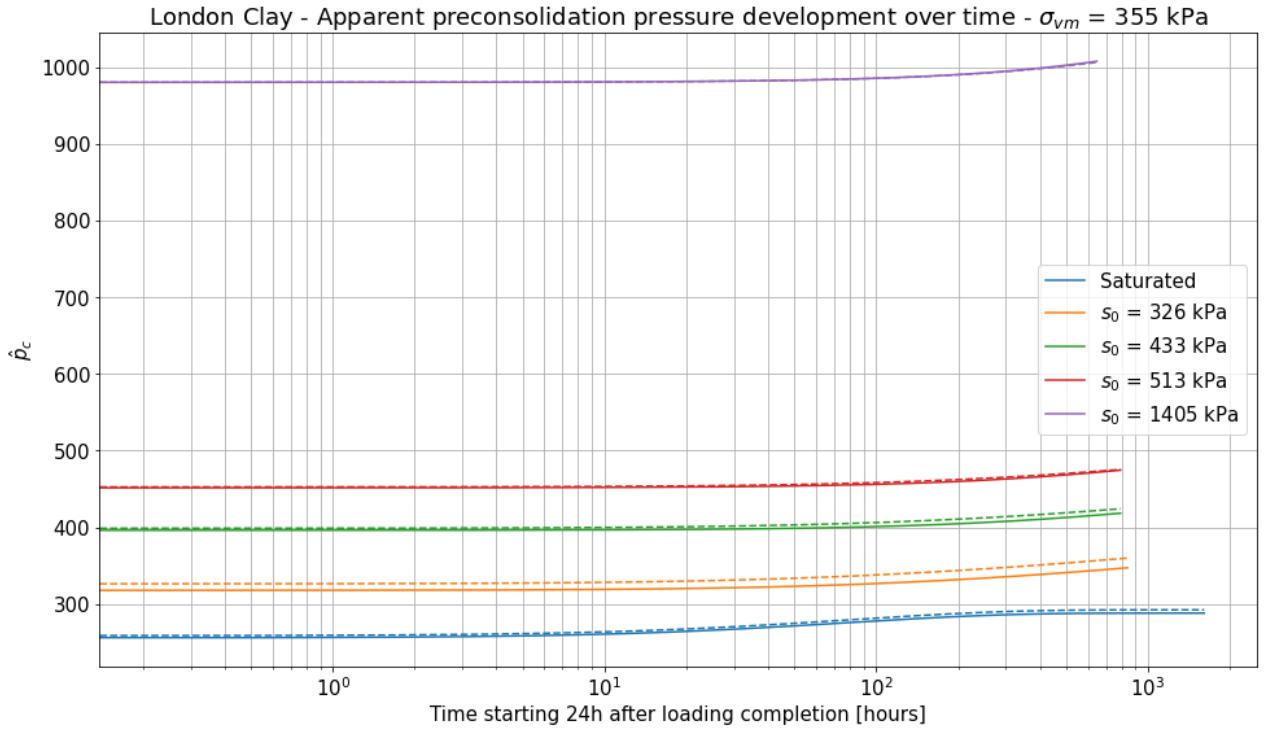

(c) σ_{vm} = 355 kPa.

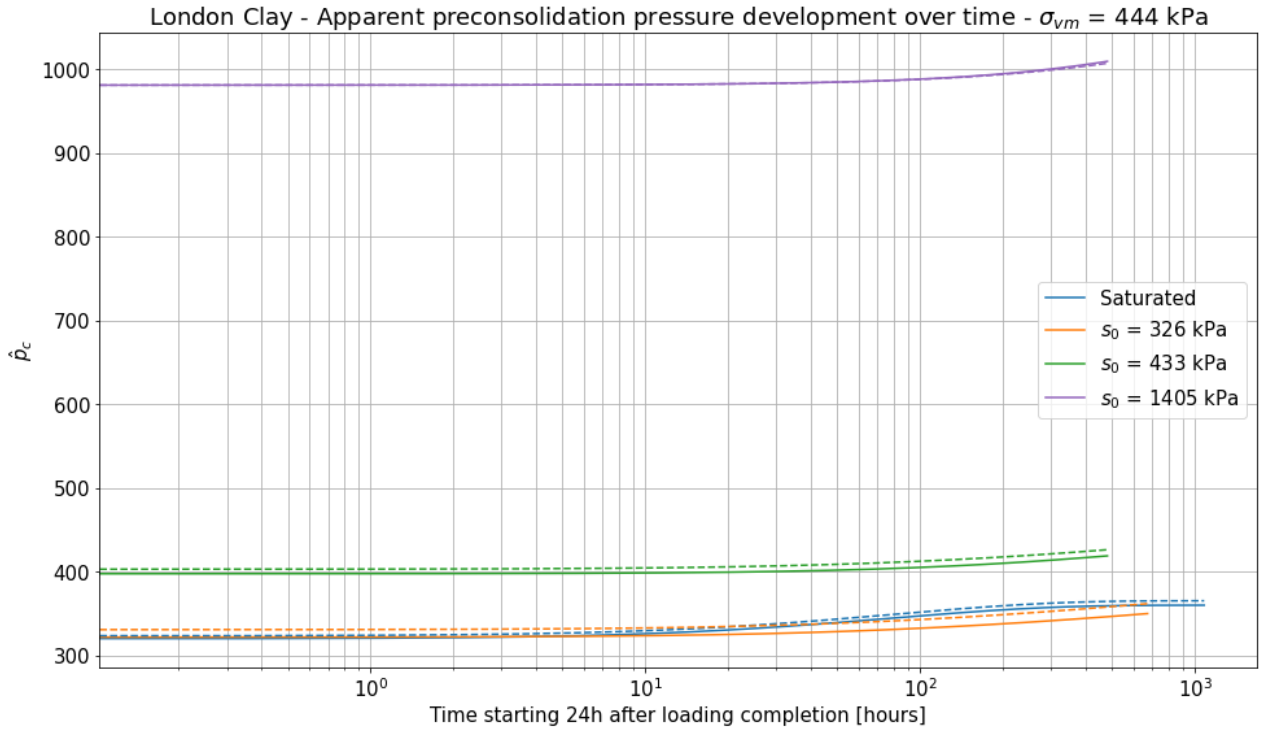

(d) σ_{vm} = 444 kPa.

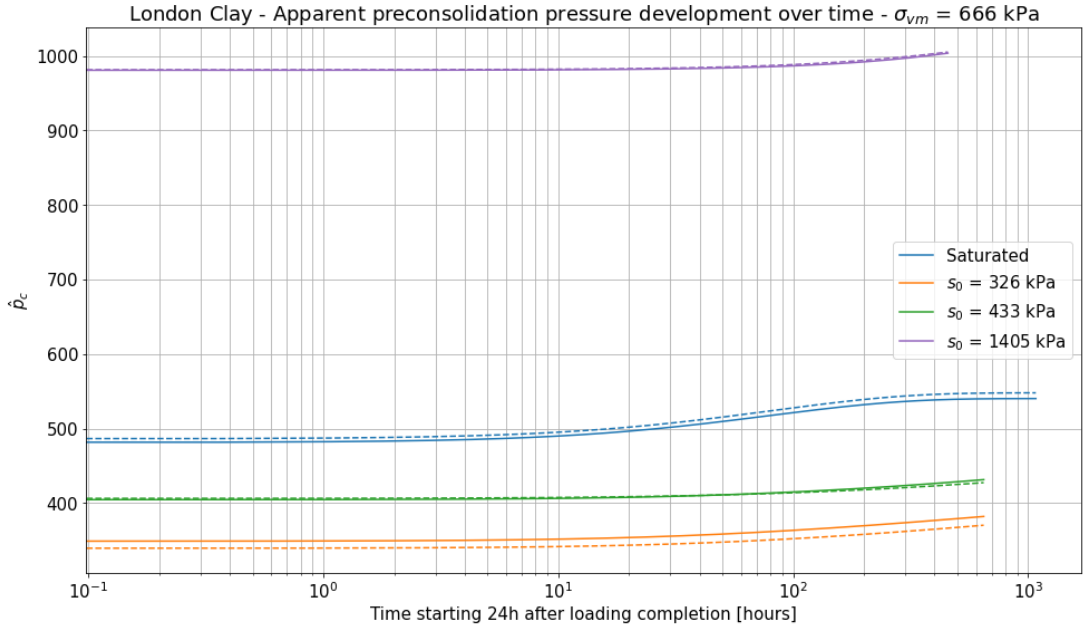

(e) σ_{vm} = 666 kPa.

Figure 80: $\hat{p}_c$ development over time.

Next to the results presented above, the change of $\hat{p}_c$ over the long duration simulation presented in figure 78 is available as well. These results are presented below, the notation is the same as in figure 78.

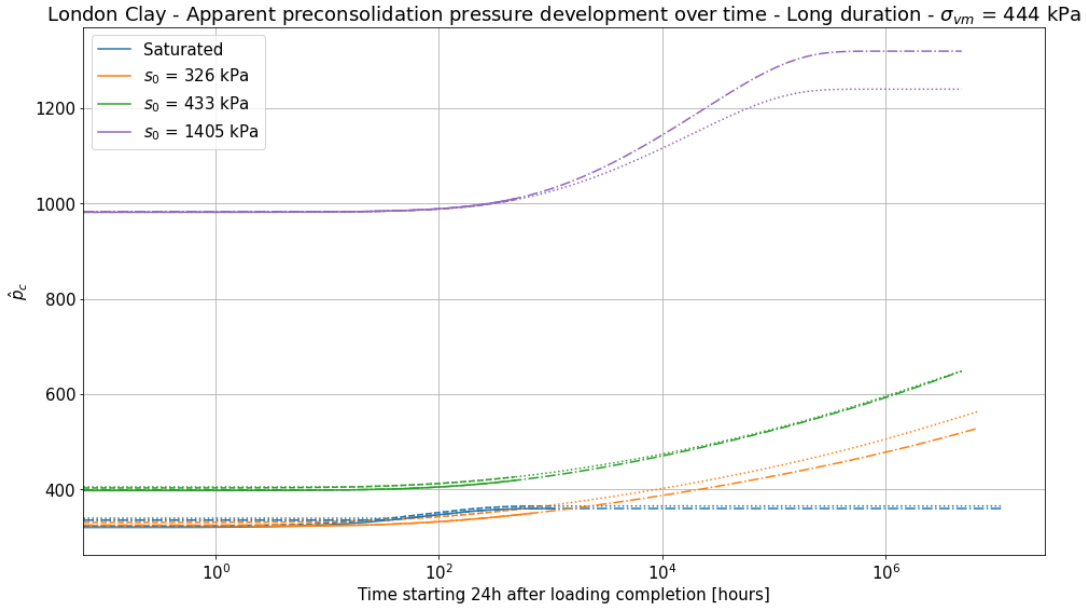

Figure 81: $\hat{p}_c$ development over time - long duration.

It can be seen that, regarding the change in apparent preconsolidation pressure, almost no difference is found between an anisotropic and isotropic approach.

In the next chapter, all the presented results are discussed to interpret what can be taken away from them, where the model difficulties lie and what the practical relevance of the findings is.

7 Discussion

In this chapter, the obtained results are discussed. The focus is on the most recently acquired results showing the change in K_0 over time at different suctions but the earlier presented results in the model validation sections are touched on as well. The performance of the different model versions and their difficulties have already been discussed in their respective sections though so therefore they are not treated in full detail again. Other points which are discussed are the role of anisotropy, the newly introduced model parameters, the suction range in which the model works accurately and the practical relevance of the findings.

7.1 Stress state changes over time at different suctions

In the previous section, the prediction of K_0 with time for samples with different suctions was presented. Since no experimental data is available, no conclusions can be drawn on the accuracy of the model prediction. However, this does not mean that the results cannot be discussed. From the literature study it is known that for saturated samples in general K_0 increases with time and for unsaturated samples it decreases with suction. Looking at the results, it can be seen that using the anisotropic approach, an increase with time is only found for samples with a low to moderate suction or a high applied load (figure 75e). This initial increase however was followed by a decrease later on which continued until the yield surface reached the stress point as is shown in figure 76. For low loads and high suctions, a monotonic decrease with time was found (figure 75b). Looking at the value of K_0 with suction it can be seen that if the suction increases, the value of K_0 is lower which is in line with what was found in the literature study.

The isotropic approach shows more straightforward behaviour with time. It is still observed that at low loads and high suctions the value of K_0 decreases with time (figure 77b) but the samples that show an increase with time no longer show a decrease after a certain time. An explanation for this behaviour is found by comparing the stress paths, shown below are first both the anisotropic and isotropic stress path of the sample with $s_0 = 326$ kPa and $\sigma_{vm} = 444$ kPa. After this, the individual stress paths are presented with corresponding SYS and DLS, for these plots, only the first year of the creep response is presented since the biggest changes take place in this time frame.

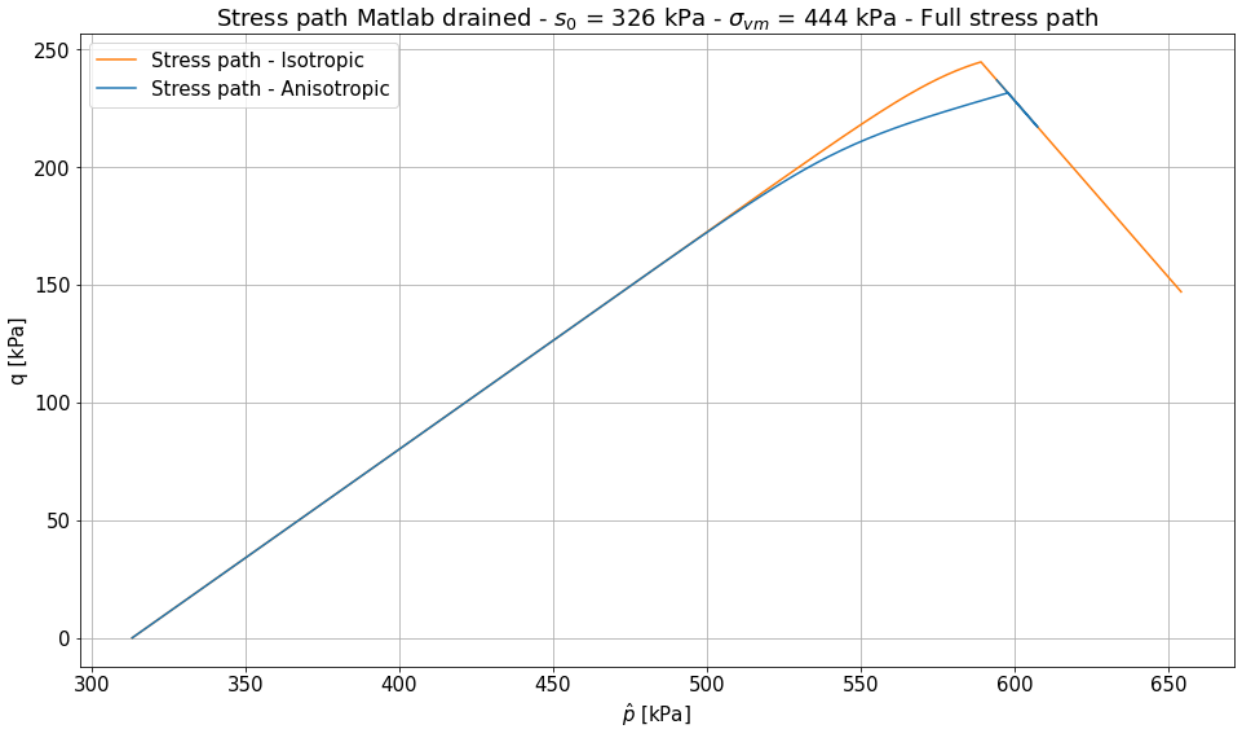

Figure 82: Stress paths for the long duration simulation of the sample with $s_0 = 326$ kPa and $\sigma_{vm} = 444$ kPa.

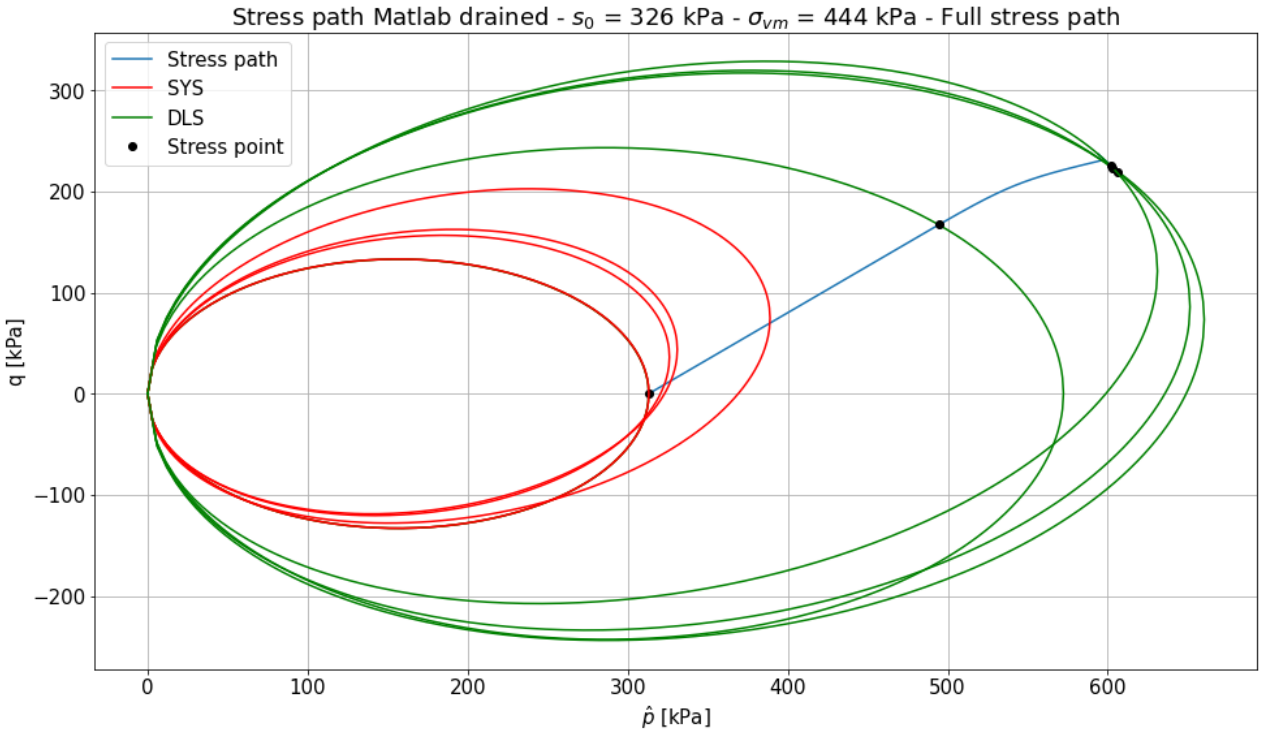

Figure 83: Stress path for the long duration simulation of the sample with $s_0 = 326$ kPa and $\sigma_{vm} = 444$ kPa - anisotropic approach.

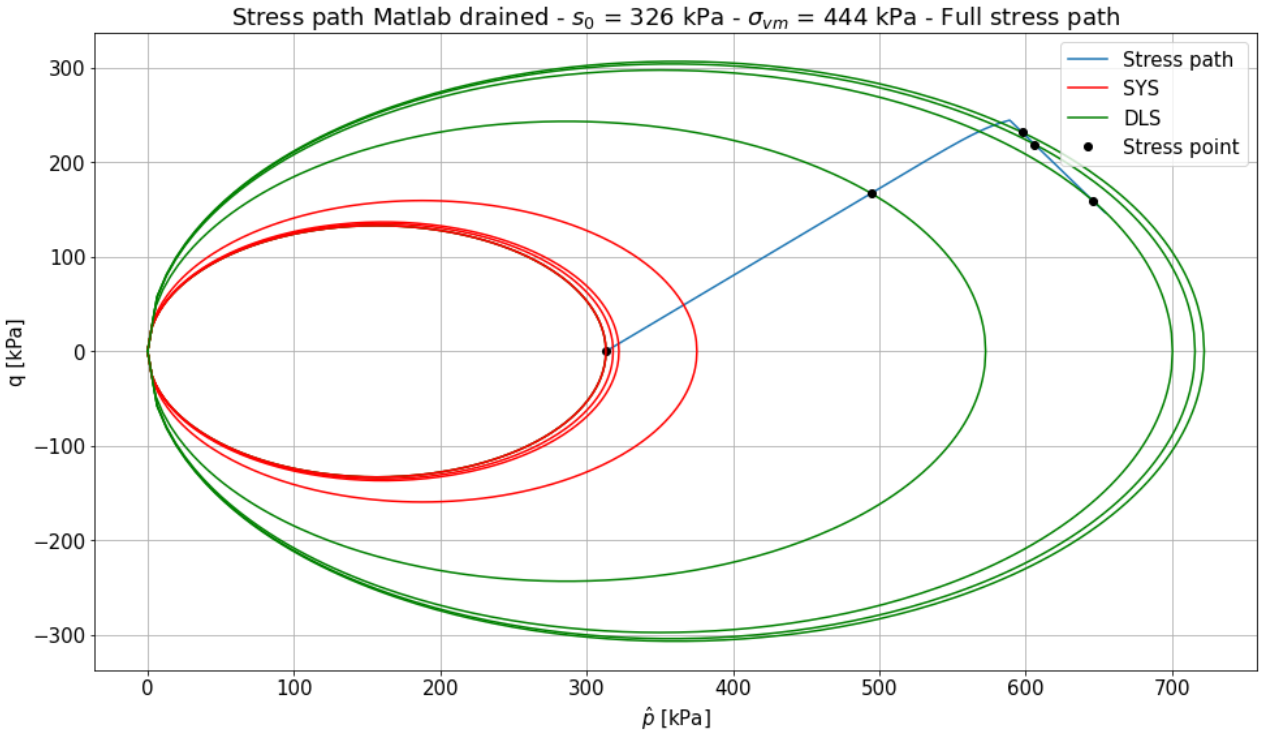

Figure 84: Stress path for the long duration simulation of the sample with $s_0 = 326$ kPa and $\sigma_{vm} = 444$ kPa - isotropic approach.

Figure 82 shows that for the anisotropic approach the stress path in $\hat{p}$-q space first moves towards the bottom right after which it turns around and moves to the top left. The movement towards the bottom right is accompanied by an increase in horizontal stress giving an increase of K_0. The movement towards the top left indicates the opposite behaviour (decrease of horizontal stress and thus a decrease of K_0). The explanation for this behaviour is found in figures 83 and 84. It can be seen that due to the rotation of the SYS and with it the DLS in figure 83, the stress path is forced to change direction. Using the isotropic approach, no rotation is present and therefore the stress path can continue to move towards the bottom right in $\hat{p} - q$ space.

A direct comparison between the K_0 predictions using anisotropic and isotropic approaches was presented in figure 78. It was found that for the same sample, the value of K_0 continues to increase until the yield surface reaches the stress point using the isotropic approach whereas using the anisotropic approach resulted in a decrease of K_0 with time.

A point worth noting is that in figure 77e, the sample with a suction of 326 kPa reaches a K_0 value higher than the saturated sample. Looking at the figure it is likely that the sample with a suction of 433 kPa will also reach this. No direct reason can be given to explain why K_0 for the unsaturated sample increases more than the saturated one. Without the presence of experimental data it is not possible to conclude if this observed behaviour is correct. It is also not possible to conclude whether the anisotropic or the isotropic approach captures the (qualitative) change of K_0 with time accurately.

The final results that were presented showed the change of apparent preconsolidation pressure with time. The results showed that $\hat{p}_c$ increased with time for all samples as was to be expected since the static yield surface will expend towards the stress point. Comparing the long duration simulation results (figure 81), it can be seen that not only does $\hat{p}_c$ continue to increase until the stress point is reached but the difference between prediction using an anisotropic and isotropic approach is minimal. The increase of $\hat{p}_c$ with time was also found for OVP clay as shown in figure 54.

7.2 Role of anisotropy

The role of anisotropy is clearly present in the results in the previous section. The K_0 prediction over time at different suction levels becomes more straightforward using an isotropic approach but there is no evidence if this is also the real soil behaviour.

Literature shows that for saturated soils, isotropic models tend to overpredict the value of K_0. For example, looking at the isotropic Cam Clay and Modified Cam Clay models, Federico et al. (2009) state that the original Cam Clay model predicts values much higher than the measured K_0, the Modified Cam Clay model overpredicts the measured value less but still does not match experimental results accurately. Wheeler et al. (2003) show that the correct K_0^{NC} prediction is found by adjusting the rotation of the yield surface which supports the previous findings. This work was summarised by Sivasithamparam and Castro (2016) who stated that 'the authors believe that trying to fit K_0^{NC} values with isotropic plastic potential surfaces is not realistic.'

It has to be noted that the findings above are found for saturated conditions only. Romero and Jommi (2008) evaluated the importance of anisotropy for unsaturated soils and found evidence for an anisotropic material response. This can serve as a starting point to evaluate the importance of anisotropy in assessing the initial stress state of a soil.

Another point worth noting is that the above theory states that for saturated soils an anisotropic approach is needed to get a correct prediction of K_0, this is coming from the fact that it is found that isotropic approaches overpredict K_0. However, looking at the obtained results it can be seen that the initial K_0 value is roughly the same for the anisotropic and isotropic prediction but that using an isotropic approach, K_0 reaches higher values than for the anisotropic alternative. This is not in line with the findings for saturated soils so therefore blindly assuming that the anisotropic approach is correct based on the above theory cannot be done. This emphasises the need for lab tests to confirm which soil behaviour is correct.

7.3 Suction dependent viscous nucleus parameters

The developed viscous nucleus introduced two new parameters, s_{ref} and n_{suc}. In both the isotropic and anisotropic approach, these parameters show dependency on suction and stress. s_{ref} shows a linear increase with suction and no dependency to the stress level. n_{suc} on the other hand shows a decrease with suction but a higher starting value depending on the stress (figures 73, 74 and 79). A preliminary attempts was made to fit analytical functions to the obtained values of which the results are shown below. Note that this preliminary analysis is only performed on the anisotropic data since the majority of this work has included anisotropy.

The following functions are proposed for s_{ref} and n_{suc} respectively.

$$s_{ref} = \alpha_{suc} * s \tag{46}$$

where α_{suc} is a fitting parameter governing the slope of the increase of s_{ref} with suction.

$$n_{suc} = n_{suc,sat}\sigma_v - \beta_{suc}(\sigma_v)s \tag{47}$$
$$\text{with, } \beta_{suc}(\sigma_v) = a_n * \sigma_v^2 + b_n * \sigma_v + c_n$$

where $n_{suc,sat}$ is the value of n_{suc} at the saturated state normalised by the stress level it is determined at. a_n, b_n and c_n are fitting parameters to determine the slope of the decrease of n_{suc} with suction.

Using the experimental data the following parameter values were obtained.

Table 28: Fitted values s_{ref} and n_{suc} function parameters.

Parameter	Unit	Value
α_{suc}	[-]	0.047
$n_{suc,sat}$	kPa^{-1}	0.01
a_n	kPa^{-2}	-3.66e-09
b_n	kPa^{-1}	8.30e-06
c_n	[-]	-1.21e-03

Using the values given above, the function were fitted through the s_{ref} and n_{suc} data of which the results are shown below.

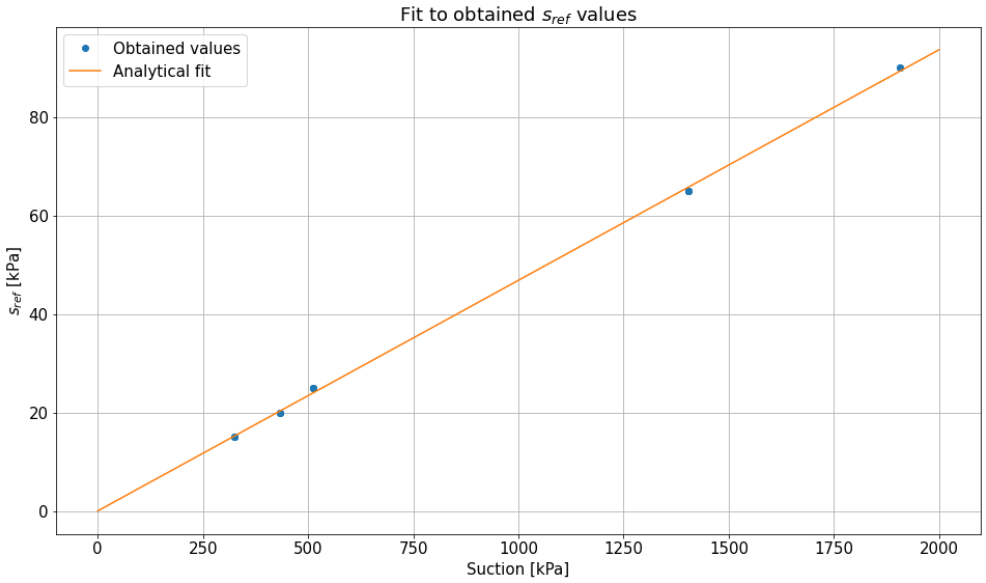

Figure 85: Fit to obtained s_{ref} values.

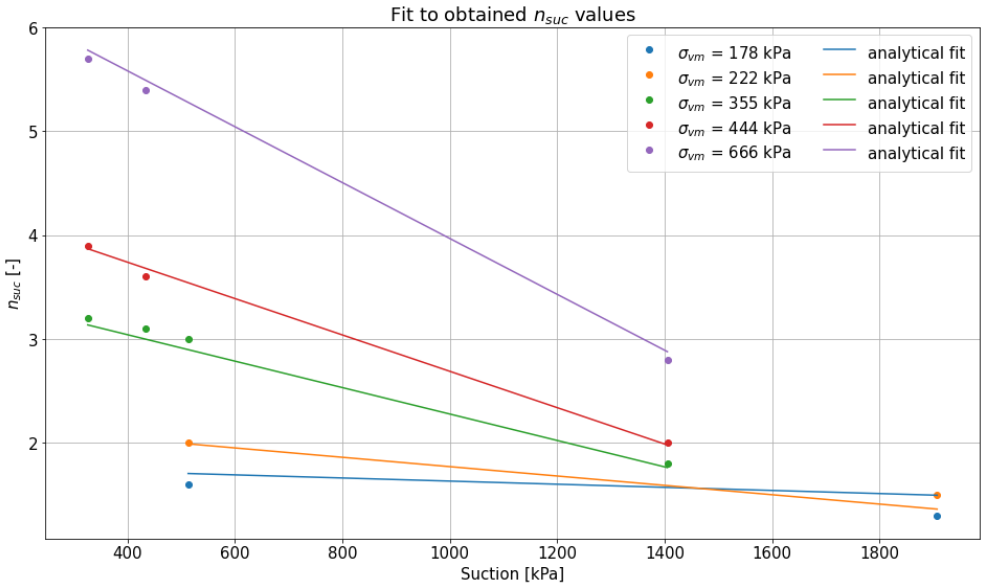

Figure 86: Fit to obtained n_{suc} values.

It can be seen that the fit for s_{ref} is accurate but that it is more difficult to properly fit a function for n_{suc}. It is therefore possible to replace s_{ref} with α_{suc} multiplied by the suction with only α_{suc} having to be determined based on the used material. This avoids having to calibrate s_{ref} for each sample.
For n_{suc}, the proposed function needs to be refined further, the main difficulty is found in calibrating the slope correctly based on the stress level. The currently proposed law has a constant slope at constant stress and would result in negative n_{suc} values at suctions beyond 2 MPa. Potential could be found in fitting an exponential curve through the obtained values. However, attention needs to be paid to three aspects. The first one is that if a law is fitted which remains valid for higher values of suctions. The second point is that if a law like this is proposed, the accuracy at low suctions (which are more relevant in lab testing as shown before) needs to be secured. The final point is that the goal of the proposed function is to make the calibration process easier. This means that a proposed function cannot contain too many new parameters because this could make the calibration process more difficult and therefore the proposal could lose all its value.

7.4 Suction range

It was found in section 5.5.1 that the unsaturated model works accurately for suctions < 1 MPa. For suctions starting at 1405 kPa the model was not able to predict the experimental data satisfactory. To which exact suction value the model remains accurate is not known but this is also not of high importance. What is interesting to look at is a comparison between the accurate suction range of the model and other experimental data from the literature. An investigation on unsaturated creep tests performed by other authors shows that the high suction values that are tested by Rezania et al. (2020) are not commonly encountered. Lai et al. (2014), Lai et al. (2009), Li and Yang (2018), Zhang et al. (2020), Zhu and Yu (2014), and Zou et al. (2013) all performed unsaturated tests on different soft soils. The maximum suction values reached in their testing programs ranged from 200 to 300 kPa. This shows that the suction range of the developed model in this work is good enough to model commonly found suction values in practice. Based on this literature it is likely that in a potential follow-up study where unsaturated creep tests will be performed to investigate the K_0 over time behaviour of a soil, the maximum suction value will not exceed a suction of 513 kPa until which the current model version is validated. This means that no improvement to the model are required if this is indeed the case.

If the model needs to be used beyond the validated suction values, two approaches can be adopted to obtain satisfactory results. The first option is to try to remove as much uncertainty from the experimental data as possible. Two main sources of uncertainty in the data from Rezania et al. (2020) are the void ratio with which the data is normalised and the SWRC. If both of these can be determined with higher accuracy, it could be

found that the current model version is accurate for suctions beyond 1405 kPa.
Another option of improving the model prediction is by making adaptations to the actual model itself. For example, considering double porosity as explained in section 2.2.1 and implementing this in the model could lead to an improvement of the modelling of the unsaturated conditions. Li et al. (2017) developed a model in which double porosity is considered. They split the adsorbed and capillary water and the macro- and micropores into two distinct phases. Using this approach, they developed a model and tested this to experimental data where wetting and drying cycles were applied to Boom clay and triaxial tests on Zaoyang expansive clay. The results showed that the model was able to simulate the mechanical behaviour as well as the water retention characteristics of the clays reasonably well.
Della Vecchia et al. (2013) found that next to anisotropy, the evolution of the clay aggregate size is an important aspect of clay fabric. This evolution is promoted by water exchange between inter-aggregate and intra-aggregate pores. This evolution was quantified and included in the development of a hydromechanical model. Simulations of experimental data were performed on different clays and is was found that the model was able to accurately predict many aspects of the behaviour of compacted clayey soils. Examples of these aspects are mechanical loading at constant water content and wetting-drying cycles at constant external stress.

7.5 Practical relevance

The final thing worth discussion is the practical relevance of the findings. An obvious practical relevance is found in foundation piles. These piles transfer their load to the soil through both tip resistance and sleeve friction. Roughly speaking, this tip resistance is dependent on the vertical stress in the soil but the sleeve friction is dependent on the horizontal stress. In this schematic framework, a change in K_0 would cause a change in the sleeve friction. Therefore, it is of value to improve the prediction of the change in horizontal stress through a pile's lifetime caused by a change in K_0.

A less schematic example is given by Salgado et al. (1997), they analysed the effect of K_0 on both the normalised CPT (Cone Penetration Test) tip resistance as well as the Cyclic Resistance Ratio (CRR) defined as the cyclic shear stress divided by the initial vertical effective stress. After that, they combined the relationship to evaluate when the soil would liquefy. The result of this is shown below.

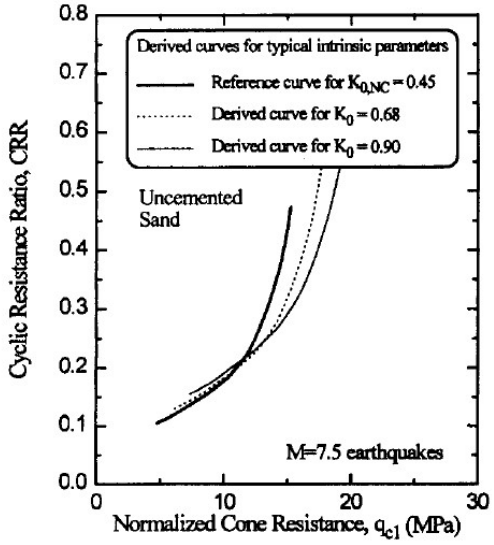

Figure 87: CRR vs normalised q_c relationship at different values of K_0.

In the figure above, the soil suffers liquefaction when the state moves to the top left of the line. It can be seen that as K_0 increases to above K_0^{NC}, the line moves to the right. This means that at a high normalised q_c, the soil liquefies earlier than the original K_0^{NC} curve shows. Because of this it is of importance to get a good prediction of the K_0 change with time to contribute avoiding liquefaction problems.

8 Conclusions and recommendations

In this final chapter, the research questions are answered. Following this is the recommendations section in which the recommendations for further research are given.

8.1 Conclusions

The answer to the main research question is found in the answers of the subquestions. Because of this, the subquestions will be answered first after which the answer to the main research question is formulated.

1. **Is there an agreement in literature on the influence of creep and drying/wetting on the soil stress state and is there solid physical reasoning behind this?**
   Investigation into the results of experimental tests performed by other researchers showed good agreement on the individual influences of both creep and unsaturated conditions on K_0. It was found that, for saturated samples, K_0 increases as a soil is left subjective to creep. This was not only found to be true for clays but data on peat also showed this behaviour. The only set of experimental results predicting a decrease of K_0 with time was presented as well (Wijeyesekera & Mohamed, 2000) but using other literature (Grimstad et al., 2021) it was shown that this decrease was not the final soil behaviour and that after a while this data also showed an increase of K_0 with time. Physical reasoning behind creep was touched on extensively. Five causes were elaborated upon focussing on the grains and the pores individually. For the grains, structural rearrangement was mentioned where due to sliding, breaking of bonds and jumping of molecules, the grains rearrange themselves under constant effective stress. Looking at the pores, reasoning for creep was found in water flow in a double pore system. Work from Akagi (1994) was referred to who showed experimentally that during creep water drains from the micropores present in clays.

   The effect of unsaturated conditions was harder to capture. This is because experimental data can be presented using different stress approaches and the choice of stress approach affects the obtained results. From a qualitative point of view it was found that K_0 decreases as the suction increases using both Bishop's and Fredlund's stress approaches. When for example the suction stress approach was used, a unique value for K_0 with suction was found. No work was found in which an increase of K_0 with suction was presented which indicates the agreement in literature that K_0 either decreases or remains constant with suction.
   Physical reasoning was found in the elaboration of the suction stress approach. This approach captures the processes at the particle level showing that as the soil desaturates these processes become important.

2. **How can the influences be validated?**
   The influences of creep and unsaturated conditions were validated by implementing their effects in a constitutive model. The basis for the model was based on the saturated elastoplastic SANICLAY model. In order to validate the influence of creep, this model was extended to become saturated elasto viscoplastic by introducing time dependency through Perzyna's approach. This new version of the model was validated using experimental data on OVP clay from the literature and the results showed that the model was able to follow stress paths and predict creep deformation accurately. Experimental data from Polinder (2019) was used to assess the K_0 change with time but due to significant scatter in the data this assessment was difficult. An attempt was made nonetheless comparing the model output to this experimental data and the results showed that the experimental K_0 roughly increased with time and that the numerical K_0 prediction increased with time as well. This numerically predicted increase was however a lot smaller than the rough experimental trend.

   Unsaturated conditions were analysed by adopting the average soil skeleton approach as developed by Jommi (2000). This approach was implemented in the original saturated elastoplastic model resulting in an unsaturated version of this model. The reason for this is that this way it was possible to first assess the influence of the unsaturated conditions independently of creep. This version of the model was again tested using experimental data from the literature. Loading/Unloading tests were analysed at different suctions and the results showed that the model was able to accurately predict the soil behaviour up to a suction of 1 MPa. For higher suctions, the model performance was worse but it has to be noted that

at high suctions the uncertainty in the experimental data increased so therefore it is hard to conclude if this decreased model performance is due to the model capabilities or the quality of the experimental data.

3. **What is the influence of drying/wetting on the creep behaviour of a soil?**
   Upon validating the individual influences of creep and unsaturated conditions, a model version was constructed where both Perzyna's and the average soil skeleton stress approach were implemented which resulted in an unsaturated elasto viscoplastic model. This model was tested to experimental unsaturated creep tests and the results showed that the model predicted the creep deformation to occur too quickly. The deviation from the experimental data increased as the suction increased. Because of this, a coupled effect was introduced. The viscous nucleus in Perzyna's approach was adapted to include a term dependent on suction. This introduced two new parameters s_{ref} and n_{suc} which were found to be dependent on suction and load. With this model adaptations it was possible to predict the creep deformation with a higher level of accuracy. The need for a coupling effect showed that unsaturated conditions do have an influence on the creep behaviour of a soil and that this can be accounted for in a model.

4. **What is the influence of anisotropy on the initial stress state?**
   As a final analysis, it was investigated what the role of anisotropy is in the model prediction of the soil behaviour. It was found that the same creep deformation prediction could be obtained by tuning n_{suc}. A comparison between the K_0 prediction with time using an anisotropic and isotropic approach showed that using the anisotropic approach, K_0 would initially increase with time after which it would decrease to a value lower than the starting value. For high suctions (>1 MPa) and low loads (<222 kPa) only a decrease was found. The isotropic approach showed that the initial increase continued and K_0 would no longer decrease with time. The decrease at high suctions and low loads was still present. Which of the two predictions is correct from a qualitative point of view cannot be concluded due to the lack of experimental data on unsaturated K_0 development with time.

Using the answers to the subquestions, the main research question can now be answered. This question was formulated as follows.

Can the prediction of K_0 be improved for unconventional stress histories including creep and drying/wetting cycles?

From a qualitative point of view, the prediction of K_0 can be improved by accounting for creep and unsaturated conditions. The trends that were found in the literature study showing an increase of K_0 with creep and a decrease with suction are predicted by the developed unsaturated elasto viscoplastic model. Whether the prediction can also be improved from a quantitative point of view cannot currently be determined. In order to do this, lab tests are required to which the model prediction can be compared.

The prediction improvement does have some limitations, it was found that the model has difficulties dealing with high suctions and the K_0 prediction with time at low loads showed a decrease with time. Based on the available experimental data this decrease would intuitively be deemed to be incorrect. It has to be stated though that the available experimental data includes only saturated tests. It could be the case that future unsaturated tests show that at low loads the value of K_0 does indeed decrease with time which would mean that the accurate prediction range of the model is larger than can be concluded based on current day's knowledge.

8.2 Recommendations

In this section, recommendations are given for future research. This work presented a first approach in developing an unsaturated elasto viscoplastic constitutive model with a coupled effect for which the need as indicated by available experimental data. The developed model showed some clear limitations for example at high suction levels so therefore room of improvement is definitely present. The following recommendations are given based on the findings of this project.

1. The most important recommendation is that unsaturated creep lab tests need to be performed in order to assess experimentally the change of K_0 with time for unsaturated soft soils. Using the results of these lab tests, the model performance can be evaluated starting from a qualitative point of view. Performing unsaturated creep tests is however not that straightforward to do due to the requirement of controlling the suction or water content over long periods of time. Therefore, these tests would require proper care and attention. The type of test that is recommended is a set of triaxial tests with automatic K_0 control. What is meant by this is that the apparatus automatically corrects the pressures in order to obtain negligible radial strains and therefore preserve the sample in K_0 conditions. This type of test is described in Muraro and Jommi (2019).

2. The loading/unloading experimental data that was used in the validation of the unsaturated elastoplastic model included a significant amount of uncertainty. The data was normalised with an unknown void ratio and the Soil Water Retention Curve that was used was not determined accurately at high suction levels. It is recommended to attempt to remove as much uncertainty from the experimental data as possible by either redoing the loading/unloading tests in the lab or by further analysing the data and the SWRC. This allows for a better model performance assessment and will lead to a clearer overview of the model capabilities and accurate suction range.

3. Upon validation of the K_0 prediction with time, the unsaturated viscous nucleus parameters (s_{ref} and n_{suc}) can be determined with a higher accuracy. Once they are known at each combination of suction and load it is recommended to define analytical functions for both parameters dependent on stress and suction. A proposal was presented in the previous chapter and this suggestion can be used as a starting point. If analytical functions can be fitted, the calibration process will become easier since parameter values will only need to be determined for the relevant material instead of for each sample.

4. The parameter calibration procedure should be performed with care. Starting off with the parameters belonging to the elastoplastic part of the model, these can be determined through experimental data (M_c, c_M, λ^*, κ^*), other parameters can be taken from literature such as the Poisson's ratio, equations are suggested for N and x and finally trial runs should be performed to calibrate the value of C.
   Then, the initial state variables can be determined. The preconsolidation pressure should be determined based on the sample preparation. The initial void ratio needs to be calculated or taken from a test description and the initial rotation can be calculated through a given equation. The initial stresses and strains can reasonably be assumed.
   The viscosity parameters are calibrated through the execution of trial runs with starting values to be taken from relevant literature.
   The unsaturated parameters belong to the SWRC and the loading collapse rule. The SWRC parameters can be fitted to an experimentally determined SWRC whereas the loading collapse rule parameters are calibrated by fitting the experimental preconsolidation pressure at different suctions.
   Finally, the suction dependent viscous nucleus parameters need to be determined through the execution of trial runs, as stated above it is proposed to fit analytical functions for both parameters to make the calibration process easier.

5. For future model development it is recommended to look at the double porosity approach such as Della Vecchia et al. (2013) and Li et al. (2017) as mentioned in chapter 7 to improve the unsaturated model performance. For improvement of the time dependent aspect of the model, a possible starting point is including creep strains inside the yield surface as suggested by Cresseri and Jommi (2005) and Liingaard et al. (2004). This could for example improve the initial prediction of the loading/unloading data which were found to not be perfectly elastic.

6. The final recommendation that is made is to include the unsaturated elasto viscoplastic approach in a Finite Element Model (FEM). If it can be validated using FEM analyses that the approach is able to predict soil behaviour well, the approach could become more practically relevant.

9 References

Abrantes, L. G., & de Campos, T. M. P. (2019). Evaluation of the coefficient of earth pressure at rest (K0) of a saturated-unsaturated colluvium soil. *E3S Web of Conferences*, *92*, 1–6. https://doi.org/10.1051/e3sconf/20199207006

Adams, J. (1963). A comparison of field and laboratory measurement in peat. *Mukeg. Res. Conf. Ontario Hydro Res. Q.*, *15*, 1–7.

Akagi, H. (1994). Physico-chemical approach to the consolidation mechanism of soft clays. *Soils and Foundations*, *34*(4), 43–50. https://doi.org/10.3208/sandf1972.34.4_43

Andersland, O. B., & Douglas, A. G. (1970). Soil deformation rates and activation energies. *Geotechnique*, *20*(1), 1–16. https://doi.org/10.1680/geot.1970.20.1.1

Bagheri, M., Nezhad, M. M., & Rezania, M. (2020). A CRS oedometer cell for unsaturated and non-isothermal tests. *Geotechnical Testing Journal*, *43*(1), 20–37. https://doi.org/10.1520/GTJ20180204

Bishop, A. (1958). Test requirements for measuring the coefficient of earth pressure at rest. *Brussels Conference on earth pressure problems*, 2–14.

Bishop, A. (1959). The principle of effective stress. *Tek. Ukeblad*, *106*(39), 859–863.

Brooker, E. W., & Ireland, H. O. (1965). Earth Pressures at Rest Related to Stress History. *Canadian Geotechnical Journal*, *2*(1), 1–15. https://doi.org/10.1139/t65-001

Collins, I. F., & Yu, H. S. (1996). Undrained cavity expansions in critical state soils. *International Journal for Numerical and Analytical Methods in Geomechanics*, *20*, 489–516. https://doi.org/10.1002/(sici)1096-9853(199607)20:7⟨489::aid-nag829⟩3.0.co;2-v

Cresseri, S., & Jommi, C. (2005). Snow as an elastic viscoplastic bonded continuum: a modelling approach. *RIVISTA ITALIANA DI GEOTECNICA*, *4*, 43–58. http://hdl.handle.net/11311/267441

Dafalias, Y. F. (1987). An Anisotropic Critical State Soil Plasticity Model. *Mechanics Research Communications*, *13*(6), 341–347.

Dafalias, Y. F., Manzari, M. T., & Papadimitriou, A. G. (2006). SANICLAY : simple anisotropic clay plasticity model. *International Journal for Numerical and Analytical Methods in Geomechanics*, 1231–1257. https://doi.org/10.1002/nag.524

Dafalias, Y. F., & Taiebat, M. (2013). Anatomy of rotational hardening in clay plasticity. *Géotechnique*, *63*(16), 1406–1418.

de Campos, T., de C. Viana, A., Silva, T., & Abrantes, L. (2021). Evaluation of the at-rest coefficient of earth pressure in unsaturated residual soil with a new suction-controlled device, 373–391.

de Jong, G. (1966). On the secondary consolidation of soils.

de Jong, G. (1968). Consolidation models consisting of an assembly of viscous elements on a cavity channel network. *Géotechnique*, *18*(2), 195–228.

Della Vecchia, G., Jommi, C., & Romero, E. (2013). A fully coupled elastic – plastic hydromechanical model for compacted soils accounting for clay activity. *International Journal for Numerical and Analytical Methods in Geomechanics*, *37*, 503–535. https://doi.org/10.1002/nag.1116

Donath, A. D. (1891). Unteruschungen uber Erdduck Stutzwande. *Zeitschrift fur Bauwessen.*

Ellithy, G. S., & Stark, T. D. (2020). Case Study : Unsaturated Embankment Failure on Soft Soils. *Journal of Geotechnical and Geoenvironmental Engineering*, *146*(12), 1–10. https://doi.org/10.1061/(ASCE)GT.1943-5606.0002382

Federico, A., Elia, G., & Murianni, A. (2009). The at-rest earth pressure coefficient prediction using simple elasto-plastic constitutive models. *Computers and Geotechnics*, *36*, 187–198. https://doi.org/10.1016/j.compgeo.2008.01.006

Fern, E. J., de Lange, D. A., Zwanenburg, C., Teunissen, J. A. M., Rohe, A., & Soga, K. (2017). Experimental and numerical investigations of dyke failures involving soft materials. *Engineering Geology*, *219*, 130–139. https://doi.org/10.1016/j.enggeo.2016.07.006

Fredlund, D. G., & Morgenstern, N. R. (1977). Stress State Variables for Unsaturated Soils. *Journal of the Geotechnical Engineering Division*, *103*(5). https://doi.org/10.1061/AJGEB6.0000423

Fredlund, D. G., & Rahardjo, H. (1993). *Soil Mechanics for Unsaturated Soils.* John Wiley & Sons.

Gasparre, A. (2005). *Advanced Laboratory Characterisation of London Clay* (Doctoral dissertation). Imperial College London.

GeotechniCAL. (1996). Consolidation. Retrieved, from http://environment.uwe.ac.uk/geocal/SoilMech/consol/soilcons.htm

Gjengstø, B. A. (2016). *Et Laboratoriestudie på Hviletrykkskoeffisientens Utvikling under Kryp for både Uforstyrret og Omrørt , Rekonsolidert Tillerleire [A laboratory study on the evolution of the earth pressure coefficient under creep for both undisturbed and remoulded tiller]* (Master's thesis). NTNU.

Golpasand, M. R. B., Do, N. A., Dias, D., & Nikudel, M. R. (2018). Effect of the lateral earth pressure coefficient on settlements during mechanized tunneling. *Geomechanics and Engineering*, *16*(6), 643–654. https://doi.org/10.12989/gae.2018.16.6.643

Grimstad, G., Long, M., Dadrasajirlou, D., & Amiri, S. A. G. (2021). Investigation of Development of the Earth Pressure Coefficient at Rest in Clay During Creep in the Framework of Hyper-Viscoplasticity. *International Journal of Geomechanics*, *21*(1), 04020235. https://doi.org/10.1061/(asce)gm.1943-5622.0001883

Gupta, B. (1964). *Creep of saturated soil at different temperatures.* (Doctoral dissertation). The University of British Columbia, Vancouver 8, Canada.

Heeres, O. M., Suiker, A. S., & de Borst, R. (2002). A comparison between the perzyna viscoplastic model and the consistency viscoplastic model. *European Journal of Mechanics - A/Solids*, *21*(1), 1–12. https://doi.org/https://doi.org/10.1016/S0997-7538(01)01188-3

Hendron, A. J. J. (1963). *THE BEHAVIOR OF SAND IN ONE-DIMENSIONAL COMPRESSION* (Doctoral dissertation). University of lllinois at Urbana- Champaign, Urbana. https://doi.org/10.1016/0003-6870(76)90053-3

Huang, W., Fityus, S., Bishop, D., Smith, D., & Sheng, D. (2006). Finite-Element Parametric Study of the Consolidation Behavior of a Trial Embankment on Soft Clay. *International Journal of Geomechanics*, *6*(5), 328–341. https://doi.org/10.1061/(ASCE)1532-3641(2006)6

Jaky, J. (1944). The coefficient of earth pressure at rest. (In Hungarian: A nyugalmi nyomas tenyezoje). *J. Soc. Hung. Eng. Arch. (Magyar Mernok es Epitesz-Egylet Kozlonye)*, 355–358.

Jaky, J. (1948). Pressure in silos. *Proceedings of the 2nd International Conference on Soil Mechanics and Foundation Engineering*, 103–107.

Jommi, C. (2000). Remarks on the constitutive modelling of unsaturated soils. *Experimental Evidence and Theoretical Approaches in Unsaturated Soils*, 139–153.

Kavazanjian, J. J., & Mitchell, J. K. (1984). Time Dependence Of Lateral Earth Pressure. *Journal of Geotechnical Engineering*, *110*(4), 530–533.

Krieg, S., & Goldscheider, M. (1993). Some resuits concerning the development of K0 during one-dimensional creep of peat. *Advances in Understanding and Modelling the Mechanical Behaviour of Peat*, 71–75. publicaties.minienm.nl/download-bijlage/64175/20063.pdf

Kuhn, M., & Mitchell, J. (1993). New perspectives on soil creep. *Journal of Geotechnical Engineering*, *119*. https://doi.org/10.1061/(ASCE)0733-9410(1993)119:3(507)

Lai, X. L., Wang, S., Ye, W. M., & Cui, Y. J. (2014). Experimental investigation on the creep behavior of an unsaturated clay. *Canadian Geotechnical Journal*, *51*, 621–628. https://doi.org/10.1139/cgj-2013-0064

Lai, X., Wang, S., Qin, H., & Liu, X. (2009). Unsaturated creep tests and empirical models for sliding zone soils of Qianjiangping landslide in the Three Gorges. *Journal of Rock Mechanics and Geotechnical Engineering*, *2*(2), 149–154. https://doi.org/10.3724/SP.J.1235.2010.00149

Lazari, M., Sanavia, L., di Prisco, C., & Pisanò, F. (2019). Predictive potential of Perzyna viscoplastic modelling for granular geomaterials. *International Journal for Numerical and Analytical Methods in Geomechanics*, *43*, 544–567. https://doi.org/10.1002/nag.2876

Le, T. M., Fatahi, B., & Khabbaz, H. (2012). Viscous Behaviour of Soft Clay and Inducing Factors. https://doi.org/10.1007/s10706-012-9535-0

Leonards, G. A., & Altschaeffl, A. G. (1964). Compressibility of clay. *Journal of the Soil Mechanics and Foundations Division*, *90*(5), 133–155. https://doi.org/10.1061/JSFEAQ.0000649

Li, J., Yin, Z. Y., Cui, Y., & Hicher, P. Y. (2017). Work input analysis for soils with double porosity and application to the hydromechanical modeling of unsaturated expansive clays. *Canadian Geotechnical Journal*, *54*, 173–187. https://doi.org/10.1139/cgj-2015-0574

Li, J., & Yang, Y. (2018). Creep behavior of unsaturated reticulate red clay under matric suction. *KSCE Journal of Civil Engineering*, *22*(2), 582–587. https://doi.org/10.1007/s12205-017-0092-1

Liingaard, M., Augustesen, A., & Lade, P. V. (2004). Characterization of Models for Time-Dependent Behavior of Soils. *International Journal of Geomechanics*, *4*(3), 157–177. https://doi.org/10.1061/(asce)1532-3641(2004)4:3(157)

Lindgård, A., & Ofstad, C. (2017). *Field and laboratory investigations to evaluate the coefficient of earth pressure at rest – NGTS Tiller-Flotten quick clay test site*, Norwegian Geotechnical Institute.

Lo, K. Y., & Morin, J. P. (1972). Strength anisotropy and time effects of two sensitive clays. *Canadian Geotechnical Journal*, *9*(3), 261–277. https://doi.org/10.1139/t72-030

Low, P. F. (1962). Influence of adsorbed water on exchangeable ion movement. *Clays and Clay Minerals*, *9*(1), 219–228.

Lu, N., Godt, J. W., & Wu, D. T. (2010). A closed-form equation for effective stress in unsaturated soil. *Water Resources Research*, *46*, 1–14. https://doi.org/10.1029/2009wr008646

Lu, N., & Likos, W. J. (2006). Suction Stress Characteristic Curve for Unsaturated Soil. *Journal of Geotechnical and Geoenvironmental Engineering*, *132*(2), 131–142. https://doi.org/10.1061/(asce)1090-0241(2006)132:2(131)

Mayne, P. W., & Kulhawy, F. H. (1982). K0-OCR relationships in soil. *108*(6), 851–869. https://doi.org/10.1016/0148-9062(83)91623-6

McDowell, G. R., & Hau, K. W. (2004). A generalised Modified Cam clay model for clay and sand incorporating kinematic hardening and bounding surface plasticity. *Granular Matter*, *6*, 11–16. https://doi.org/10.1007/s10035-003-0152-8

Mesri, G. (1973). Coefficient of Secondary Compression. *Journal of the Soil Mechanics and Foundations Division*, *99*(1). https://doi.org/10.1061/JSFEAQ.0001840

Mesri, G., & Castro, A. (1987). C α/C c concept and K0 during secondary compression. *Journal of Geotechnical Engineering*, *113*(3), 230–247.

Mesri, G., & Hayat, T. M. (1993). The coefficient of earth pressure at rest. *Canadian Geotechnical Journal*, *30*, 647–666. https://doi.org/10.1139/t93-056

Muraro, S., & Jommi, C. (2019). Experimental determination of the shear strength of peat from standard undrained triaxial tests: correcting for the effects of end restraint. *Géotechnique*, 1–12. https://doi.org/10.1680/jgeot.18.P.346

Oh, S., Lu, N., Kim, T.-K., & Lee, Y. H. (2013). Experimental Validation of Suction Stress Characteristic Curve from Nonfailure Triaxial K0 Consolidation Tests. *Journal of Geotechnical and Geoenvironmental Engineering*, *139*(9), 1490–1503. https://doi.org/10.1061/(asce)gt.1943-5606.0000880

Peryzna, P. (1963). the Constitutive Equations for Rate Sensitive Plastic Materials. *Quarterly of Applied Mathematics*, *20*, 321–332. https://doi.org/https://doi.org/10.1090/qam/144536

Pirjalili, A., Garakani, A. A., Golshani, A., & Mirzaii, A. (2020). A suction-controlled ring device to measure the coefficient of lateral soil pressure in unsaturated soils. *Geotechnical Testing Journal*, *43*(6), 1379–1396. https://doi.org/10.1520/GTJ20190099

Polinder, H. B. (2019). *Development of the Yield Stress due to Aging*. TU Delft.

Rezania, M., Bagheri, M., & Nezhad, M. M. (2020). Creep and consolidation of a stiff clay under saturated and unsaturated conditions. *Canadian Geotechnical Journal*, *57*(5), 728–741. https://doi.org/10.1139/cgj-2018-0398

Rezania, M., Taiebat, M., & Poletti, E. (2016). A viscoplastic saniclay model for natural soft soils. *Computers and Geotechnics*, *73*, 128–141. https://doi.org/https://doi.org/10.1016/j.compgeo.2015.11.023

Romero, E., & Jommi, C. (2008). An insight into the role of hydraulic history on the volume changes of anisotropic clayey soils. *Water Resources Research*, *44*, 1–16. https://doi.org/10.1029/2007WR006558

Salgado, R., Boulanger, R. W., & Mitchell, J. K. (1997). Lateral Stress Effects on CPT Liquefaction Resistance Correlations. *Journal of Geotechnical and Geoenvironmental Engineering*, *123*(8), 726–735. https://doi.org/10.1061/(asce)1090-0241(1997)123:8(726)

Schmertmann, J. H. (1983). A simple question about consolidation. *Journal of Geotechnical Engineering*, *109*(1), 119–122. https://doi.org/10.1061/(ASCE)0733-9410(1983)109:1(119).

Schmidt, B. (1966). Earth pressure at rest related to stress history. *Canadian Geotechnical Journal*, 239–242. https://doi.org/10.1139/t66-028

Schmidt, B. (1967). Lateral stresses in uniaxial strain. *Geoteknisk Institut (The Danish Geotechnical Institute)*, 5–12.

Sivasithamparam, N., & Castro, J. (2016). An anisotropic elastoplastic model for soft clays based on logarithmic contractancy Nallathamby. *International Journal for Numerical and Analytical Methods in Geomechanics*, *40*, 596–621. https://doi.org/10.1002/nag

Sletten, J. R. (2015). *On the earth pressure coefficient at rest during creep*. NTNU.

Wang, Y. H., & Gao, Y. (2013). Examining the behavior and mechanisms of structuration in sand under the K0 condition. *Granular Matter*, *16*, 55–68. https://doi.org/10.1007/s10035-013-0457-1

Wegman, T. G. (2020). *Analysis of undrained soil behaviour of Dutch organic clay in K_0-consolidated triaxial tests*. TU Delft.

Wheeler, S. J., Näätänen, A., Karstunen, M., & Lojander, M. (2003). An anisotropic elastoplastic model for soft clays. *Canadian Geotechnical Journal*, *40*, 403–418. https://doi.org/10.1139/t02-119

Wijeyesekera, D. C., & Mohamed, S. M. (2000). K0 Development In Kaolin-Bentonite Mixtures.

Yang, R., Xiao, P., & Qi, S. (2019). Analysis of slope stability in unsaturated expansive soil: A case study. *Frontiers in Earth Science*, *7*, 292. https://doi.org/10.3389/feart.2019.00292

Yao, Y.-p., Qi, S.-j., Che, L.-w., Chen, J., Han, L.-m., & Ma, X.-Y. (2018). Postconstruction Settlement Prediction of High Embankment of Silty Clay at Chengde Airport Based on One-Dimensional Creep Analytical Method : Case Study. *18*(7), 1–8. https://doi.org/10.1061/(ASCE)GM.1943-5622.0001191

Yin, Z. Y., & Karstunen, M. (2011). Modelling strain-rate-dependency of natural soft clays combined with anisotropy and destructuration. *Acta Mechanica Solida Sinica*, *24*(3), 216–230. https://doi.org/10.1016/S0894-9166(11)60023-2

Zeevaert, L. (1986). *Consolidation in the intergranular viscosity of highly compressible soils: Testing and evaluation* (R. Yong & F. Townsend, Eds.). ASTM International. https://compass.astm.org/DIGITAL_LIBRARY/STP/PAGES/STP34619S.htm

Zhang, C., Li, J. Z., & He, Y. (2020). Experimental Study on Viscoplastic Property of Unsaturated Reticulate Red Clay Used as an Engineered Barrier. *Geofluids*, 1–13. https://doi.org/10.1155/2020/1523659

Zhang, J., Gong, B., WangJ., Zhou, X., & Liu, J. (2010). Field study of landslide of swelling rock slope under Artificial Rainfall. *Journal of Yangtze River Scientific Research Institute*, *27*(9), 47–52.

Zhang, R., Zheng, J., & Yang, H. (2009). Experimental study on k_0 consolidation behavior of recompacted unsaturated expansive soil, 27–32. https://doi.org/10.1061/41044(351)5

Zhu, Y. b., & Yu, H. m. (2014). An improved Mesri creep model for unsaturated weak intercalated soils. *Journal of Central South University*, *21*, 4677–4681. https://doi.org/10.1007/s11771-014-2476-4

Zou, L., Wang, S., & Lai, X. (2013). Creep model for unsaturated soils in sliding zone of Qianjiangping landslide. *Journal of Rock Mechanics and Geotechnical Engineering*, *5*, 162–167. https://doi.org/10.1016/j.jrmge.2013.03.001

A Sensitivity Analysis

A.1 Elastoplastic parameters

In this appendix, the sensitivity of the elastoplastic model to each of its parameters will be analysed. The sensitivity analysis is performed by changing one parameter while keeping all the other ones constant. For each parameter, five values are tested. These are 80, 90, 100, 110 and 120% of the original determined parameter value. This results in two analyses with a lower value than the original one and two with a higher value. In doing so the change of the model output can be determined. This does not mean that every parameter has to be set to one of the five values used here. The sensitivity analysis purely serves as an indication of the change in model output to a change in parameter.

The model output is compared to the data from Wegman (2020). More specifically, the stress path in p'-q space and the void ratio vs log(p') plot are used since these plots indicate the influence of the model parameters well. The test which is used is the slightly overconsolidated one (TRX_5) since this is deemed to be the most representative. The saturated EP model is used since the elastoplastic parameters are determined before the viscoplastic ones and therefore with the EP model their sensitivity can already be analysed before the viscoplastic parameters are determined.

The following model parameters are used in the analysis.

Table 29: Elastoplastic parameter values - Sensitivity analysis EP parameters.

Parameter	Lowest (80%)	Low (90%)	Default (100%)	High (110%)	Highest (120%)
λ^*	0.104	0.117	0.130	0.143	0.156
κ^*	0.011	0.013	0.014	0.015	0.017
ν	0.16	0.18	0.20	0.22	0.24
N	1.18	1.33	1.48	1.63	1.78
x	1.37	1.54	1.71	1.88	2.05
k_f	1.6	1.8	2.0	2.2	2.4

M_c and c_M are not analysed with respect to their sensitivity since they are taken directly from Wegman (2020) and there is no uncertainty in their values. They are kept at 1.61 and 0.84 throughout all analyses.
Dafalias et al. (2006) stated that C ranges from 3 to 20, therefore a wider range of values are selected for this parameter. The values at which C is tested are 3.0, 4.0 (Default), 8.0 and 9.0. For values above 9.0, the model failed to converge so therefore it is not possible to test the entire range of values for C.

Only the sensitivity of the model parameters are tested since the initial state variables can be determined accurately enough from the description of the test in Wegman (2020). For convenience, they are repeated here.

Table 30: Initial state variables - Sensitivity analysis EP parameters.

Parameter	Unit	Meaning	Value
$\boldsymbol{\varepsilon_0}$	[-]	Initial strain	[0.0, 0.0, 0.0, 0.0, 0.0, 0.0]
$\boldsymbol{\sigma_0}$	[kPa]	Initial total stress	[5.0, 5.0, 5.0, 0.0, 0.0, 0.0]
$\boldsymbol{\alpha_0}$	[-]	Initial rotation of plastic potential	[-0.65/3*1, -0.65/3*1, 0.65/3*2, 0.0, 0.0, 0.0]
$\boldsymbol{\beta_0}$	[-]	Initial rotation of yield surface	[-0.65/3*1, -0.65/3*1, 0.65/3*2, 0.0, 0.0, 0.0]
$p_{c,0}$	[kPa]	Initial mean preconsolidation pressure	22.9
e_0	[-]	Initial void ratio	2.59 (Wegman, 2020)

Sensitivity λ^*

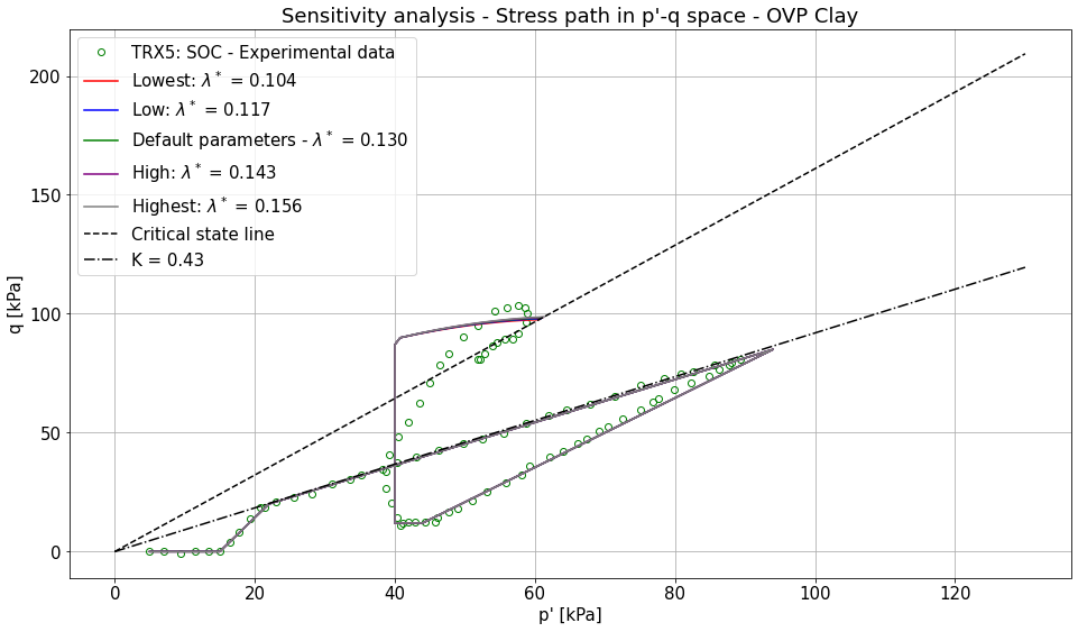

(a) Sensitivity presented in stress path in p'-q space.

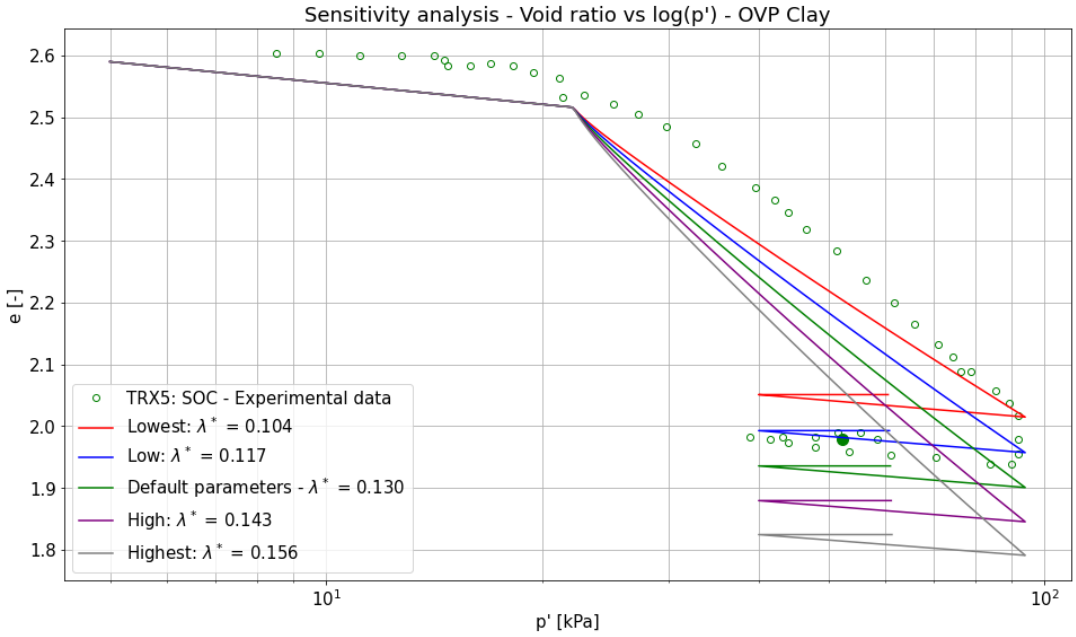

(b) Sensitivity presented by change in void ratio with mean effective stress.

Figure 88: Sensitivity λ^*.

Since λ^* governs the slope of the virgin compression line it was to be expected that changing λ^* would have no significant effect on the stress path in p'-q space. The effect is clearly visible in figure 88b, for a higher value of λ^*, the slope of the virgin compression line increases and as a consequence so does the final value of the void ratio.

Sensitivity κ^*

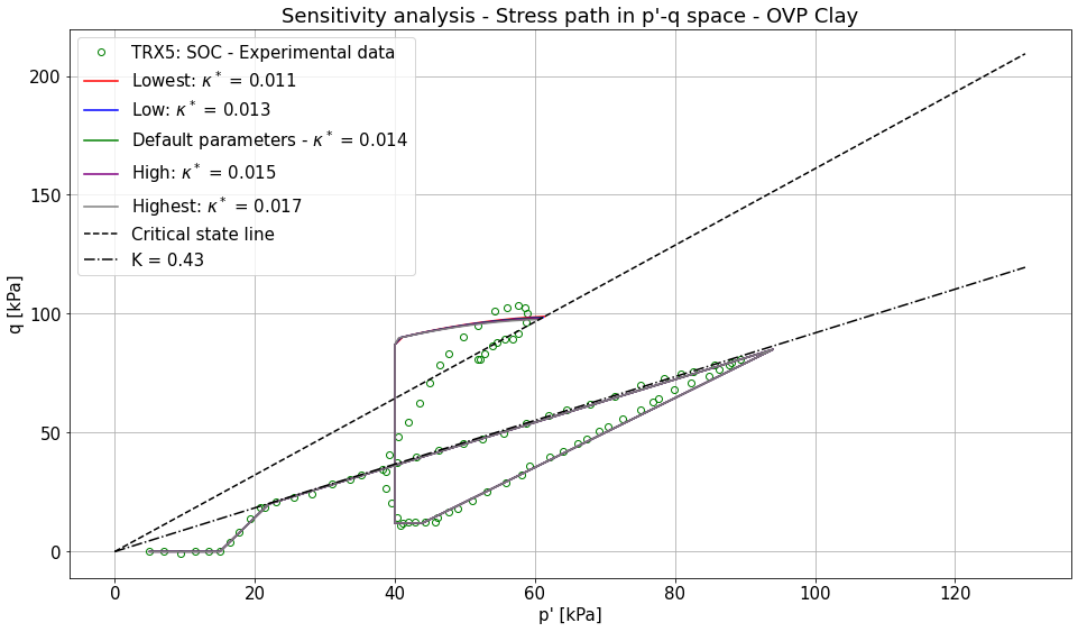

(a) Sensitivity presented in stress path in p'-q space.

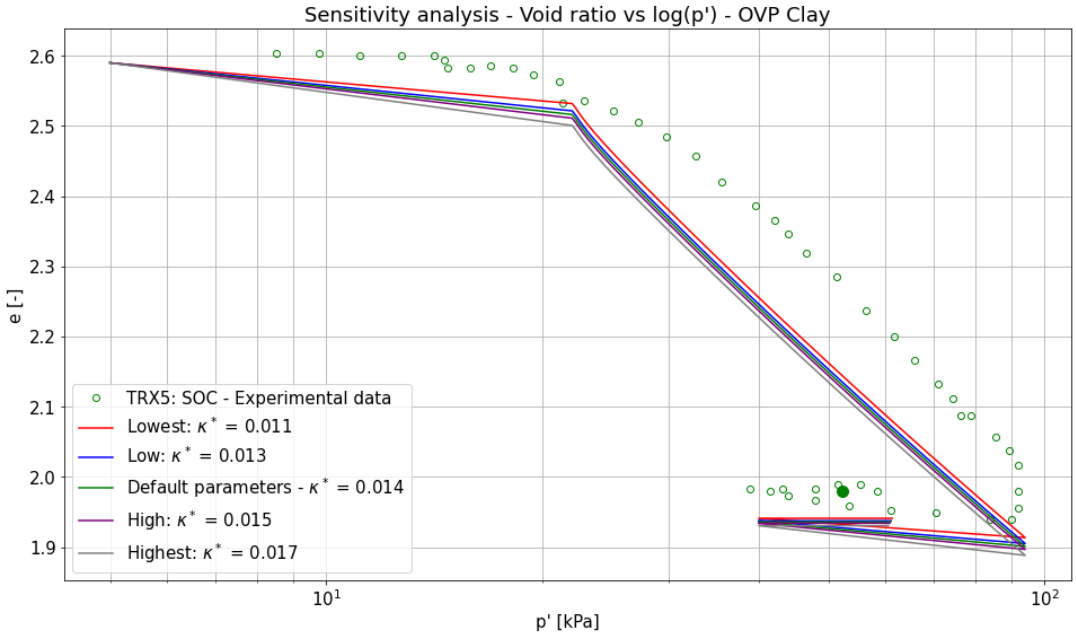

(b) Sensitivity presented by change in void ratio with mean effective stress.

Figure 89: Sensitivity κ^*.

Similar to λ^*, κ^* has no significant effect on the stress path in p'-q space this time because κ^* governs the slope of the recompression line. The effect of κ^* is shown in figure 89b, for higher values of κ^*, the slope of the recompression line increases.

Sensitivity ν

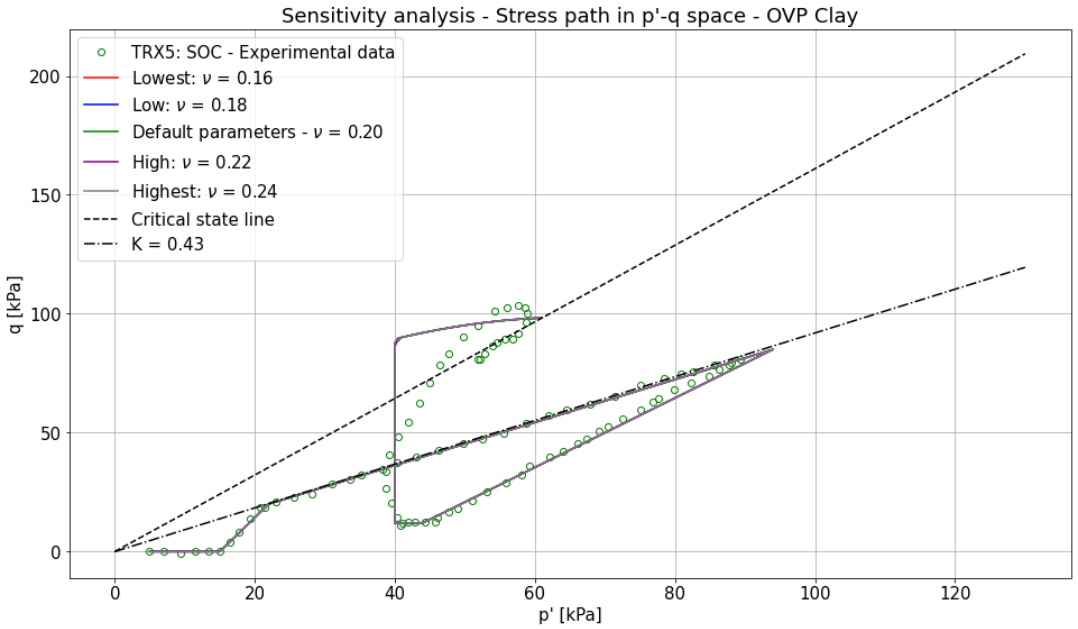

(a) Sensitivity presented in stress path in p'-q space.

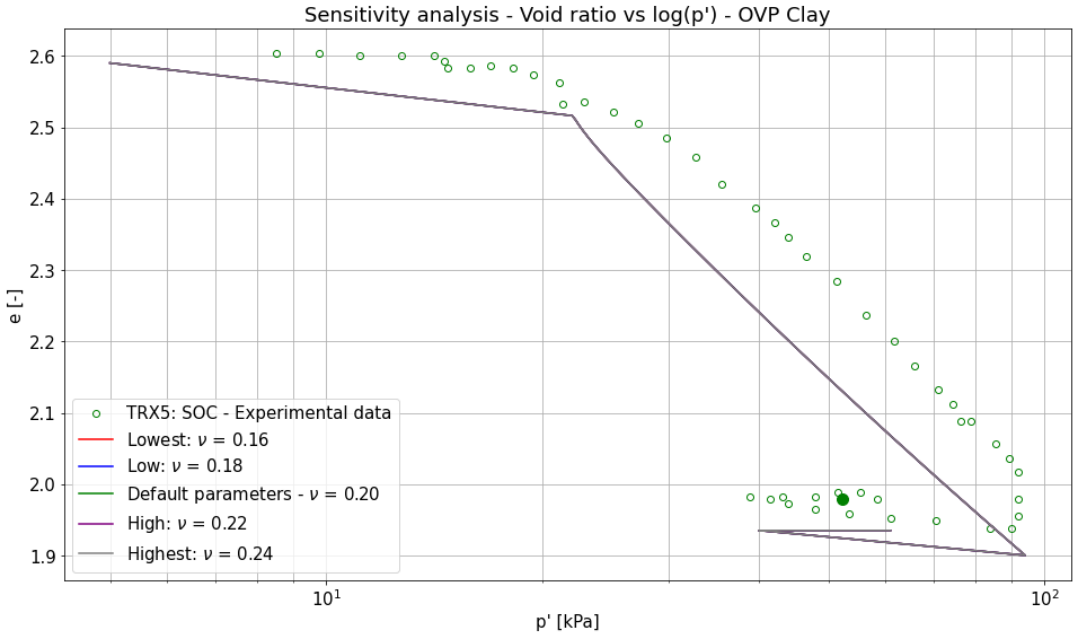

(b) Sensitivity presented by change in void ratio with mean effective stress.

Figure 90: Sensitivity ν.

It can be seen that the model is insensitive to the chosen value of ν.

Sensitivity N

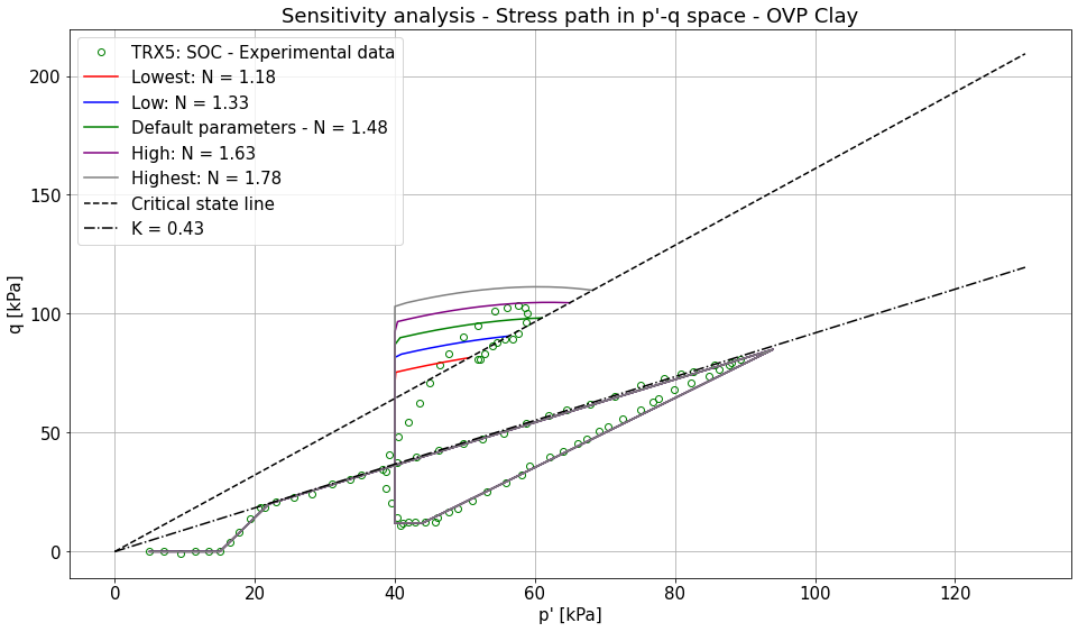

(a) Sensitivity presented in stress path in p'-q space.

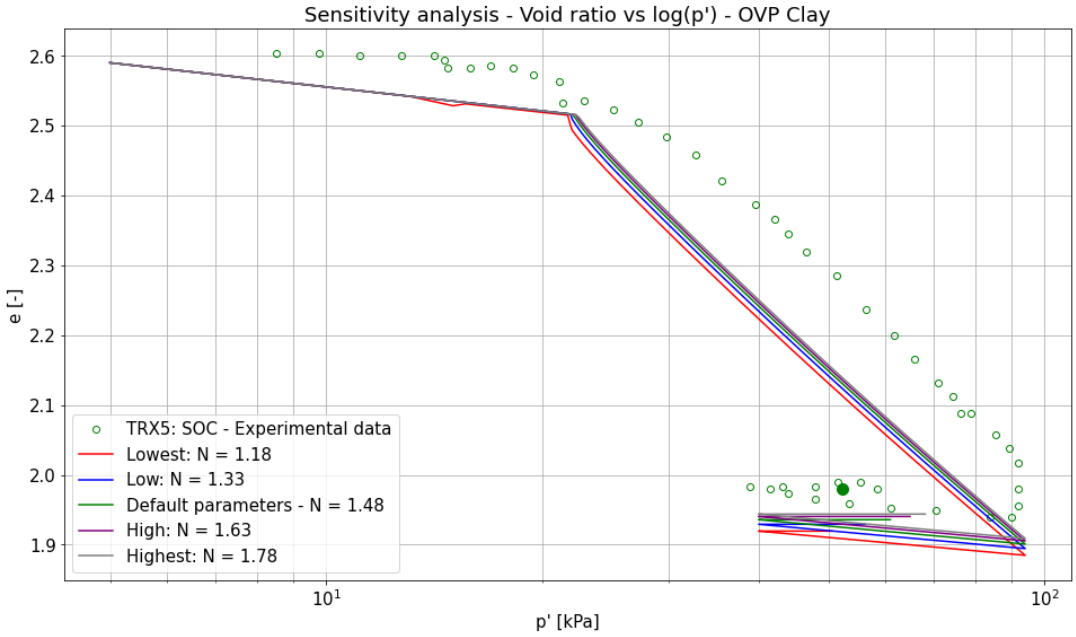

(b) Sensitivity presented by change in void ratio with mean effective stress.

Figure 91: Sensitivity N.

The value of N changes the shape of the yield surface and therefore changes the moment where the soil sample reaches the plastic domain under shearing and starts going towards the critical state line. In the void ratio vs log(p') plot, the effect can be seen upon reaching the preconsolidation pressure. For lower values of N there is a bigger initial change in void ratio after which the slope of the plot is recovered to be similar to the other lines.

Sensitivity x

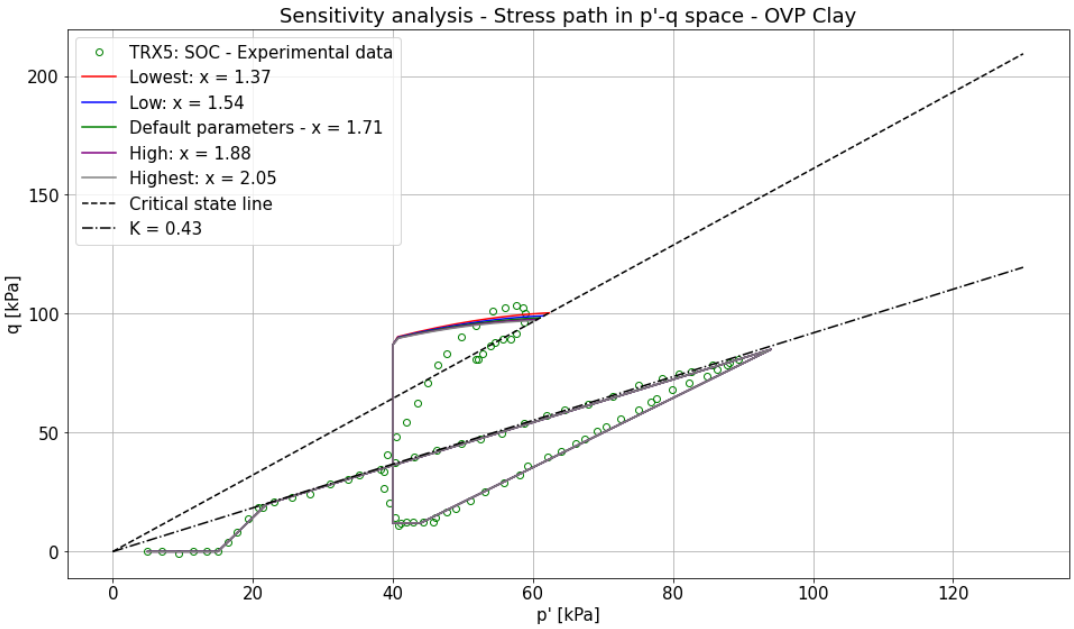

(a) Sensitivity presented in stress path in p'-q space.

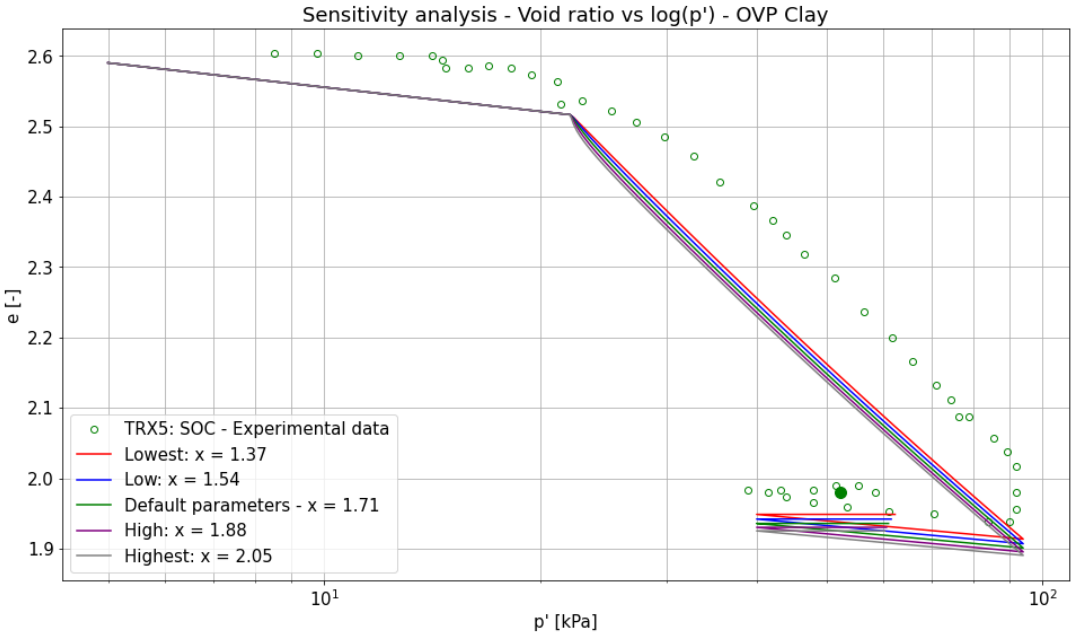

(b) Sensitivity presented by change in void ratio with mean effective stress.

Figure 92: Sensitivity x.

The value of x only changes the initial part of the virgin compression line. Overall it can be stated that the model is relatively insensitive to the value of x.

Sensitivity C

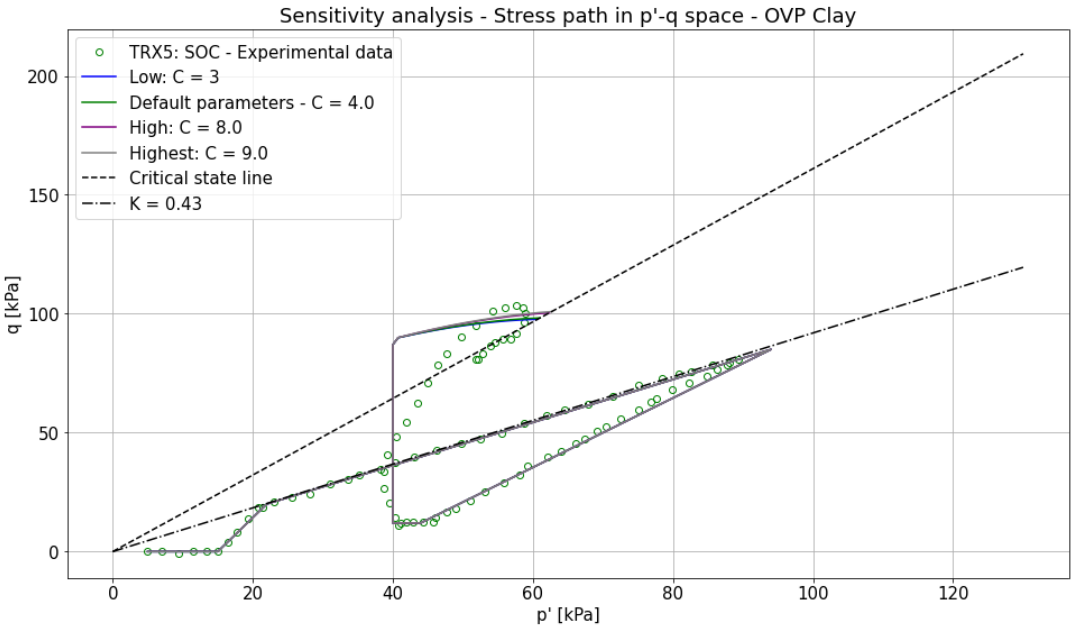

(a) Sensitivity presented in stress path in p'-q space.

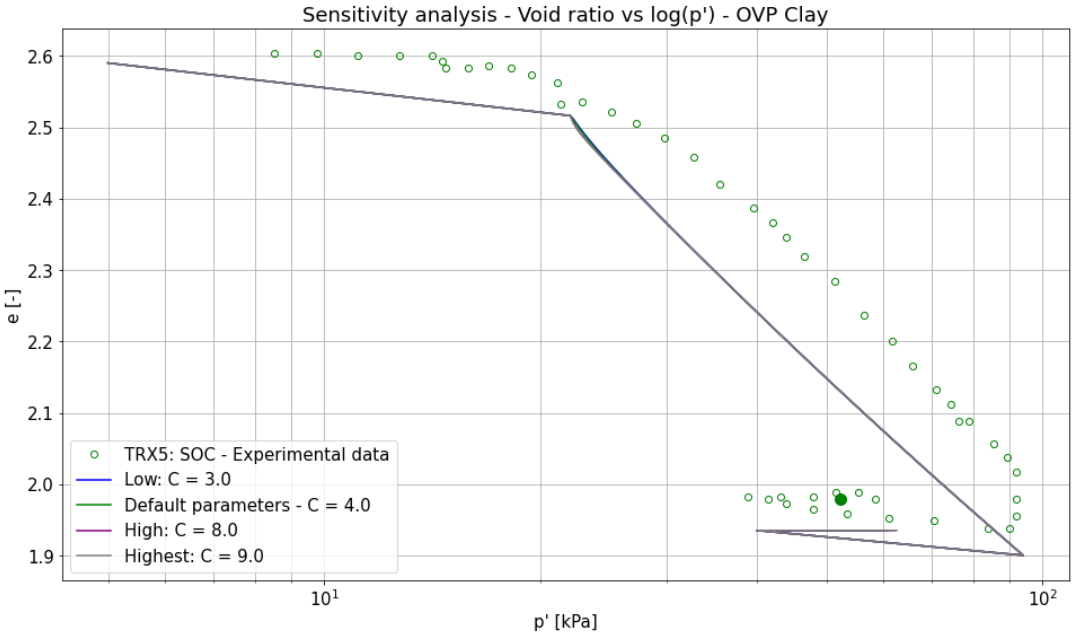

(b) Sensitivity presented by change in void ratio with mean effective stress.

Figure 93: Sensitivity C.

The model is insensitive to the changes made to C. The range of values for C as reported by Dafalias et al. (2006) is higher than the values that are tested here. For values higher than 9.0, the model runs into convergence problems. Therefore it is desired to keep C at a low value. The default value of 4.0 gives good results.

Sensitivity k_f

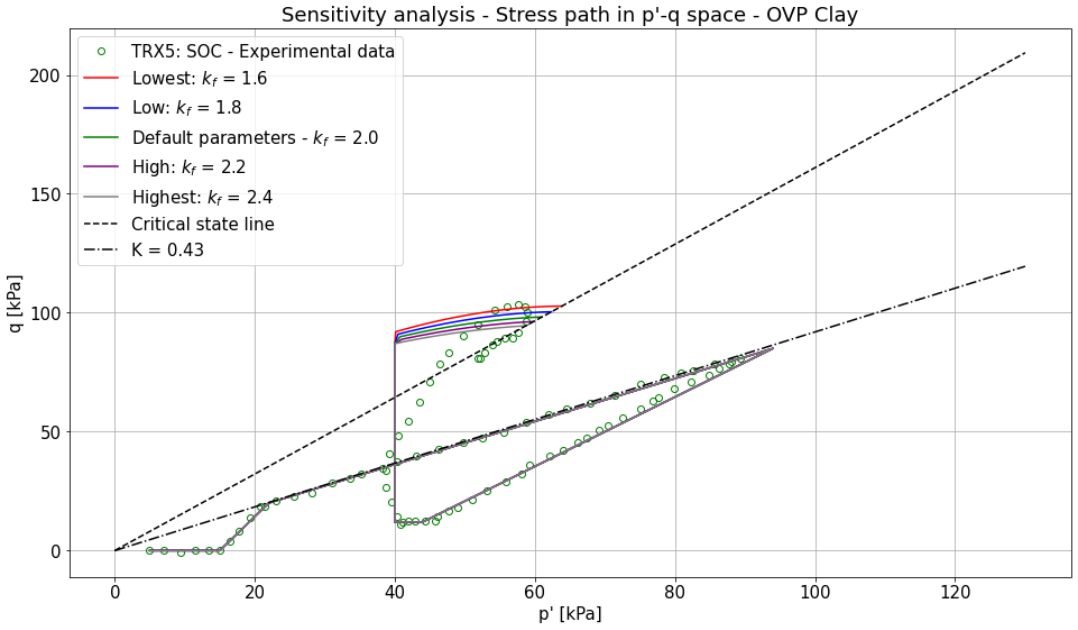

(a) Sensitivity presented in stress path in p'-q space.

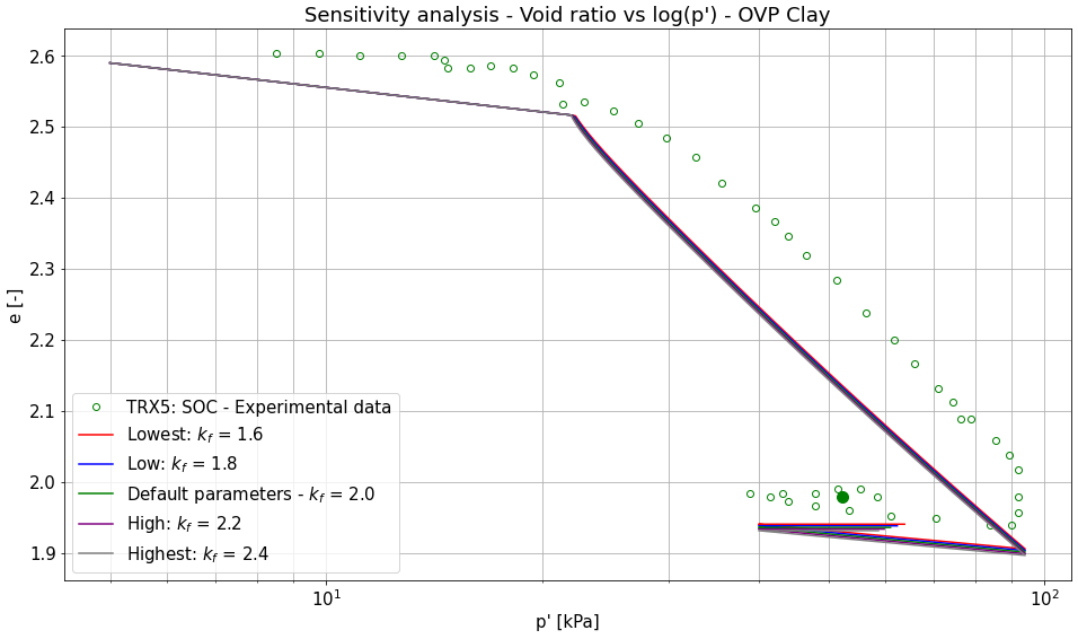

(b) Sensitivity presented by change in void ratio with mean effective stress.

Figure 94: Sensitivity k_f.

The value of k_f also manages the shape of the yield surface. Figure 94a shows that for a lower value of k_f shearing towards the critical state line occurs later. The influence of k_f on the void ratio vs log(p') plot is small.

A.2 Viscosity parameters

In this appendix, the sensitivity of the EVP model to the viscosity parameters μ and N_ϕ is analysed. For both the soils that are being used in this thesis, different tests are performed. Whereas for the elastoplastic parameters, the sensitivity analysis on the OVP clay gives enough insight to calibrate these parameters for the London clay (LC) as well, this is not the case for the viscosity parameters. The test that is performed in the sensitivity analysis of μ and N_ϕ on OVP clay is different from the one performed on the LC clay to the point that the first test is not viable in the calibration of μ and N_ϕ for LC. Because of this, the sensitivity analysis for μ and N_ϕ is performed twice starting with the one for OVP clay and afterwards for the LC.

A.2.1 OVP clay

The sensitivity of the model to μ and N_ϕ is determined using test data from Polinder (2019), more specifically a sample which has undergone 10 days ageing is used. The sensitivity of μ is analysed first since it was shown that the sensitivity of N_ϕ only showed under low values of μ. The values that are tested are a wider range than the elastoplastic parameters, this is because the initial values for μ and N_ϕ had to be guessed and are therefore less certain. The values that are used are shown below.

Table 31: Viscosity parameter values - Sensitivity analysis OVP clay.

Parameter	Unit	Value								
μ	[s^{-1}]	7e-2[1]	7e-3	7e-4	7e-5	7e-6	7e-7	7e-8	7e-9	7e-10
N_ϕ	[-]	8	9	10	11	12	13	14	15	16

[1] The test with $\mu =$ 7e-2 s^{-1} was not able to complete due to convergence problems and is therefore not included in the results.

For the sake of clarity, the other parameter values are shown below.

Table 32: Overview elastoplastic parameters - Sensitivity analysis OVP clay.

Parameter	Meaning	Value
M_c	Value of stress ratio q/p at critical state in compression	1.61
c_M	M_e/M_c	0.84
λ^*	Slope of compression line in ln(ν)-ln(p') plane	0.13
κ^*	Slope of rebound line in ln(ν)-ln(p') plane	0.014
ν	Poisson's ratio	0.20
N	Shape of the yield surface (1)	1.48
x	Saturation limit of anisotropy under constant stress ratio	1.71
C	Rate of evolution of anisotropy	4
k_f	Shape of the yield surface (2)	2.0
k_g	Shape of the plastic potential (always equal to 2.0)	2.0

Table 33: Initial state variables - Sensitivity analysis OVP clay.

Parameter	Unit	Meaning	Value
$\boldsymbol{\varepsilon_0}$	[-]	Initial strain	[0.0, 0.0, 0.0, 0.0, 0.0, 0.0]
$\boldsymbol{\sigma_0}$	[kPa]	Initial total stress	[5.0, 5.0, 5.0, 0.0, 0.0, 0.0]
$\boldsymbol{\alpha_0}$	[-]	Initial rotation of plastic potential	[-0.65/3*1, -0.65/3*1, 0.65/3*2, 0.0, 0.0, 0.0]
$\boldsymbol{\beta_0}$	[-]	Initial rotation of yield surface	[-0.65/3*1, -0.65/3*1, 0.65/3*2, 0.0, 0.0, 0.0]
$p_{c,0}$	[kPa]	Initial mean preconsolidation pressure	22.9
e_0	[-]	Initial void ratio	2.59

Sensitivity μ

The sensitivity analysis of μ was performed with N_ϕ equal to 12. The results are shown below.

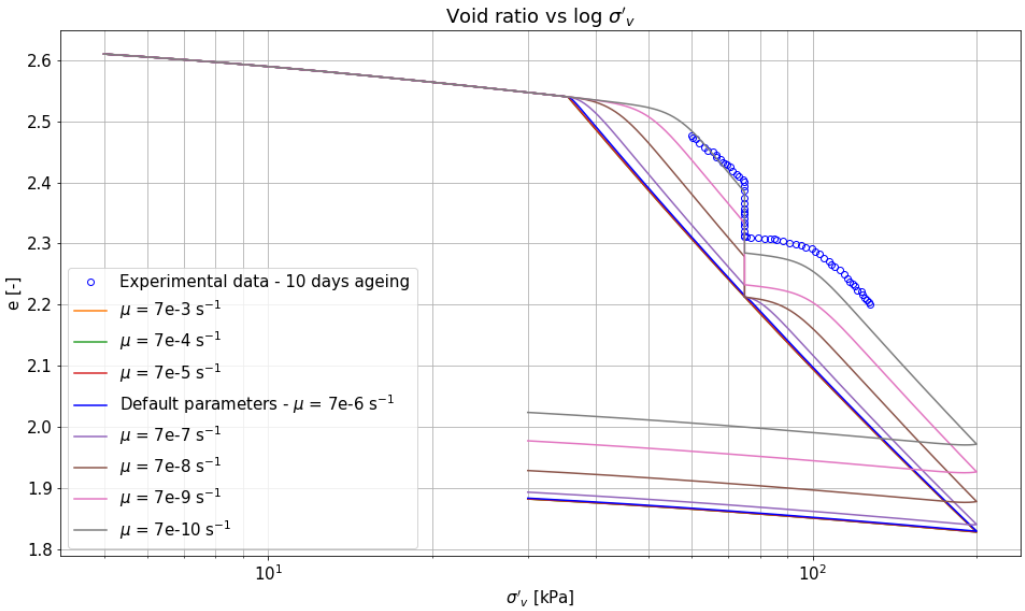

Figure 95: Sensitivity μ - Void ratio vs $\log(\sigma'_v)$.

Sensitivity N_ϕ

It was experienced that only for low values of μ, the sensitivity of N_ϕ could be analysed properly. Therefore, the sensitivity analysis of N_ϕ is performed with μ equal to 7e-10 s^{-1}.

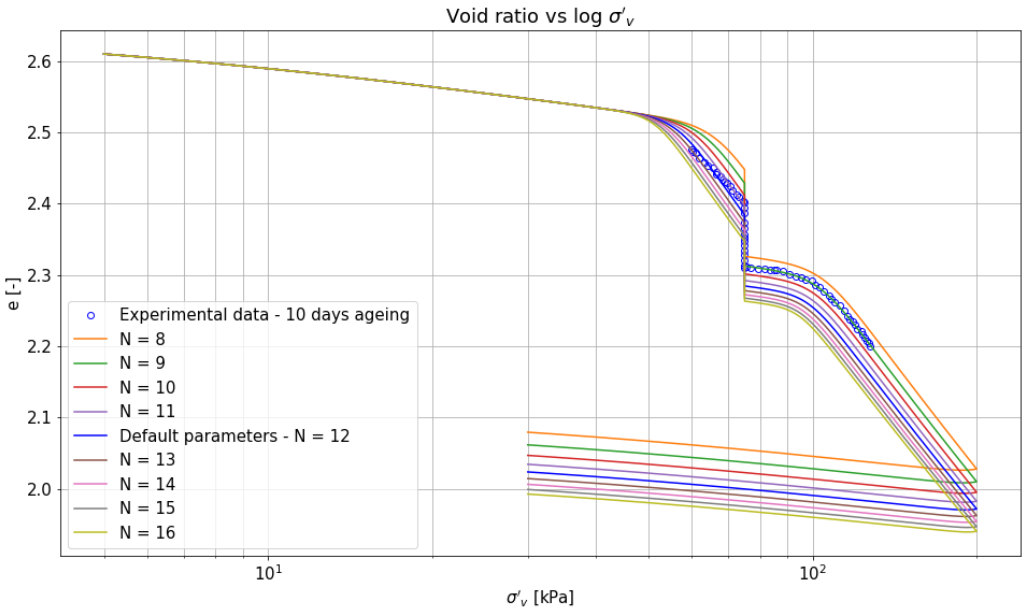

Figure 96: Sensitivity N_ϕ - Void ratio vs $\log(\sigma'_v)$.

It can be seen that a low value of μ is required to fit the results accurately. N_ϕ mostly controls the amount of deformation during a constant effective stress.

A.2.2 London clay

In this appendix, the sensitivity of the model to μ and N_ϕ is analysed again but this time using a test from Rezania et al. (2020) on the London clay. The test that is being used is a saturated sample which is loaded to 355 kPa. The reason why a saturated test is used is because for saturated samples the model behaves like the already validated saturated EVP model and therefore the viscosity parameters can be determined without any potential influence of suction. Shown below is a table indicating which parameter values are tested.

Table 34: Viscosity parameter values - Sensitivity analysis London clay.

Parameter	Unit	Value								
μ	[s^{-1}]	1e-2	1e-3	1e-4	1e-5	1e-6	1e-7	1e-8	1e-9	1e-10
N_ϕ	[-]	9	10	11	12	13	14	15	16	17

The sensitivity analyses for μ is performed with N_ϕ constant and equal to 13.0, the sensitivity analysis for N_ϕ is performed with μ constant and equal to 1e-7 s^{-1}.

For the sake of overview, the elastoplastic parameters and state variables are presented first. After this, the results of the sensitivity analysis are shown. Because changing the parameters changes e_p, the results cannot be presented on a non-normalised axis as is done in the main document.

Table 35: Overview elastoplastic parameters - Sensitivity analysis London clay.

Parameter	Unit	Value
M_c	[-]	0.85
c_M	[-]	1.0
λ^*	[-]	0.087
κ^*	[-]	0.021
ν	[-]	0.3
N	[-]	0.85
x	[-]	1.84
C	[-]	4.0
k_f	[-]	2.0
k_g	[-]	2.0
α	[kPa^{-1}]	0.0036
n	[-]	4.5
m	[-]	0.05
a	[kPa]	1e6
b_1	[-]	1.0
b_2	[-]	0.5
$S_{r,aev}$	[-]	0.97
$S_{r,res}$	[-]	0.23

Table 36: Initial state variables - Sensitivity analysis London clay.

Variable	Unit	Value
$\boldsymbol{\varepsilon_0}$	[-]	[0.0, 0.0, 0.0, 0.0, 0.0, 0.0]
$\boldsymbol{\sigma_0}$	[kPa]	[11.0, 11.0, 11.0, 0.0, 0.0, 0.0]
$\boldsymbol{\alpha_0}$	[-]	0.26
$\boldsymbol{\beta_0}$	[-]	0.26
$p^*_{c,0}$	[kPa]	61.0
e_0	[-]	0.93

Sensitivity μ

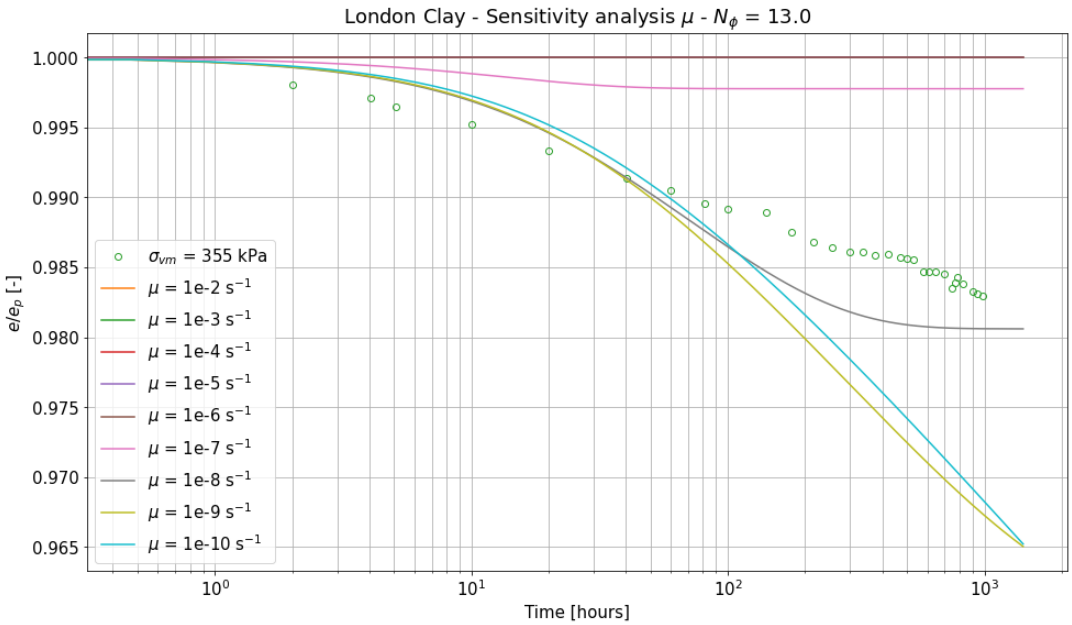

Figure 97: Sensitivity analysis μ - experimental data from Rezania et al. (2020).

Sensitivity N_ϕ

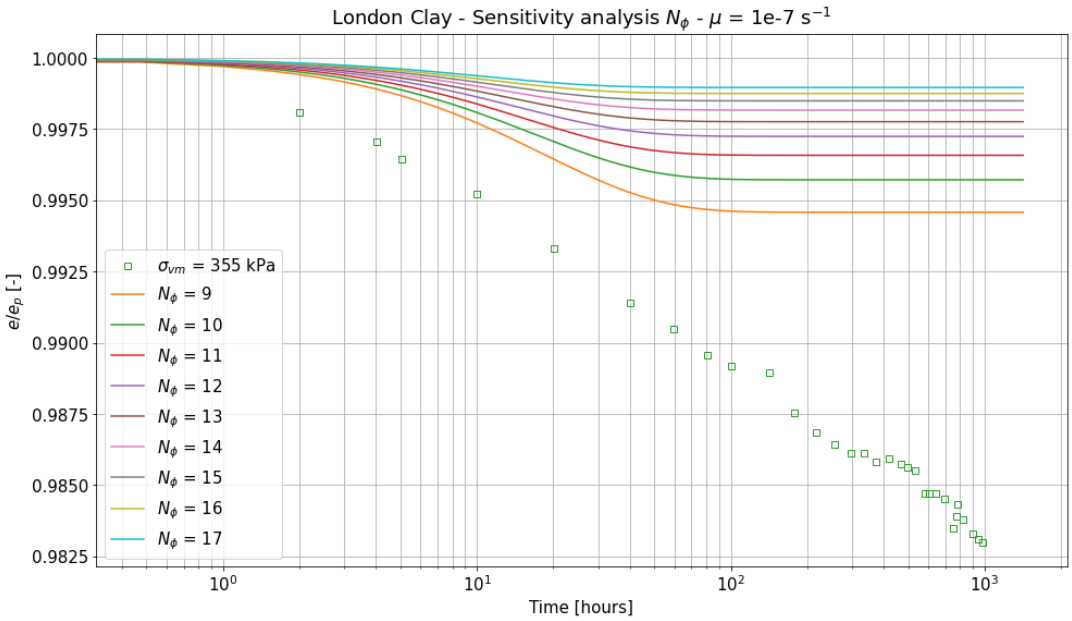

Figure 98: Sensitivity analysis N_ϕ - experimental data from Rezania et al. (2020).

A.3 Elastoplastic parameters EVP model

It was found that the EVP model behaved differently than the EP model when the same set of parameters was used. The results with the EVP model were not accurate (figure 47) so therefore the parameters need to be tuned. In this appendix, the sensitivity to the elastoplastic parameters in the EVP model is analysed. The same parameter values are tested as in appendix A.1, the other parameters are presented below.

Table 37: Elasto viscoplastic parameter values - Sensitivity analysis EP parameters - EVP model.

Parameter	Unit	Meaning	Value
μ	[s^{-1}]	Fluidity parameter	3e-10
N_ϕ	[-]	Strain rate coefficient	9

Table 38: Initial state variables - Sensitivity analysis EP parameters - EVP model.

Parameter	Unit	Meaning	Value
$\boldsymbol{\varepsilon_0}$	[-]	Initial strain	[0.0, 0.0, 0.0, 0.0, 0.0, 0.0]
$\boldsymbol{\sigma_0}$	[kPa]	Initial total stress	[5.0, 5.0, 5.0, 0.0, 0.0, 0.0]
$\boldsymbol{\alpha_0}$	[-]	Initial rotation of plastic potential	[-0.65/3*1, -0.65/3*1, 0.65/3*2, 0.0, 0.0, 0.0]
$\boldsymbol{\beta_0}$	[-]	Initial rotation of yield surface	[-0.65/3*1, -0.65/3*1, 0.65/3*2, 0.0, 0.0, 0.0]
$p_{c,0}$	[kPa]	Initial mean preconsolidation pressure	22.9
e_0	[-]	Initial void ratio	2.59 (Wegman, 2020)

Again, M_c and c_M are kept constant and equal to 1.61 and 0.84 respectively. The results of the sensitivity analysis are presented below.

Sensitivity λ^*

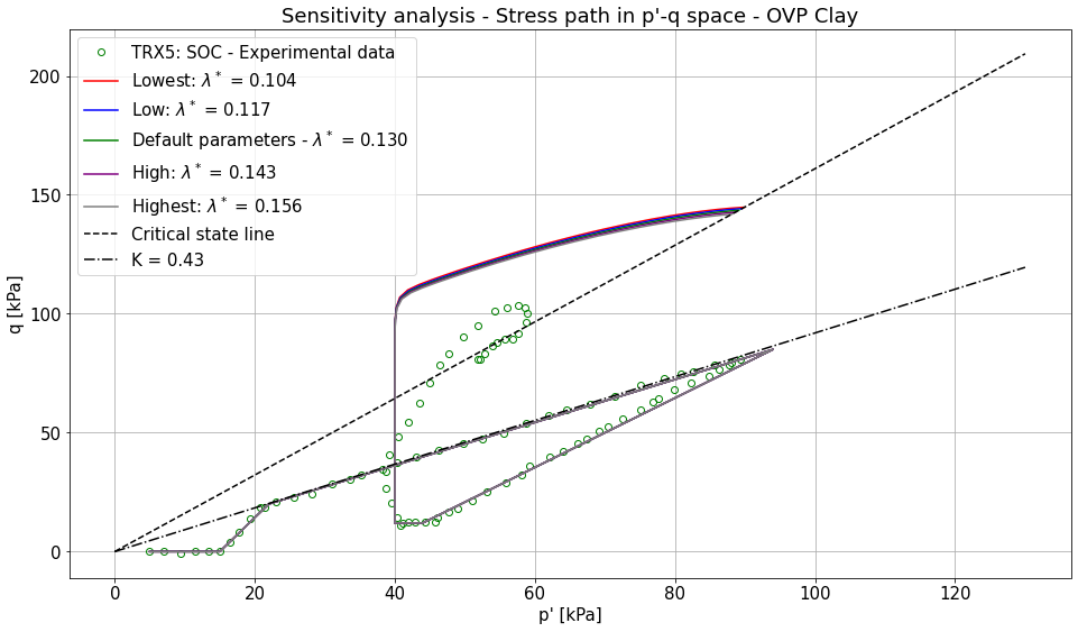

(a) Sensitivity presented in stress path in p'-q space.

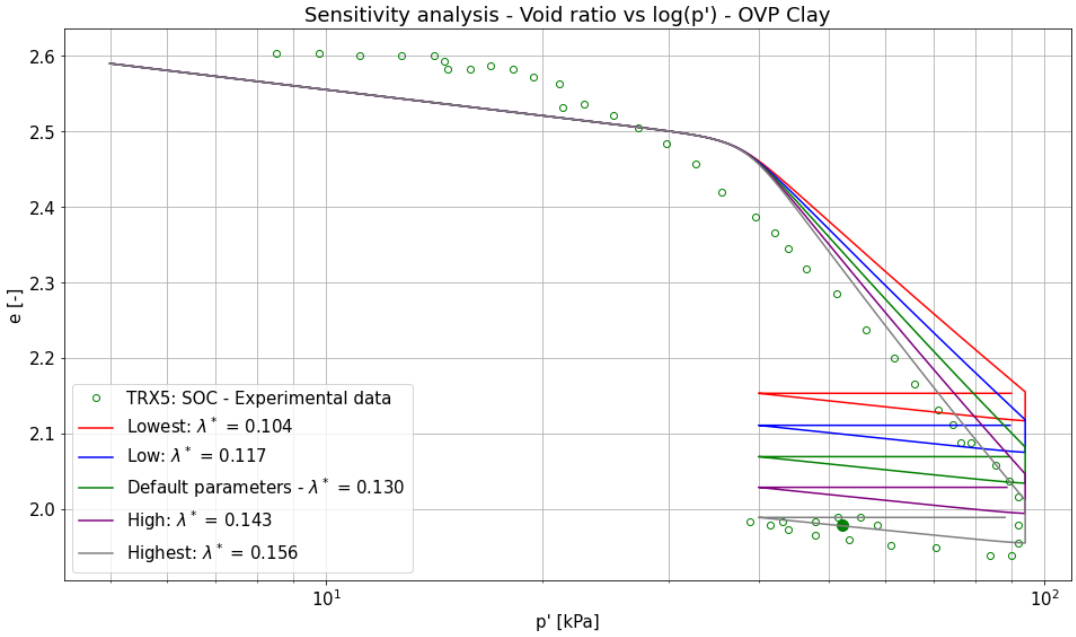

(b) Sensitivity presented by change in void ratio with mean effective stress.

Figure 99: Sensitivity λ^* - EVP Model.

Sensitivity κ^*

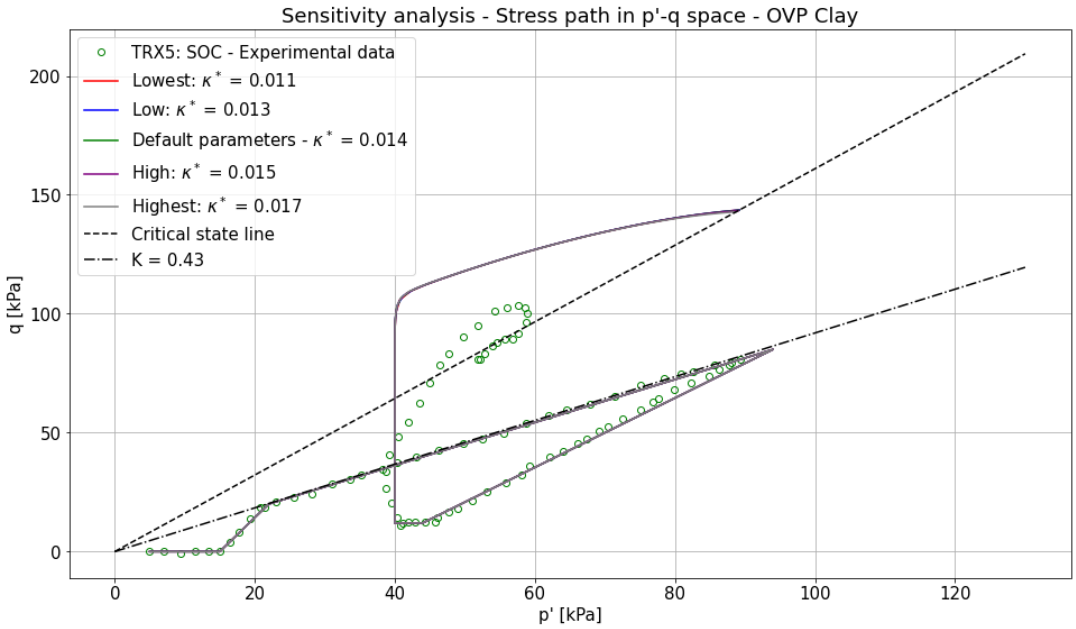

(a) Sensitivity presented in stress path in p'-q space.

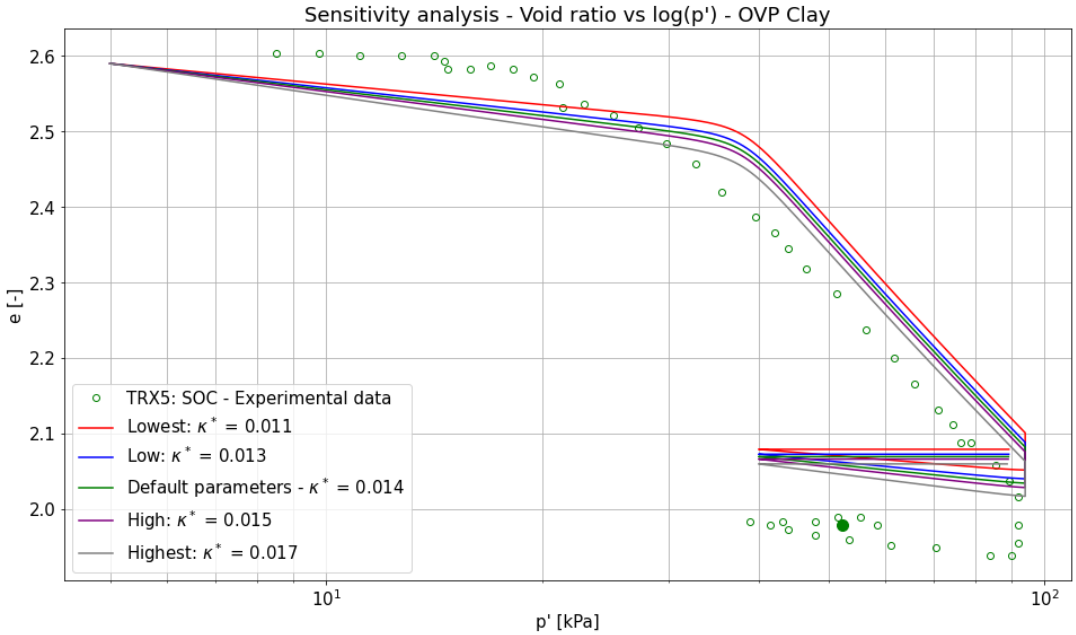

(b) Sensitivity presented by change in void ratio with mean effective stress.

Figure 100: Sensitivity κ^* - EVP Model.

Sensitivity ν

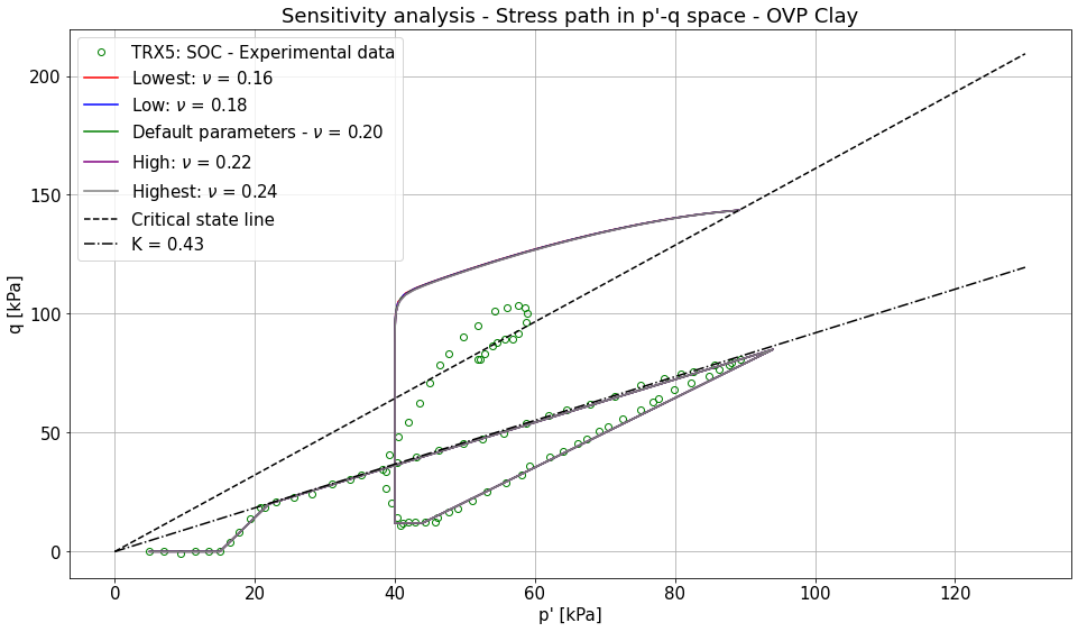

(a) Sensitivity presented in stress path in p'-q space.

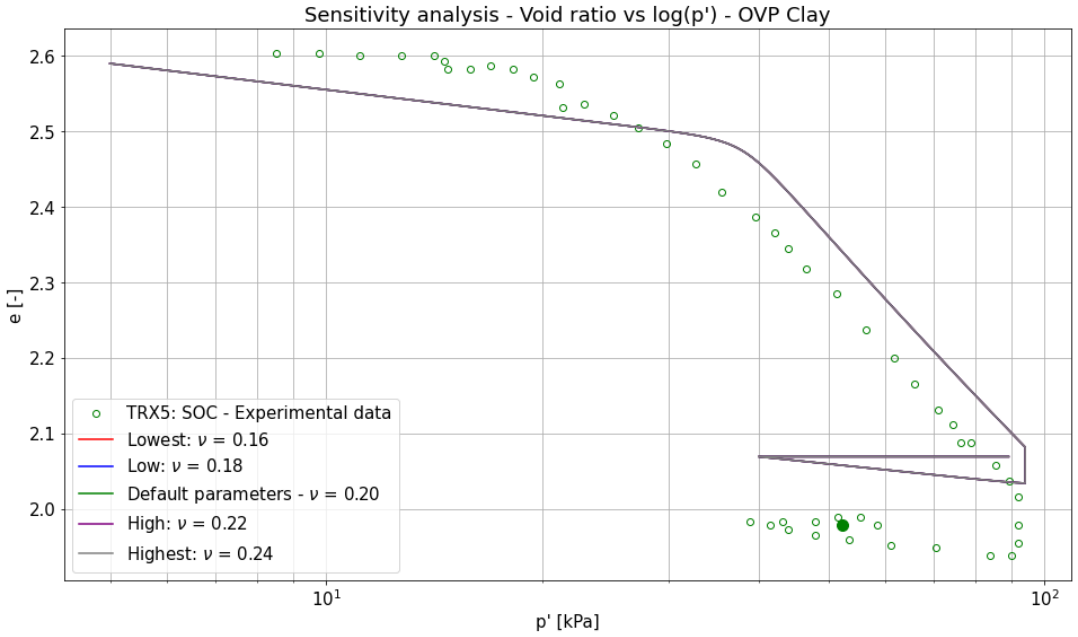

(b) Sensitivity presented by change in void ratio with mean effective stress.

Figure 101: Sensitivity ν - EVP Model.

Sensitivity N

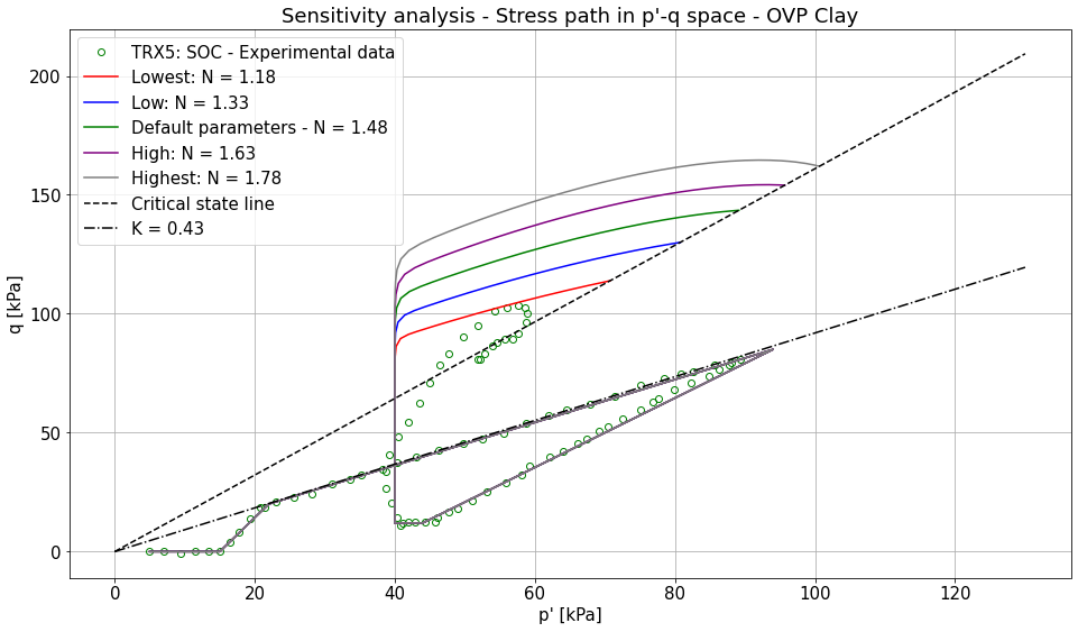

(a) Sensitivity presented in stress path in p'-q space.

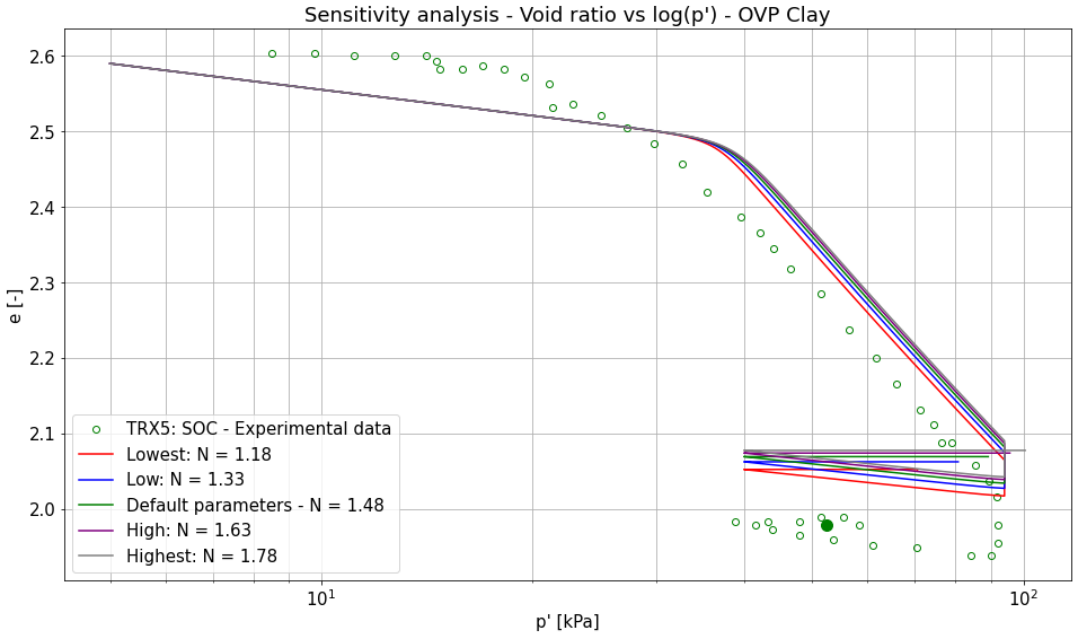

(b) Sensitivity presented by change in void ratio with mean effective stress.

Figure 102: Sensitivity N - EVP Model.

It can be seen that a lower value of N fits the data better than the default determined value.

Sensitivity x

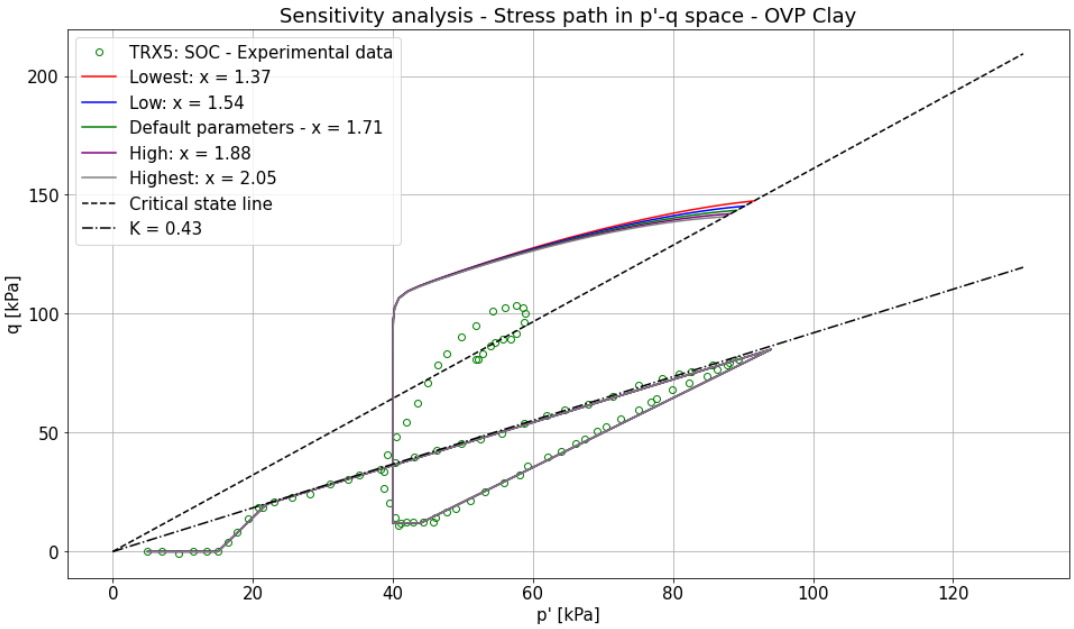

(a) Sensitivity presented in stress path in p'-q space.

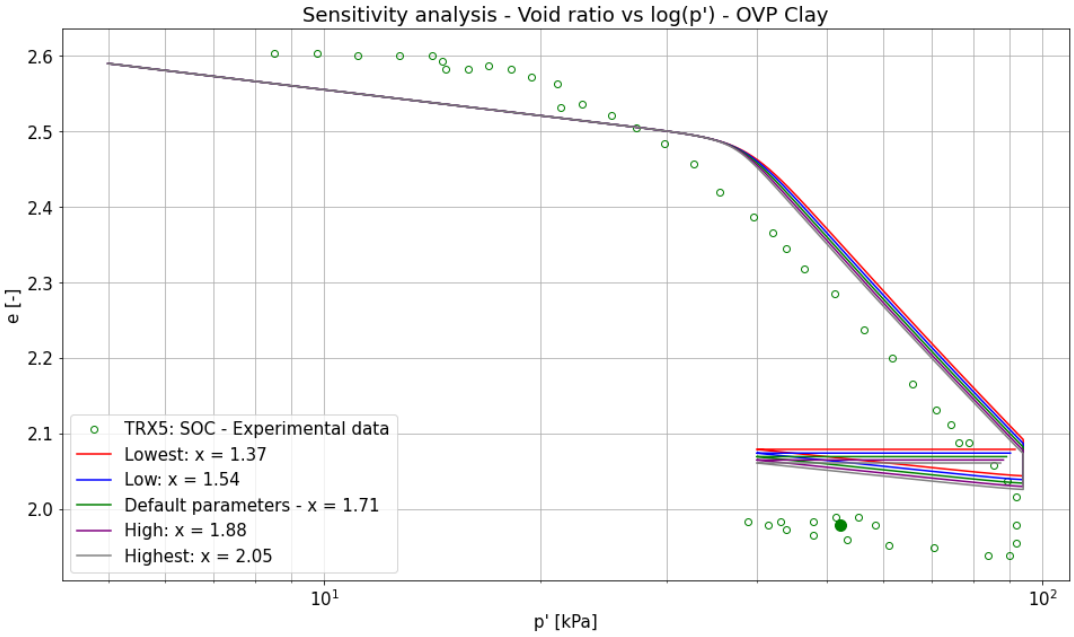

(b) Sensitivity presented by change in void ratio with mean effective stress.

Figure 103: Sensitivity x - EVP Model.

Sensitivity C

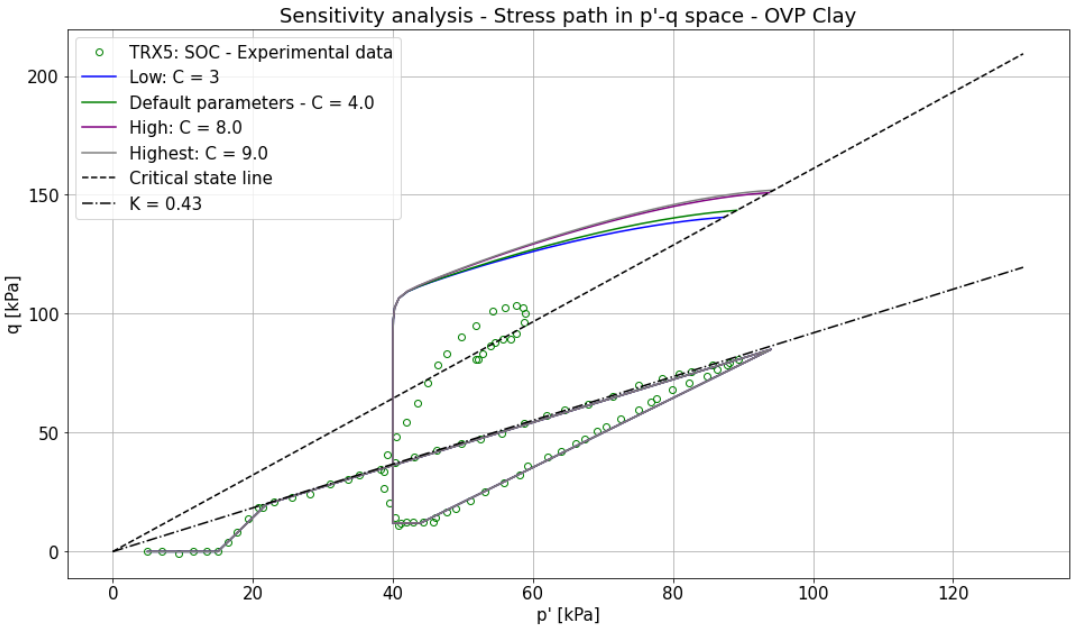

(a) Sensitivity presented in stress path in p'-q space.

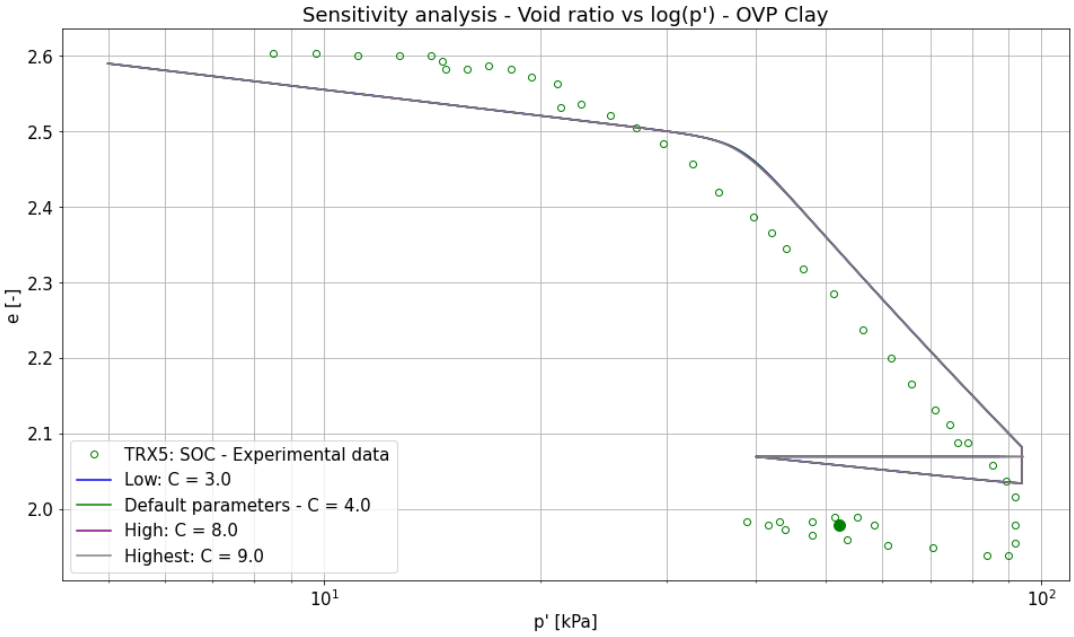

(b) Sensitivity presented by change in void ratio with mean effective stress.

Figure 104: Sensitivity C- EVP Model.

Sensitivity k_f

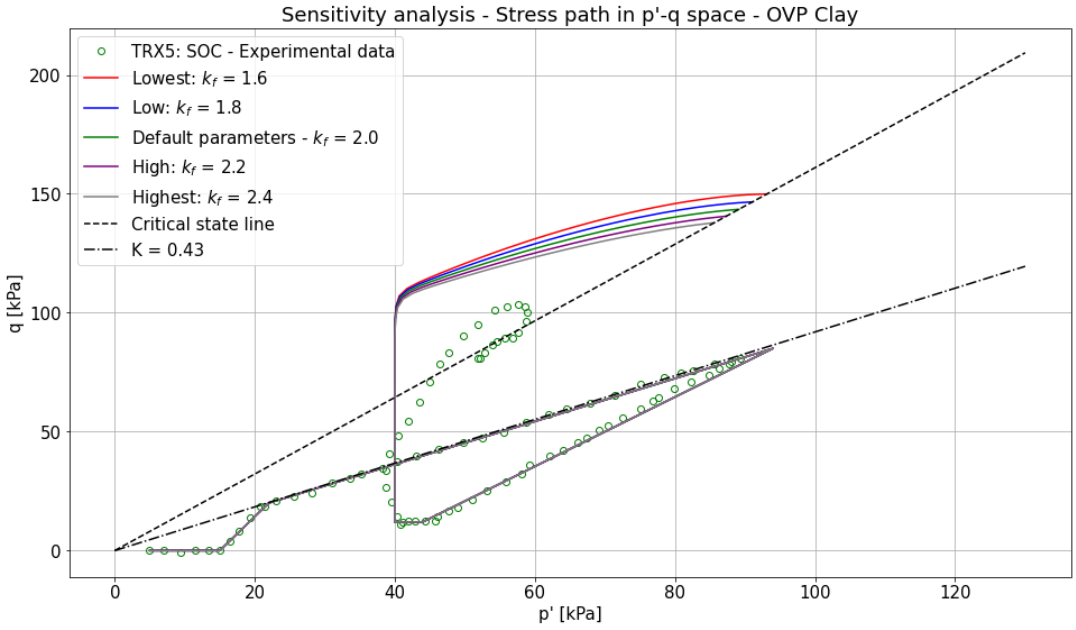

(a) Sensitivity presented in stress path in p'-q space.

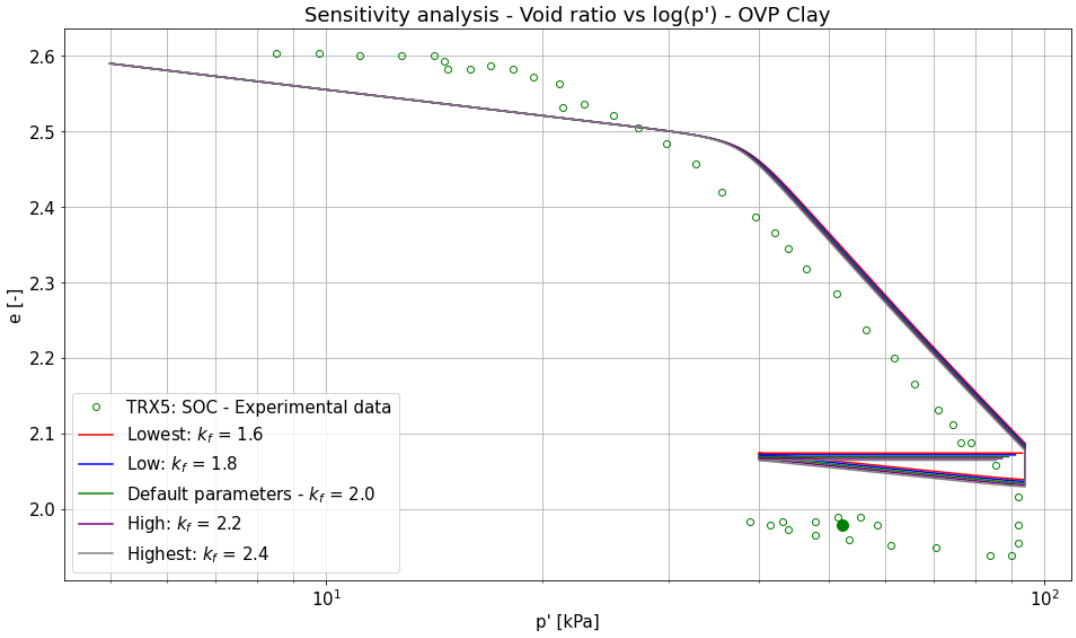

(b) Sensitivity presented by change in void ratio with mean effective stress.

Figure 105: Sensitivity k_f - EVP Model.

A.4 Unsaturated parameters

In this section, the sensitivity of the model to the unsaturated parameters is analysed. First, the SWRC parameters are analysed after which the newly introduced suction dependent viscous nucleus parameters are investigated.

A.4.1 SWRC parameters

In this subsection, the influence of the SWRC parameters is determined. In total, four parameters need to be calibrated to the experimentally determined SWRC for London clay reported by Bagheri et al. (2020) and Rezania et al. (2020). These parameters are a, n, m and α.
Starting values for the parameters are taken from Romero and Jommi (2008) who fitted the same SWRC equation to Boom clay. Due to the different soil properties between Boom clay and London clay, a relatively wide range of parameters is tested. The values at which the sensitivity analysis is performed is presented below. The default values of the parameters are indicated in the middle column.

Table 39: Viscosity parameter values - Sensitivity analysis London clay.

Parameter	Unit			Default		
a	[kPa]	4e3	4e4	4e5	4e6	4e7
n	[-]	0.10	0.50	0.95	1.5	2.0
m	[-]	0.10	0.20	0.41	0.60	0.80
α	[kPa^{-1}]	0.0001	0.0005	0.0014	0.0030	0.0050

The results of the sensitivity analysis are presented below.

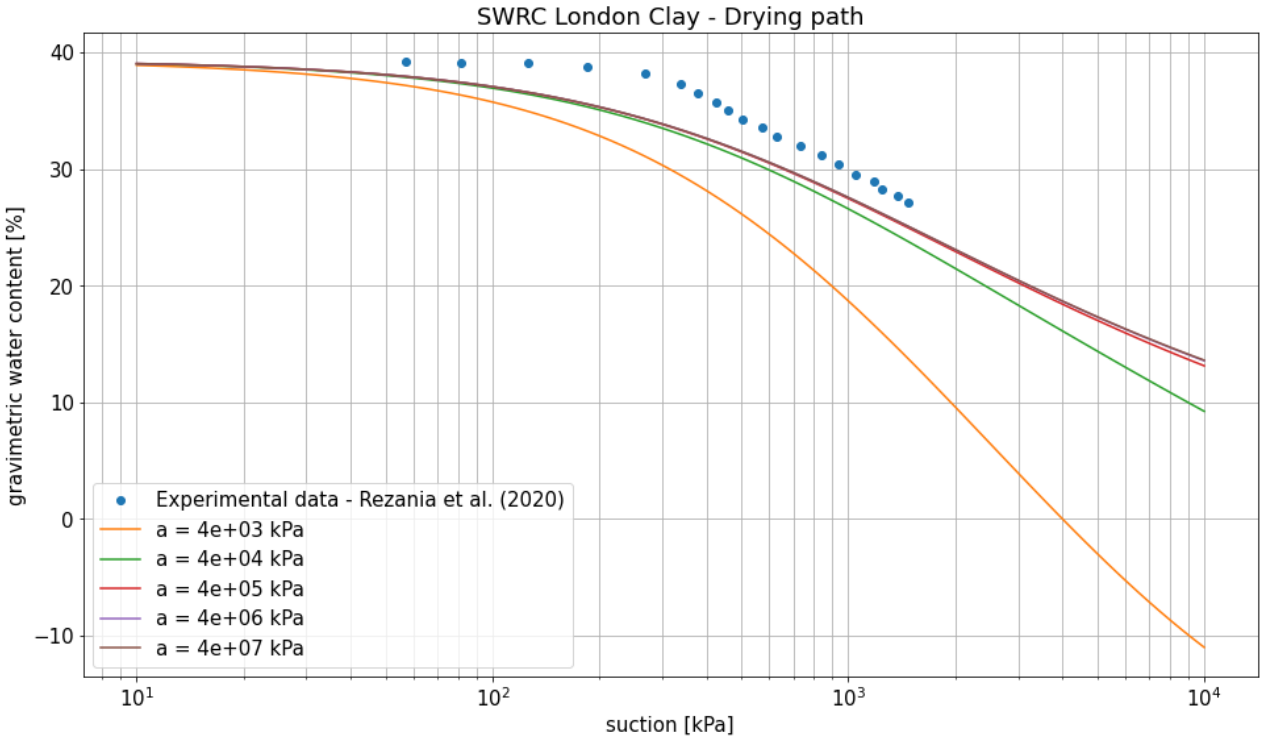

(a) Sensitivity a.

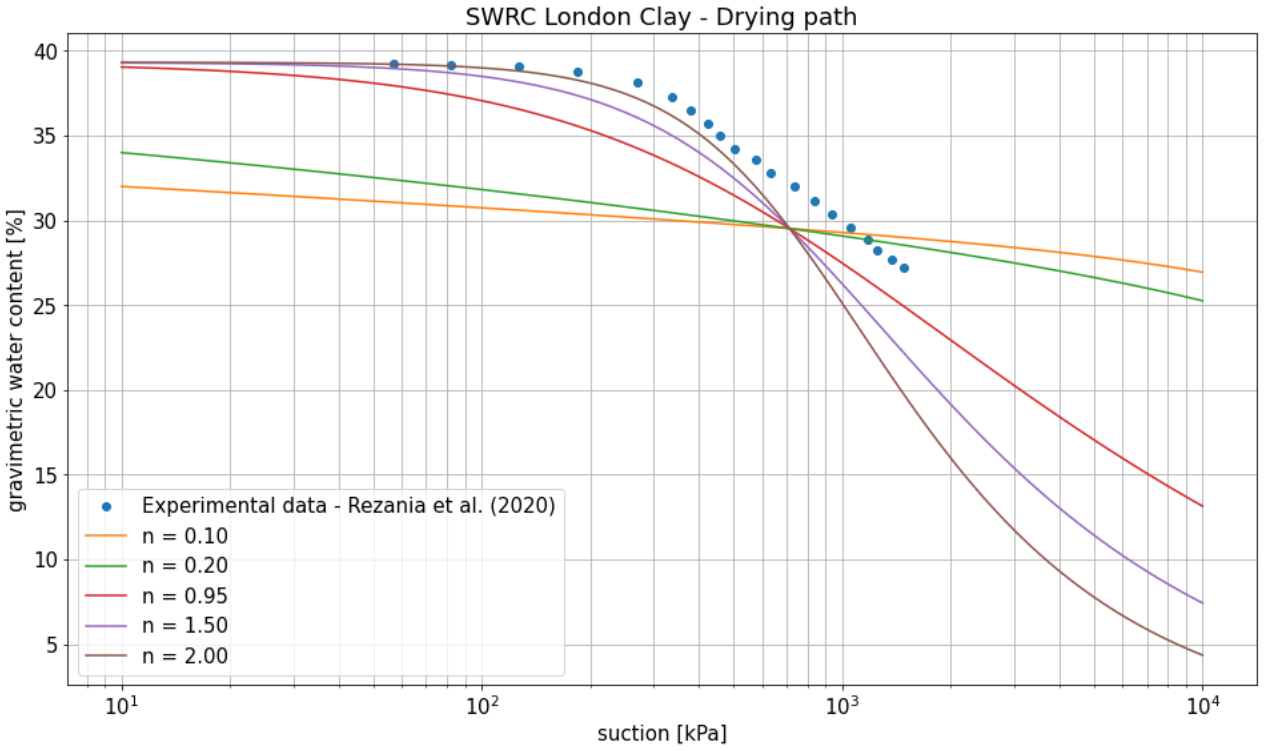

(b) Sensitivity n.

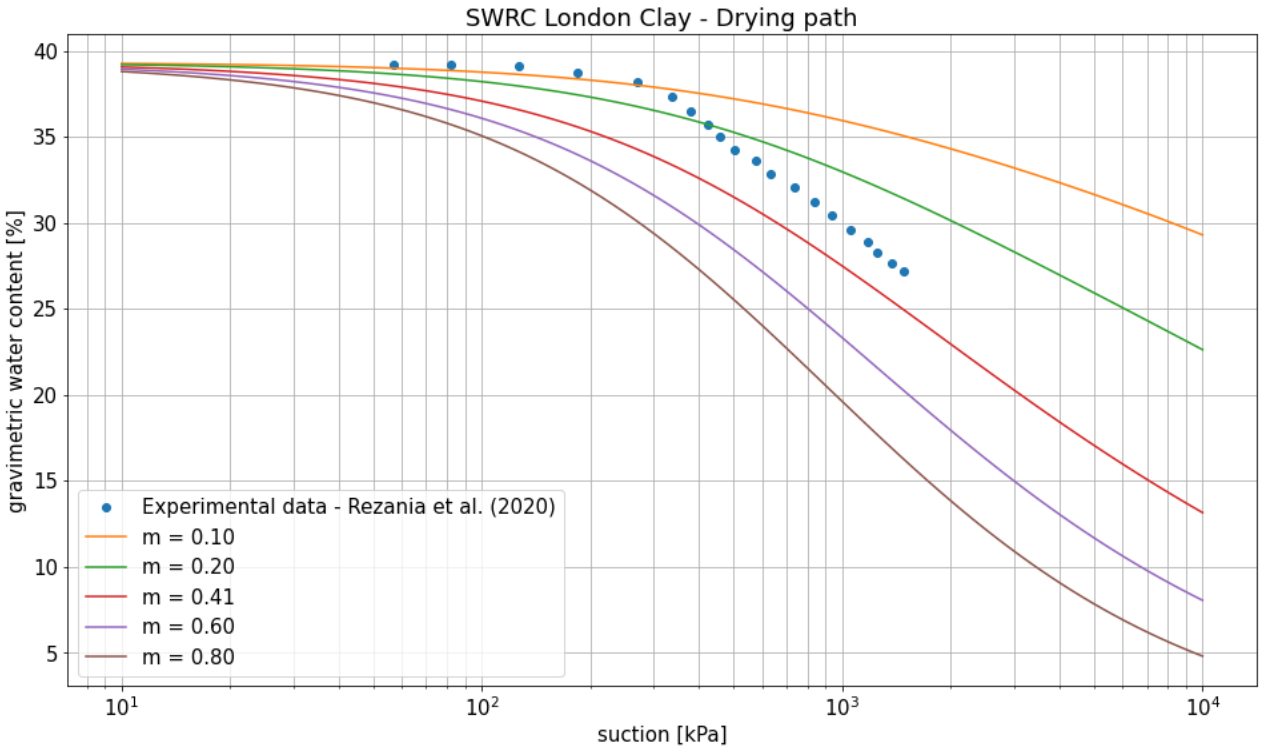

(c) Sensitivity m.

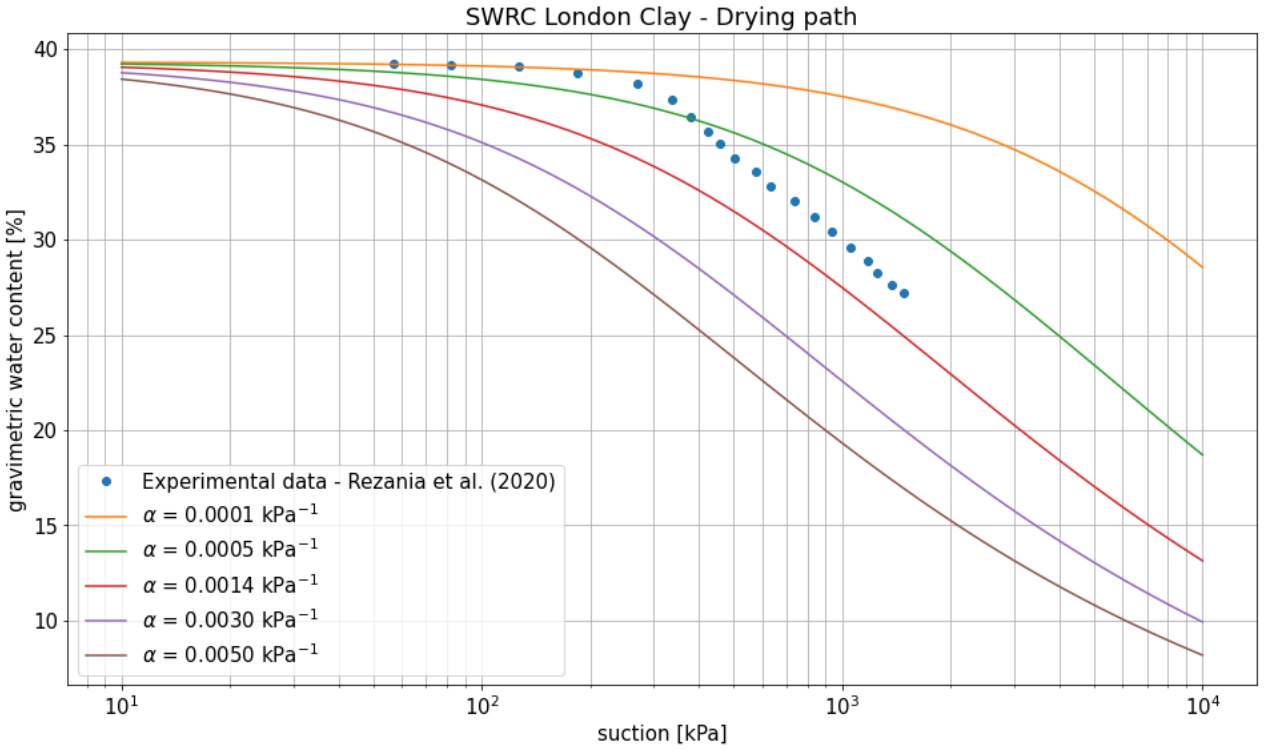

(d) Sensitivity α.

Figure 106: Calculated SWRC compared to experimental SWRC for different values of the SWRC parameters.

The sensitivity analysis shows that for a, a relatively high value is needed to get close to the experimental data. For n, a high value is needed as well, for this parameter low values change the shape of the SWRC completely. Looking at m, a low value is needed, the shape of the SWRC is not much affected by this parameters. Finally, for α it is found that this parameter governs at which suction the SWRC becomes steeper, the best match is found at around 0.0030 kPa^{-1}.

A.4.2 Suction dependent viscous nucleus parameters

Since the parameters belonging to the suction dependent viscous nucleus are newly introduced. Their values need to be determined through the execution of trial runs. This process can be aided by the use of a sensitivity analysis. The experimental data is taken from Rezania et al. (2020), more specifically, the sample with an initial suction of 513 kPa and an applied load of 355 kPa is used. This sample is chosen because it has a median value for both the suction and the load and is therefore deemed to be representative. Shown below are first the tested values in a table after which the results are presented. The other parameter values are found in tables 35 and 36 with μ = 1e-8 s^{-1} and N_ϕ = 13.0.

Table 40: Suction dependent viscous nucleus parameter values - Sensitivity analysis London clay.

Parameter	Unit	Value									
s_{ref}	[kPa]	10	20	30	40	50	60	70	80	90	100
n_{suc}	[-]	0.5	1.0	1.5	2.0	2.5	3.0	3.5	4.0	4.5	5.0

For the sensitivity analysis of s_{ref}, n_{suc} is set to 2.5, for the sensitivity analysis of n_{suc}, s_{ref} is set to 20 kPa.

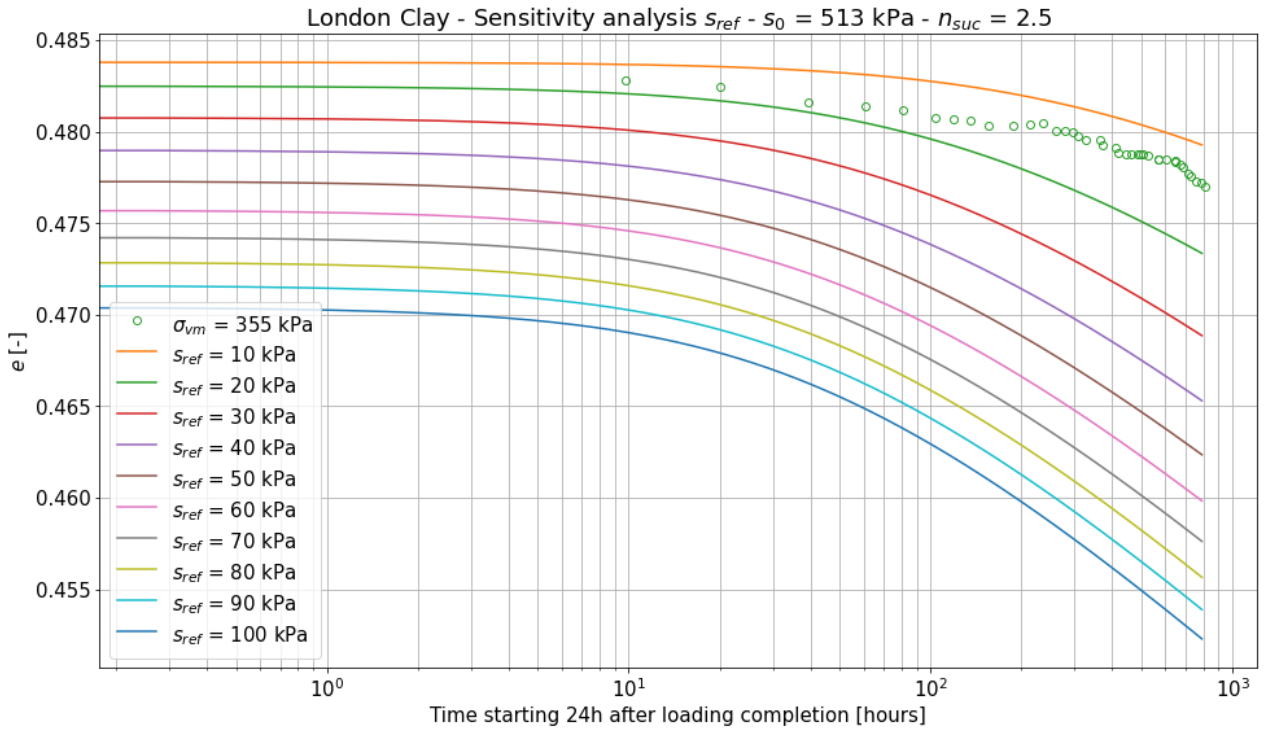

Figure 107: Sensitivity analysis s_{ref}.

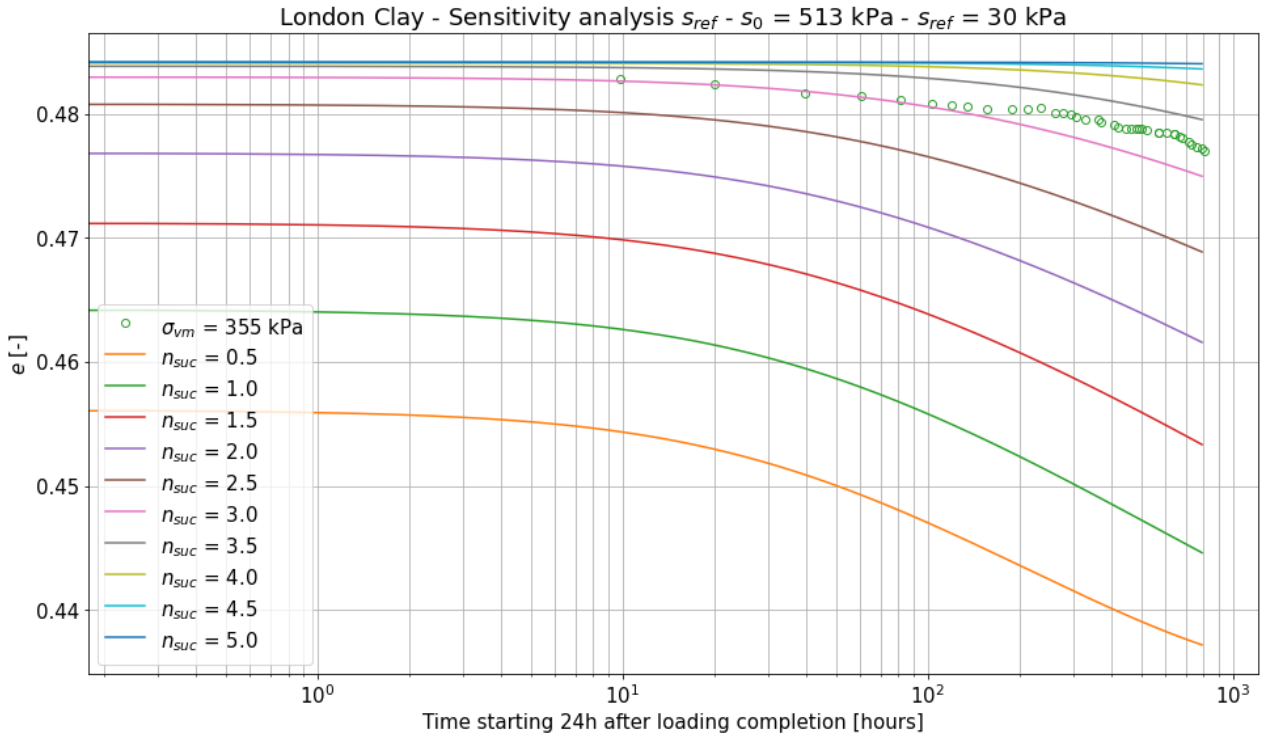

Figure 108: Sensitivity analysis n_{suc}.

B Unsaturated elastoplastic plots

As has been stated in section 5.5, both the hydromechanical and the mechanical driver can be used to simulate the loading/unloading tests by Rezania et al. (2020). In this appendix, the plots for all six samples are presented. In each plot, the drained model prediction by both the hydromechanical and mechanical driver are shown. For four of the samples, Rezania et al. (2020) gave the value of the suction throughout the tests. This information is exploited to also perform a model run with the hydromechanical driver where the suction is governed throughout the tests. This final model simulation is labeled as 'suction applied' in the figures below.

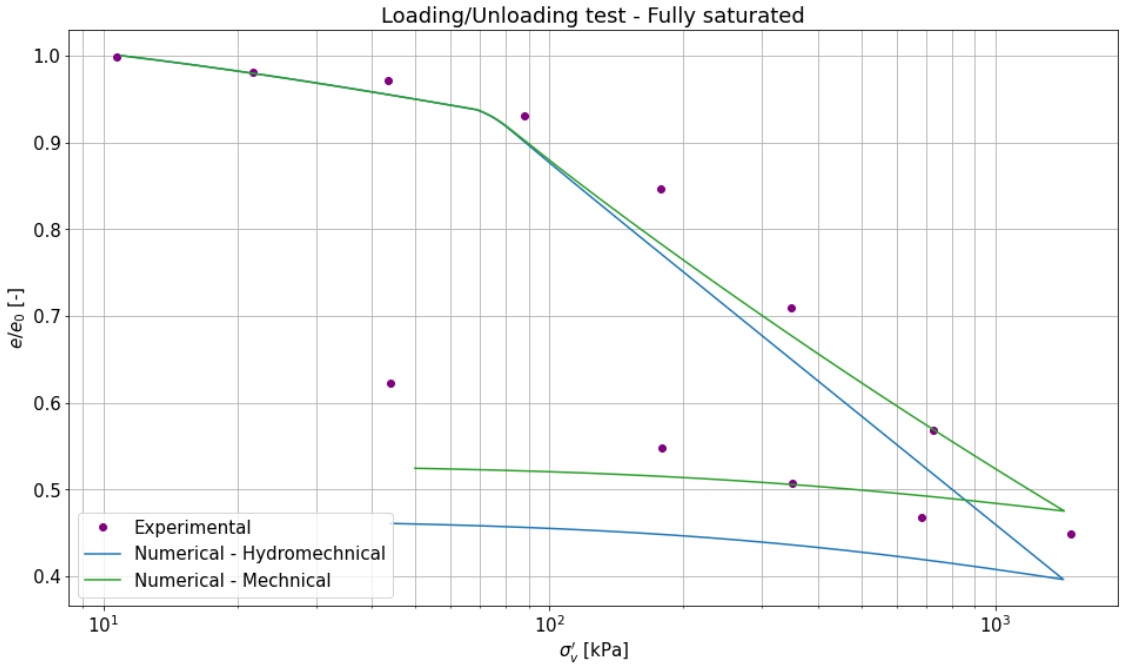

(a) Saturated sample.

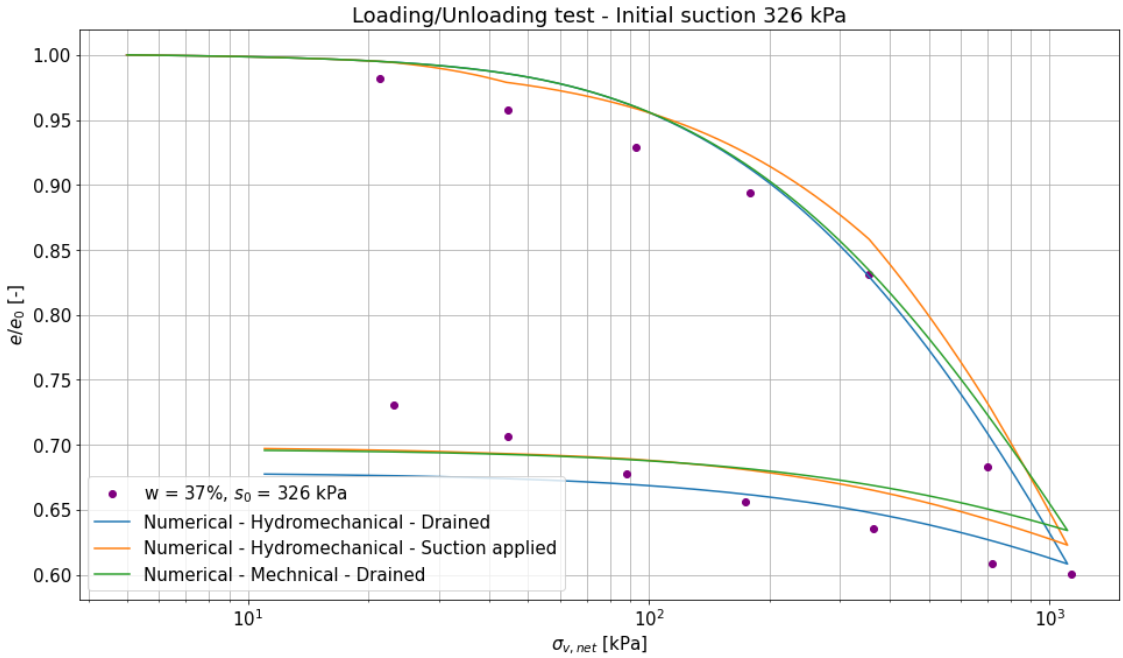

(b) $s_0 = 326$ kPa.

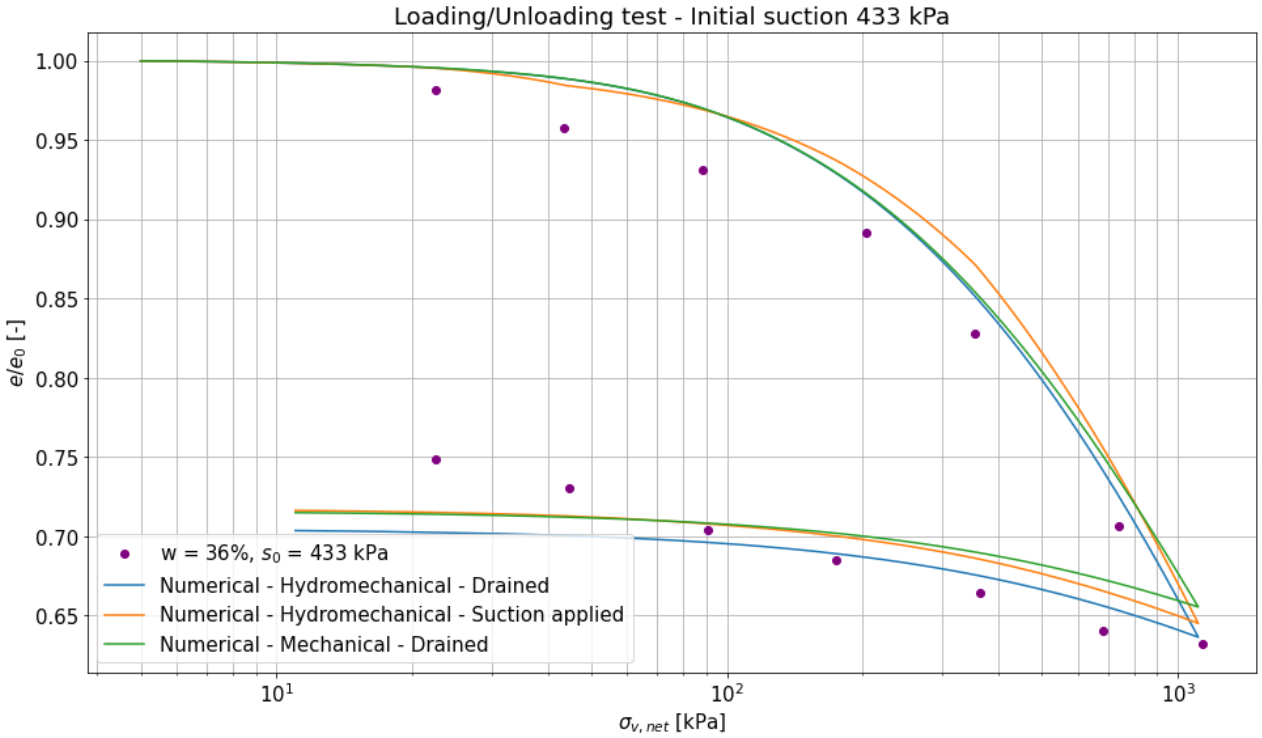

(c) $s_0 = 433$ kPa.

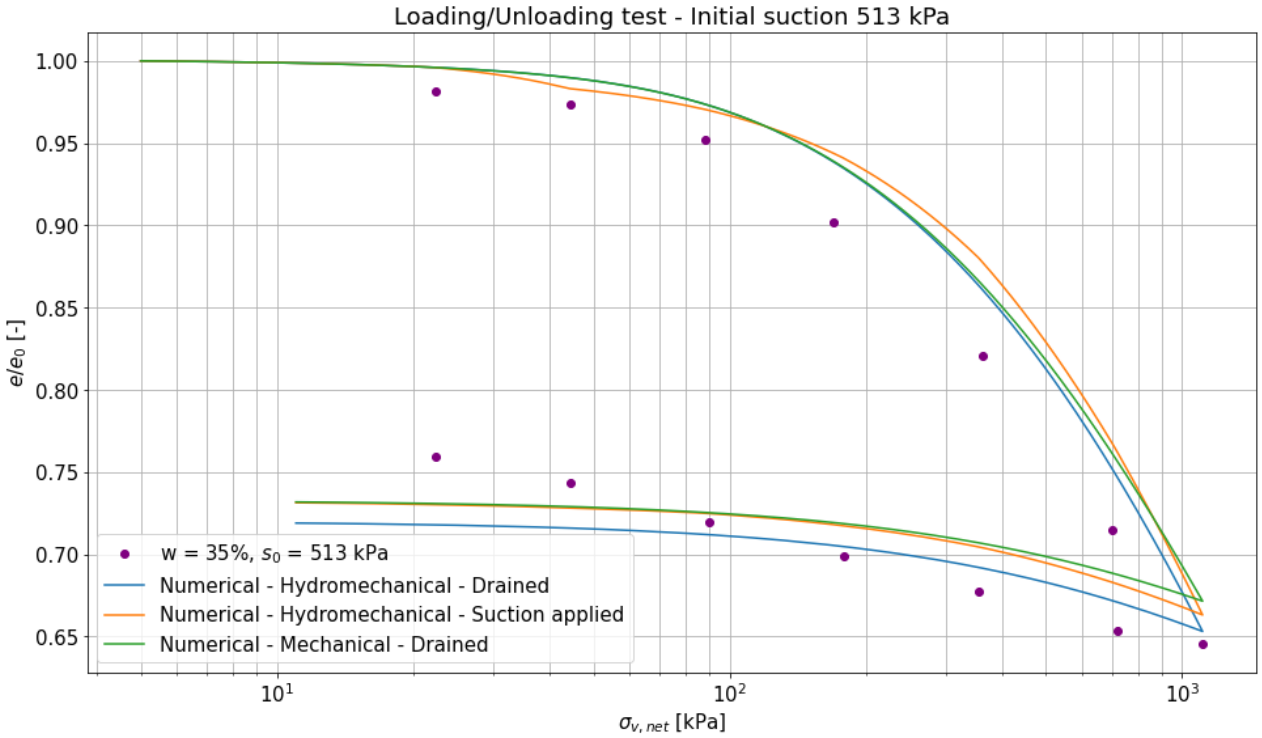

(d) $s_0 = 513$ kPa.

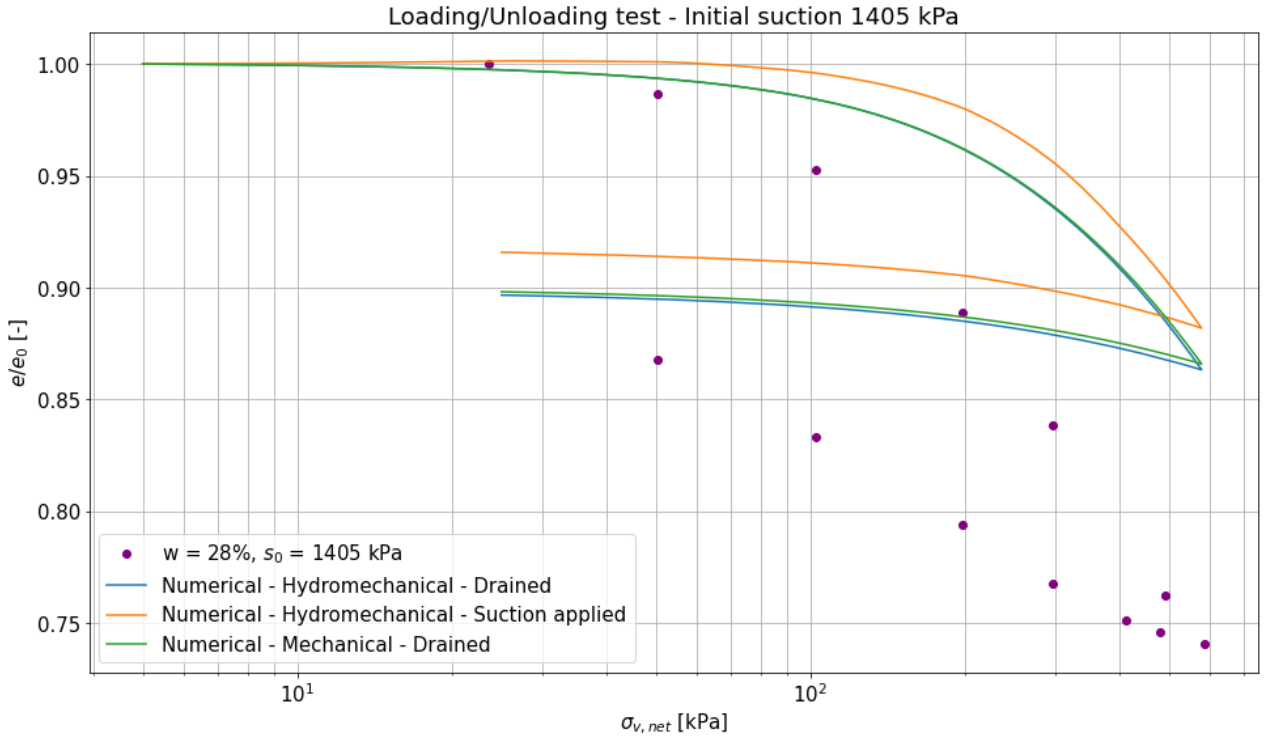

(e) $s_0 = 1405$ kPa.

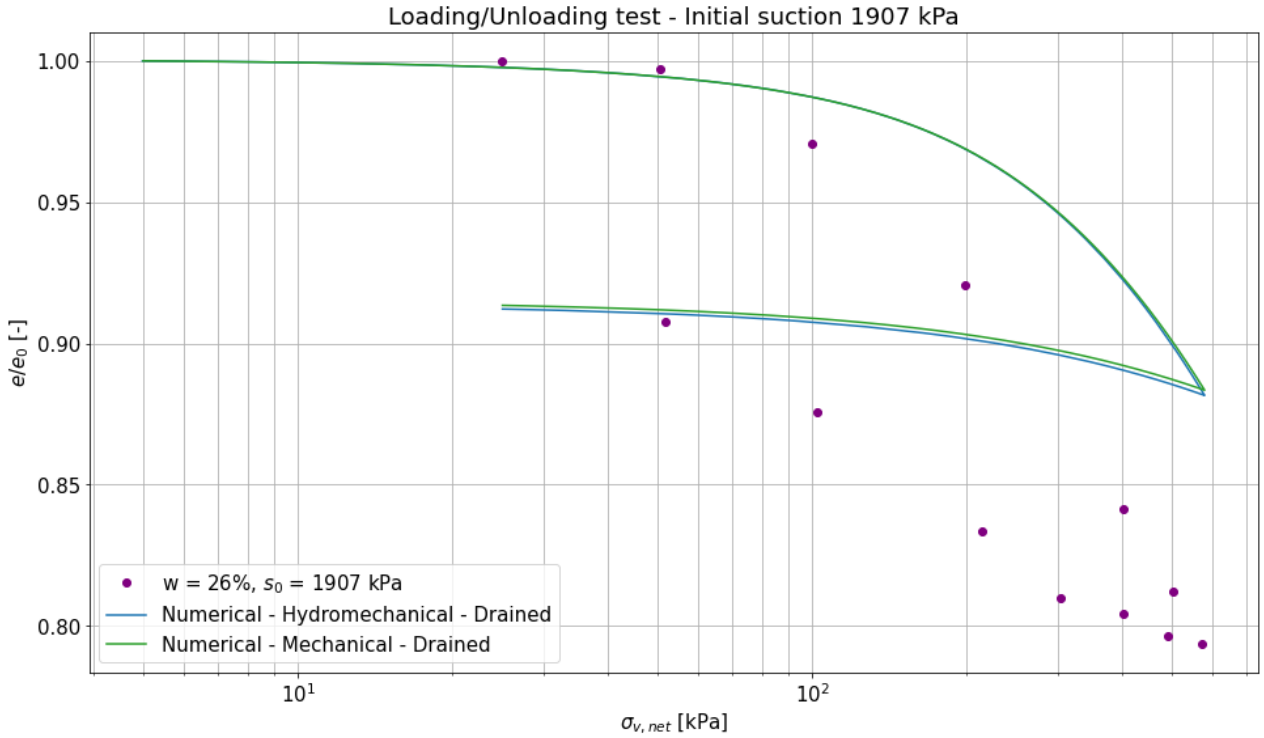

(f) $s_0 = 1907$ kPa.

Figure 109: Deformation predicted by hydromechanical and mechanical driver.

Date 03/12/2021
Contact person Prof. Dr. Cristina Jommi
Telephone/fax +31 15 27 84173
E-mail C.Jommi@tudelft.nl
Subject Bosmans MSc plagiarism check

Delft University of Technology

Faculty of Civil Engineering and Geosciences
Department of Geoscience & Engineering

Visiting address
Stevinweg 1
2628 CN Delft
Postal address
P.O. Box 5048
2600 GA DELFT
The Netherlands

www.gt.citg.tudelft.nl

R. Bosmans final MSc report: plagiarism check

I hereby declare that I fully checked the final report on

Influence of creep and drying/wetting on the initial stress state of clays
by Rutger (R.P.A.) Bosmans

for the degree of Master of Science in Civil Engineering at the Delft University of Technology.

The document properly refers to previous literature knowledge, summarised by the author in an autonomous way. The main core of the dissertation consists of original theoretical developments, which have never been published before. All sources of data and information are correctly quoted.

Regards

Cristina Jommi

Prof. Dr. Cristina Jommi
Supervisor and Chair of the MSc committee